Responsive Polymer–Based pH Sensors and Environmental Remediation Technologies

by

Andrews Ahiabu

A thesis submitted in partial fulfillment of the requirements for the degree of

Doctor of Philosophy

Department of Chemistry
University of Alberta

Abstract

My Ph.D. research involved the generation of stimuli responsive poly(*N*-isopropylacrylamide) (pNIPAm)-based microgels and the modification of their chemistry to generate a series of pH responsive microgel-based optical devices (etalons). The pH responsivity of the synthesized microgels was used also for drug delivery applications by taking advantage of the different ionizable groups that can be incorporated during the microgel synthesis. pH responsive microgels were used also as sorbents for environmental remediation applications, i.e., to remove heavy metal ions from solution. The porous nature and versatility of microgels made them possible to be incorporated into other remediation technologies. Specifically, they have been used to stabilize zero valent iron, which suffers aggregation in the remediation process.

In Chapter 1, I present a brief introduction of stimuli responsive polymers and hydrogels, with emphasis on their structure and swelling theories. Chapter 2 focuses on the synthesis of a library of pH responsive microgels using different ionizable groups and the evaluation of their response to solution pH changes. The response kinetics to solution pH for a series of pH responsive microgels differing only in their alkyl pendant groups was investigated in Chapter 3. The longer alkyl group chains yielded the fastest response rate, with nearly a 1000 fold increase in response rate when compared to the shortest alkyl chain microgel. The knowledge obtained from pH responsive microgels in Chapter 2 was implemented in drug delivery applications in Chapter 4. Two ionizable groups of opposite charges at different pH regimes were used to load and release model drugs in a controlled manner through the aggregation (drug loading) and disaggregation (drug

releasing) of the microgels controlled by solution pH. In Chapter 5, the microgels were used as sorbents for the remediation of heavy metal ions, such as Cd^{2+} and Pb^{2+}. The role that crosslinking density, type and composition of the microgels, played in remediating these ions was presented. An attempt to expand the remediating capability of these microgels to other recalcitrant contaminants such as selenium, which is a metalloid, failed. However, the microgels played a significant role in dispersing zero valent iron (ZVI), which is an emerging technology capable of remediating many contaminants, ranging from halogenated organic compounds to heavy metals and metalloids. However, its propensity to aggregate limits its use. In Chapter 6, I present the enhanced ability to remove Se with microgel stabilized ZVI as compared to either N_2 purged or pristine ZVI. In Chapter 7, conclusions and future suggestions are presented for further directions to the work presented.

Preface

This dissertation is an original work by Andrews Ahiabu (A. Ahiabu), being supervised by Dr. Michael J. Serpe (M. J. Serpe).

Chapter 3 of this thesis has been published as A. Ahiabu, and M. J. Serpe, Rapidly Responding pH and Temperature-Responsive Poly (*N*-Isopropylacrylamide)-Based Microgels and Assemblies. *ACS Omega*, **2017**, *2*, 1769-1777. I was responsible for the experiment design, data collection and analysis as well as the manuscript composition. M. J. Serpe was the supervisory author and was involved with research design and manuscript composition.

Chapter 4 of this thesis has been published as Y. Gao, A. Ahiabu, and Michael J. Serpe, Controlled Drug Release from the Aggregation-Disaggregation Behavior of pH-Responsive Microgels. *ACS Appl. Mater. Interfaces*, **2014**, *6*, 13749-13756. I was responsible for the experiment design, data collection and analysis as well as the manuscript composition. Y. Gao assisted equally with the experimental design, data collection as well as the manuscript composition and contributed equally with me. M. J. Serpe was the supervisory author and was involved with research design and manuscript composition.

I would like to dedicate this thesis to my late father John K. Ahiabu. Papa, it was your tireless effort and determination that has brought me this far. May your soul rest in perfect peace!

Acknowledgements

To God be the glory for the great things He has done! I am grateful to God Almighty for how far He has brought me throughout my academic journey, especially the pursuit of my Ph.D. He has in diverse ways used people along the journey to accomplish what I am and have today and I would like to acknowledge them.

The first acknowledgment goes to my Ph.D. advisor, Dr. Michael J. Serpe, affectionately called Mike! As I recount my first day in the lab, far away from home, the warmth and comfort you gave me to feel at home, made this journey more embracing. Your continuous help in diverse ways; through the thick and thin, you have been my guide. As I walk down your office confused, I come out with clarity and energized to fight on. Words cannot express my gratitude to you Mike, I am truly grateful!

I would like to thank both past and current Serpe Group members for their willingness to help and the friendly atmosphere that enabled continuous research. A special thanks to my Supervisory committee members, Dr. Charles A. Lucy, Dr. Chris Le and Dr. Eric Rivard for your constructive criticism each time I approached you. Your invaluable contributions and suggestions towards my journey are well appreciated. I am grateful also to Dr. Joao Soares and Dr. Stefan Zauscher for agreeing to serve as arm's length and external examiner, respectively, for my doctoral examination. I am thankful to Dr. Anna Jordan for her tireless effort in proof reading this thesis; for dotting my i's and crossing my t's.

I would like to thank my family, my Mom, my brothers, Eric and Moses and my other siblings for your support and encouragements. A thank you to the many friends I have met along the journey. Last but not least, I would like to thank my lovely Fiancée, Rachel who has been there for me through the tough times and kept encouraging me for the past year we have known each other. I appreciate your sincere love towards me and I love you dearly Rachel!

Table of Contents

Abstract ii

Preface iv

Acknowledgements vi

List of Tables xii

List of Schemes xiii

List of Figures xiv

List of Symbols xxiii

List of Abbreviations xxiv

Chapter 1 1

General Introduction to Hydrogels and Microgels 1

1.1 General Hydrogel/Microgel Theory 2

1.1.1 Physical Structure 2

1.1.2 Equilibrium Swelling Theory 3

1.2 Stimuli Responsive Polymers 6

1.2.1 Temperature Responsive Polymers 6

1.2.1.1 Swelling Theory 7

1.2.2 pH Responsive Polymers 10

1.2.2.1 Polymer Composition and Swelling Behavior 13

1.3 Applications of Stimuli Responsive Polymers 16

1.3.1 pH Responsive Photonic Sensors 16

1.3.2 pH Responsive Hydrogels for Controlled Drug Release 19

1.3.3 Water Remediation Applications 22

1.3.3.1 Polymer-Based Sorbents for Water Remediation 27

1.3.3.2 Zero Valent Iron for Water Remediation 28

1.4 Polymerization Synthesis and Mechanism 31

1.5 Conclusions 33

Chapter 2 35

pH Responsive Microgels as Sensors and their Response in High Salt Concentrations 35

2.1 Introduction 35

2.2 Experimental Section: 39

2.3 Results and Discussion 43

2.4 Conclusions 63

Chapter 3 64

Rapidly Responding pH and Temperature-Responsive Poly (*N*-Isopropylacrylamide)-Based Microgels and Assemblies 64

3.1 Introduction 65

3.2 Experimental Section 69

3.3 Results and Discussion 73

3.4 Conclusions 89

Chapter 4 91

Controlled Drug Release from the Aggregation–Disaggregation Behavior of pH-Responsive Microgels 91

4.1 Introduction 92

4.2 Experimental Section 94

4.3 Results and Discussion 97

4.4 Conclusions 111

Chapter 5 113

Poly (*N*-Isopropylacrylamide)-Based Microgels as Sorbents for Pb^{2+} and Cd^{2+} Removal: Effect of Comonomer and Crosslinking Densities 113

5.1 Introduction 113

5.2 Experimental Section 117

5.3 Results and Discussion 119

5. 4 Conclusions 130

Chapter 6 131

Enhanced Selenium Removal by Microgel Stabilized Zero Valent Iron 131

6.1 Introduction 131

6.2 Experimental Section 134

6.3 Results and Discussion 139

6.4 Conclusions 149

Chapter 7 150

Conclusions and Future Outlook 150

References: 153

Appendices 168

Appendix A: Crown Ether Functionalized Microgels for Selective Removal of Metal Ions 169

Appendix B: Ion Selective Membranes for Selective Sensing of Chromium Ions 171

Appendix C: Oil Sands Processed Affected Clay (OSPC) as Sorbents for Organics and Heavy Metal Ions 174

Appendix D: Hybrid Clay-Hydrogel Sorbents for Organic Dye Removal from Water . 182

Appendix E: Putting Waste to Use: A Case of Cigarette Butts 185

Appendix F: Unexpected Ionic Strength Response by Confined Microgels 188

List of Tables

Table 2-1. pH in different tissues and cellular compartments. 21

Table 1-2. Guidelines for Canadian drinking water quality for the above heavy metals . 25

Table 2-1. Distinctive IR functional groups and their representative vibrational frequencies for BAAc monomer. 44

Table 3-1. Comonomer feed and compositions in microgel. 89

Table C-1. Zeta potential (ZP) measurements at different pH for sorbents used in this study. 179

Table C-2. Adsorption capacity values at different initial concentrations of CV for the three sorbents studied. 180

List of Schemes

Scheme 2-1. Swelling/shrinking mechanism of (a) pNIPAm-*co*-4VP, (b) pNIPAm-*co*-BAAc and (c) pNIPAm-*co*-AAc+APBA microgels. 47

Scheme 3-1. (a) Structures of pH-responsive monomers used in this Chapter, (b) synthesis of 2-butylacrylic acid and (c) polymerization scheme used to generate poly(N-Isopropylacrylamide-*co*-Butylacrylic acid) (pNIPAm-*co*-BAAc) microgels 73

Scheme 4-1. Aggregate formation and the trapping of a model drug (methylene blue) when microgels are mixed at pH values that render both microgels charged. 98

Scheme 4-2. A schematic representation of the drug release experimental set up. 108

Scheme 5-1. A schematic presentation for the removal of heavy metal ions by the microgels and their quantitation by ICP-OES 118

Scheme 5-2. Proposed sorption mechanism for Cd^{2+} and Pb^{2+} by microgels..... 119

Scheme 6-1. A synthetic scheme for microgel stabilized zero valent iron. 137

Scheme C-1. Experimental procedure for removal of CV from aqueous solution by OSPC..... 175

List of Figures

Figure 1-1. Some common temperature responsive polymers..... 7

Figure 1-2. Temperature dependence of crosslinked poly (N,N'-alkyl substituted acrylamides). 9

Figure 1-3. pH-Responsive polymers of different architectures..... 12

Figure 1-4. Some common pH responsive monomers..... 16

Figure 1-5. (a) Structure of a microgel–based etalon: (i) glass substrate, (ii) Cr/Au base layer (iii) monolithic microgel, (iv) Cr/Au over layer. (b) Instrumental setup for obtaining spectroscopic information from the device. (c) A characteristic reflectance spectrum obtained from the setup in (b) 19

Figure 1-6. Reduction mechanism of oxidic-shell-free ZVI in the removal of As in both oxic and anoxic conditions..... 31

Figure 1-7. pNIPAm-based microgel synthesis scheme 33

Figure 2-1. (a) FTIR spectra of BAAc and (b) mass spectrum of BAAc, with its molecular ion peak of (M-H) at 127.0764. 44

Figure 2-2. (a) A schematic representation of etalons and their behavior in different pH conditions for etalons, which swell at pH above the pK_a of the acid comonomer. The etalon is composed of monolithic microgel (ii) sandwiched between two Cr/Au layers (i and iii) on a glass substrate (iv), (b) a representative reflectance spectrum, showing a red shift from response in panel (a). 46

Figure 2-3. (a) pH response of pNIPAm-*co*-4VP, (b) pNIPAm-*co*-AAc, (c) pNIPAm-*co*-BAAc and (d) pNIPAm-*co*-AAc+4APBA devices. 49

Figure 2-4. Linear pH response ranges for (a) pNIPAm-*co*-4VP (3.5–5.3), (b) pNIPAm-*co*-AAc (4.0–7.0), (c) pNIPAm-*co*-BAAc (4.8–8.5) and (d) pNIPAm-*co*-AAc+4APBA (7.7–11.5) devices. 51

Figure 2-5. Reversibility of pH response to (a) pNIPAm-*co*-4VP, (b) pNIPAm-*co*-AAc, (c) pNIPAm-*co*-BAAc and (d) pNIPAm-*co*-AAc+4APBA devices. 53

Figure 2-6. The repeatability of (a) pNIPAm-*co*-4VP, (b) pNIPAm-*co*-AAc, (c) pNIPAm-*co*-BAAc and (d) pNIPAm-*co*-AAc+4APBA etalon's response to solution pH changes. 55

Figure 2-7. pH response of pNIPAm-*co*-AAc-*co*-APBA terpolymer microgel and their devices. (a) DLS size measurement of microgel's response to pH, (b) etalon of terpolymer in response to solution pH. Shaded regions represent areas where the device is fully collapsed/swollen. Between the shaded regions are the linear response ranges of the device. (c) Reversibility of the terpolymer device and (d) independent pH-step cycling of the device in response to pH from 3–7 and from pH 7–12, followed by the reverse order and so forth 57

Figure 2-8. Kinetics of the response of pNIPAm-*co*-AAc etalon to decreasing pH (a) and increasing pH (b). Kinetics of the response of pNIPAm-*co*-AAc-*co*-APBA etalon to decreasing pH (c) and increasing pH (d). 59

Figure 2-9. pH response of pNIPAm-*co*-BAAc etalon to different salt concentrations and mixtures 61

Figure 2-10. (a) pH response of pNIPAm-*co*-BAAc etalon to different salt concentration mixtures (NaBr:NaCl) in a narrow pH range. (b) Reversibility of pH response of

pNIPAm-*co*-BAAc etalon to different salt mixture concentrations between pH 6 and 8..... 62

Figure 3-1. (a) Structure of etalon: (i) glass substrate, (ii) Cr/Au underlayer, (iii) microgel layer, (iv) Cr/Au overlayer. (b) A representative reflectance spectrum from a microgel-based etalon showing multiple peaks as a result of the order term "m" in Eq. 3-1..... 74

Figure 3-2. DIC images of (a) pNIPAm-*co*-AAc, (b) pNIPAm-*co*-MAAc, (c) pNIPAm-*co*-EAAc and (d) pNIPAm-*co*-BAAc microgels. 75

Figure 3-3. DLS measured diameter of (□) pure pNIPAm microgel, (O) pNIPAm-*co*-AAc microgel, (▽) pNIPAm-*co*-MAAc microgel, (△) pNIPAm-*co*-EAAc microgel and (◊) pNIPAm-*co*-BAAc microgel..... 76

Figure 3-4. DLS microgel diameter as a function of solution temperature at the indicated solution pH. (a) pNIPAm, (b) pNIPAm-*co*-MAAc, (c) pNIPAm-*co*-EAAc and (d) pNIPAm-*co*-BAAc at (☐) pH 3 and (O) pH 10, respectively..... 77

Figure 3-5. Kinetics of the response of (a) pNIPAm-*co*-BAAc, (b) pNIPAm-*co*-EAAc, (c) pNIPAm-*co*-MAAc and (d) pNIPAm-*co*-AAc etalons to solution pH changes.. 79

Figure 3-6. (a) Shifts in the reflectance peak position as a function of pH for the pNIPAm-*co*-BAAc etalons: (□) increasing pH and (O) decreasing pH. (b) The repeatability of the pNIPAm-*co*-BAAc etalon's response to solution pH..... 81

Figure 3-7. (a) Reflectance spectra from pNIPAm-*co*-BAAc etalons at the indicated temperatures at pH 3. (b) Peak position as a function of temperature. (c) Temperature cycling of pNIPAm-*co*-BAAc etalons between 25 °C to 41 °C at pH 3.

(d) Temperature response of a pNIPAm-*co*-BAAc etalon at (O) pH 10 (below the pK_a of BAAc) and (□) pH 3 (above its pK_a). 83

Figure 3-8. DLS microgel diameter as a function of temperature for (a) pNIPAm, (b) pNIPAm-*co*-AAc, (c) pNIPAm-*co*-MAAc, (d) pNIPAm-*co*-EAAc and (e) pNIPAm-*co*-BAAc microgels.. 84

Figure 3-9. Temperature response kinetics for (a) pNIPAm-*co*-BAAc and (b) pNIPAm-*co*-AAc etalons..... 86

Figure 3-10. FTIR spectra of pNIPAm-*co*-BAAc, pNIPAm-*co*-EAAc, pNIPAm-*co*-MAAc and pNIPAm-*co*-AAc 87

Figure 3-11. Potentiometric and conductometric titration of (a) pNIPAm-*co*-BAAc, (b) pNIPAm-*co*-EAAc, (c) pNIPAm-*co*-MAAc and (d) pNIPAm-*co*-AAc 88

Figure 4-1. A photograph of microgel-based aggregates in solutions of the indicated pH values. 99

Figure 4-2. Scanning electron microscope (SEM) images of samples recovered after the two sets of microgels were mixed in solutions of pH (a) 2; (b) 5; (c) 7; (d) 12. 100

Figure 4-3. SEM images showing the relative aggregate sizes of the microgels at different pH values.. 100

Figure 4-4. Photographs of methylene blue (MB) solutions at the indicated pH (a) before and (b) after addition and aggregation of the individual sets of microgels. 102

Figure 4-5. A control experiment with (a) only pNIPAm-*co*-DMAPMA microgels and (b) pNIPAm-*co*-AAc microgels at different pH values..... 103

Figure 4-6**.** UV-Vis absorption spectrum for methylene blue at pH 5 (red) and pH 10 (black). 104

Figure 4-7. (a) UV-Vis absorbance values from MB solutions at the indicated pH (□) before and (○) after microgel aggregation (and removal from solution). Photographs of the remaining solutions at the indicated pH (b) before and (c) after microgel aggregation. 105

Figure 4-8. Absorbance values for MB solutions at the indicated pH values. (A) MB solutions before addition of microgels, (B) after microgel aggregation and (C) after addition of just the pNIPAm-*co*-AAc microgels alone and centrifugation to remove the microgels from solution 106

Figure 4-9. Zeta potential measurements of individual pNIPAm-*co*-AAc (black) and pNIPAm-*co*-DMAPMA (blue) microgels at different pH values..... 107

Figure 4-10. Drug release profiles in (□) pH=2 and (○) pH=10 solutions for aggregates formed at (a) pH=5 and (b) pH=7 solutions. 109

Figure 4-11. A photograph of the release of MB from the aggregates at (a) pH and at (b) pH 10..... 110

Figure 4-12. Triggered small molecule release from the microgel-based aggregates upon changing the solution pH from 10 to 2 at the time indicated by the shaded region.111

Figure 5-1. Calibration curves for (a) Cd^{2+} (226.502 nm) and (b) Pb^{2+} (220.353 nm) used to quantify the amount of Cd^{2+} and Pb^{2+} sorbed by the microgels. 120

Figure 5-2. Influence of pH and temperature on 10 ppm lead uptake by 2000 ppm pNIPAm-*co*-BAAc (10Bu-10B) 122

Figure 5-3. Contact time comparison on removal efficiency of (a) Cd^{2+} and (b) Pb^{2+} ions.. 122

Figure 5-4. Effect of monomer composition on uptake of (a) Cd^{2+} and (b) Pb^{2+} ions. A: acrylic acid and B: BIS (numbers preceding letters represent amount in %) 124

Figure 5-5. Effect of crosslinking density on removal efficiency of (a) Cd^{2+} and (b) Pb^{2+} ions. A: acrylic acid and B: BIS (numbers preceding letters represent amount in %).. 125

Figure 5-6. A Comparison of the removal efficiency of three comonomers with the same amount (10%) and the same crosslinking density (10%). A: acrylic acid, M: methacrylic acid and Bu: 2-butylacyrlic acid 126

Figure 5-7. A scanning electron micrograph of different monomer and crosslinking density of pNIPAm-*co*-MAAc microgels. (a) 10M-10B (b) 1M-10B (c) 10M-5B (d) 10M-1B. M: methacrylic acid and B: BIS (numbers preceding letters represent amount in %). 128

Figure 5-8. FTIR spectra of pNIPAm-*co*-AAc microgel (Gel), pNIPAm-*co*-AAc microgel sorbed Cd^{2+} (Gel-Cd) and pNIPAm-*co*-AAc microgel sorbed Pb^{2+} (Gel-Pb)..... 129

Figure 6-1. TEM images of (a) microgel, (b) zero valent iron and (c) microgel stabilized zero valent iron 140

Figure 6-2. Helium ion micrographs of pristine (a) ZVI, with a scale bar of 100 nm, (b) microgel stabilized ZVI (ZVI–MG), with a scale bar of 200 nm and (c) ZVI–MG after Se uptake, with a scale bar of 500 nm, operating on a helium ion beam with an accelerated voltage of 34 kV and a beam current of 0.1–1.1 pA. 141

Figure 6-3. (a) DSC measurements of MG and ZVI, (b) FTIR spectra of ZVI, MG and ZVI–MG and (c) XRD spectra of MG and ZVI–MG. 143

Figure 6-4. XPS survey scans of (a) blank ZVI–MG and (b) spent ZVI–MG after Se sorption. XPS focus scans for Se in (c) blank ZVI–MG and (d) after Se sorption. Note the scales in both (c) and (d) 144

Figure 6-5. XPS focus scans for Fe peaks in (a) blank ZVI–MG and (b) spent ZVI–MG after Se sorption. XPS high resolution scans for C peaks in (c) blank ZVI–MG and (d) spent ZVI–MG after Se sorption. 145

Figure 6-6. Zeta potential measurements of ZVI to estimate the point of zero charge. . 146

Figure 6-7. (a) Se uptake studies on only BAAc-based microgels, (b) kinetics of Se uptake by ZVI (c) uptake efficiency for ZVI, degassed ZVI and ZVI–MG using ~40 mg sorbent loaded with 10 ppm Se for 30 min and (d) ZVI–MG sorbent dose studies using 10 ppm Se 148

Figure 6-8. A calibration curve for Se (VI) (196.026 nm) used for the quantification of Se uptake by ZVI-based particles. 149

Figure A-1. Synthesis of 4-acrylamidobenzo-18-crwon-6 (4-AB18C6). The synthesized 4-AB18C6 was used to synthesize microgels similarly to that shown in previous Chapters. 170

Figure A-2. 4'-AB18C6 based microgel- based etalons' response to different metal ions 170

Figure B-1. (a) Experimental procedure for casting ion selective membrane on top of etalon, (b) chemical structure of Aliquat 336, the ionophore used in this study and (c) schematic representation of Cr ion passage through the ion channels of the membrane. 171

Figure B-2. Etalon response to different heavy metals with or without Cr ion selective membrane. 172

Figure B-3. A comparison of the membrane-etalon response to all metal ions, with Cr ions showing the highest response. 173

Figure C-1. PH effect and sorbent dose studies. (a) Effect of pH on stability of 4 ppm CV at 1 h contact time, sorbent dose studies with 20 ppm of CV for (b) OSPC, (c) Kaolin and (d) Bentonite 176

Figure C-2. A contact time study for removal of CV by OSPC at less contact time (a) and higher contact time (b). Red cycles in (a) represent control samples without the OSPC and the black squares are the data after CV contact with OSPC. 176

Figure C-3. (a) Calibration curve for CV used to calculate the removal efficiency of CV by the OSPC, (b) adsorption of CV by OSPC in the form of adsorbed amount (q_e) as a function of initial sorbate concentration (C_0) 177

Figure C-4. Adsorption isotherms for (a) OSPC, (b) Kaolin and (c) Bentonite in their uptake of CV.. 177

Figure C-5. (a,d) Langmuir, (b,e) Freundlich and (c,f) Temkin isotherms to fit the adsorption of CV data by (a-c) OSPC and (d-f) Kaolin 178

Figure C-6. Kinetics study of the adsorption of CV by the OSPC. (a) Pseudo first order kinetics and (b) Pseudo second order kinetics 179

Figure C-7. Calibration curves for the Cd^{2+} and Pb^{2+} used to quantify the uptake efficiency of Cd^{2+} and Pb^{2+} by the OSPC. 181

Figure C-8. Concentrations of ions before (black) and after removal by OSPC (red stripes) for (a) Cd^{2+} and (b) Pb^{2+} 181

Figure D-1. (a) UV-Vis spectrum of CV showing the removal efficiency of different sorbent dose at 150 min of contact, (b) UV-Vis absorbance showing the uptake of CV over time at different sorbent dose, (c) absorbance showing the removal of CV by different composition of sorbents and (d) photographs of equilibrium concentrations of CV after 150 min contact time with 20 mg sorbent dose. C represents OSPC and B represents BIS 183

Figure D-2. SEM images of (a) 0C-6B and (b) 6C-0B. Figure (a) shows a dense packed structure of the sorbents, with a possible blocking of some sorption sites. Figure (b) shows honey-comb-like structures, with void spaces that can enhance removal of CV. 184

Figure E-1. Cigarette butt removal of CV from aqueous solution. (a) Sorbent dose effect on uptake of CV, (b) photographs showing uptake of initial 4 ppm CV after 30 min of contact time, (c) adsorption capacity studies shown as a plot of percent uptake as a function of initial concentrations of CV and (d) photograph showing the uptake capacity 186

Figure E-2. (a) Uptake of MB as a function of initial concentration using 0.2 g of sorbent. As seen here, even at higher dose of sorbate, there is still a higher uptake. Chemical structures of (b) MB and (c) CV. 187

Figure F-1. Ionic strength response of p(NIPAm-*co*-AAc) microgel etalon at pH 6.5 at (a) low concentrations and (b) high concentrations. 189

Figure F-2. Particle size dependence on ionic strength of p(NIPAm-*co*-AAc) microgel at pH 6.5. Particle size measurement was done with dynamic light scattering. 190

List of Symbols

a	Gel size
C_i^g	Concentration of mobile ions of species *i* in the gel
C_i^s	Mobile ion concentration of species *i* in the surrounding medium
D	Diffusion coefficient
d	Distance between the two Au mirrors
m	Order of a reflected peak
N	Average number of segments in the network chain
n	Refractive index of the dielectric medium
R	Universal gas constant
T	Kelvin temperature
V_s	Molar volume of solvent
ΔG	Gibbs free energy
θ	Angle of incident light
λ	Wavelength of reflection
π	Osmotic pressure
τ	Gel swelling time
v_2	Volume fraction of polymer in the hydrogel
v_2^0	Volume fraction of polymer just after its synthesis and before solvation
χ	Polymer–solvent interaction parameter

List of Abbreviations

4APBA	4-Aminophenylboronic acid
4VP	4-Vinylpyridine
5-FU	5-Fluorouracil
AAc	Acrylic acid
AAm	Acrylamide
APBA	3-(Acrylamido)phenylboronic acid
APS	Ammonium persulfate
BAAc	2-Butylacrylic acid
BIS	*N*, *N'*-Methylene(bisacrylamide)
CV	Crystal violet
DFT	Density functional theory
DI	Deionized
DMAPMA	N-[3-(Dimethylamino)propyl]methacrylamide
EAAc	2-Ethylacrylic acid
EDC	1-Ethyl-3-(3-dimethylaminopropyl)carbodiimide
IS	Ionic strength
LCST	Lower critical solution temperature
MA	Methyl acrylate
MAAc	Methacrylic acid
MB	Methylene blue

MIM	Macroinimer
NIPAm	*N*-isopropylacrylamide
OSPC	Oil sands processed affected clay
pAMPS	Poly(2-acrylamido-2-methylpropane sulfonic acid)
pAPTMACl	Poly(3-acrylamidopropyl)trimethylammonium chloride
pDMAEMA	Poly[2-(dimethylamino)ethyl methacrylate]
pMVE	Poly (methyl vinyl ether)
pNIPAm	Poly (N-isopropylacrylamide)
pNIPAm-*co*-AAc	Poly (N-isopropylacrylamide)-*co*-acrylic acid
pNIPAm-*co*-DMAPMA	Poly (N-isopropylacrylamide)-*co*- N-[3-(Dimethylamino)propyl]methacrylamide
pOEGMAs	Poly (oligo (ethylene glycol) methacrylates)
pSSA	Poly(4-styrenesulfonic acid)
pVCL	Poly (*N*-vinyl caprolactam)
pVP	Poly (N-vinyl pyrrolidone)
RMP	Rounds Per Minute
SEM	Scanning electron microscopy
TEM	Transmission electron microscopy
UCST	Upper critical solution temperature
VPTT	Volume phase transition temperature
XPS	X-ray photoelectron spectroscopy
ZVI	Zero valent iron

Chapter 1

General Introduction to Hydrogels and Microgels

Hydrogels are defined as three dimensional crosslinked networks of polymeric chains joined together via chemical and/or physical bonds. The hydrogels swell in water up to their thermodynamic equilibrium swelling state. The use of hydrogels has become widespread in numerous applications for over 50 years. Even though Paul Flory set the basic theories of hydrogels, they had been prepared long before the establishment of his original theoretical treatment of the hydrogels. Flory was awarded the Nobel Prize in 1974 for setting the main framework of analysis of gels using his thermodynamic theories, statistical mechanical analysis, and the first analysis of critical miscibility characteristics of hydrogels. Since his work, there have been variations in the basic definition of hydrogels and deviations from the thermodynamic and structural equations that characterized their performance.[1] Hydrogels are considerably "soft" mainly due to their hydrophilic nature, which permits uptake of water that is sometimes up to about 90% of the hydrogel's mass; they have found their way into biomedical applications. More importantly, hydrogels become valuable when used as "smart" materials, which are able to respond in a defined manner to their environment. Hydrogel particles (microgels) have attracted considerable attention as well because of their smaller dimensions. The response rate of hydrogels to environmental stimuli is inversely proportional to the size of the hydrogels.[2] Therefore, microgels (smaller dimensions compared to bulk hydrogels)

have become indispensable in areas where fast response rates to environmental stimuli are desired.[2-7]

1.1 General Hydrogel/Microgel Theory

1.1.1 Physical Structure

Hydrogels are composed of hydrophilic polymers that are crosslinked into insoluble, yet hydrophilic structures. The crosslinks that form the hydrogel can be strong (via covalent bonds), or weak (via hydrogen bonds, ionic bonds, entanglement, and/or other dipolar interactions). The crosslinked structure can be generated by polymerization in the presence of an appropriate crosslinker. A common crosslinker used for this purpose is *N,N'*-methylenebisacrylamide (BIS), and is the primary crosslinker used in this dissertation. In other cases, linear polymers can be crosslinked post-polymerization to form hydrogels; glutaraldehyde has been used widely for this purpose.[8,9] Regardless of when the crosslinking is done, the hydrogels formed can take many forms. These different forms reflect the wide range of monomers that can make up the hydrogel structure. Either natural monomers, such as alginate and starch, or synthetic monomers, such as *N*-isopropylacrylamide (NIPAm), acrylamide or acrylic acid, can be used. The final characteristic of the hydrogel is a function of the monomer composition and their ratios, the polymerization synthesis procedure and the solvent used.[10] Based on the monomers incorporated, the final hydrogel can have a variety of charged states/densities: neutral, cationic, anionic or zwitterionic. The final charge of hydrogels is strongly pH

dependent, much like other macromolecules, such as proteins or nucleic acids, reflecting the charge state or protonation state of the incorporated comonomer.

The primary monomer used in this dissertation was NIPAm, whose polymeric form is thermoresponsive and has been copolymerized with other functional comonomers to impart a different charge state or functionality to the whole gel. To impart anionic properties to the microgel, carboxylic acid comonomers or pendant groups are used. Specifically, acrylic acid (AAc), methacrylic acid (MAAc), ethylacrylic acid (EAAc) and butylacrylic acid (BAAc) were used to study the different functionality that was imparted to the microgel in response to the pH of the solution. Meanwhile, amine containing pendant groups or comonomers are used to impart cationic properties to the microgel. 4-Vinylpyridine(4VP) and *N*-[3-(dimethylamino)propyl] methacrylamide (DMAPMA) were used to achieve this. Other amine containing pendant groups have been used by other researchers to impart cationic characteristics to the entire gel.[11,12]

1.1.2 Equilibrium Swelling Theory

The equilibrium swelling state of a polymer network immersed in a suitable solvent is obtained when a thermodynamic equilibrium exists between the solvent inside the network and outside the polymer network. The Flory–Rehner (F–R) theory,[13] which assumes that an equilibrium for a hydrogel is reached through a balance of enthalpic mixing and elastic forces, is appropriate for the quantitative analysis of nonionic hydrogel systems. The F–R theory assumes that the enthalpy of mixing promotes swelling while the elastic forces are imposed by the crosslinked chains of the hydrogels, which promote

contraction. Hence, the balance of these two forces leads to the equilibrium swelling and contraction of the hydrogels. The basis of the F–R theory is:

$$\Delta G_{total} = \Delta G_{elastic} + \Delta G_{mixing} \qquad (1\text{-}1)$$

where ΔG is the Gibbs free energy. However, the direct application of the F–R theory to ionic hydrogels is incorrect because there are additional forces that shift the hydrogels' swelling equilibrium. These forces are those from ionic interactions that exist within the hydrogels and in the surrounding medium. To compensate for this additional ionic term, ΔG_{ionic} is introduced:

$$\Delta G_{total} = \Delta G_{elastic} + \Delta G_{mixing} + \Delta G_{ionic} \quad (1\text{-}2)$$

This can be written in terms of the osmotic pressure (π) of the gel as:

$$\pi = \pi_{el} + \pi_{mix} + \pi_{ion} \qquad (1\text{-}3)$$

which determines whether the gel swells or shrinks. The π_{mix} in Eq. 1-3 represents the tendency of mixing the polymer and the solvent, π_{el} denotes the elastic response as a result of crosslinking of the gel, and π_{ion} represents the osmotic pressure as a result of the difference in the ionic concentrations between the swollen gel and its surrounding medium. According to the Flory–Huggins theory, the osmotic pressure due to mixing (π_{mix}) is:

$$\pi_{mix} = -\frac{RT}{V_s}\{ln(1-\upsilon_2) + \upsilon_2 + \chi\upsilon_2^2\} \qquad (1\text{-}4)$$

where V_s is the molar volume of the solvent, υ_2 is the volume fraction of the polymer in the hydrogel, χ is the polymer-solvent interaction parameter (also called the Flory–Huggins interaction parameter), R is the universal gas constant and T is the Kelvin temperature. According to the simplest model that describes the behavior of gels, the elastic contribution π_{el} to the swelling pressure is:

$$\pi_{el} = -\frac{RT}{V_s} N^{-1} (v_2^{1/3} (v_2^0)^{2/3} - {v_2}/{2}) \qquad (1\text{-}5)$$

where N is the average number of segments in the network chain, v_2^0 is the volume fraction of polymer just after its synthesis and before solvation and π_{ion} is the ionic contribution from the gel to the swelling pressure due to the difference in concentration of counter ions between the swollen gel and its surrounding medium. While the ideal Donnan theory simplifies the ionic contribution π_{ion} as the pressure difference of mobile ions in and out of the gel, a complete description of the ionic contribution will take into account the ion-ion, ion-solvent and ion-polymer interactions:

$$\pi_{ion} = RT\left(C_i^g - C_i^s\right) \qquad (1\text{-}6)$$

where C_i^g is the concentration of mobile ions of species i in the gel, and C_i^s is the mobile ion concentration of species i in the surrounding medium.

According to the Tanaka–Fillmore (T–F) theory[2] of gel swelling, the time taken for swelling (τ) is proportional to the square of the gel size (a) and inversely proportional to the diffusion coefficient (D):

$$\tau = \frac{a^2}{D} \qquad (1\text{-}7)$$

Thus, the swelling response of gels depends on the size and shape of the gels. According to Eq. 1-7, since it is almost impossible to increase the value of D by a factor $\geq 10^2$, the only way to achieve a faster response is to reduce the size of the gel. Microgels, which are a colloidally stable crosslinked network of hydrogel particles, with dimensions ranging from ~0.1–10 μm, show a faster response than slab/macroscopic gels. The response time is of the order of seconds compared to hours or even days for the slab gels to reach swelling equilibrium in response to changes in their chemical environment.

Mainly microgels were used in this dissertation. Chapter 3 compares the kinetic response of different pH responsive microgels differing in their pendant alkyl chain length.

1.2 Stimuli Responsive Polymers

Stimuli responsive polymers (or simply responsive polymers) that respond to their environment by undergoing changes in chemical and/or physical properties have been known for a number of decades. Specifically, responsive polymers have been developed, which respond to changes in solution pH,[14-18] temperature,[18-23] ionic strength (IS)[24,25] and the application of an electric field,[26] magnetic field[27] and/or light.[19,28] Only temperature and pH responsive polymers will be discussed below because they form the foundation of this thesis. Readers are referred to other resources for an in-depth knowledge of other stimuli responsive polymers.[29,30]

1.2.1 Temperature Responsive Polymers

Temperature responsive (thermoresponsive) polymers fall under two categories: negative and positive thermoresponsive systems. These systems are characterized by having a lower critical solution temperature (LCST) or an upper critical solution temperature (UCST), respectively. Of the various stimuli responsive polymers, those that respond to changes in temperature have been studied most extensively. Among these, poly (*N*-isopropylacrylamide) (pNIPAm) has emerged as the most popular one over the past few decades.[23] Since its first discovery in 1968,[31] pNIPAm has been used for numerous applications including sensing and biosensing,[32,33] drug delivery,[34-36] tissue engineering,[37] anti-fouling coatings[38] and "smart" optical systems.[21] The widespread use

is due partially to pNIPAm's volume phase transition temperature (VPTT) at 32 ºC, which is near the range of physiological relevance. Specifically, below this temperature, pNIPAm exists as a random coil (extended state) and transitions into a globular conformation (collapsed state) above 32 ºC. Furthermore, pNIPAm is "hydrated" below the VPTT and "dehydrated" above the VPTT; this transition is fully reversible. Figure 1-1 lists examples of some common temperature responsive polymers.

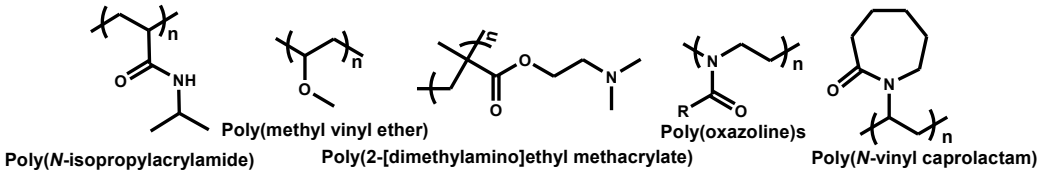

Figure 1-1. Some common temperature responsive polymers

1.2.1.1 Swelling Theory

The physical stimulus that has been studied most widely is temperature. Gels swell/deswell near a critical temperature, referred to as the transition temperature. There are two classes of transition temperatures that gels undergo: the lower critical solution temperature (LCST) and the upper critical solution temperature (UCST).

The Lower Critical Solution Temperature (LCST) is more encountered frequently than the UCST. When dissolved polymers, like pNIPAm, are heated above their LCST, their gelation point will show aqueous insolubility where aggregation of desolvated gels can occur.[39] As pNIPAm has both hydrophobic isopropyl groups and hydrophilic amide groups, the LCST response of pNIPAm and other alkyl substituted acrylamides is due to the balance of these hydrophobic and hydrophilic groups as well as the entropic and

enthalpic contributions required to solvate these groups. As the temperature is increased above the LCST, the interactions among the isopropyl groups of pNIPAm increase. In a study on the temperature dependence of the swelling/deswelling behavior of *N*-*N'*-alkyl substituted acrylamides in water,[40] a slight positive swelling response from only poly (acrylamide) was observed due to the lack of the hydrophobic amide alkyl group. In such a case, the only contribution to the swelling behavior is the hydrogen bonding characteristics. However, pNIPAm and poly (*N,N'*-diethyl acrylamide), the only two polymers studied with the most hydrophobic *N*-alkyl substituted acrylamides, exhibited a critical phase shift. Another major conclusion from their study is the entropic contribution to the χ parameter. To hydrate the hydrophobic isopropyl segments, a significant formation of water cages around them is required. Thus, the polymer is hydrated by the balance between the water cages and the insoluble hydrophobic backbone in water. There is an entropic cost to the water cage formation. This cost is balanced by the formation of hydrogen bonds by the amide groups. Increasing the temperature further increases this entropic cost, as seen in Figure 1-2, where the entropic cost reaches a maximum at the LCST. Then, the system is forced to react to compensate for this entropic cost by expelling water from the gel, leading to an eventual collapse of the gel. Other polymers that exhibit LCST characteristics in water include poly[2-(dimethylamino)ethyl methacrylate] (pDMAEMA),[41] poly (methyl vinyl ether) (pMVE),[42] poly (2-oxazoline)s,[43] poly (*N*-vinyl caprolactam) (pVCL),[44] poly (oligo (ethylene glycol) methacrylates) (pOEGMAs)[45] and their analogues.

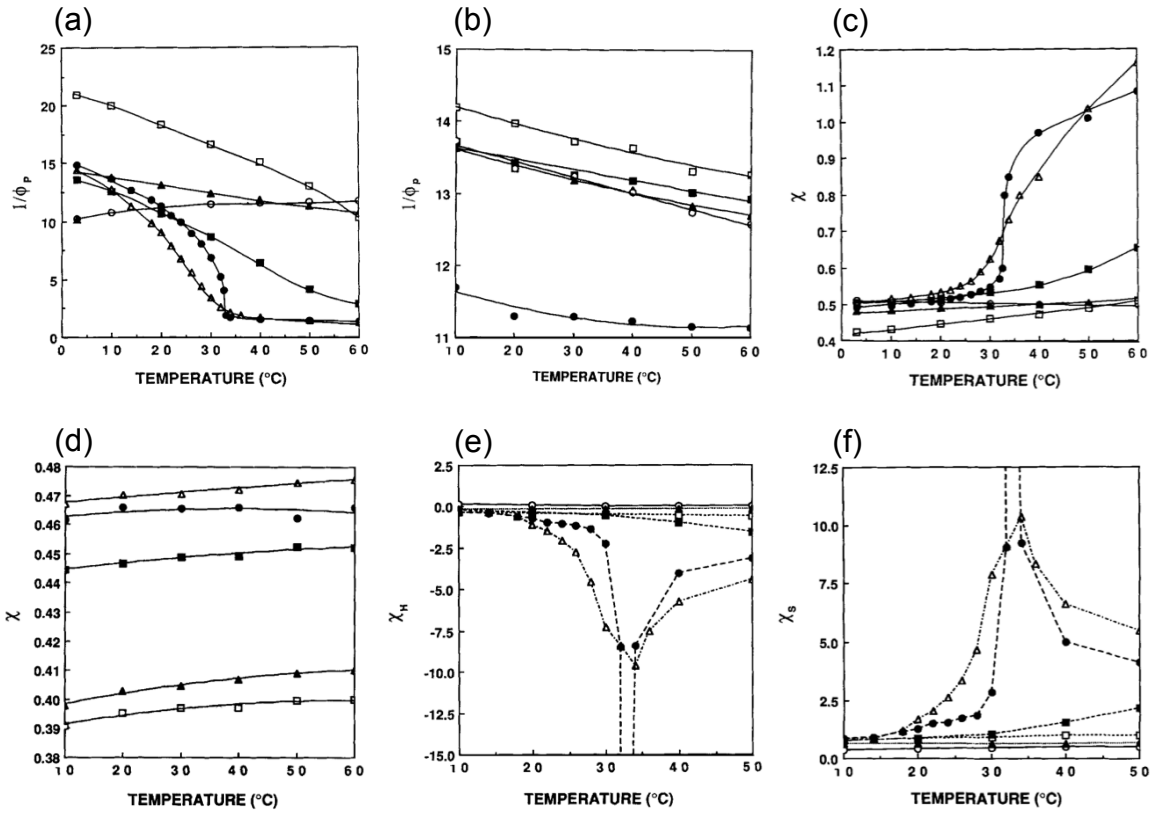

Figure 1-2. Temperature dependence of crosslinked poly (N,N'-alkyl substituted acrylamides). Equilibrium swelling in: (a) water and (b) ethanol as a function of temperature. Polymer interaction parameter (χ) in: (c) water and (d) ethanol. (e) Enthalpic contribution to the polymer interaction parameter in water (χ_H). (f) Entropic contribution to the polymer interaction parameter in water (χ_S). (o) poly(acrylamide), (▲) poly(dimethyl acrylamide), (□) poly(ethyl acrylamide), (■) poly(acryloylpyrolidine), (**Δ**) poly(diethylacrylamide), (●) poly(*N*-isoproylacrylamide). Reprinted with permission from Ref.[40] Copyright 1990, John Wiley & Sons, Inc.

The Upper Critical Solution Temperature (UCST). UCST systems are less common. The driving force for the UCST behavior is associated mostly with hydrogen bonding, (for example between acrylic acid (AAc) and acrylamide (AAm) groups in the case of an interpenetrating network composed of AAc and AAm), forcing the gel to collapse at low temperatures. This effect is described as the "zipper" effect. At high temperatures, the enthalpic gains from these hydrogen bonds are far less than the entropic loss of water separation from the polymer phase. This critical temperature "unzips" the network allowing the gel to be hydrated, leading to swelling at higher temperatures. Contributions from ionic strength and pH play a significant role in the swelling behavior of UCST polymers, and thus, limit their use *in vivo*.

1.2.2 pH Responsive Polymers

pH responsive polymers respond to changes in environmental pH by undergoing changes in their conformation, surface activity, configuration or solubility. Typically, changes in the environmental pH results in swelling/deswelling of the polymer. Measurement of pH is essential in both the environment and in the human body, and most biological processes are pH dependent.[46] For example, protein synthesis, DNA and RNA synthesis, cell cycle control and the activity of other key enzymes and metabolic processes are regulated by pH.[47] Therefore, pH measurements have been of particular interest in biomedical applications, primarily because of the different pH ranges (either as in normal function or in disease state) in different parts of the body. Variations in pH exist in different parts of the body such as in blood vessels, extracellular tumor environments, inflamed tissue wounds, intracellular vesicles and the gastrointestinal tract;

these different pH environments can trigger pH response. pH responsive hydrogels (or microgels) have been used extensively in drug delivery applications, of which one is described in Chapter 4.

Structurally, pH-responsive polymers can be linear, branched or crosslinked into a network. Their responses to solution conditions, such as pH, differ as well as their structural (re)organization, which takes different shapes depending on their structures. For example, a pH change can cause protonation/deprotonation of functional groups in polymer chains, while in other cases, a pH change can cause precipitation, flocculation and chain collapse-extension, especially for homopolymers. The same pH change could result in self-assembly, as in the formation of vesicles, gels, micelles, unimers, swelling and deswelling.[48] Architectures such as block (co)polymers, branched (co)polymers and star (co)polymers with pH responsive block(s) respond in some defined ways to solution pH. The changes observed in polymers of different architectures by solution pH change are shown in Figure 1-3.

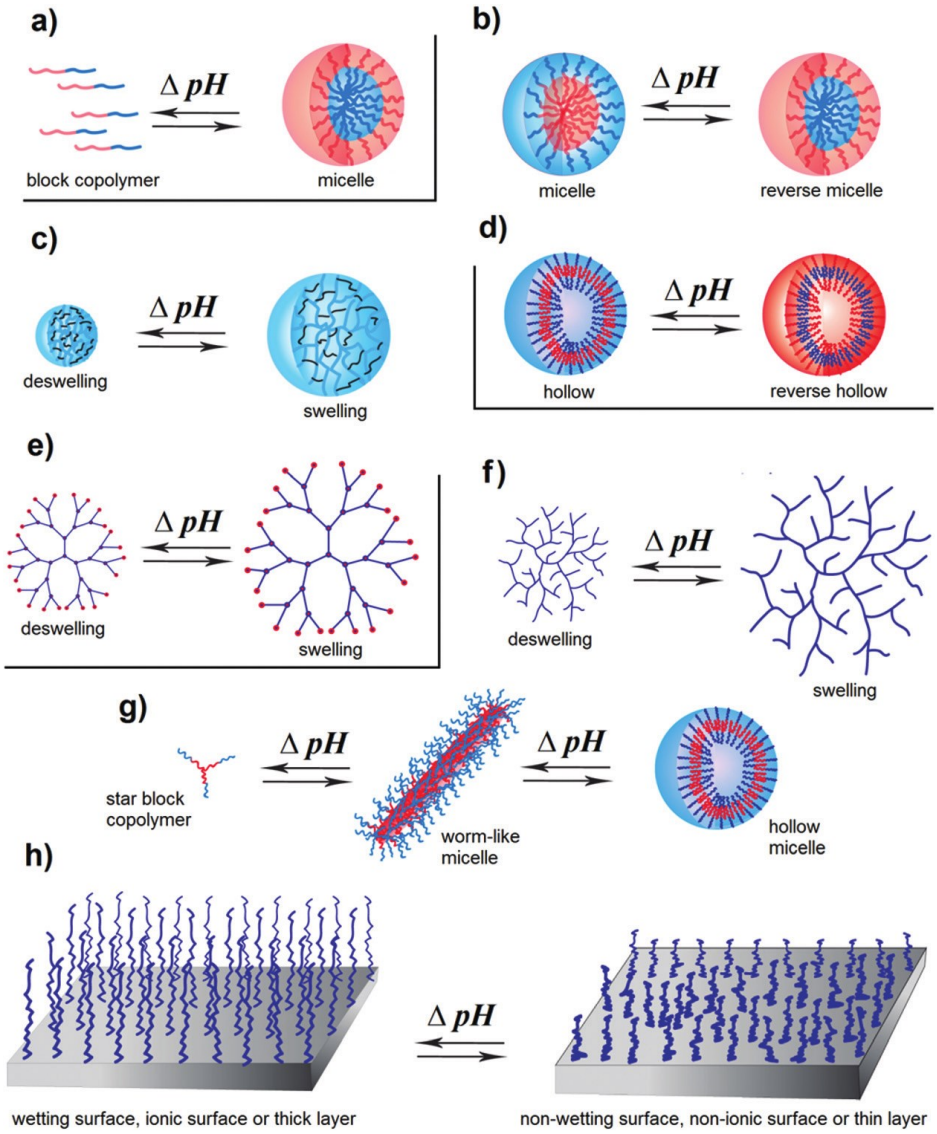

Figure 1-3. pH-Responsive polymers of different architectures: (a) unimer–micelle, (b) micelle–reverse micelle, (c) nanogels or microgels, (d) hollow–reverse hollow, (e) dendrimer, (f) hyper–branched, (g) micelle morphology changes (from worm–like to hollow) and (h) polymer brushes. Adapted with permission from Ref.[48] Copyright 2017, The Royal Society of Chemistry.

1.2.2.1 Polymer Composition and Swelling Behavior

The incorporation of ionizable groups into the polymer (hydrogel or microgel) synthesis imparts pH responsiveness to the gel. When these gels are exposed to an aqueous solution of the appropriate pH and ionic strength, the pendant ionizable groups ionize and cause a buildup of fixed charges along the polymer backbone. These fixed charges generate Coulombic repulsive forces, which control the swelling/deswelling of the gel, as well as an increased osmotic pressure due to the build up of counter ions.[49] The mechanism of hydrogel swelling involves: (1) water diffusion into the hydrogel network, (2) polymer chain loosening due to hydration, and (3) hydrogel network expansion upon relaxation of polymer chains.[50] Three categories of water molecule association can be identified: (i) primary bound water, which is due to the attraction of water molecules towards the polar and hydrophilic groups of the hydrogels; (ii) secondary bound water, which is formed as a result of swelling contributed from the primary bound water, which interacts with the exposed hydrophobic groups; and (iii) free water, which is the additional water that moves into the hydrogel under osmotic pressure. At this point, the hydrogel is said to have reached its equilibrium, where there is a balance between the elastic forces of the chains and osmotic pressure, as explained by the Flory and Rehner theory.[50] pH responsive hydrogels can be categorized as anionic or cationic, differing in their ionization state and swelling characteristics.

Hydrogel networks containing anionic pendant groups such as AAc, are ionized in a solution of pH above their acid dissociation constant (pK_a). As an example, AAc, one of the most common anionic comonomers used, has a pK_a of 4.25 and in a solution of pH > 4.25, the deprotonated state of AAc dominates. The ionized state results in an

electrostatic negative charge repulsion and increased in osmotic pressure, with a concomitant swollen gel at a pH > pK_a. At a lower pH, however, the AAc moieties of the gel become protonated (and neutralized), resulting in deswelling of the gel. The same phenomenon holds for other anionic gels with swollen state at a pH > pK_a of the ionizable groups in the gel and a deswollen state at a pH < pK_a of the anionic groups. Anionic monomers can be of carboxylic acid, phosphonic acid, sulfonic acid, or boronic acid groups.

Carboxylic acid groups. Monomers containing weak carboxylic acid groups have a dominant carboxylate groups above the pK_a of the acid, resulting in anionic polyelectrolytes. The carboxylic acid groups accept protons at low pH and become neutral macromolecules. Acrylic acid, methacrylic, 2-ethylacrylic acid, and 2-butyl acrylic acid are all carboxylic acid based monomers that have been studied in this work.

Phosphonic acid groups. (Meth)acrylate monomers with phosphorous containing groups have been used widely in the synthesis of hydrogels, which swell under conditions of high pH, due to deprotonation.[51]

Sulfonic acid groups. Polymers containing sulfonic acid groups are good candidates for preparing hydrogels as the hydrogels swell significantly at high pH conditions above the pK_a of the acidic group in the hydrogel. The most widely used polymers containing sulfonic acid groups are poly(2-acrylamido-2-methylpropane sulfonic acid) (pAMPS) and poly(4-styrenesulfonic acid) (pSSA).[52]

Boronic acid groups. Polymers containing boronic acid groups can be prepared either via a direct polymerization of acrylamidophenylboronic acid or via the post polymerization modification using the carbodiimide coupling method. These groups of polymers have found applications primarily in glucose sensing. Polymers containing boronic acid groups were prepared in Chapter 2 of this dissertation and showed rapid response rate to solution pH.

Cationic pendant groups, on the other hand, are more ionized at a pH lower than their pK_a, resulting in a swollen hydrogel network at a pH < pK_a. For example, DMAPMA, one of the cationic monomers used in this work, has a pK_a of 8.4 and is mainly positively charged at a pH < 8.4. The amine groups of DMAPMA are protonated, and a buildup of fixed positive charges and increased osmotic pressure results in swelling of the whole gel at pH < 8.4. The gels deswell in pH environments > 8.4, much like other cationic gels that are neutral and shrink at a pH > pK_a of the cationic pendant group.

Figure 1-4 shows the chemical structures of some cationic and anionic monomers. Often, the application at stake may necessitate the choice of one of these two types (anionic or cationic) or a combination of them with their appropriate composition. It is, therefore, possible to prepare pH responsive polymers with a pK_a ranging from ~1–14. This is described in detail in Chapter 2. In Chapter 4, a combination of anionic and cationic pendant groups were utilized to capture and release model drug molecules in a pH triggered fashion through their aggregation (drug loading) and disaggregation (drug release) at specific pH regions.

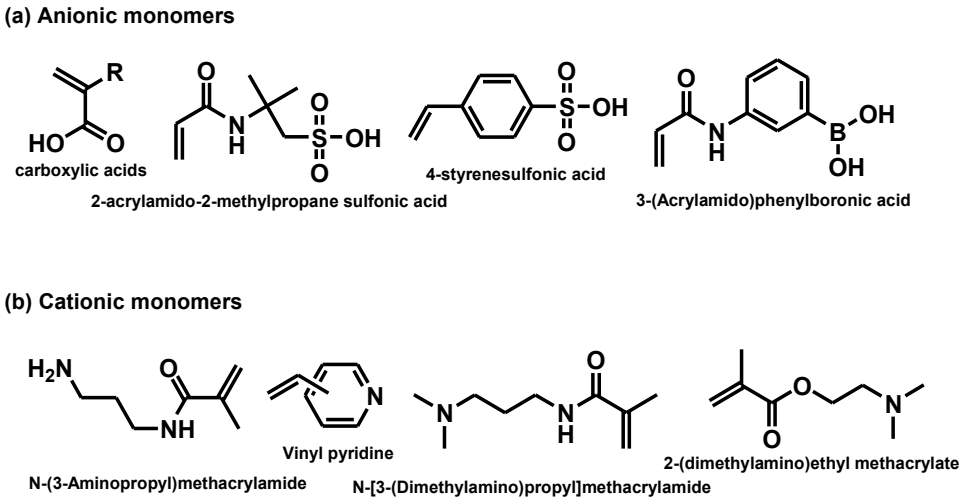

Figure 1-4. Some common pH responsive monomers

1.3 Applications of Stimuli Responsive Polymers

There are numerous applications of stimuli responsive polymers in the field of biology and medicine, for example, in sensors and biosensors,[32,33] actuators, tissue engineering,[37] antifouling coatings[38] and "smart" optical systems.[21] This section focuses on the applications of stimuli responsive polymers in environmental pH monitoring/sensing, controlled drug release, and environmental remediation.

1.3.1 pH Responsive Photonic Sensors

The importance of pH measurements cannot be overemphasized, particularly in the environment and in humans. Most biological processes are pH dependent.[46] The many roles that pH plays both in the environment and in the body have resulted in the development of different approaches to pH measurements. pH responsive polymers are widely used for pH sensing due to the flexibility of being able to tune the pH selectivity

range. Thus, the ability to incorporate different functional monomers of different pK_a into the main polymer backbone has made them attractive and versatile for pH sensing. The driving mechanism for most of the work presented here is dependent on the pH responsiveness of the system used.

The Serpe group fabricates 1–dimensional (1D) photonic materials that mimic the *Fabry Pérot* etalon. The construct, shown in Figure 1-5, is composed of a monolithic layer of microgels that are sandwiched between two thin metal (Au) layers. As light impinges on the etalon, the light resonates between the cavities with some light wavelengths being reflected while others are transmitted. A constructive and destructive interference results in a multipeak reflectance spectrum, according to the following equation:

$$\lambda = \frac{2nd\cos\theta}{m} \qquad (1\text{-}8)$$

where λ is the reflected wavelength at a given order (m) of reflection, n is the refractive index of the dielectric medium, d is the distance between the two Au mirrors, θ is the angle of incident light and m is the order of a "reflected" peak. The value of θ was maintained at 0; with a negligible change in n and for a particular order m, there is a direct relationship between λ and d. Therefore, any stimuli that can change the etalon's d–spacing will result in a color change; this is useful for sensing applications. Under different pH environments, swelling/deswelling of the gels results in a change in distance between the two Au mirrors, resulting in a blue/red shift. This phenomenon was used to characterize the pH sensors used in this thesis. Also, as temperature changes due to the hydrophilic/hydrophobic balance within the pNIPAm–based microgels, the gels swell/shrink, with a concomitant increase/decrease in the wavelength in lieu of a diameter

change. The ability to tune the Au mirror distance leading to a wavelength shift as a result of the swelling/shrinking behavior of the microgels has been used in a variety of applications by the Serpe group, such as for sensing and biosensing applications,[32,53] molecular weight determination,[54] electrochemical response[26] and controlled drug release.[34,55,56] This transduction mechanism has been exploited to develop microgel–based pH sensors that cover the entire pH range. The etalon only acts as a transducing element and does not offer any form of specificity, unless the same specificity is introduced to the device via some other means. Thus, any analyte (or recognition element) capable of causing a shrinking/swelling of the microgels will result in a detectable wavelength change. This is the major drawback to the use of the etalon; however, because of the ease of functionalization that comes with the synthesis of microgels, some form of specificity can be introduced. In the Appendix section, the use of the etalon as a transducer has been demonstrated. An ionophore–based membrane was fabricated on the surface of the etalon, which allows the selective passage of ions, while the etalon served as the transducer. This assembly was used for the selective detection of Cr (VI), specific to the ionophore present in the membrane. Ideally, the etalon responds to all cations, however, the ion-specific membrane provided a channel for the passage of certain ions of interest through a combination of different mechanisms, such as size, shape and charge match.

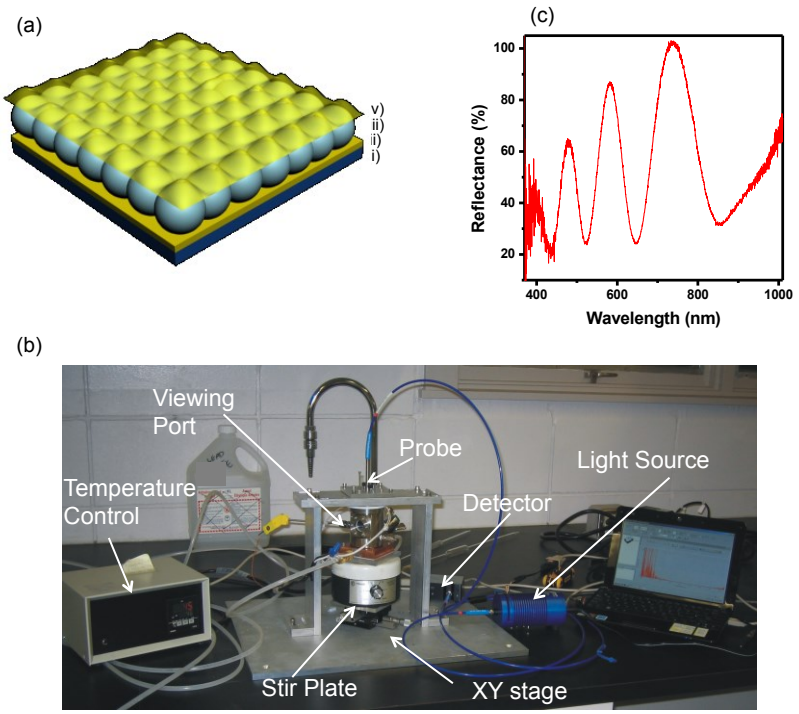

Figure 1-5. (a) Structure of a microgel–based etalon: (i) glass substrate, (ii) Cr/Au base layer (iii) monolithic microgel, (iv) Cr/Au over layer. (b) Instrumental setup for obtaining spectroscopic information from the device. (c) A characteristic reflectance spectrum obtained from the setup in (b). Figure (a) and (c) are reprinted with permission from Ref.[57] Copyright 2017, American Chemical Society. Figure (b) is reprinted with permission from Ref.[58] Copyright 2013, Springer.

1.3.2 pH Responsive Hydrogels for Controlled Drug Release

Controlled drug delivery systems have been developed to deliver model small molecules (therapeutic drugs) at predetermined rates and at predefined periods of time. Hydrogels have played a significant role in the development of smart drug delivery systems. These gels can respond reversibly in the presence of environmental stimuli to

release drugs in a controlled manner via structural changes of the hydrogel.[59] Importantly, hydrogels protect the drug from hostile environments, such as a low pH in the stomach.[60] Although different triggers, such as temperature, light,[61] pressure and pH,[59,60] have been used for the controlled release of drugs, the different pH environments that exist in the human body[62] (Table 1-1) have made the use of pH as a trigger for drug delivery applications more attractive.[50] The ability to load drugs into gels and trigger their release at a certain pH in a controlled manner has been demonstrated by many researchers. In some cases, the microgel can be designed to release the model drug only in acidic conditions, which is especially useful for cancer treatment applications due to the low pH of tumor sites. For example, the groups of Wu and Zhou[63] developed pH–responsive chitosan-based nanogels for the encapsulation and delivery of a model anti-cancer drug 5-fluorouracil (5-FU). The nanogels were prepared by physical interpenetration of chitosan chains into a nonlinear poly(ethylene glycol) (nonlinear PEG) chain network. At a tumour extracellular pH (6.5–7.2) the nanogels' surface charge transition from a neutral to a positive state where cell internalization is facilitated. Following the significantly increased acidity in the subcellular compartment (~5.0), the nanogels are protonated further, with swelling and a subsequent release of 5-FU. Gao *et al.* have used pH as triggers for releasing loaded model drug molecules from pNIPAm-microgels and their assemblies at both acidic and alkaline environments.[17,34,55,56]

In addition, the gels can be designed to release model drugs in the alkaline intestine region, as demonstrated by the work of Bai *et al*.,[64] with the release of insulin through pH and temperature responsive microgels. In the acidic condition of the stomach, the microgels are protonated and are in their collapsed state, keeping the insulin intact.

Insulin is only released within the alkaline intestines due to deprotonation and subsequent swelling of the microgels.

Table 1-1. pH in different tissues and cellular compartments. Adapted from Ref.[62]

Tissue/cellular compartment	pH
Blood	7.34–7.45
Colon	7.0–7.5
Tumor, extracellular	6.5–7.2
Early endosome	6.0–6.5
Inflamed tissue/wound	5.4–7.4
Late endosome	5.0–6.0
Upper small intestine	4.8–8.2
Lysosome	4.5–5.0
Vagina	3.8–4.5
Stomach	1.0–3.0

Finally, amphiphilic/zwitterionic microgel systems capable of delivering model therapeutic drugs of both polarities have been fabricated by the Georgiou group.[65,66] They used a microfluidic approach to fabricate pH responsive anionic amphiphilic microgels of hydrophilic AAc and hydrophobic non-ionic *n*-butylacrylate (BuA). The amphiphilic nature of the microgels offered the flexibility to encapsulate and release both hydrophilic Trypan Blue dye and hydrophobic Sudan I dye. Hydrophobic drugs were encapsulated at neutral pH and released in alkaline conditions, and the release mechanism was based on

pH-dependent swelling. Manipulating the hydrophobic content of the microgels can control the release rate also. Hydrophilic drugs, on the other hand, were loaded at a higher pH and released at neutral pH conditions.

In Chapter 4, we harnessed the ionization state of different microgels at varying pH values to load and release model drugs in a pH-controlled manner. As stated in previous sections, copolymerization of anionic monomers imparts their charge state to the whole microgel. The microgels are, therefore, more deprotonated at a pH greater than the corresponding pK_a of the ionizing group. Cationic monomers, on the other hand, are more protonated at a pH less than the pK_a of the ionizable group. When the right combinations of these groups are present in separate microgels, an interesting phenomenon occurs: The microgels aggregate at certain pH ranges that render both the anionic and cationic ionizable groups charged, and they form aggregates due to electrostatic interaction. This aggregation mechanism was used to load model drug molecules within these pH ranges. At pH values above and below the pK_a of both the anionic and cationic groups, the combined microgels disaggregate, and the loaded drugs are released. A detailed description of this phenomenon is presented in Chapter 4, demonstrating an application of pH responsive gels. Many other applications of pH responsive microgels for controlled drug release have been studied by our group[55,67-69] and others.[63-66,70-72]

1.3.3 Water Remediation Applications

One of the major issues facing the 21st century is the lack of access to clean drinking water. In addition to the challenge of quality, quantity is becoming another

threat, given the rising population growth. Currently, more than a third of the world's population lacks access to safe drinking water.[73] Growing industrialization demands that efficient remediation technologies be put in place to mitigate the impact of the release of pollutants into the environment, especially into water bodies. Contaminating the environment via anthropogenic means, leading to an excessive deposit of heavy metals and other organic pollutants into the environment, in particular, aquifers and biota, is a major concern. Although the exact impact of pollutants on the prevalence of disease is unknown, about 70–90 % of disease risks are due to changes in the environment.[74] In this regard, there has been extensive research into remediation technologies by a myriad of researchers. Most of these pollutants are bioavailable and is even more problematic for humans, as the pollutants get transported up the food chain, with humans being the ultimate victims. Heavy metals are not biodegradable, and most of them are known toxins or carcinogens. Particularly, mercury, lead, cadmium, nickel, copper, chromium and zinc are threats in wastewater treatment:

- Mercury is a neurotoxin, capable of causing damage to the central and peripheral nervous systems.[75] The inhalation of mercury vapor can result in harmful effects on the nervous, digestive and immune systems, lungs and kidneys, and may be fatal. High mercury concentrations result in impairment of kidney function, chest pain and dyspnoea;[75] an extreme example of mercury poisoning is that which occurred in Minamata Bay, with severe methylmercury contamination.
- Lead can damage the central nervous system, kidney, liver and reproductive system, basic cellular processes and brain functions. The toxic symptoms are

anemia, insomnia, headache, dizziness, irritability, weakness of muscles, hallucination and renal damages.[76]

- According to the U.S. Environmental Protection Agency, cadmium is a probable human carcinogen. There are severe human health risks associated with cadmium exposure; chronic exposure to cadmium results in kidney dysfunction while high levels of exposure results in death.[77]
- Nickel is also a known human carcinogen, and concentrations exceeding the critical level may result in serious lung and kidney problems, gastrointestinal distress, skin dermatitis and pulmonary fibrosis.[78]
- Copper is an essential element in animal metabolism. However, excessive ingestion of copper results in serious toxicological anxieties, such as cramps, convulsions, vomiting and death in some cases.[79]
- Chromium in an aquatic environment exists mainly in two states: Cr(III) and Cr(VI). Cr(VI) is more toxic than Cr(III). Cr(III) distorts the physiology of humans and accumulates in food; the outcome of this distortion is severe health problems, such as lung carcinoma.[80]
- Zinc is an essential trace element for human health; it regulates many biological processes, and it is a key component for the physiological functioning of living tissues. Nonetheless, just like most essential heavy metals, too much of it can result in serious health problems, such as skin irritation, vomiting, stomach cramps, nausea and anemia.[81]

The impacts of environmental contamination on human health cannot be overemphasized. Table 1-2 lists the above heavy metal ions and their maximum acceptable concentrations.

Table 1-2. Guidelines for Canadian drinking water quality for the above heavy metals[a]

Parameter	Maximum acceptable concentration (mg/L)
Mercury	0.001
Lead	0.010
Cadmium	0.005
Nickel	0.1
Copper	1.3
Chromium	0.05
Zinc	5

With stringent regulations in place, it is necessary to develop strategies for removing these heavy metals to protect human life and the environment. Different remediation strategies have been explored over the years such as chemical precipitations, membrane filtration, ion exchange, flotation, electrochemical treatment and adsorption.[82] Activated carbon[83] has emerged as one of the best-known adsorbents. However, due to its expensive regeneration cost and reduced performance owing to adsorbent loss, there has

[a] https://www.canada.ca/en/health-canada/services/environmental-workplace-health/reports-publications/water-quality/guidelines-canadian-drinking-water-quality-summary-table-health-canada-2012.html (accessed on November 17, 2017)

been growing interest in developing competitive adsorbents. Dichtel and coworkers[84] recently reported a porous polymer of β-cyclodextrin that is capable of removing micropollutants, with an adsorption rate constant of about 15 to 200 times greater than those of activated carbon. The growing diverse technologies arising in water remediation technology are all geared towards finding efficient means to reduce/eliminate the detrimental impacts of these pollutants on human health.[85] However, researchers ought to be mindful of the possibility of generating adducts of toxicological concern in the attempt to remove toxins with certain technologies. A classical example is the remediation via oxidative water treatment, such as ozonation and advanced oxidation by $KMnO_4$ addition or ferrate, has proven to be efficient. Nonetheless, there is the likelihood of the oxidation leading to formation of persistent abiotic oxidation byproducts of toxicological concern.[86]

Ion-exchange approach has been used widely over the years for the removal of heavy metal ions from wastewater. The high treatment capacity, high removal efficiency and fast exchange (kinetics) have played significant roles in the widespread use of the ion-exchange process for the remediation of heavy metals from aqueous media. Whether synthetic or natural, ion-exchange resins have the specific ability to exchange their cations with the metals in the wastewater to be treated. Strongly acidic resins with sulfonic acid groups and weakly acidic resins with carboxylic acid groups are the most common cation exchangers. The hydrogen ions in each of these groups are exchanged for the metal ions in the test solution. Factors such as temperature, pH, initial concentration of metal ion and the contact time, affect the uptake capacity of the metal ions in solution. A careful control of these parameters can enhance the uptake capacity of the heavy metal ions, which will be discussed in Chapter 5.

1.3.3.1 Polymer-Based Sorbents for Water Remediation

Diverse materials have been employed in the above remediation strategies, but the focus here will be limited to the use of stimuli responsive polymers for environmental remediation. The driving force for the removal of heavy metals by these polymers is the presence of donor atoms (N, O or F) on the backbone of the polymers. In other cases, polymers containing carboxylic acid functional groups have been used as effective sorbents for removal of heavy metal ions. Yildiz *et al.*[87] synthesized hydrogels made of the homopolymer *N*-vinyl pyrrolidone (pVP) and copolymer VP with methyl acrylate (pVP-*co*-MA) using a macroinimer (MIM). Inherent in the MIM are the properties of macromonomers, macrocrosslinkers and macroinitiator in a macrostructure.[88] The synthesized hydrogels displayed enhanced uptake of Cu^{2+} over Ni^{2+}, Zn^{2+} and Cd^{2+}. The preferential adsorption of Cu^{2+} was attributed to the *Jahn–Teller Effect* and that Cu^{2+} easily forms coordination compounds with oxygen and nitrogen containing ligands. The main driving force for the removal of these metals in the case of pVP is coordination between the donor *N* atoms and the metal ions. The removal capacity for the other ions was $Ni^{2+} > Zn^{2+} > Cd^{2+}$. Barring all other factors, such as the chemical nature of the metal ion, hydrogel, environmental changes and morphology, the observed trend was attributed to the increasing ionic radii of the ions. pVP-*co*-MA had a higher uptake capacity for all ions tested over pVP. This phenomenon is due to the added donor atoms, oxygen, with more coordination capability.

Several developments and attempts have been made to explore various adsorbents for removing contaminants. While some are specific to certain metal ions of interest, others generally are capable of removing ions with better sorption capacity for some ions

over others.[89-91] In Rehman *et al.*'s[92] recent work on the removal of As (V) ions, they employed cationic poly(3-acrylamidopropyl)trimethylammonium chloride (p(APTMACl)) microgels and found an improved As (V) adsorption capacity over the pAPTMACl hydrogel or cryogel.[93] More importantly, the ability to recycle the used pAPTMACl was improved further by employing a magnetic pAPTMACl. With this, an external magnet could be used for efficient separation of the adsorbed ions from solution.

Earlier studies in the Serpe group revealed the capability of pNIPAm-based microgels and their assemblies for the removal of organic dyes from water,[94-98] due to a combined electrostatic effect and water absorption phenomenon. A part of this thesis is focused on the remediation of heavy metal ions with pH responsive microgels and metalloids, specifically selenium (Se) using zero valent iron. As described earlier, microgels are porous, and the incorporation of functionalities like carboxylic acid based moieties make them excellent candidates for water remediation, especially in the remediation of heavy metal ions. Remediation by microgels are through a combination of electrostatic and coordination effect and a likely absorption phenomenon to remove contaminants of interest.

1.3.3.2 Zero Valent Iron for Water Remediation

Zero valent iron (ZVI) has emerged as a competitive adsorbent to activated carbon. Research has shown that ZVI is capable of removing contaminants ranging from heavy metals and metalloids to organic contaminants (mostly chlorinated compounds).[99,100] However, there is a stability challenge with the use of ZVI. Oxide layers form on the surface of the ZVI no matter how hard researchers try to degas the ZVI solution during its preparation.[101] Ultimately, this results in decreased activity and

removal efficiency. To decrease the oxide layer formation or to eliminate dissolved oxygen, so as to increase the removal efficiency, some researchers purge the system with high-purity nitrogen before the introduction of the ZVI.[99,102] Another challenge that limits the use of ZVI is aggregate rapidly due to weak van der Waals forces, high surface energy and intrinsic magnetic interactions.[103,104] To improve the dispersion of ZVI, many researchers have employed different kinds of surface modifications or metal doping methods where the ZVI particles are coated with stabilizers through steric hindrance and electrostatic repulsion.[85] The removal efficiency of selenium (Se contamination spans a broad spectrum of human activities, ranging from the most basic agricultural practices to the advanced technological industrial processes)[105] by the microgels was low. However, a hybrid of microgels and ZVI led to an enhanced removal efficiency as a result of stabilization by the microgel. This will be described in Chapter 6.

Remediation Mechanism by Zero Valent Iron

The earlier discovery of ZVI technology for the remediation of environmental contamination[106] has seen a tremendous growth in the use of this technology for remediating numerous contaminants. Despite the growing interest, there is still a debate about the true mechanism of action in remediating environmental contaminants.[85] The main interaction mechanism could be through adsorption, reduction and oxidation.

In an *adsorption mechanism*, the presence of surface oxygen-containing functional groups presents many active sites. The adsorption mechanism has been considered the main mechanism in removing heavy metal ions. In arsenic (As) removal studies using nanoscale-ZVI by Choi and coworkers,[107] the formation of ZVI-As(III)

inner sphere complexes, evidenced by laser light scattering analysis, was observed. Recently, theoretical calculation and models are being considered in an attempt to elucidate the interaction mechanism between ZVI-based materials and environmental pollutants.[108] Lazar and Otyepka[108] used density functional theory (DFT) to study the adsorption process in water on the iron. Their DFT calculations showed that the adsorbed water could change into H-Fe-OH species with a positive activation barrier, favorable for the adsorption process of heavy metal ions on ZVI-based materials, which are capable of interacting with heavy metal ions.

Heavy metal ions with multiple oxidation states interact mainly with ZVI via the *reduction mechanism*. Two distinct mechanisms are possible for reduction: (1) direct reduction of heavy metals by (Fe^0),[109] and (2) initial adsorption of a heavy metal followed by a gradual reduction by Fe^{2+} from the ZVI.[110] Most heavy metal ions that do not have an intermediate oxidation state are reduced to the lowest oxidation state possible. Those with intermediate oxidation state are adsorbed first, followed by Fe^{2+} reduction. Multiple remediation mechanisms are possible in some cases. For example Liu *et al.*[109] used $Mg(OH)_2$ supported ZVI and observed an exceptional removal capacity of Pb(II) ions from aqueous solution due to a synergistic effect of adsorption, reduction and precipitation mechanisms. A recent study by Zbořil and coworkers,[102] using ^{57}Fe Mössbauer spectroscopy and X-ray photoelectron spectroscopy (XPS) for the mechanistic study of the removal of arsenic, revealed a reduction mechanism and compared the reduction in both oxic and anoxic conditions, as shown in Figure 1-6.

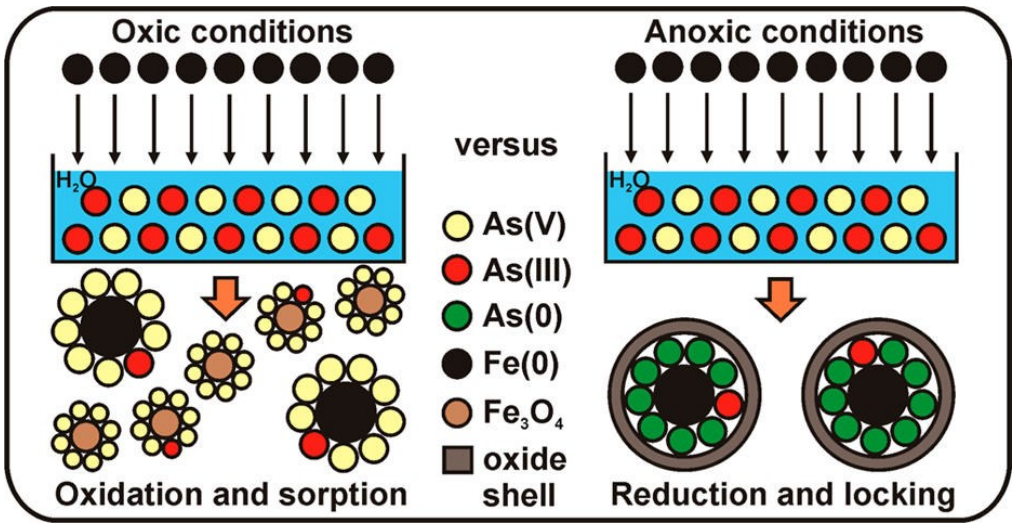

Figure 1-6. Reduction mechanism of oxidic-shell-free ZVI in the removal of As in both oxic and anoxic conditions. Adapted with permission from Ref.[102] Copyright 2017, American Chemical Society.

Another plausible pathway through which heavy metal ions are remediated by ZVI-based materials is *oxidation*. This is evidenced by the mechanistic study of Bhowmick *et al.*[111] on the removal of Arsenic using Montmorillonite–supported nanoscale zero valent iron (Mt-ZVI). As(V) reduction was not observed, but rather complete oxidation of As(III) to As(V) was revealed by the XPS analysis**.**

1.4 Polymerization Synthesis and Mechanism

While there exist many forms of polymerization methods, free radical precipitation polymerization was employed to synthesize the microgels in this dissertation.[112] The primary monomer used for the polymerization was *N*-isopropylacrylamide (NIPAm). Other functional comonomers used included AAc,

MAAc, EAAc, BAAc, 4-vinylpyridine (4VP), DMAPMA and 3-(acrylamido)phenylboronic acid (APBA), depending on the application. Though other crosslinkers have been used in free radical precipitation polymerization, *N,N'*-methylene(bisacrylamide) (BIS) was the main crosslinker used. Ammonium persulfate (APS) was the initiator used, as the polymerization medium was deionized (DI) water. Precipitation polymerization is classified as a heterogeneous polymerization where, initially monomer(s) and initiator are soluble until the onset of initiation, and the formed polymers become insoluble and precipitate out of solution. In a typical free radical precipitation polymerization, the monomer(s) and crosslinker are charged for about 1 h and degassed while raising the polymerization temperature to 70 °C. When desired, a comonomer is added to the soluble monomer and crosslinker solution, followed by the addition of the initiator. At the polymerization temperature, free radicals are generated from the initiator (chain initiation), which attack a free monomer or crosslinker to generate "macro" radicals (chain propagation). At the same time, the increase in temperature causes the formation of seed particles as the particles collapse upon reaching the critical temperature. The nuclei particles (the nucleation process) proceed by chain precipitation until the primary aggregates have garnered enough charge to repel smaller charged particles.[113] During the polymerization process, phase separation occurs between the growing polymer chains and the homogenous bulk solution via enthalpic or entropic precipitation.[114] As the crosslinker is theoretically twice as reactive as NIPAm, the formed microgels have an uneven distribution of density, where the core is denser than the corona. Delayed introduction of the crosslinker may result in evenly distributed densities. Though the polymerization was done at a higher temperature (70 °C), there are

cases where the polymerization can be done at lower temperatures by using solvent mixtures, such as methanol/water, which decrease the LCST of the formed microgels.[115]

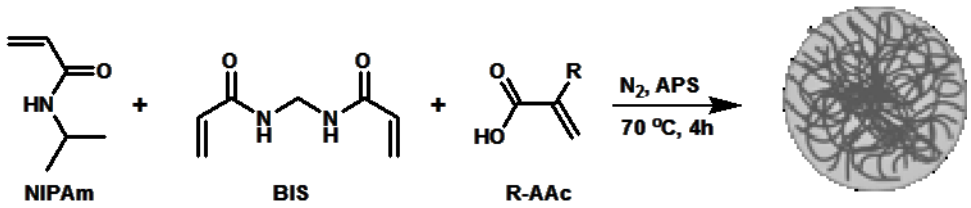

Figure 1-7. pNIPAm-based microgel synthesis scheme

1.5 Conclusions

Even though stimuli responsive polymer materials have been studied over the past decades, the growing interest in smart materials, suggests that the field of stimuli responsive polymers will receive yet a considerable attention for the next few decades. Smart materials that respond to environmental stimuli, such as pH and temperature, are desirable. Structurally, hydrogels or microgels are composed of monomer(s) that can be crosslinked to different degrees to form different architectures. The use of ionizable groups imparts pH responsivity to the final gel. This has been utilized to develop a library of pH responsive microgel-based sensors in Chapter 2. The swelling and shrinking mechanism of stimuli responsive microgels have been used to develop these sensors, whose sensing approach is dependent on the solvation state of the microgels. The design principles employed for the pH sensors described in this thesis involved the direct polymerization of monomers with desired pH responsive ranges. There are other approaches to fabricate pH-responsive sensors; especially for *in vivo* studies, inert or responsive polymers can be functionalized with pH-sensitive dyes such as

fluorescein.[116,117] Depending on the charge state of the microgels, a combination of oppositely charged microgels at different pH ranges has been used to develop a facile means of loading and releasing model drugs that are triggered by a pH controlled manner in Chapter 4.

In Chapter 3, a system that responds in a rapid manner to solution pH changes will be discussed. Even though a system that responds to two stimuli was developed in Chapter 3, developing systems that respond to multiple external stimuli in a smart way are highly desirable. However, developing these systems can be challenging. Although some examples have been reported,[118-120] considerable research into this area still remains to be carried out before the realization of their practical applications. The application of stimuli responsive polymer systems in drug delivery applications has seen tremendous growth. However, there are still some challenges, such as designing multiple stimuli responsive systems for compartmentalization and designing drug delivery systems with stimuli responsive polymers that are biocompatible.

The beauty of stimuli responsive polymer systems is that they are flexible because they can be introduced into other systems. For example, this thesis shows that responsive polymers are introduced into environmental remediation technologies. Several other areas can benefit from this "composite" capability of stimuli responsive polymers. Moreover, they can be introduced into many existing materials at relatively low cost, as often times only a very thin coating is needed.[121] A traditional, yet important area where stimuli responsive polymers can find tremendous application is in the oil and gas industry,[122] and research into this area is highly recommended.

Chapter 2

pH Responsive Microgels as Sensors and their Response in High Salt Concentrations

In this Chapter, a library of pH responsive microgels covering the spectrum of pH range was synthesized and characterized with respect to their response to solution pH changes. An optical construct (etalon) was made from these pH responsive microgels and their response to solution pH was characterized via a reflectance spectroscopy, taking advantage of the microgels' swelling/shrinking behavior, which translates into a diameter change of the microgel, and a subsequent shift in the wavelength maxima observed in the reflectance spectra. Further, one of the devices was shown to withstand a high salt concentration and yet maintained its pH responsiveness.

2.1 Introduction

Stimuli responsive polymers or hydrogels whose response depends on environmental changes, such as solution pH,[14-18] temperature,[18-23] ionic strength,[24,25] application of an electric field,[26] magnetic field,[27] light[19,28] and biomolecules[21] have attracted considerable attention.[30] These intelligent materials have been used in the biochemical, biomedical,[123] sensing and biosensing,[124,125] the oil industry,[126] coatings,[127]

organic dye removal[128] and the food industry.[129] pH measurement in particular is essential in both the environment and in the human body and most biological processes are pH dependent.[46] For example, protein synthesis, DNA and RNA synthesis, cell cycle control and the activity of other key enzymes and metabolic processes are regulated by pH.[47] Water and soil pH are parameters that are crucial to water quality or soil quality; these parameters are frequently monitored in their respective fields. Knowledge of different pH range sensors is useful for developing multi-pH range targeted drug release systems or developing low cost pH sensors that are capable of remote sensing applications.

pH responsive hydrogel particles (microgels) can either be weakly acidic (anionic) or weakly basic (cationic), depending on the nature of the ionizable pendant groups on the backbones of the polymer. The presence of these ionizable groups impart their pH responsivity to the bulk microgel and their swelling/shrinking behavior is controlled by factors such as hydrophobicity/hydrophilicity, elasticity, charge density and pK_a. Based on the swelling/shrinking behavior of hydrogels, the following principles have been used in detecting pH values for sensors: resonance frequency shifts of a quartz crystal microbalance,[130] holographic diffraction wavelength changes in optical Bragg grating sensors,[131] in microgravimetric sensors,[132] bending of micromechanical bilayer cantilevers,[133] microfluidic devices[134,135] and deflection of silicon membranes in piezoresistive pressure sensors.[136]

In this Chapter, microgels composed of weakly acidic or weakly basic comonomers of varying pK_a were synthesized and used to build optical devices, with the goal of building a library of pH sensors that operate in different pH ranges. Microgels

containing acidic groups can be ionized in basic conditions according to the following equation:

$$[RCOOH]_{gel} + H_2O \rightleftharpoons [RCOO^-]_{gel} + [H_3O^+] \qquad (2\text{-}1)$$

Under this condition, the density of carboxylate charged anions increases, resulting in the swelling of the microgels due to Coulombic repulsion of like charges and osmotic pressure within the microgels.[49,137] However, when the microgels are in acidic environments, they are neutralized according to the equation:

$$[RCOO^-]_{gel} + [H^+]_{aq} \rightleftharpoons [RCOOH]_{gel} \qquad (2\text{-}2)$$

resulting in a decrease of the charge density and the amount of mobile counter ions within the microgels, leading to shrinkage of the microgels. The microgels used in this Chapter were synthesized by direct free radical precipitation polymerization, and composed of poly-(*N*-isopropylacrylamide-*co*-acrylic acid) (pNIPAm-*co*-AAc), poly-(*N*-isopropylacrylamide-*co*-butylacrylic acid) (pNIPAm-*co*-BAAc) (both of which contain the weakly acidic comonomers AAc and BAAc respectively), poly-(*N*-isopropylacrylamide-*co*-4vinyl pyridine) (pNIPAm-*co*-4VP) (containing the weakly basic comonomer 4VP). The last category of microgels was synthesized via an indirect post polymerization modification approach, where pNIPAm-*co*-AAc was first synthesized and later functionalized with 4-aminophenylboronic acid (4APBA) using 1-ethyl-3-(3-dimethylaminopropyl)carbodiimide (EDC). To quantify the swelling/shrinking behavior of the pH responsive microgels, pH sensors have been developed with different transducing mechanisms as mentioned above. For example, Grimes and coworkers[138] developed a mass-sensitive pH sensor based on a stimuli-responsive polymer, poly(acrylic acid-*co*-isooctyl acrylate) hydrogel. Using a microfluidic platform, Lu *et*

al.[135] fabricated pH sensors based on the hydrophilic, pH-responsive acrylic acid and the hydrophobic, non-ionic *n*-butyl acrylate. They applied the device in the encapsulation and release of two model hydrophilic and hydrophobic drugs.

The Serpe group fabricates a low cost sensing device, called etalon. It is made by coating a thin layer of Au on a glass substrate, followed by "painting"[139] a monolithic microgel layer on top of the Au coated glass and finally depositing another layer of Au on the microgels. The complete construct mimics the *Fabry Pérot* etalon, where light impinging on the device resonates within the cavity, leading to a constructive and destructive interference, which results in a characteristic spectrum. The observed wavelengths of reflected lights in the spectrum are characteristic of the device thickness according to the following equation:

$$\lambda = \frac{2nd\cos\theta}{m} \qquad (2\text{-}3)$$

where λ is the reflected wavelength at a given order (m) of reflection, n is the refractive index of the dielectric medium, d is the distance between the two Au mirrors, θ is the angle of incident light and m is the order of a "reflected" peak. Maintaining θ at 0º, with a negligible change in n and for a particular order m, λ is directly proportional to d. Therefore, tuning the thickness by virtue of the swelling/shrinking behavior of the microgels is useful to quantify the signal vs. solution pH. This work is a step in building an inexpensive wireless, passive device for remote pH sensing/monitoring. To develop a useful pH sensor based on pH-responsive microgels, it is desired that the microgels respond rapidly and reversibly to changes in pH and that their response can be used over multiple cycles without losing their efficiency. These characteristics were evaluated for the developed pH sensors. Their pH response in high salt concentrations was evaluated

also. Unlike other salt independent sensors[140,141] that use dual sensors to achieve one goal, this Chapter demonstrates that a single device remains passive to different salt environments in their response to solution pH changes.

2.2 Experimental Section:

Materials: All reagents were from Sigma-Aldrich (Oakville, ON, Canada), unless specified. *N*-isopropylacrylamide (NIPAm) was from TCI (Portland, Oregon) and purified by re-crystallization from hexanes and vacuum dried. *N*, *N'*-methylene(bisacrylamide) (BIS), ammonium persulfate (APS), 4-vinylpyridine (4VP), acrylic acid (AAc), 3-acrylamidophenyboronic acid (APBA), 4-aminophenylboronic acid (4APBA), *n*-butylmalonic acid, ethyl acetate and anhydrous $MgSO_4$ were used without further purification. 1-Ethyl-3-(3-dimethylamino- propyl)carbodiimide hydrochloride (EDC) and BupH 2-(*N*- morpholino)ethanesulfonic acid (MES) buffered saline packets were from Thermo Scientific (Rockford, IL) and were used according to the package instructions. 2-Butylacrylic acid was synthesized following a previously reported procedure[142] with some modifications.[57] A pH meter (JENCO 6173 pH, San Diego, CA, USA) was used to prepare solutions with known pH using sodium hydroxide (NaOH) and hydrochloric acid (HCl) to adjust the pH. Millipore water (18.2 MΩ.cm) from a Milli-Q Plus system (Fisher, Z00QSVC01, Toronto, ON, Canada) was used for all experiments. A Rotovap RV 8 (IKA®, Wilmington, NC, USA) was used to remove organic solvents. Glass cover slips were 25 × 25 mm and purchased from Fisher Scientific (Ottawa, Ontario). Au and Cr (99.999%) were obtained from ESPI (Ashland, OR). Au annealing

was done in a Thermolyne muffle furnace from Thermo Fisher Scientific (Ottawa, Ontario).

Synthesis of BAAc:

BAAc was synthesized as previously published.[57] Specifically, piperidine (7.5 mmol) and formaldehyde (31.3 mmol) were added to a solution of n-butylmalonic acid (6.2 mmol) in ethanol (11.6 mL). The solution was heated to 85 °C under reflux while stirring and a white precipitate appeared that steadily re-dissolved over 1 h. The mixture was stirred at 85 °C (under reflux) overnight and cooled to room temperature. The solvent was removed under reduced pressure using rotoevaporation. Then, the residue was dissolved in ethylacetate (12 mL) and transferred into a separatory funnel. The mixture was washed successively with 1.0 M HCl and brine (5%), dried over anhydrous $MgSO_4$ and vacuum-filtered (Whatman #1 filter paper), yielding a clear oil. ^{1}H NMR ($CDCl_3$, 500 MHz): δ_H 6.27 (s, 1H), 5.63 (s, 1H), 2.32–2.28 (m, 2H), 1.49–1.23 (m, 4H), 0.91 (t, 3H). Mass spectrometry (MS) was used to characterize the BAAc and revealed the molecular ion peak of (M–H) at 127.0764. FTIR characterization was done also on BAAc. Both the MS and FTIR data are shown in Figure 2-1, with the expected IR vibrational frequencies shown in Table 2-1

Synthesis of pNIPAm-Based Microgels:

The microgels were synthesized by free radical precipitation polymerization, similarly to a previously published procedure.[143,144] NIPAm (11.928 mmol) and BIS (0.702 mmol) were weighed into a 250 mL beaker and dissolved in 99 mL deionized

water. The mixture was stirred for 30 min and filtered through a 0.2 μm filter into a 3-neck round-bottom flask. A reflux condenser was added to the flask, along with a N_2 gas inlet (needle) and a temperature probe. The solution was charged with N_2 gas and heated to 70 °C for 1.5 h. One of the comonomers, 4VP/AAc/BAAc (1.403 mmol) was added to the heated reaction mixture in one aliquot and the polymerization was initiated immediately by the addition of APS (0.2 mmol) dissolved in 1 mL of deionized water. The solution turned white/cloudy after ~1 min, indicating successful initiation. Then, the reaction was allowed to proceed at 70 °C for 4 h under a blanket of N_2 gas. The resulting suspension was allowed to cool overnight, followed by filtration through glass wool to remove any large aggregates. The microgel solution was distributed into centrifuge tubes and purified via centrifugation at ~10000 rpm for ~30 min to form a pellet, followed by removal of the supernatant and resuspending them in deionized water; this was repeated 6x. The purified microgels were stored for further use.

Preparation of Etalons:

Etalons were fabricated according to our group's previously published "paint on" protocol.[139] Briefly, Au coated coverslips (etalon underlayer) were fabricated by depositing 2 nm Cr and 15 nm of Au onto a 25 x 25 mm ethanol-rinsed and N_2 gas dried glass coverslip (Fisher's Finest, Ottawa, ON) via thermal evaporation at a rate of 1 Å s^{-1}, and 0.15 Å s^{-1}, respectively (Torr International Inc., thermal evaporation system, Model THEUPG, New Windsor, NY, USA). The Cr/Au substrates were annealed at 250 °C for 3 h (Thermolyne muffle furnace, Ottawa, ON, Canada) and cooled to room temperature prior to microgel film deposition. The annealed glass slides were rinsed with ethanol and

water followed by N_2 gas drying. The concentrated microgel pellets obtained via centrifugation were vortexed to loosen and homogenize the microgels. A 40 μL aliquot of the concentrated microgels was spread onto the annealed 25 mm x 25 mm Au-coated glass coverslips. The films were allowed to dry on a 30 °C hotplate for 2 h, followed by rinsing of the excess microgels with DI water. The devices were soaked overnight at 30 °C in a DI water bath to remove any non-specific microgel adsorption. The devices were then rinsed with DI water, dried with N_2 and another Au overlayer (2 nm Cr for adhesion, followed by 15 nm Au) was deposited under the same conditions as the underlayer. The completed devices were soaked in DI water overnight at 30 °C, after which the etalons (Figure 2-2a) were ready for spectral analysis.

4-Aminophenylboronic acid Functionalization of Etalon Via EDC Coupling

The device, made previously by copolymerizing NIPAm with AAc and coating a monolithic layer of pNIPAm-*co*-AAc microgels on a glass slide that was coated previously with Cr/Au, was used for the EDC functionalization. The device was soaked in deionized water overnight and later soaked in pH 4.7 MES buffered saline followed by the addition of 9 mg 4APBA. The mixture was placed on a gyratory water bath shaker G76 (Brunswick Scientific Co., New Brunswick, NJ) to mix for 1 h. Then, 20 mg of EDC was added to the buffered 4APBA solution and sample, with swirling to dissolve the EDC, and placed in the refrigerator for 5 h. An additional 4.5 mg of 4APBA was added to each sample and the mixture was allowed to mix on the gyration shaker table for 30 min. Finally, an additional 20 mg per sample of EDC was added and the reaction was allowed to proceed overnight at 4 °C. The samples were rinsed with deionized water and soaked

in pH 7.2, 10 mM PBS buffer (with 150 mM NaCl ionic strength) for 2 h to remove any unreacted reagents. The samples were rinsed with DI water, N_2 dried and placed in a gold evaporation apparatus as above. Two nm Cr (adhesion layer) and 15 nm Au were evaporated onto the functionalized films at a rate of 1 and 0.15 Å s^{-1} respectively. The completed etalons were soaked in DI water and are now ready for use.

2.3 Results and Discussion

The addition of functionality to microgels can be accomplished via two approaches: direct (copolymerization) and indirect approach (post polymerization modification). In the direct approach, monomers with the desired chemical functionality are directly copolymerized with the primary monomer, NIPAm, during the polymerization process. The indirect approach is preferred in cases where there is no polymerizable monomer available, but a small molecule is present with the desired functionality or the conditions for the direct polymerization approach are unfavorable to the functional comonomer. This modification method can be approached either by functionalizing amine containing moieties via a direct EDC coupling reaction with the synthesized microgel that bears carboxylic acid groups, or the modification can be done on the microgels in the device. Here, the modification was done on the prepared device, where the device preparation protocol was used followed by the EDC coupling with amine as described here and elsewhere.[145] Another means to address the unavailability of the monomer is to synthesize the monomer prior to its use for the direct polymerization. This was the case for BAAc, which was synthesized and characterized by means of ^{1}HNMR, as described in the synthesis section. MS and FTIR were also used to

characterize the BAAc and the results are shown in Figure 2-1. The expected vibrational frequencies from the FTIR analysis are shown in Table 2-1.

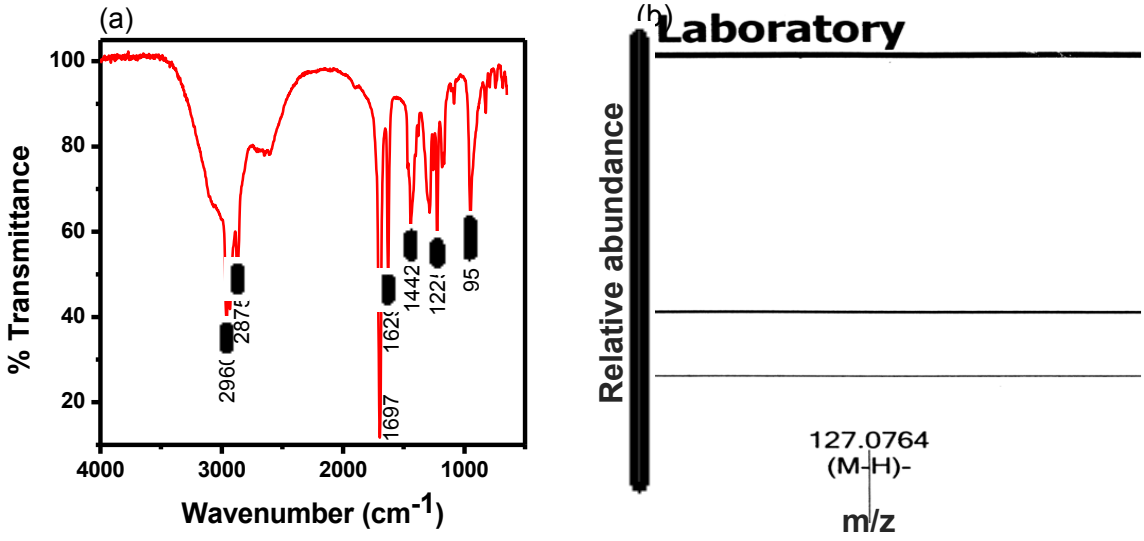

Figure 2-1. (a) FTIR spectra of BAAc and (b) mass spectrum of BAAc, with its molecular ion peak of (M-H) at 127.0764.

Table 2-1. Distinctive IR functional groups and their representative vibrational frequencies for BAAc monomer.

Functional group	Wavenumbers (cm^{-1})
O–H stretching	2960
=C–H stretching	2875
–C=O carboxyl stretching	1697
C=C stretching	1629
C–H bending	1442
C–O stretching	1225
=C–H bending	951

Five sets of microgels were prepared with NIPAm as the main monomer, with comonomers comprising of 4VP, AAc, BAAc, 4APBA functionalization and a terpolymer of NIPAm, AAc and APBA. Devices were prepared from these microgels and their response to solution pH was evaluated by immersing them in a solution of pH in a range that encompasses the pK_a of the acidic/basic comonomer or the functional small molecule. A representative structure of the prepared etalon and their behavior in different pH conditions is shown in Figure 2-2a. The characteristic spectrum that results under the conditions of Figure 2-2a is shown in Figure 2-2b. PNIPAm microgels by themselves do no exhibit pH responsivity. The incorporation of either weakly acidic or basic comonomers renders the microgel pH responsive.

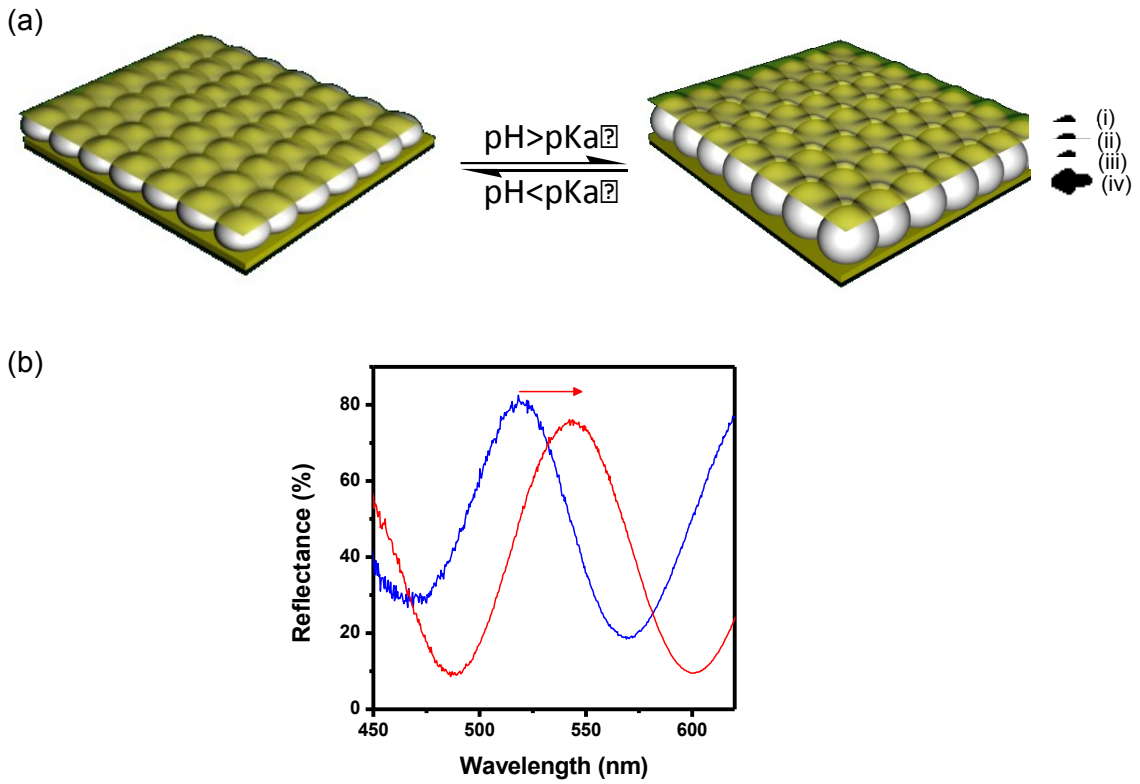

Figure 2-2. (a) A schematic representation of etalons and their behavior in different pH conditions for etalons, which swell at pH above the pK_a of the acid comonomer. The etalon is composed of monolithic microgel (ii) sandwiched between two Cr/Au layers (i and iii) on a glass substrate (iv), (b) a representative reflectance spectrum, showing a red shift from response in panel (a). The blue peak represents the reflectance spectrum of pNIPAm-*co*-BAAc etalon soaked in a pH 5.5 solution while the red peak is the spectrum of the same device in pH 6.5 solution.

A schematic representation of the synthesized microgels' behavior in different pH environments is shown in Scheme 2-1. At pH below the pK_a of 4VP for example, the microgels are positively charged due to protonation of the N group of the 4VP. This

causes the microgels to swell due to Coulombic repulsion and osmotic pressure build up within the microgel networks.[49,137]

Scheme 2-1. Swelling/shrinking mechanism of (a) pNIPAm-*co*-4VP, (b) pNIPAm-*co*-BAAc and (c) pNIPAm-*co*-AAc+APBA microgels. pNIPAm-*co*-AAc shows a similar swelling/shrinking mechanism to that of (b). Different charge states are present at pH around the pK_a, however the pH description here is shown for simplicity.

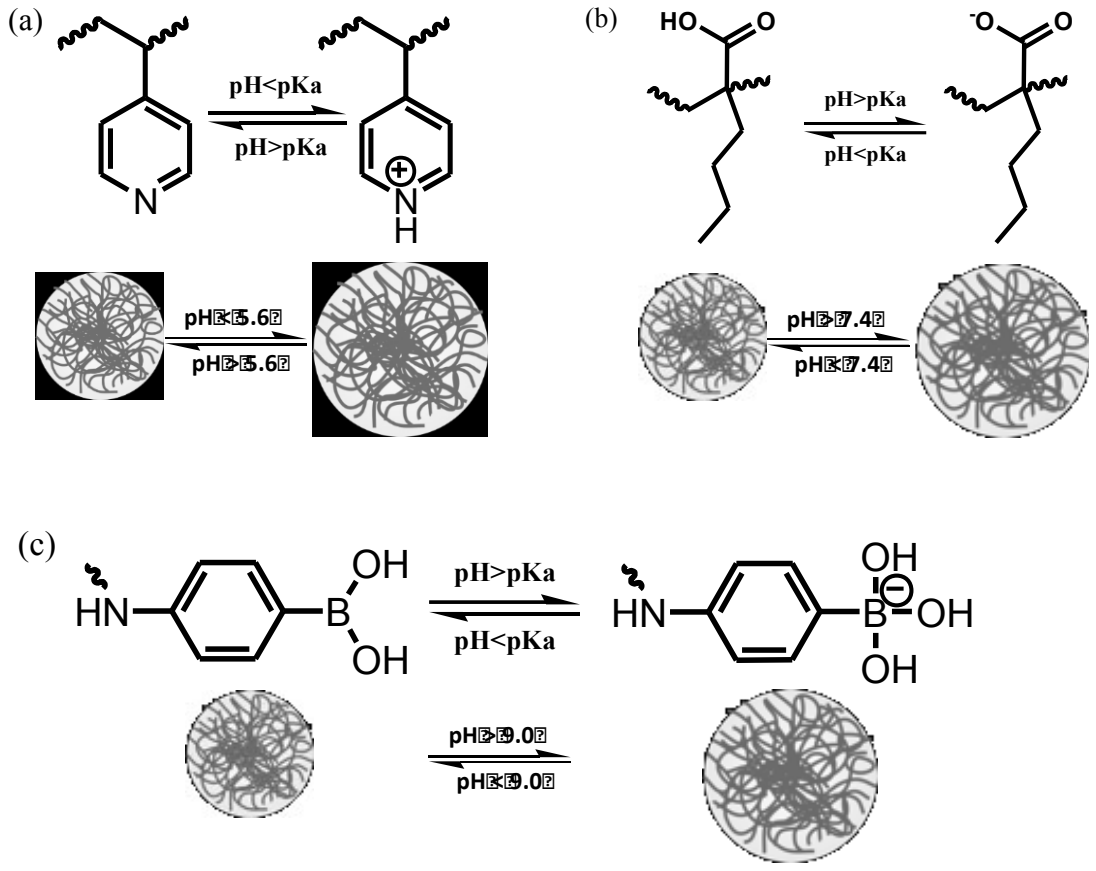

The swelling induces an increased distance between the two Au mirrors, leading to a red shift, according to Eq. 2-3. As seen in Figure 2-3a, the peak blue shifted with increasing pH, with an effective pH range of 3.5-5.5 (Figure 2-4a). The gradual decrease in wavelength with increasing pH signified the various degrees of neutralization, and the presence of the plateau region shows the complete neutralization of the 4VP group within the microgels. The reverse response to pH occurs (Figures 2-3b-d). AAc, BAAc both are deprotonated at pH above their pK_a, causing an increased Coulombic repulsion of negative, and a concomitant red shift. Similarly to Figure 2-3a, the gradual increase in wavelength with pH for Figures 2-3b and 2-3c depicted the various degrees of deprotonation. A complete deprotonation was marked by the plateau region, as seen in Figure 2-3c at pH above 8. For pH regions where there was no direct monomer available with pK_a within the pH region of interest, or if available but cannot withstand the polymerization conditions, an indirect approach becomes indispensable. Figure 2-3d is a typical result where EDC coupling was used to functionalize 4APBA unto pNIPAm-*co*-AAc microgels through the carboxylic acid moieties of the microgels. Unlike the state of the microgels in Figures 2-3b and 2-3c, 4APBA in Figure 2-3d is hydroxylated. The boron atom acquired a negative charge, resulting in charge-charge repulsion due to Coulombic force, with an increased osmotic pressure that causes the microgel to swell. The swelling of the microgels caused the Au mirrors distance to increase, leading to a red shift that is observed in the reflectance spectrum. In all cases, the swelling observed in Figure 2-3a at low pH and that observed in Figures 2-3b-d at high pH can be attributed to an increase in hydrophilicity as the microgels are ionized, allowing water to enter into the microgels.[137]

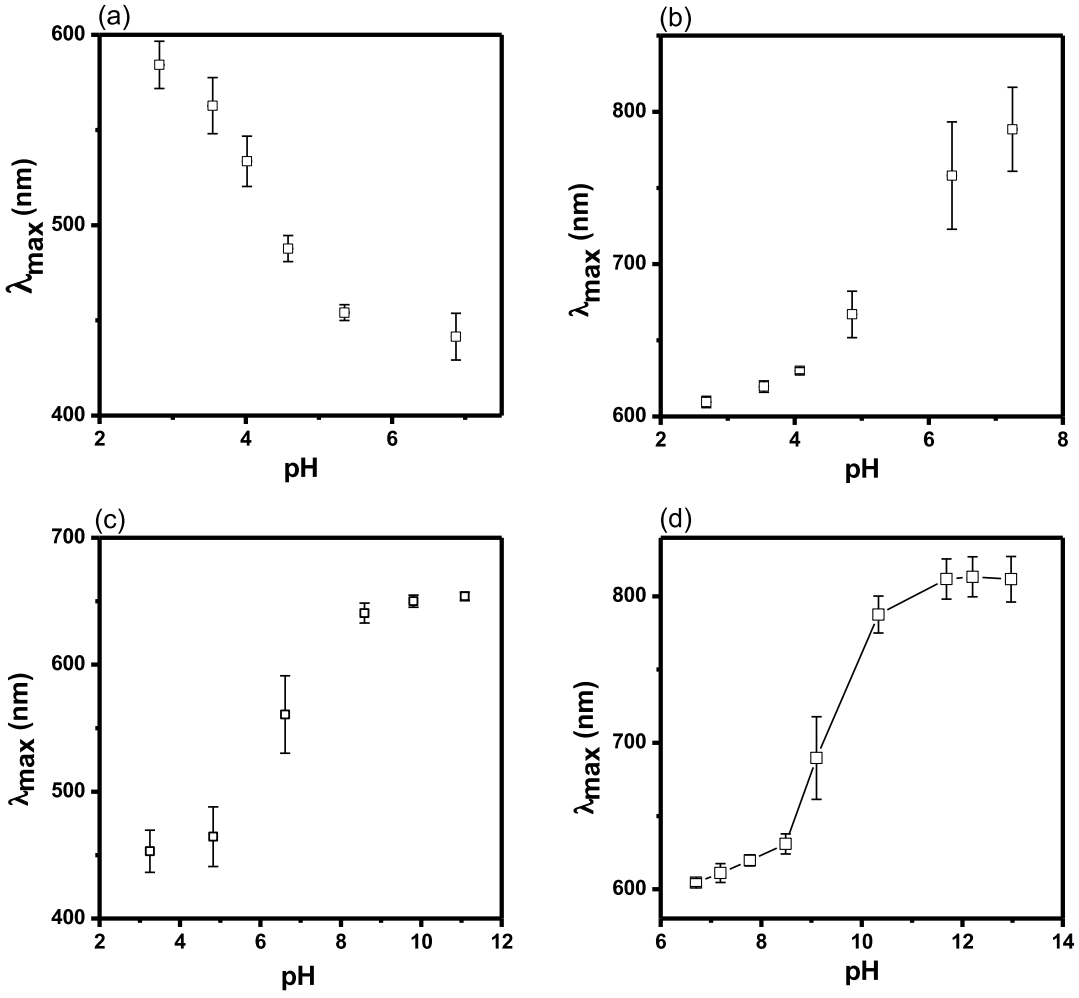

Figure 2-3. (a) pH response of pNIPAm-*co*-4VP, (b) pNIPAm-*co*-AAc, (c) pNIPAm-*co*-BAAc and (d) pNIPAm-*co*-AAc+4APBA devices. The devices were immersed in high pH solutions to cause (a) to fully collapse and (b-d) to fully swell. The solution pH was then decreased gradually while recording the spectrum. Data point represents average peak position of three devices and error bars represent their standard deviation. The line drawn through (d) is for an eye-guide.

A dramatic change in wavelength shift occurred when the pH approached the vicinity of the pK_a of the acidic/basic functional comonomer, as the degree of ionization of weak acids and bases change rapidly at pH values near the pK_a of the weak acid/base. The response from each of the sensors was marked by three distinct regions: the *creeping* region, characterized by a small increase (or decrease in the case of 4VP) in wavelength in response to pH; the *exponential* region, where there is a sharp rise/fall of the wavelength in response to pH change. This region can be considered the linear range of the sensors, as detailed in Figure 2-4. The final region, the *plateau* region, is the pH range at which the device is either fully swollen or fully collapsed (for sensors made of 4VP).

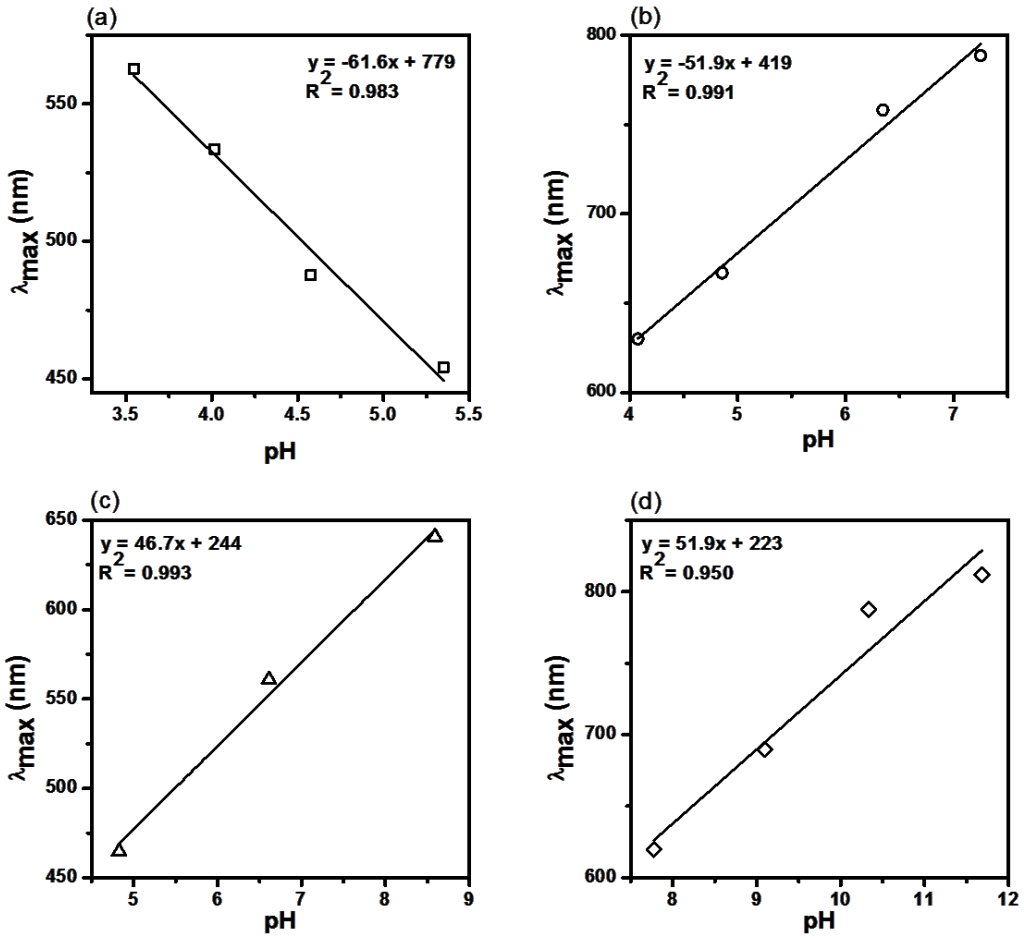

Figure 2-4. Linear pH response ranges for (a) pNIPAm-*co*-4VP (3.5–5.3), (b) pNIPAm-*co*-AAc (4.0–7.0), (c) pNIPAm-*co*-BAAc (4.8–8.5) and (d) pNIPAm-*co*-AAc+4APBA (7.7–11.5) devices. Data were fit to the linear fit model of OriginLab Pro version 8.5 program software.

As described earlier, a stimuli responsive system should respond reversibly to applied stimuli. Thus, upon the reversal of the applied stimuli, the system should return to their initial state. To investigate the reversibility of the devices, each of them was placed in a solution of pH that is high enough to cause the device to fully collapse (Figure 2-5a)

or fully swell (Figures 2-5b-d), followed by a gradual decrease in pH values while monitoring the corresponding peak shift. After attaining a pH value below the pK_a of the corresponding comonomers, the pH was increased again gradually with their corresponding peak shift being recorded. The devices show significant response upon the reversal of the applied stimuli, as in Figure 2-5. The observed signal drift in response to the reversal of pH can be attributed to signal hysteresis,[15,146] which occurs with pH cycling from a high to low pH and vice-versa.

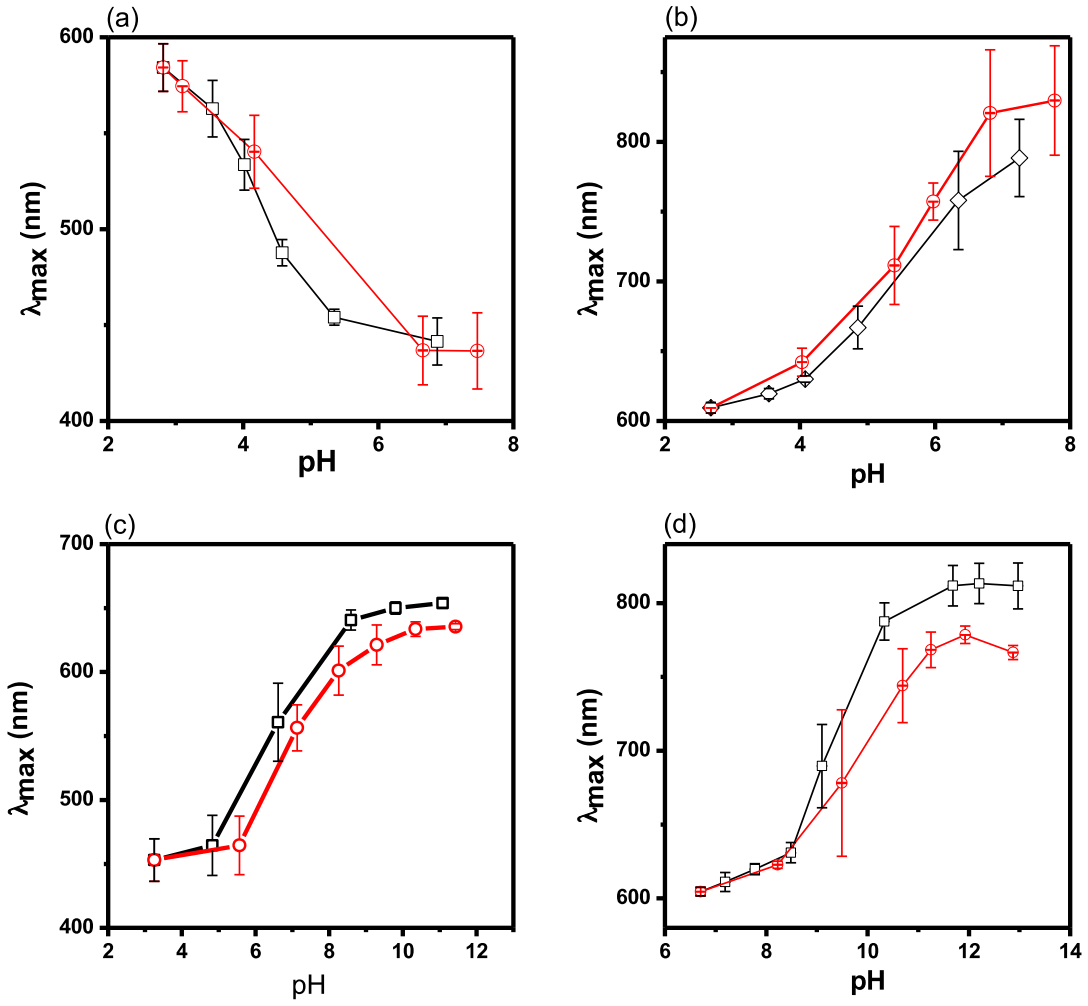

Figure 2-5. Reversibility of pH response to (a) pNIPAm-*co*-4VP, (b) pNIPAm-*co*-AAc, (c) pNIPAm-*co*-BAAc and (d) pNIPAm-*co*-AAc+4APBA devices. The devices were immersed in high pH solutions to cause (a) to fully collapse and (b-d) to fully swell. Then, the solution pH was decreased gradually below the pK_a value of the ionizable group while recording the spectrum (black curve). Again, the pH was increased gradually with their corresponding peak shift being recorded (red curve). Data point represents average peak position of three devices and the error bars

represent their standard deviation. The lines drawn through the data points are eye-guides.

The reversibility of a sensor is desired. However, the reusability of a single device over multiple times is more desirable. These pH-sensing devices showed multiple usages without losing their sensitivity to pH changes. In this setup, each device was placed in a solution of high pH where the device was fully collapsed (Figure 2-6a) or fully swollen (Figures 2-6b-d). After recording their corresponding peak position, the pH was decreased to the indicated pH in each figure: to about pH 3 for the devices composed of pNIPAm-*co*-4VP (Figure 2-6a) and pNIPAm-*co*-AAc (Figure 2-6b); to about pH 2 for the device made of pNIPAm-*co*-BAAc (Figure 2-6c); and pH 7 for the device made of pNIPAm-*co*-AAc+4APBA (Figure 2-6d). The devices, as shown are capable of maintaining their pH response even after several cycles of pH changes; this can be beneficial from an economic point of view. The ability of the sensors to respond even under extremely low/high pH showed the stability of the devices in harsh pH conditions.

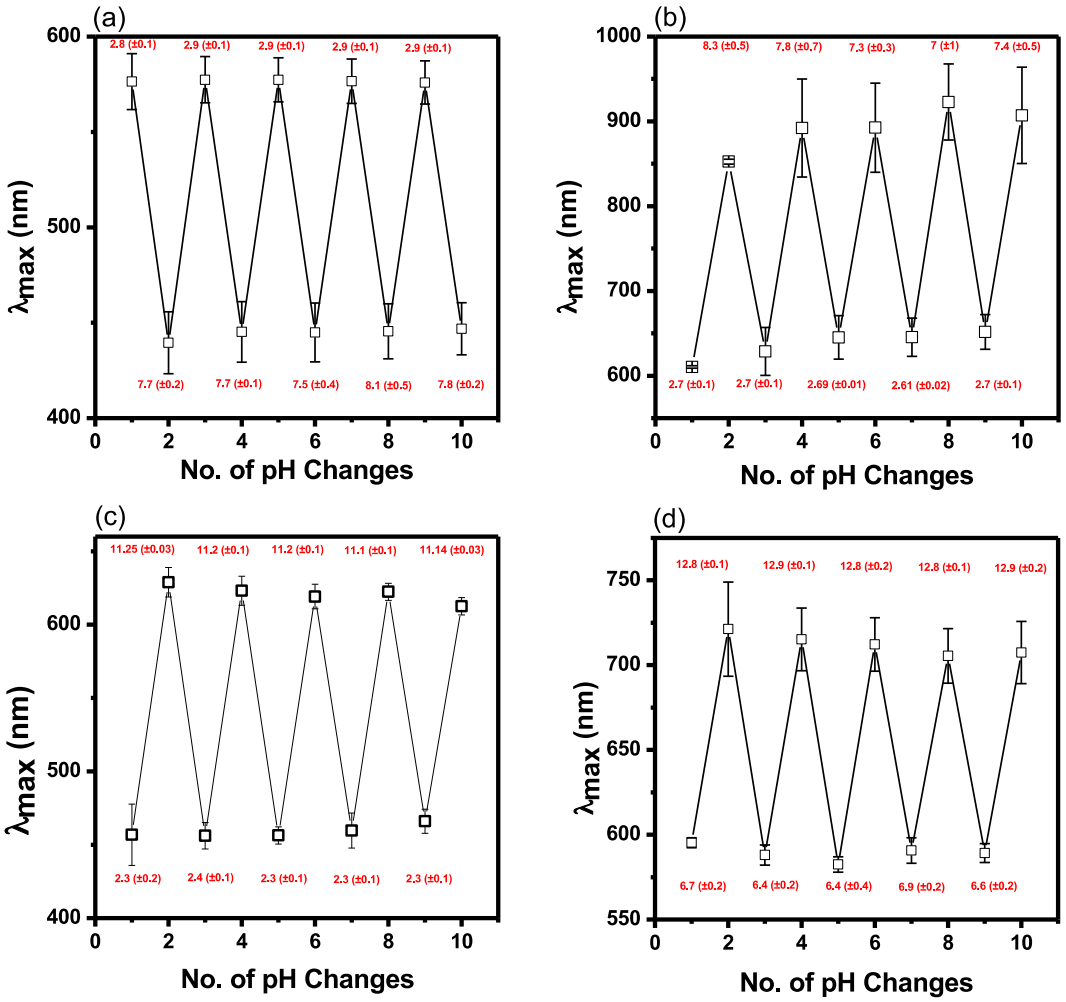

Figure 2-6. The repeatability of (a) pNIPAm-*co*-4VP, (b) pNIPAm-*co*-AAc, (c) pNIPAm-*co*-BAAc and (d) pNIPAm-*co*-AAc+4APBA etalon's response to solution pH changes (average pH values are indicated in the plot with their standard deviations in parentheses). Each data point is the average obtained from three separate etalons with the error bars showing their standard deviation.

A high-demand sensor would be one that can respond to different pH ranges with high sensitivity and accuracy. To fabricate a single device with the ability to respond to different pH ranges, the two comonomers AAc and APBA, with pK_a of 4.25 and 9.0, respectively were used together with NIPAm to synthesize multi-pH responsive microgels. The microgels respond almost linearly to solution pH in the range of 3.5–7 and from 7–12, respectively. A dynamic light scattering (DLS) size measurement for the microgel at different pH, shown in Figure 2-7a, shows clearly defined regions where each of the pH responsive comonomer responded linearly to pH: in the ranges 3.5–7 and from 7–12. Devices were then fabricated from this terpolymer microgel as before, and the devices showed a response that is comparable to their microgels in solution. The device in response to pH, as shown in Figure 2-7b, marked a gradual increase in peak position, steeped around the pK_a of AAc and eventually plateaued at pH 6.5. The second inflection region was due to the presence of the 4APBA, whose pH response is in the higher range of 7–12. The shaded regions represent states in which the microgels are fully collapsed/swollen. Between the shaded regions are the linear response ranges encompassing the pK_a of the functional comonomer. The device's reversibility is presented in Figure 2–7c, where upon decreasing the pH, the peak blue shifted. Finally, to demonstrate the independent pH response over many cycles, the device was cycled between pH 3–7 and from pH 7– 12, followed by the reverse order and so forth. Similar to Figure 2-6, the results of Figure 2-7d showed that the multi pH-range responsive device is repeatable and can be used over multiple times without losing its efficiency.

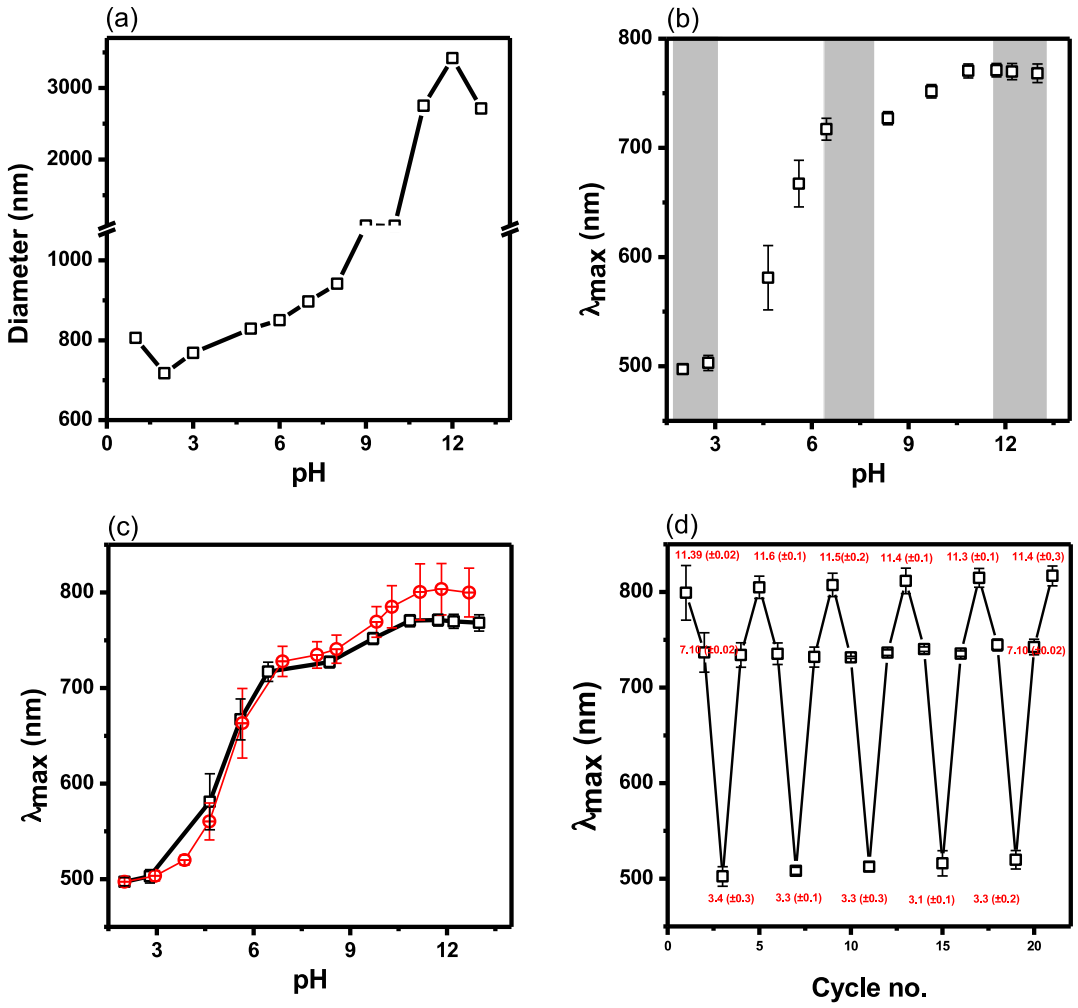

Figure 2-7. pH response of pNIPAm-*co*-AAc-*co*-APBA terpolymer microgel and their devices. (a) DLS size measurement of microgel's response to pH, (b) etalon of terpolymer in response to solution pH. Shaded regions represent areas where the device is fully collapsed/swollen. Between the shaded regions are the linear response ranges of the device. (c) Reversibility of the terpolymer device and (d) independent pH-step cycling of the device in response to pH from 3–7 and from pH 7–12, followed by the reverse order and so forth. Each data point is the average obtained

from three separate measurements with the error bars showing their standard deviation. The lines are guides to the eye.

The incorporation of the APBA into the terpolymer dramatically enhanced the kinetic response. As will be described in detail in Chapter 3, the bulky nature of the APBA might have increased the diffusibility of water in and out of the gel. An increased in hydrophobicity as suggested in Chapter 3 is seen here as well. The results of Figures 2-8a and 2-8c were obtained by immersing the respective devices in high pH solutions followed by an instant decrease in the pH with 1.0 M HCl at constant stirring rate. The reverse was done for Figures 2-8b and 2-8d, by immersing the respective devices in low pH solution followed by an instant increase in solution pH with 1.0 M NaOH. A slow kinetic response was observed without the presence of the APBA, as shown in Figure 2-8a and 2-8b for pNIPAm-*co*-AAc. However, the incorporation of APBA enhanced the kinetics from about 30 min for AAc, to about 2 s, as shown in Figures 2-8c and 2-8d for pNIPAm-*co*-AAc-*co*-APBA. The bulky nature of the incorporated APBA created an interstitial space within the microgels, leading to an increased void space that resulted in an enhanced diffusion of water in and out of the microgel network. A gradual decrease is seen in Figure 2-8a, while an instantaneous decrease in diameter in the form of a blue shift is seen in Figure 2-8c. The reversibility of the devices, shown in Figures 2-8b and 2-8d were demonstrated by a rapid increase in pH using 1.0 M NaOH. Comparable to Figure 2-8a, a gradual increase in λ_{max} was observed over time for pNIPAm-*co*-AAc (Figure 2-8b), whereas a sharp increase in λ_{max} resulted over time for pNIPAm-*co*-AAc-*co*-APBA (Figure 2-8d).

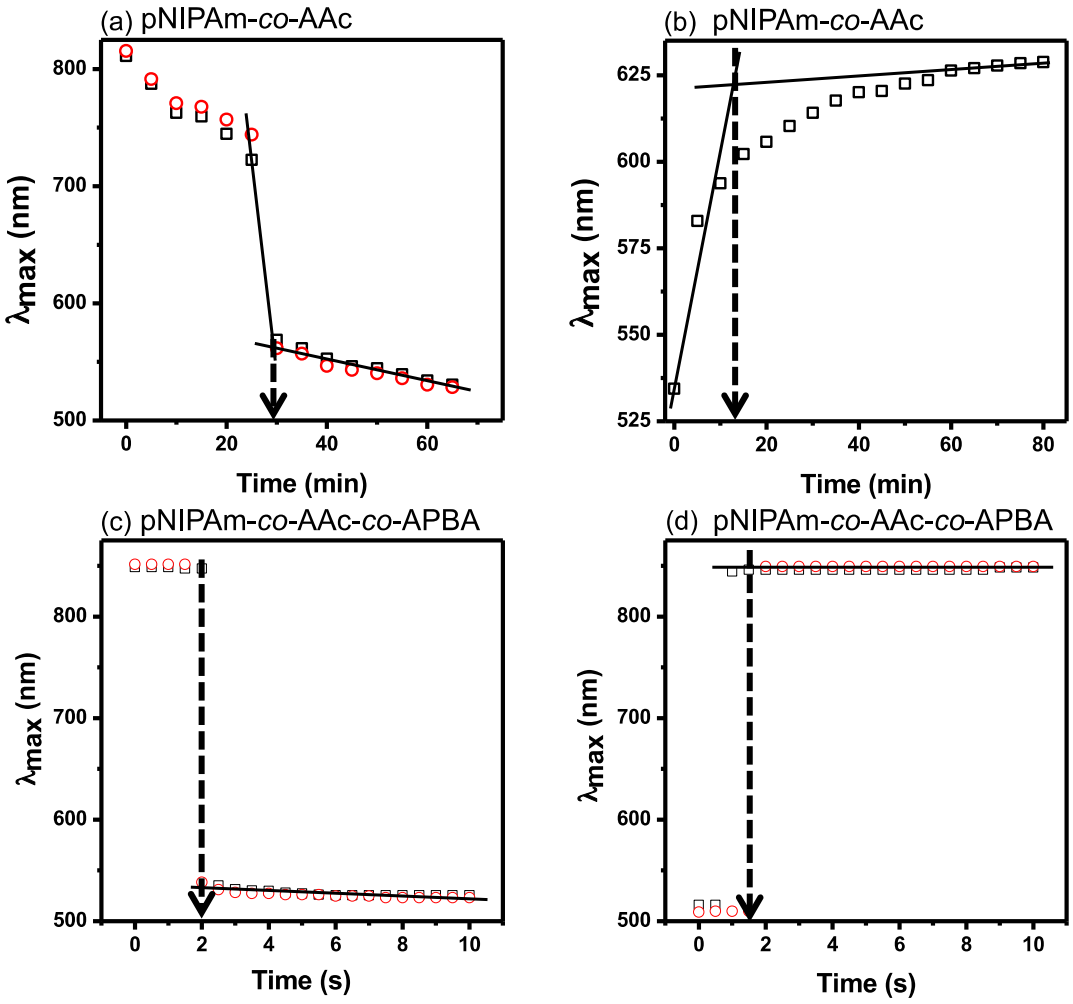

Figure 2-8. Kinetics of the response of pNIPAm-*co*-AAc etalon to decreasing pH (a) and increasing pH (b). Kinetics of the response of pNIPAm-*co*-AAc-*co*-APBA etalon to decreasing pH (c) and increasing pH (d). Solution pH was cycled between pH 7 to 3 and vice versa for (a) and (b) respectively; and from pH 12 to 3 and vice versa for (c) and (d) respectively. The different data symbols represent data from separate devices, while the arrows point to the critical time that the devices completed their response to pH.

Devices that respond to solution pH in the neutral range are particularly useful for physiological applications, such as the monitoring of gastric pH for diagnosis of gastroesophageal reflux disease.[141] However, the mixed response due to the variable salt concentration and pH environment hinders the successful application of the pH sensor. Similarly, for applications such as in water disinfection, the presence of Cl^- or Br^- inhibits the use of pH sensors in these industries. Therefore, the effects of salt (NaBr and NaCl) were investigated on the pH response of the developed sensors. The device was immersed in salt solutions of different concentrations and the solution pH was gradually increased while monitoring the peak shift in the reflectance spectrum. The pH responsivity of the device was still maintained even at high salt concentrations of 5000 ppm, as seen in Figure 2-9.

Fouling,[147] which is a major challenge for most surface coating devices, is seen to be minimal in this case as the device's response to pH was still attainable under high salt concentrations. The differences in response to different concentrations and types of salts are within the standard deviations obtained for the same device shown in Figure 2-3c (without the presence of salt). The significance of this pH sensor, unlike others is that, a single device can be used even at high salt concentrations. Some salt independent devices use a dual responsive polymer system where one set of polymer responds to both salt and pH whereas the other polymer responds only to salt but not pH.[141]

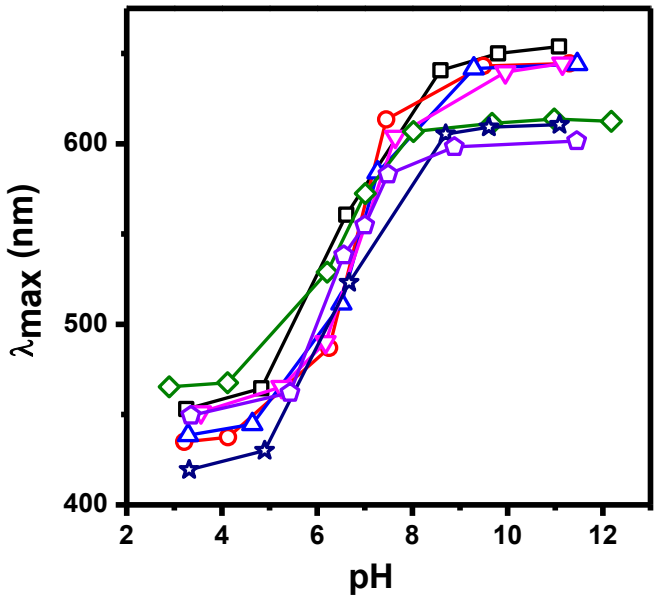

Figure 2-9. pH response of pNIPAm-*co*-BAAc etalon to different salt concentrations and mixtures: 0 ppm salt (black □), 2500:2500 ppm (24.3:42.8 mM) NaBr:NaCl (red□○□, 1000 ppm (9.72 mM) NaBr (blue Δ), 1000 ppm (17.1 mM) NaCl (magenta ▽), 2000 ppm (19.4 mM) NaBr (olive ◊), 5000 ppm (48.6 mM) NaBr (navy star), 5000 ppm (85.6 mM) NaCl (violet pentagon). The lines are eye-guides.

To narrow the pH window and investigate the pH response between pH 6 and 8, which are typical pH ranges in most water related samples, the device's response to small incremental pH changes was investigated. The incredible sensitivity of the device is worth mentioning; a small change in pH yielded a significant change in peak shift, as shown in Figure 2-10a. This pH sensitive sensor can be a very useful sensor in regions where infinitesimal pH changes are required. The device was immersed in a mixture of NaCl and NaBr at different concentrations. The repeatability of the device immersed in a

salt mixture of different concentrations, is shown in Figure 2-10b, with the device maintaining their response to pH with prolonged/multiple exposure to high salt concentrations.

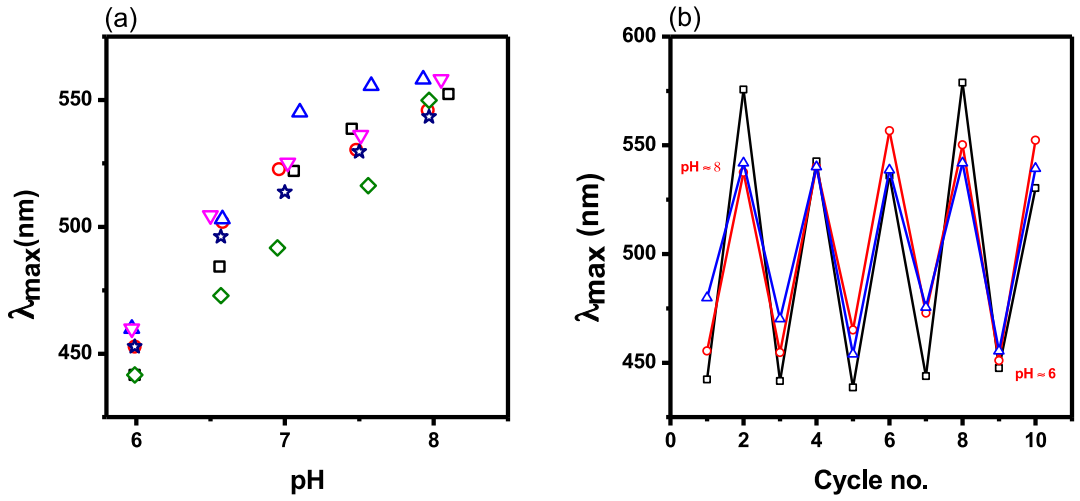

Figure 2-10. (a) pH response of pNIPAm-*co*-BAAc etalon to different salt concentration mixtures (NaBr:NaCl) in a narrow pH range: 1000:1000 ppm (9.72: 17.1 mM) (black □), 2000:2000 ppm (19.4:34.2 mM) (red□○□, 5000:5000 ppm (48.6:85.6 mM) (blue Δ), 1000:1000 ppm rev. (magenta ▽), 2000:2000 ppm rev. (olive ◊), 5000:5000 ppm rev. (navy star). *Rev*. represents response upon reversing solution pH. (b) Reversibility of pH response of pNIPAm-*co*-BAAc etalon to different salt mixture concentrations between pH 6 and 8: 1000:1000 ppm (black □), 2000:2000 ppm (red□○□, 5000:5000 ppm (blue Δ).

2.4 Conclusions

Microgels of varying functionalities have been synthesized and used to develop pH sensors that span most of the entire pH range. In pH ranges where there is no available monomer with a pK_a within the desired pH range of interest, or in cases where the monomer is susceptible to degradation due to the polymerization conditions, an indirect post-polymerization modification becomes indispensable. These sensors, costing only a few cents can be of great benefit in building wireless, remote sensors for diverse applications such as soil pH monitoring as well as real time pH monitoring during water disinfection. The devices show great reversibility and have demonstrated their potential for multiple uses without losing their efficiency. The scope of pH sensing by a single device have been expanded through the copolymerization of different functional comonomers whose pK_a encompass the pH range of interest. The incredible sensitivity of the device, especially within the physiological pH range of 6–8 was demonstrated. Not only can these devices survive harsh pH conditions, but also, they are resistant to fouling caused by salt accumulation.

Chapter 3

Rapidly Responding pH and Temperature-Responsive Poly (*N*-Isopropylacrylamide)-Based Microgels and Assemblies[b]

In this Chapter, a series of pH responsive microgels were synthesized that differ only in their pendant alkyl chain length. The microgels were composed of NIPAm and the following anionic functional monomers: acrylic acid (AAc), methacrylic acid (MAAc), ethylacrylic acid (EAAc) and butylacrylic acid (BAAc). Etalons were fabricated from these microgels, and their response to solution pH was investigated. The highlight of this Chapter is the investigation of the response speed and the hypothesis that was proven to show that the pendant alkyl chain length was responsible for the various degrees of response time. The response rate to solution pH changes under identical experimental conditions was in the order BAAc>EAAc>>MAAc>>>AAc.

[b] This Chapter has been adapted from previously published article: A. Ahiabu, M. J. Serpe.* *ACS Omega*, 2017, 2, 1769-1777.

3.1 Introduction

In the world of sensing and biosensing, actuation and drug delivery systems, a desired stimuli responsive system is one that responds rapidly to the applied stimuli. Thermo- and pH-responsive materials have been among the most widely studied stimuli and can be triggered at a physiologically relevant temperature and pH. This Chapter shows how a "homologous series" of acids based on the acrylic acid (AAc) backbone and that are independently incorporated into *N*-isopropylacrylamide (NIPAm)-based microgels differ in terms of their response rate to applied pH and temperature. Specifically, the acids used were AAc, MAAc, EAAc and BAAc, which have pK_a's in the range of 4.25 to 7.4. Subsequently, the microgels were used to generate optical devices (etalons) and their pH and temperature response was investigated, which showed that devices composed of BAAc-modified microgels exhibited unusually fast response kinetics relative to the rest of the devices. The speed of the response decreased as the length of the acid pendant group decreased, with AAc-modified microgel-based devices exhibiting the slowest response kinetics. Finally, the kinetics of the device's temperature response also decreased as the length of the acid pendant group decreased, which was possibly due to a consequence of the hydrophobicity of the acid groups, i.e., increased hydrophobicity lead to faster responses. Understanding this behavior can lead to the rational design of fast responding materials for the applications mentioned above.

It was of interest to fabricate pH sensors from responsive polymers composed of monomers with pK_a covering the entire pH scale, as shown in the previous Chapter. In the process of fabricating these pH sensors, it was observed that variations in the alkyl chain length of the pendant group on acrylic acid-based comonomers shifted the pK_a

towards a more physiologically relevant pH, which is similar to what was observed by Grainger *et al*.[148] More importantly, it was observed that the speed of the response was significantly improved as the length of the pendant alkyl chain increased. As mentioned, materials with fast response kinetics to pH changes are needed for various applications, such as: actuators for chemical valves,[149] artificial muscles[150] and 'on/off' switches for controlling chemical reactions.[151] To achieve such materials, Zhang *et al.*[152] fabricated a comb-type grafted hydrogel by grafting free pNIPAm and pDMAEMA chains onto the backbone of a crosslinked pNIPAm-*co*-pDMAEMA network. They reported a faster swelling rate and a higher swelling degree (at lower pH) for the grafted hydrogels compared to the native crosslinked pNIPAm-*co*-pDMAEMA hydrogels. In another example, Yan *et al.*[153] copolymerized a polymeric surfactant, poly(2-(methacryloyl-oxy)decyl phosphate) with pNIPAm to generate gels with improved response kinetics. They observed an 88% swelling ratio within 30 min and complete collapse within 120 min (from the swollen state) in response to temperature. This was in contrast to a 24% swelling ratio within 30 min for the unmodified pNIPAm gels. To obtain macroscopic gels with fast response to external stimuli, Richtering and coworkers[154] embedded pNIPAm-based microgels in a polyacrylamide hydrogel matrix. The embedded microgels rendered the microgel-polyacrylamide composite thermoresponsive, yielding a faster response relative to the hydrogels themselves. Several other studies have been devoted to improving the response time of pH/thermo-responsive systems using various grafting approaches. [155-157]

This Chapter demonstrates that the pH dependent response kinetics can be varied by manipulating the chain length of the pendant group attached to the second carbon of AAc. Specifically, the response kinetics to solution pH changes became faster as the alkyl chain length increased. To investigate this, a series of acid modified microgels was synthesized via free radical precipitation polymerization. The weak acid monomers differed from one another by the length of their alkyl group, i.e., acrylic acid (AAc), methacrylic acid (MAAc), ethylacrylic acid (EAAc) or butylacrylic acid (BAAc) microgels. The resultant microgels were characterized by differential interference contrast (DIC) microscopy and dynamic light scattering (DLS) at various solution temperatures and pH. Similarly to microgels made of AAc, the microgels composed of MAAc, EAAc and BAAc could be ionized at a solution pH above their respective pK_a of 5.5, 6.3 and 7.4.[148]

Next, optical sensing devices (etalons[139]) were constructed from these microgels and were used to monitor real time solution pH. This was accomplished by constructing layered materials composed of two thin Au layers sandwiching the pNIPAm-based microgels; a schematic of the structure of the etalons can be seen in Figure 3-1a. They were generated by depositing a thin layer of Au (typically 15 nm) on top of a glass substrate, followed by the deposition of a microgel layer and a subsequent layer of Au on top. This device exhibited color and multipeak reflectance spectra, as seen in Figure 3-1b. This was due to light impinging on the device resonating in the microgel-based cavity, leading to constructive/destructive interference, which allowed certain wavelengths of light to be reflected, according to Eq. (3-1):

$$\lambda = \frac{2nd\cos\theta}{m} \qquad (3\text{-}1)$$

where λ is the reflected wavelength at a given order (m) of reflection, n is the refractive index of the dielectric medium, d is the distance between the two Au mirrors, θ is the angle of incident light and m is the order of a "reflected" peak. The value of θ was maintained at 0º; with a negligible change in n and for a particular order m, a direct relationship between λ and d can be seen. Therefore, any stimuli that can change the etalon's d-spacing will result in a color change, which can be used for sensing applications. While these devices exhibit optical properties that depend on temperature due to the thermoresponsive behavior of the pNIPAm-based microgels, the presence of AAc, MAAc, EAAc and BAAc in the microgels also renders the device's color dependent on pH. That is, when the surrounding solution has a pH > pKa, the microgel's acid groups are ionized, resulting in their swelling and a change in d and the wavelength of light reflected from the device, leading to a color change. The response kinetics was observed to be much faster for the BAAc microgel-based devices compared to the others. Specifically, the BAAc microgel-based devices responded to pH changes within 2 s, while the others responded in 30 min (AAc), 3.5 min (MAAc) and 6.5 s (EAAc). The fast response of BAAc microgel-based devices was a result of the relatively long pendant alkyl group of the BAAc and its increased hydrophobicity. This phenomenon created a larger interstitial space between chains, which increased chain mobility and yielded faster shrinking/swelling kinetics.[158,159] This fast response can be used for various potential applications, e.g., for the fabrication of rapid smart sensors, actuators and rapid drug delivery systems.

3.2 Experimental Section

Materials. Unless otherwise specified, all reagents were from Sigma-Aldrich (Oakville, ON, Canada). *N*-isopropylacrylamide (NIPAm) was purified by re-crystallization from hexanes and vacuum dried. *N*, *N*'-methylene(bisacrylamide) (BIS), ammonium persulfate (APS), acrylic acid, methacrylic acid, ethylacrylic acid, piperidine, formaldehyde, ethanol, n-butylmalonic acid, ethyl acetate and anhydrous $MgSO_4$ were used without further purification. 2-Butylacrylic acid was synthesized following the procedure reported by Pratt et al.[142] with some modifications. A pH meter (JENCO 6173 pH, San Diego, CA, USA) was used to prepare solutions with known pH, using sodium hydroxide (NaOH) and hydrochloric acid (HCl) to adjust the pH. A conductivity meter (Orion Star A212, Indonesia) was used for conductivity measurements. Millipore water (18.2 MΩ.cm) from a Milli-Q Plus system (Fisher, Z00QSVC01, Toronto, ON, Canada) was used for all experiments. A Rotovap RV 8 (IKA®, Wilmington, NC, USA) was used to remove organic solvents.

Synthesis of BAAc

BAAc was synthesized using a modified version of what was reported by Pratt et al.[142] Specifically, piperidine (7.5 mmol, 0.74 mL) and formaldehyde (31.3 mmol, 2.3 mL) were added to a solution of n-butylmalonic acid (6.2, mmol, 1.00 g) in ethanol (11.6 mL). The solution was heated to 85 °C under reflux while stirring, and a white precipitate appeared that steadily re-dissolved over 1 h. The mixture was stirred at 85 °C (under reflux) overnight and then cooled to room temperature. The solvent was removed under reduced pressure using rotoevaporation. Then, the residue was dissolved in ethylacetate

(12 mL) and transferred into a separatory funnel. The mixture was washed successively with 1.0 M HCl and brine (5%), dried over anhydrous $MgSO_4$ and vacuum-filtered (Whatman #1 filter paper), yielding a clear oil. ^{1}H NMR, MS and FTIR characterizations are shown in Chapter 2.

Synthesis of pNIPAm-based microgels

The microgels were synthesized by free radical precipitation polymerization, similarly to a previously published procedure.[143,144] NIPAm (11.928 mmol) and BIS (0.702 mmol) were weighed into a 250 mL beaker with 99 mL deionized water. The mixture was stirred for 0.5 h and filtered through a 0.2 μm filter into a 3-neck round-bottom flask. A reflux condenser was added to the flask, along with a N_2 gas inlet (needle) and temperature probe. The solution was bubbled with N_2 gas and allowed to heat to 70 °C for 1.5 h. One of the acids, e.g., BAAc/EAAc/MAAc/AAc (1.403 mmol) was added to the heated reaction mixture in one aliquot, and the polymerization was initiated immediately by the addition of APS (0.2 mmol) dissolved in 1 mL of deionized water. The solution turned white/cloudy after ~1 min, indicating successful initiation. Then, the reaction was allowed to proceed at 70 °C for 4 h under N_2 gas. The resulting suspension was allowed to cool overnight, followed by filtration through glass wool to remove large aggregates. Next, the microgel solution was distributed into centrifuge tubes and purified via centrifugation at ~10000 rpm for ~30 min to form a pellet, followed by removal of the supernatant and resuspension in deionized water; this was repeated 6x. The purified microgels were stored for further use. The actual contents of

ionic comonomers in the microgels were estimated by potentiometric and conductometric titration.

Preparation of etalons

Etalons were fabricated according to our group's previously published "paint on" protocol.[139] Briefly, Au coated coverslips (etalon underlayer) were fabricated by depositing 2 nm of Cr and 15 nm of Au onto a 25 x 25 mm ethanol-rinsed and N_2 gas dried glass coverslip (Fisher's Finest, Ottawa, ON) via thermal evaporation at a rate of 1 Å s^{-1}, and 0.1 Å s^{-1}, respectively (Torr International Inc., thermal evaporation system, Model THEUPG, New Windsor, NY, USA). The Cr/Au substrates were annealed at 250 °C for 3 h (Thermolyne muffle furnace, Ottawa, ON, Canada) and cooled to room temperature prior to microgel film deposition. The annealed glass slides were rinsed with ethanol and water, followed by N_2 gas drying. The concentrated microgel pellets obtained via centrifugation were vortexed to loosen and homogenize the microgels, and a 40 µL aliquot of concentrated microgels was spread onto the annealed 25 mm x 25 mm Au-coated glass coverslip. The film was allowed to dry on a 30 °C hotplate for 2 h, followed by rinsing of the excess microgels with DI water. The samples were soaked overnight at 30 °C in a DI water bath. The samples were then rinsed with DI water, dried with N_2, and another Au overlayer (2 nm Cr for adhesion, followed by 15 nm Au) was deposited under the same conditions as for the underlayer. The completed device was soaked in DI water overnight at 30 °C, after which the etalon assembly (Figure 3-1a) was ready for spectral analysis.

Characterization

Differential interference contrast (DIC) microscope images were acquired on an Olympus inverted research microscope (IX71), at 100x magnification. Hydrodynamic diameters were measured on Malvern Instruments (Westborough, MA, USA) Zetasizer Nano ZS equipped with a 633 nm laser. NMR data were collected using an Agilent/Varian Inova four-channel 500 MHz spectrometer (Santa Clara, CA, USA), with $CDCl_3$ as solvent. Reflectance measurements for the etalons in response to solution pH and temperature were obtained using a Red Tide USB650 spectrometer, a LS-1 tungsten light source and a reflectance probe from Ocean Optics (Dunedin, FL, USA). The spectra were recorded using Ocean Optics Spectra Suite Spectroscopy Software over a wavelength range of 350−1000 nm. A custom-built temperature controlled chamber (Electronics Shop, Department of Chemistry, University of Alberta) was used to maintain the solution temperature and hold the etalon in a stable position. It must be pointed out that only a 0.6 □C change in temperature was observed as a result of the neutralization reaction required to change the solution pH. While this was the case, this temperature change was not significant enough to contribute to the observed kinetics. Additionally, the experimental conditions for all the devices were constant. Therefore, the temperature effect can be ignored and the response kinetics to solution pH changes directly compared. Videos were recorded using a Samsung Galaxy S6 edge, 16MP OIS (F1.9). Infrared spectra were collected on a Thermo Nicolet 8700 FTIR Spectrometer, while mass spectrometry was run on an orthogonal acceleration TOF6220 ESI in negative ion mode (Agilent Technologies, Santa Clara, CA, USA) operating on a full scan mode.

3.3 Results and Discussion

pH responsive pNIPAm-based microgels were generated from the respective pH responsive monomers (structures shown in Scheme 3-1a) using free radical precipitation polymerization under the conditions detailed in Scheme 3-1c. BAAc was synthesized following the synthetic route shown in Scheme 3-1b, which yielded clear oil.

Scheme 3-1. (a) Structures of pH-responsive monomers used in this Chapter, (b) synthesis of 2-butylacrylic acid and (c) polymerization scheme used to generate poly(N-Isopropylacrylamide-*co*-Butylacrylic acid) (pNIPAm-*co*-BAAc) microgels. A similar approach was used to generate all microgels used in this Chapter.

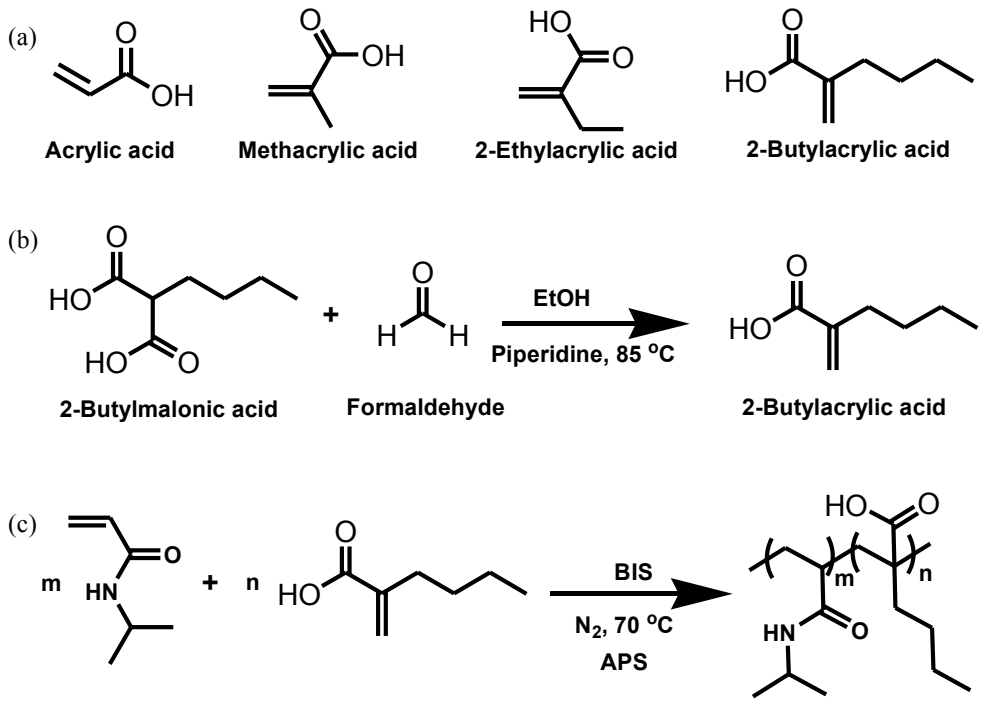

An etalon device was prepared using these synthesized microgels, and the etalon structure with a representative reflectance spectrum is shown in Figure 3-1.

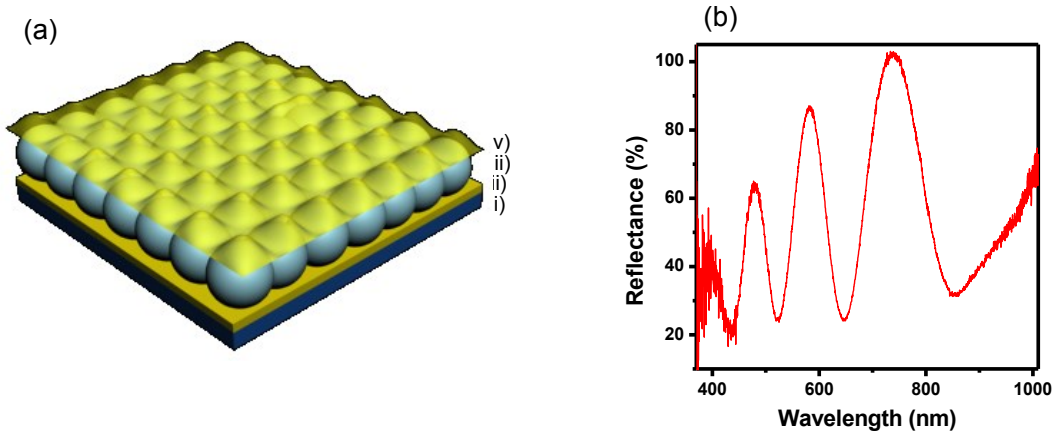

Figure 3-1. (a) Structure of etalon: (i) glass substrate, (ii) Cr/Au underlayer, (iii) microgel layer, (iv) Cr/Au overlayer. (b) A representative reflectance spectrum from a microgel-based etalon showing multiple peaks as a result of the order term "m" in Eq. 3-1.

DIC microscopy images of the synthesized pNIPAm-based microgels are shown in Figure 3-2. The resultant microgels were spherical, with homogeneously distributed sizes without the presence of observable aggregates. DLS was used also to determine the microgel diameter and the change in diameter as a result of solution pH changes.

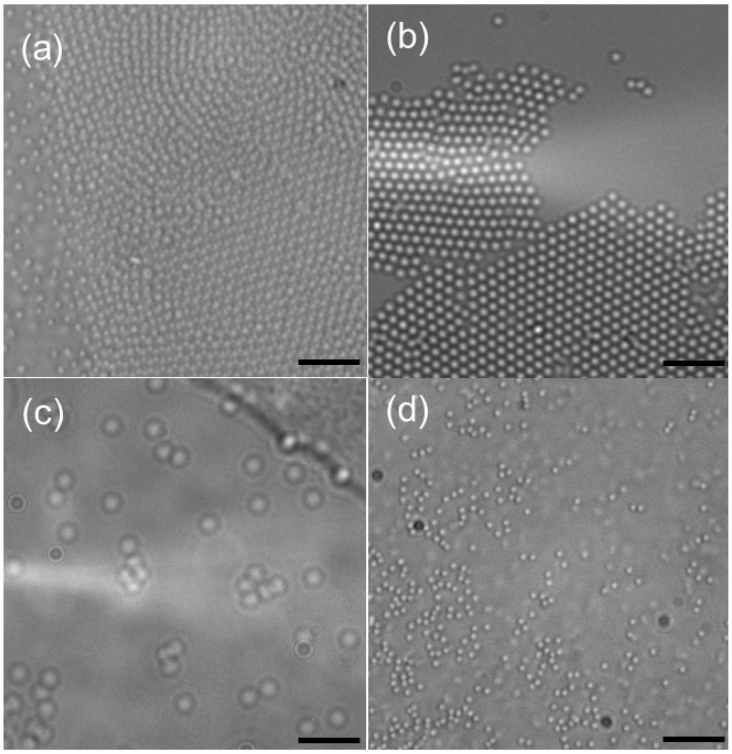

Figure 3-2. DIC images of (a) pNIPAm-*co*-AAc, (b) pNIPAm-*co*-MAAc, (c) pNIPAm-*co*-EAAc and (d) pNIPAm-*co*-BAAc microgels; the scale bar is 6 µm in each image. A dilute solution of each microgel was placed on a piece of glass slide and imaged under the DIC microscope.

An increase in the microgel diameter was expected for the corresponding comonomers mostly at pH > pK_a due to acid ionization, while the diameter was expected to decrease around pH < pK_a due to subsequent acid neutralization. In Figure 3-3 and Figure 3-4, PNIPAm-based microgels are not responsive to pH changes, while microgels composed of AAc, MAAc, EAAc and BAAc exhibit the expected pH response. That is, the pH responsive microgels exhibited an increase in diameter at pH > pK_a and returned to their initial diameter at pH < pK_a. The observed decrease in average diameter between

pH 4-6 and above pH 8 for BAAc, above 6 for AAc and above 7 for EAAc could be purely an artifact of the DLS instrument, or increased ionic strength.

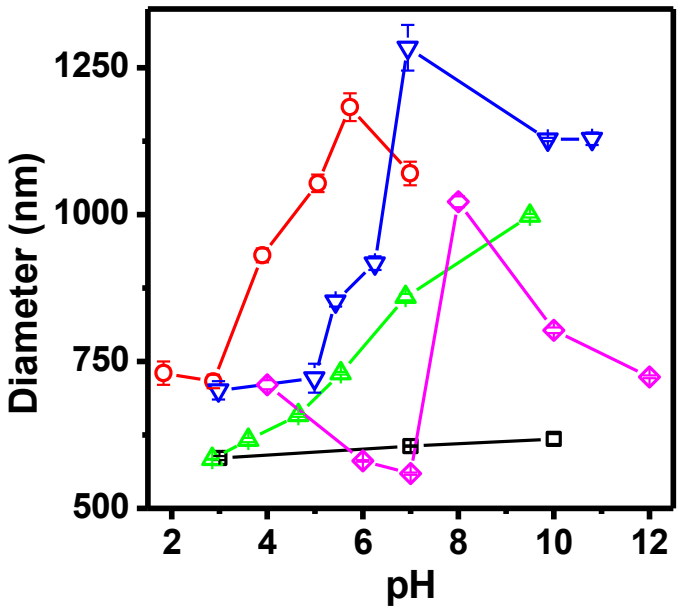

Figure 3-3. DLS measured diameter of (□) pure pNIPAm microgel, (O) pNIPAm-*co*-AAc microgel, (▽) pNIPAm-*co*-MAAc microgel, (△) pNIPAm-*co*-EAAc microgel and (◊) pNIPAm-*co*-BAAc microgel. Each symbol represents the average of three measurements, with the error bars depicting their standard deviation. The lines are eye-guides.

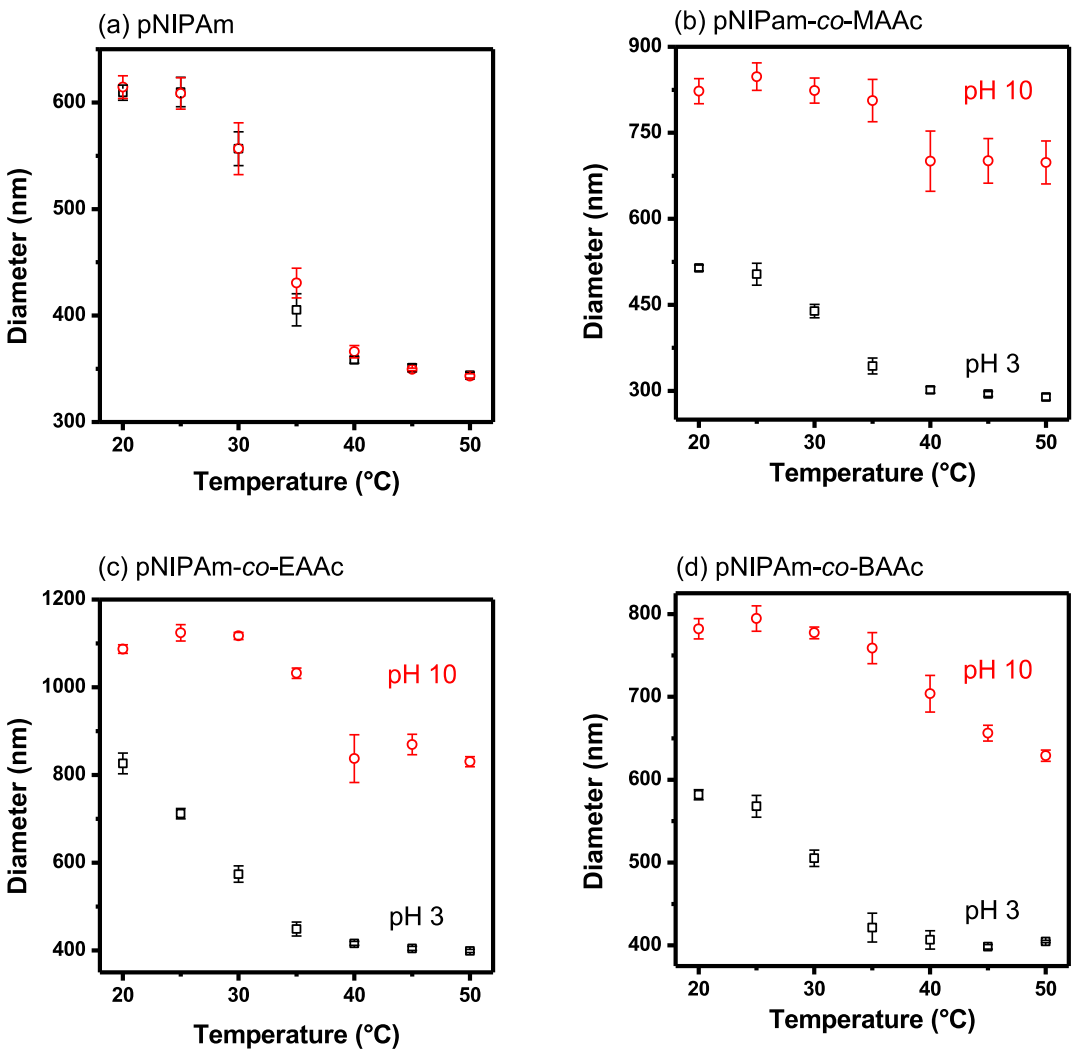

Figure 3-4. DLS microgel diameter as a function of solution temperature at the indicated solution pH. (a) pNIPAm, (b) pNIPAm-*co*-MAAc, (c) pNIPAm-*co*-EAAc and (d) pNIPAm-*co*-BAAc at (□) pH 3 and (○) pH 10, respectively. Each symbol represents the average of three measurements, with the error bars depicting their standard deviations

Next, etalons were constructed from the microgels synthesized above. This was done by painting the microgels on an Au-coated glass substrate, followed by the deposition of another Au layer on top of the formed microgel layer. This process has been described in the Experimental Section and in numerous previous publications.[144] As can be predicted from Eq. 3-1, an increase in d-spacing as a result of the deprotonation of the COOH groups (into COO^-) leads to an increase in the wavelength of light reflected from the device (i.e., a red shift). Multiple reflected wavelengths are expected from the devices as a result of the various orders of reflection (m in Eq. 3-1), which can be seen in Figure 3-1b. Hence, pH responses and response kinetics can be determined and compared by monitoring the position of a reflected peak of a given order as a function of time. To evaluate the responses of the devices to changes in solution pH, each device was immersed in an aqueous solution with a pH far above the pK_a of the acid comonomers, and the pH instantaneously decreased to well below the pK_a by fast addition of acid at a stir rate that was constant between experiments. The response kinetics for the devices to transition from a fully swollen to a fully collapsed state and vice-versa are shown in Figure 3-5. For applications such as smart actuators for chemical valves[149] and 'on/off' switches for chemical reactions,[151] a large-magnitude instantaneous response to the applied stimulus is desired. Impressively, it took less than 2 s for the pNIPAm-*co*-BAAc device to transition from a fully swollen state to a fully collapsed state. In comparison, pNIPAm-*co*-EAAc, pNIPAm-*co*-MAAc and pNIPAm-*co*-AAc took relatively longer times; about 6.5 s, 3.5 min and 30 min, respectively.

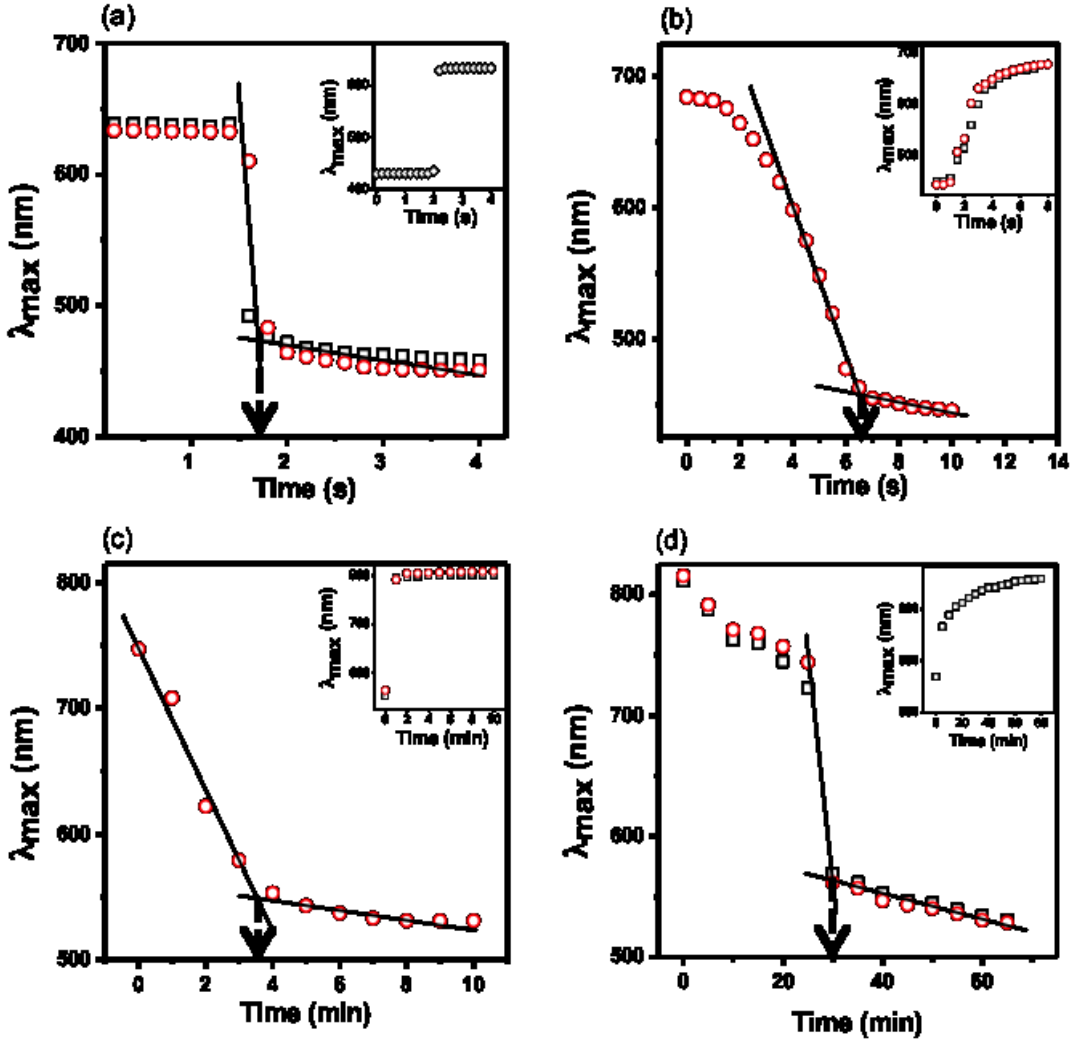

Figure 3-5. Kinetics of the response of (a) pNIPAm-*co*-BAAc, (b) pNIPAm-*co*-EAAc, (c) pNIPAm-*co*-MAAc and (d) pNIPAm-*co*-AAc etalons to solution pH changes. The main figure in each case depicts the response kinetics going from high pH (10) to low pH (4 for (a) 3 for (b-d)). The insets represent the reverse, from low pH to high pH. In all cases the solution pH was adjusted by addition of 1 M HCl or NaOH. The different data symbols represent data from different devices, while the arrows point to the critical time that the devices completed their response to pH.

All four microgels differed structurally due to the different lengths of the pendant alkyl groups on the acrylic acid backbone (Scheme 3-1a). Hence, any difference in response can be attributed primarily to the pendant group chain length. It is hypothesized that the "packing density" for a given "mass" of the microgels is higher for pNIPAm-*co*-AAc (due to the relatively smaller size of the AAc group) relative to the pNIPAm-*co*-BAAc microgels, which was predicted to have a less dense internal structure due to the larger BAAc. The implication of this hypothesis is that the diffusion rate of water in and out of the microgels increased with increasing chain length of the pendant group of the microgels. This also permitted rapid ionization and neutralization of the corresponding acid groups in the microgels.

The possibility of using the pNIPAm-*co*-BAAc etalon as a fast responding pH and temperature sensor was explored further. The pH range at which the device had the greatest response (highest sensitivity) was examined by immersing the device in a solution of low pH and gradually increasing the pH by addition of 0.1 M NaOH while monitoring the peak position. Figure 3-6a shows the device responded to pH over the range of pH 6–9. Hence it can be used over the physiologically relevant pH range. The wavelength (λ_{max}) increased gradually below pH 6 (protonated form COOH) and sharply between 6–9 (deprotonated form COO^{-}), and plateaued beyond pH 9 (fully deprotonated) (Figure 3-6a). In addition, the reversibility of the device's response to pH was probed as the pH was decreased by the addition of 0.1 M HCl. A phenomenon that is similar to the above has been observed in copolymers composed of AAc with NIPAm (pNIPAm-*co*-AAc),[16,25,144,160] MAAc with NIPAm (pNIPAm-*co*-MAAc)[161] and propylacrylic acid (PAAc) with NIPAm (pNIPAm-*co*-PAAc).[162]

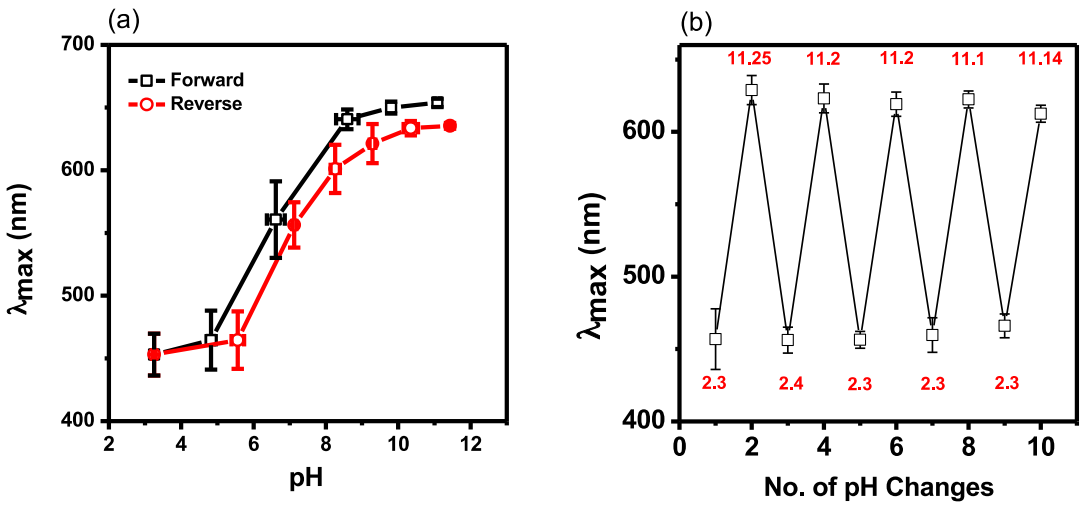

Figure 3-6. (a) Shifts in the reflectance peak position as a function of pH for the pNIPAm-*co*-BAAc etalons: (□) increasing pH and (○) decreasing pH. (b) The repeatability of the pNIPAm-*co*-BAAc etalon's response to solution pH. Each data point is the average from three separate etalons, with the error bars showing their standard deviation. The lines are eye-guides.

Next, the device's response to repeated solution pH changes was investigated. This was done by immersing a single device in a solution of pH 2, allowing it to stabilize and then recording the spectrum. After stabilization, the pH was increased to 11 by addition of 1.0 M NaOH, allowed to stabilize again and a spectrum recorded. This process was repeated multiple times. As can be seen in Figure 3-6b, the device's response to repeated solution pH changes was highly reproducible, with a low standard deviation for the magnitude of the responses between devices. The ability to reuse a single device over many times and still maintain its performance is ideal from an economic point of

view. Again, for the device to still maintain its performance between these extreme pH ranges suggested that it can survive harsh pH conditions.

Since pNIPAm is a well-known thermoresponsive polymer, copolymers composed of NIPAm were expected to maintain their thermoresponsivity.[23] Figures 3-7 and 3-8 show that the pNIPAm-based microgels and devices maintained their thermoresponsivity.

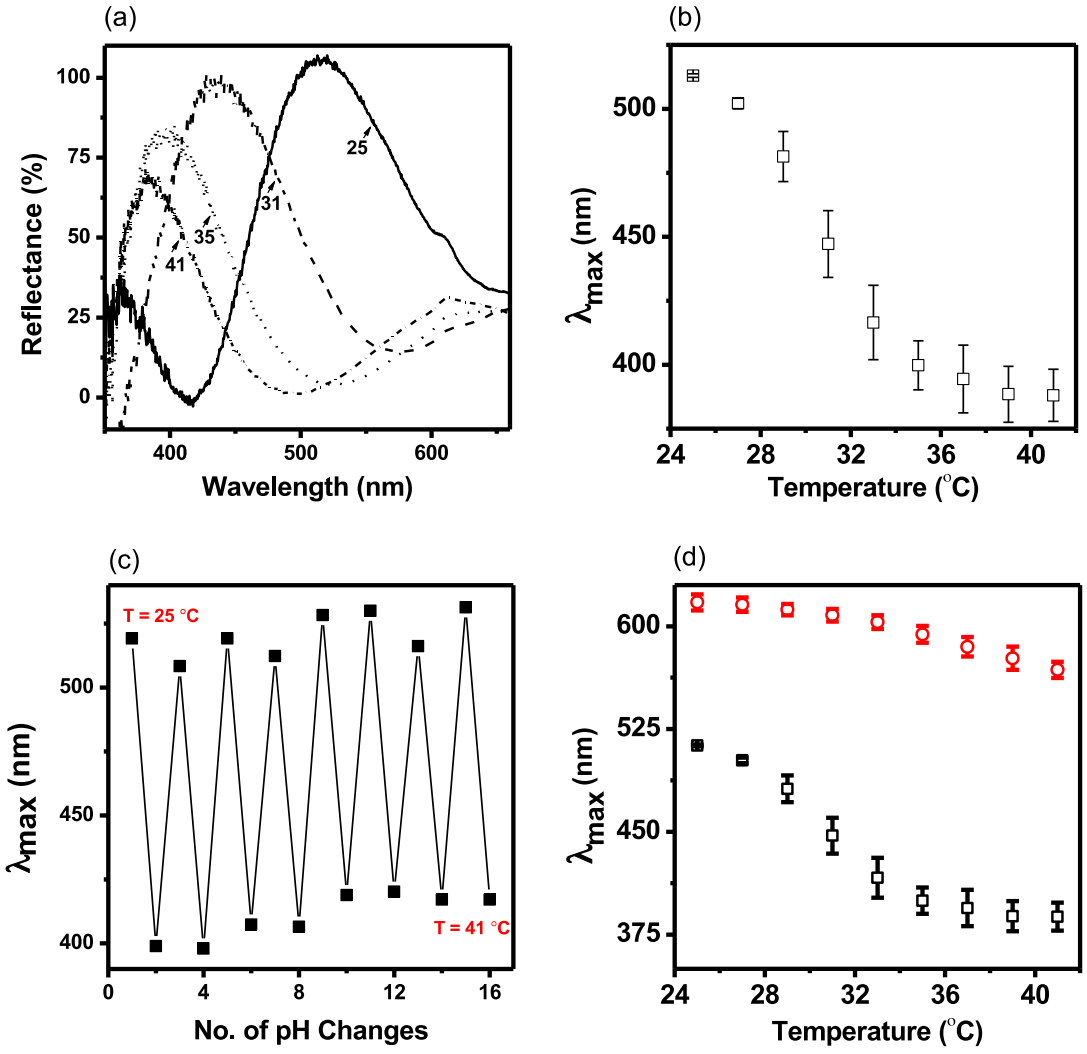

Figure 3-7. (a) Reflectance spectra from pNIPAm-*co*-BAAc etalons at the indicated temperatures at pH 3. (b) Peak position as a function of temperature. Data points in (b) are the average of three devices, and error bars represent their standard deviation. (c) Temperature cycling of pNIPAm-*co*-BAAc etalons between 25 °C to 41 °C at pH 3. (d) Temperature response of a pNIPAm-*co*-BAAc etalon at (O) pH 10 (below the pK_a of BAAc) and (□) pH 3 (above its pK_a).

In Figure 3-8, all microgels showed thermoresponsive behavior similarly to that observed for pure pNIPAm. In Figure 3-7a, increasing the solution temperature from 25 °C to 41 °C at pH 3 led to the expected blue shift of the peaks in the reflectance spectrum. The blue shift was a result of the decreased spacing between the two gold mirrors due to the collapse of the microgels. In Figure 3-7a, the spectra for 25 °C, 31 °C, 35 °C and 41 °C are shown for additional clarity. Figure 3-7b shows how the position of the reflectance peak depended on temperature. The wavelength decreased gradually as the temperature increased from 25 °C and sharply near the transition temperature of ~31 °C. Above the transition temperature, the microgels are in their collapsed state; hence, no further decrease in wavelength was observed as the temperature increased above the primary transition temperature. Upon decreasing the solution temperature, the devices returned to their initial state, and the process can be repeated multiple times, as seen in Figure 3-7c. An abrupt thermoresponsivity was observed at the pH where the pNIPAm-*co*-BAAc microgels are in the protonated state (pH 3). At this pH, the microgels have no charge and can freely collapse and swell as the temperature is increased/decreased, respectively.[163] In contrast, at the higher pH > pK_a of BAAc, the pNIPAm-*co*-BAAc

microgels are negatively charged and are swollen due to Coulombic repulsion and osmotic pressure within the microgel.[49] Therefore, any further attempt to change the microgels' diameter with temperature did not yield any significant transition since the Coulombic force of repulsion[164] is greater than the entropy-driven collapse of the microgels. This is shown in Figure 3-7d for the pNIPAm-*co*-BAAc etalon device and in Figure 3-4 for all the microgels investigated here.

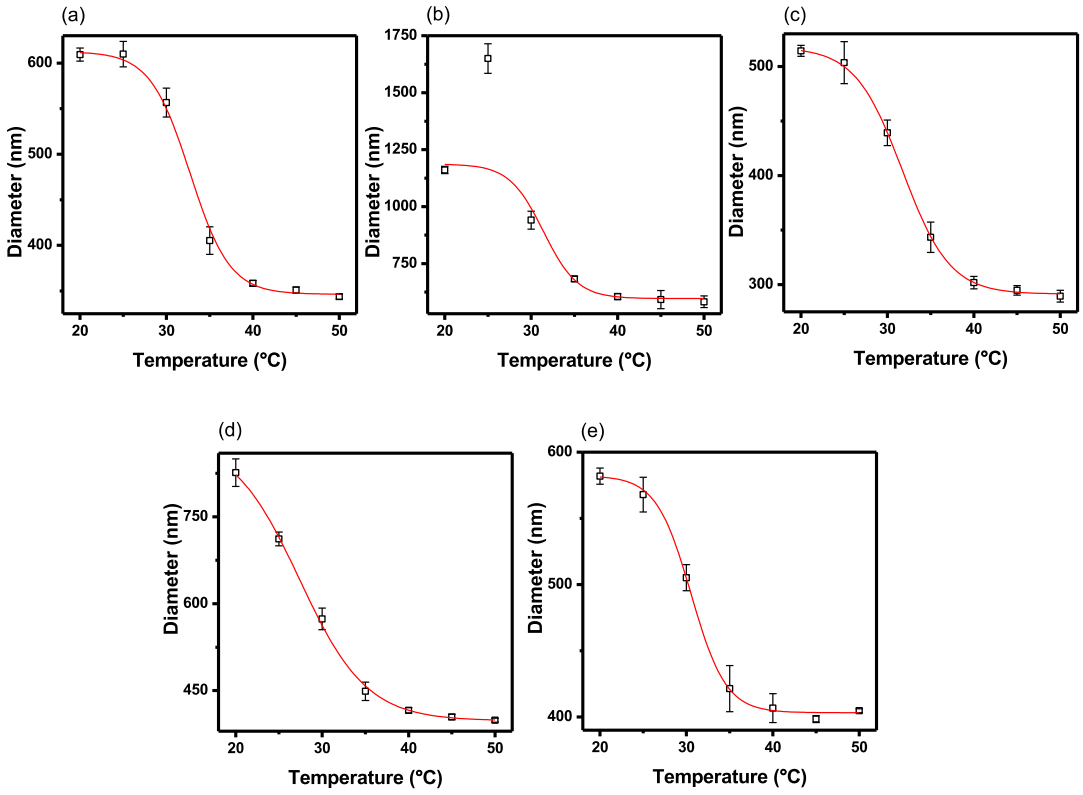

Figure 3-8. DLS microgel diameter as a function of temperature for (a) pNIPAm, (b) pNIPAm-*co*-AAc, (c) pNIPAm-*co*-MAAc, (d) pNIPAm-*co*-EAAc and (e) pNIPAm-*co*-BAAc microgels. Data points represent the average of three measurements, with

error bars representing their standard deviation. Data were fitted to a Boltzmann sigmoidal curve fitting function using OriginLab Pro 8.5 program software.

The response kinetics of pNIPAm-*co*-BAAc and pNIPAm-*co*-AAc microgel-based etalons to temperature was investigated further. The temperature control system was set to increase the solution temperature from ~23 to 60 °C at a heating rate of 0.6 °C s^{-1}. The full response curves for both the pNIPAm-*co*-BAAc and pNIPAm-*co*-AAc microgel-based etalons to this increased solution temperature is shown in Figure 3-9. A single device was used for multiple heating cycles, and each curve in Figure 3-9 represents one heating cycle. Figure 3-9a shows a rapid transition from the swollen to the collapsed state (i.e., a blue shift in reflectance peak position) was observed for the pNIPAm-*co*-BAAc etalon, while the pNIPAm-*co*-AAc etalon (Figure 3-9b) exhibited much slower response kinetics at the same heating rate and solution pH. This observation further supported the hypothesis that the hydrophobic effect (with increased void space) can lead to an increased diffusion rate of water in and out of microgels with increased chain length of the pendant group (BAAc).

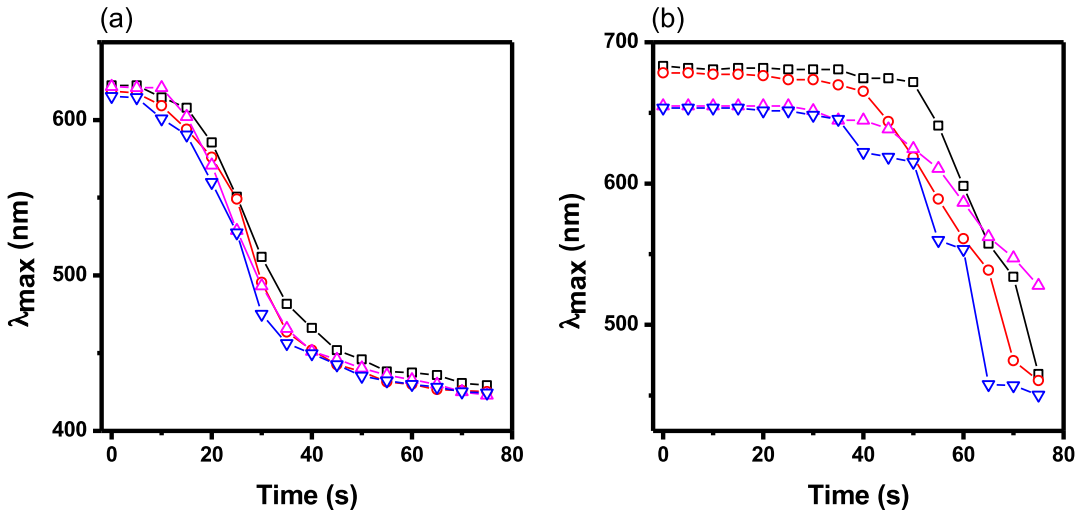

Figure 3-9. Temperature response kinetics for (a) pNIPAm-*co*-BAAc and (b) pNIPAm-*co*-AAc etalons. The temperature was set to increase from ~23 °C to 60 °C at a heating rate of 0.6 °C s^{-1}. A single device was used in each case, and the data obtained as a function of the (black □) first, (red ○) second, (magenta △) third, and (navy ▽) fourth heating cycle.

These results generated interest in knowing the actual composition of the incorporated comonomers and how they might have contributed to the overall kinetics. FTIR measurements on all the microgels synthesized and the ratio of absorbance at 1714 cm^{-1} (carboxylic acid -C=O), to that at 1645. cm^{-1} (amide I -C=O) (Figure 3-10) were compared with results obtained from potentiometric titrations (Figure 3-11). The results from these figures are summarized in Table 3-1. If the actual amount incorporated was the least for pNIPAm-*co*-BAAc but showed the fastest kinetics, it can be concluded that

the kinetic rate was solely dependent on the structural differences in the comonomers used.

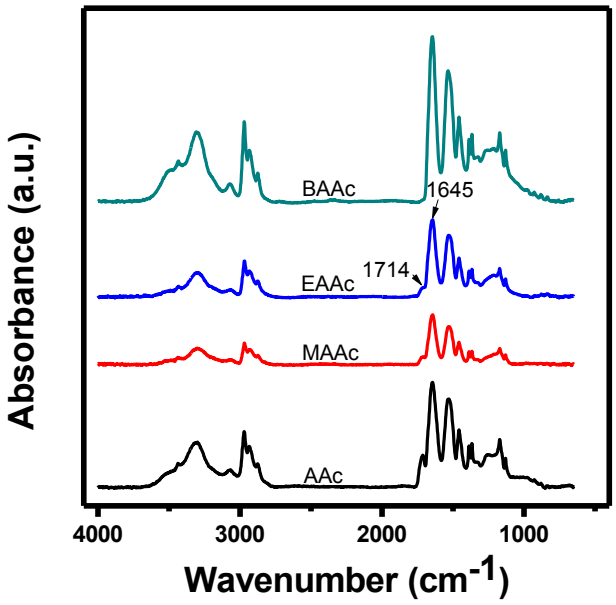

Figure 3-10. FTIR spectra of pNIPAm-*co*-BAAc, pNIPAm-*co*-EAAc, pNIPAm-*co*-MAAc and pNIPAm-*co*-AAc. The ratio of absorbance at 1714 cm^{-1} (carboxylic acid –C=O) to the absorbance at 1645 cm^{-1} (amide I –C=O) was used to estimate the amount of comonomer present in the microgels.

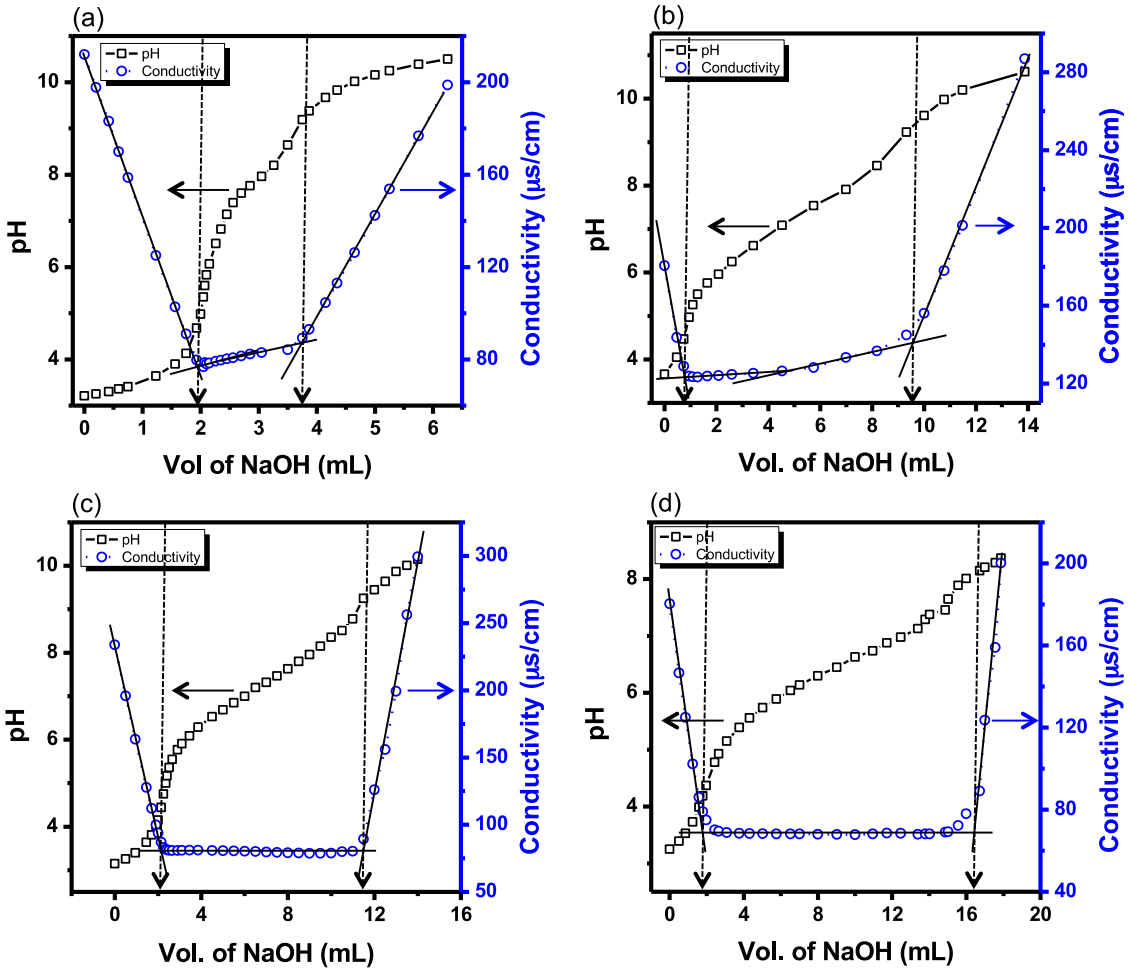

Figure 3-11. Potentiometric and conductometric titration of (a) pNIPAm-*co*-BAAc, (b) pNIPAm-*co*-EAAc, (c) pNIPAm-*co*-MAAc and (d) pNIPAm-*co*-AAc. The initial pH of each microgel was reduced to 3 with 1.0 M HCl and titrated with 0.0101 M NaOH. The first minimum on the conductivity measurement curve shows the volume of NaOH required to neutralize the added HCl, while the second minimum represents the amount of NaOH required to neutralize the acrylic acids in each of the microgels.

Table 3-1. Comonomer feed and compositions in microgel.

Comonomer	Amount added (g)	Amount in microgel (g)[1]	–C=O[2a]	–C=O[2b]	Ratio[2c]
Acrylic acid (AAc)	0.1011	0.0922	0.083	0.274	0.30
Methacrylic acid (MAAc)	0.1207	0.0810	0.021	0.13	0.16
Ethylacrylic acid (EAAc)	0.1405	0.0869	0.022	0.20	0.11
Butylacrylic acid (BAAc)	0.1798	0.0229	0.003	0.43	0.007

[1]Amount estimated from potentiometric and conductometric titration (Figure 3-11). [2a]Absorbance at 1714 cm^{-1} (carboxylic acid –C=O), [2b] absorbance at 1645 cm^{-1} (amide I –C=O), [2c] ratio of absorbance at 1714 cm^{-1} to 1645 cm^{-1} (Figure 3-10).

3.4 Conclusions

pH-responsive microgels that exhibited responses over a broad pH range have been synthesized. Furthermore, optical devices composed of the microgels that exhibited pH dependent optical properties have been generated. As a result of these studies, some of the devices exhibited unusually fast response kinetics, which depended on the length of the pendant group on the acid incorporated in the microgels. Specifically, the response to pH was fastest for the pNIPAm-*co*-BAAc etalons, while the pNIPAm-*co*-AAc etalons exhibited the slowest response. The enhanced response speed for the pNIPAm-*co*-BAAc etalons was a result of the increased hydrophobicity of the pNIPAm-*co*-BAAc microgels, which led to a faster transition to its deswollen state. In addition, the increased chain length created a lower packing density and a less dense internal structure, resulting in a larger interstitial space between chains. This resulted in increased chain mobility,

yielding faster shrinking/swelling kinetics. This hypothesis was supported further by an investigation of the temperature response kinetics, which were improved for the pNIPAm-*co*-BAAc etalons relative to the pNIPAm-*co*-AAc etalons. With this knowledge, low cost and easy to use pH (and related) sensors could be developed for a wide variety of applications where rapid response time is of great importance.

Chapter 4

Controlled Drug Release from the Aggregation–Disaggregation Behavior of pH-Responsive Microgels[c]

This Chapter describes how two sets of independent microgels with different gelation pH were exploited for the capture and controlled release of model drug molecules. The microgels were synthesized by copolymerizing two different comonomers with poly (*N*-isopropylacrylamide) (pNIPAm). The microgels copolymerized with acrylic acid exhibited over 50% negative charge above pH 4.25, while the microgels copolymerized with *N*-[3-(dimethylamino)propyl]methacrylamide exhibited a positive charge below pH 8.4; these microgels are neutral outside these pH ranges. Aggregates were formed when the two independent sets of microgels were exposed to one another in a solution that rendered them both charged. However, in solutions of pH outside the 4.25–8.4 range, the microgels disaggregated, due to one of the microgels becoming neutralized. This behavior was exploited to load (aggregation) and release (disaggregation) a small molecule model drug, methylene blue. This aggregate-

[c] This chapter has been adapted from previously published article: Y. Gao,[†] A. Ahiabu,[†] M. J. Serpe.* *ACS Appl. Mater. Interfaces*, 2014, 6, 13749-13756.

based system is one example of how pNIPAm-based microgels can be used for controlled/triggered drug delivery, which can have implications for therapeutics.

4.1 Introduction

As described in Chapter 1, pNIPAm-based micro and nanogels are synthesized most easily via free radical precipitation polymerization.[165,166] This approach is versatile in terms of the variety of chemical modifications that can be made to the microgels by simply adding functional monomers to the reaction solution prior to the initiation. Using this approach, pNIPAm-based microgels with a variety of chemical functionalities have been synthesized.[167,168] The most commonly used comonomer is acrylic acid (AAc),[169] which renders the pNIPAm-*co*-AAc microgel pH responsive and can also be used to further modify the microgels with other small molecules.[170] The pH responsivity is a result of the pK_a of the AAc group, whose pK_a is ~4.25.[171] Therefore, when the pH of the environment is < 4.25, the AAc groups are protonated and are neutral (although a slight microgel charge can exist, depending on the initiator used), and when the pH > 4.25, the microgels are deprotonated and are negatively charged.

Similarly to the copolymerization of negatively charged species, positively charged microgels can be obtained by copolymerizing with amine-containing comonomers like *N*-[3-(dimethylamino)propyl]methacrylamide (DMAPMA), whose pK_a is ~8.4.[172] Therefore, at pH < 8.4, these microgels are positively charged and exhibit attractive electrostatic interactions with negatively charged species,[173,174] while they have minimal interactions with negatively charged species at pH >8.4. This behavior is reversed completely for AAc-modified microgels, which exhibit attractive interactions

with positively charged species at pH > 4.25. Thus, these microgels are protonated at higher pH and are neutral at lower pH.

As mentioned earlier, stimuli-responsive microgels have been used and developed for drug delivery systems in the past.[175-178] A variety of different stimuli have been engineered into these systems to allow the release of small molecules in a triggered and controlled fashion. The primary triggers for release from microgel-based drug delivery systems are temperature and pH. Microgels have been used as drug carriers by exploiting different forces, such as electrostatic interactions,[179] hydrogen bonding[180] and bioconjugate interactions.[175] The drug molecules can diffuse out of the microgels by exposure to an external environment that interrupts these interactions. In most of the cases, the drug loading process is complex,[181] and the loading efficiency of the microgels (or microgel-based systems) is typically limited owing to the size of the microgels. In light of this, it is imperative to find a more effective way of minimizing these disadvantages, making microgel-based technologies viable for drug delivery.

In this Chapter, a facile method to entrap a small molecule model drug, methylene blue (MB), into microgels by aggregating microgels of opposite charges in the presence of MB was developed. PNIPAm-*co*-AAc and pNIPAm-*co*-DMAPMA microgels were used as negatively and positively charged microgel moieties, respectively. The electrostatic interaction between these two microgels (at a given pH) can cause the formation of large aggregates and a concomitant loading of the drug. Using this approach, it was envisaged that the drug loading efficiency would be dramatically increased. The pH-triggered aggregation of the microgels and the resultant release of MB from the microgels due to disaggregation at a certain pH were investigated and were shown to be a

viable option for a drug delivery system. The size of the microgels is tunable depending on the application at stake.

4.2 Experimental Section

Materials: Unless otherwise specified, all reagents were from Sigma-Aldrich**.** *N*-Isopropylacrylamide (NIPAm) was purified by re-crystallization from hexanes prior to use. *N*, *N'*-Methylene(bisacrylamide) (BIS), acrylic acid (AAc), *N*-[3-(dimethylamnino)propyl]methacrylamide (DMAPMA) and ammonium persulfate (APS) were used without further purification. Methylene blue (MB) was used as the model drug. A UV-Vis spectrometer (Hewlett Packard Diode Array Spectrometer) was used to monitor the release of the model drug. A pH meter (JENCO 6173 pH) was used to prepare the pH solutions using sodium hydroxide (NaOH) and hydrochloric acid (HCl) to adjust the pH. Millipore water (18.2 MΩ.cm) from a Milli-Q Plus system (Fisher, Z00QSVC01) was used. A scanning electron microscope (SEM) (JSM-6010LA JEOL, Peabody, MA.) was used to image the aggregates.

Synthesis of Microgels: pNIPAm-co-AAc. The microgels were synthesized following a previously published procedure.[143,169] A 3-neck flask was fitted with a reflux condenser, nitrogen inlet and temperature probe, and was charged with a solution of NIPAm (11.9 mmol) and BIS (0.703 mmol) in 99 mL deionized water, which was previously filtered through a 0.2 μm filter. The solution was purged with N_2 and allowed to heat to 70 °C for 1.5 h. AAc (1.43 mmol) was added to the heated reaction mixture in one aliquot, and the reaction was initiated immediately with a solution of APS (0.2

mmol) in 1 mL of deionized water. The reaction was allowed to proceed at 70 °C for 4 h under nitrogen. The resulting suspension was allowed to cool overnight and filtered through a Whatman #1 filter paper to remove any large aggregates. Then, the microgel solution was distributed into centrifuge tubes and was purified via centrifugation at ~10000 rpm for ~30 min to form a pellet, followed by removal of the supernatant and resuspending it 6x in deionized water.

pNIPAm-co-DMAPMA. These microgels were synthesized similarly to the above protocol. A 3-neck round-bottom flask was fitted with a reflux condenser, nitrogen inlet and temperature probe, and was charged with a solution of NIPAm (11.9 mmol) and BIS (0.703 mmol) in 99 mL deionized water, which was previously filtered through a 0.2 μm filter. The solution was purged with N_2 and allowed to heat to 70 °C for 1.5 h. DMAPMA (1.43 mmol) was added to the heated reaction mixture in one aliquot, and the reaction was initiated immediately with a solution of APS (0.2 mmol) in 1 mL of deionized water. The reaction was allowed to proceed at 70 °C for 2 h under nitrogen. The resulting suspension was allowed to cool overnight and filtered through glass wool to remove any large aggregates. Then, the microgel solution was distributed into centrifuge tubes and purified via centrifugation at ~10000 rpm for ~30 min to form a pellet, followed by removal of the supernatant and resuspending it 6x in deionized water.

Aggregation of Microgels. A 1:1 (v/v) ratio (50:50 μL) of concentrated microgels of pNIPAm-*co*-AAc and pNIPAm-*co*-DMAPMA was mixed in a glass vial containing 1.0 mL solutions of pH 2, 4, 5, 7, 9, 10 and 12. Specific pH solutions were prepared using HCl and NaOH with the ionic strength (IS) adjusted to 2.0 mM using NaCl.

UV-Vis Spectroscopy. The absorbance of the supernatant solutions from the aggregation studies was measured. In each case, 200 μL of the supernatant from all the pH solutions were diluted with 2000 μL of a solution of the same pH.

Drug Release. Efficient aggregation was observed for microgels mixed at pH 5 and 7; therefore, the drug was loaded in solutions of these pH values and released at pH 2 and 10 (where no or little aggregates were observed). The aggregated microgels were kept in a vial and were placed in a beaker containing either 5 mL of pH 2 or 10 solutions and covered. The temperature was set to 25 °C and stirred at 80 rpm. The release of the drug was monitored every 5 min for 1 h, every 10 min for another 1 h and finally every 20 min until the release profile plateaued. The controlled release of the drug was carried out by loading the drug at pH 5 and releasing it at pH 10 for 4 h, after which 0.1 M HCl was added to decrease the pH of the solution from 10 to 2 while monitoring the release for another 4 h.

Characterization of Aggregates. Scanning electron microscopy (SEM) was done on aggregates formed in solutions of different pH. The samples were taken from pH 2, 5, 7 and 12 solutions and dried for 2 days. Prior to doing the SEM measurements, the

samples were coated with a ~10 nm layer of Au by sputtering.

Zeta Potential Measurement. The zeta potential of the individual microgels was measured in different pH solutions using a Malvern Zetasizer Nano ZS instrument (Malvern, UK) with 633 nm laser at 25 °C. Briefly, about 2 μL each of the concentrated microgel pellets were dispersed in a 1000 μL pH solution (IS 2.0 mM), and 500 μL of these solutions were used for the zeta potential measurement.

4.3 Results and Discussion

The microgels used in this Chapter were synthesized via free radical precipitation polymerization, as previously described.[169] The microgels were composed of functional groups that rendered them negatively or positively charged at a certain pH, while they were neutral otherwise. This is due to the different pK_a values for AAc (~4.25) and DMAPMA (~8.4); therefore, when the pH is below the pK_a of the AAc group, pNIPAm-*co*-AAc microgels are neutral and pNIPAm-*co*-DMAPMA microgels are positively charged. On the other hand, when the pH of the solution is greater than the pK_a for DMAPMA, the pNIPAm-*co*-AAc microgels are negatively charged, while the pNIPAm-*co*-DMAPMA are neutral. In the range of pH 4.25–8.4, both sets of microgels are charged to different extents, which leads to various degrees of pNIPAm-*co*-AAc/pNIPAm-*co*-DMAPMA microgel aggregation when they are mixed. During the aggregation, small molecule model drugs in the surrounding solution can be trapped inside the aggregates, as depicted in Scheme 4-1. This phenomenon is in accordance with the scrambled egg model.[174] In this Chapter, the dye molecule methylene blue (MB) was

used as a model drug; its structure is shown in Scheme 4-1. MB is a positively charged molecule that is independent of solution pH.

Scheme 4-1. Aggregate formation and the trapping of a model drug (methylene blue) when microgels are mixed at pH values that render both microgels charged.

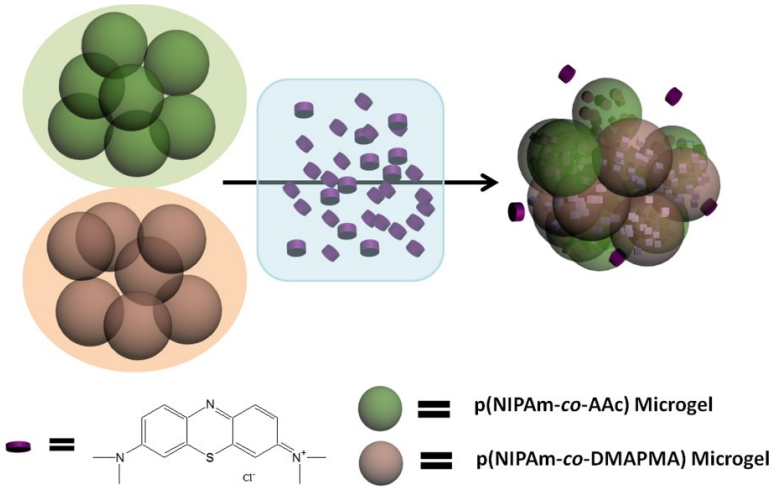

To evaluate the aggregation behavior, the microgels were mixed together at various pH values. A photograph of the aggregated microgels themselves without MB at different solution pH values is shown in Figure 4-1. The microgels at pH 2 and 12 did not visually aggregate, and the microgel solution remained turbid, indicative of the microgels remaining dispersed in the solution. This is quite different when the microgels are mixed together at pH 5 and 7, where the microgels visually aggregated into large structures.

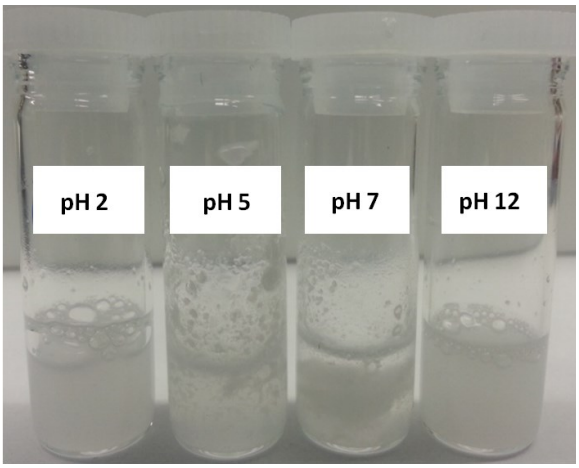

Figure 4-1. A photograph of microgel-based aggregates in solutions of the indicated pH values.

To investigate further the aggregation behavior, their size and morphology were evaluated using scanning electron microscopy (SEM), and the results can be seen in Figure 4-2. At pH 2 and 12, the SEM images clearly show that the microgels are not aggregated and appear individually on a substrate. However, at pH 5 and 7, a large aggregate was formed, with a size of about 2 mm x 4 mm, which is big enough to be seen visually. Most of the microgels were involved in the formation of the aggregates, which left the solution less turbid (because there were minimal microgels left unaggregated in the solution). The relative differences in the sizes of aggregates are shown in Figure 4-3. The SEM images show that the aggregates are tightly bound to one another; this increased their ability to uptake model small molecule drugs. This was due to the interstices between the aggregated microgels that effectively trap the small molecule, as shown previously for water remediation applications.[94,98,182,183]

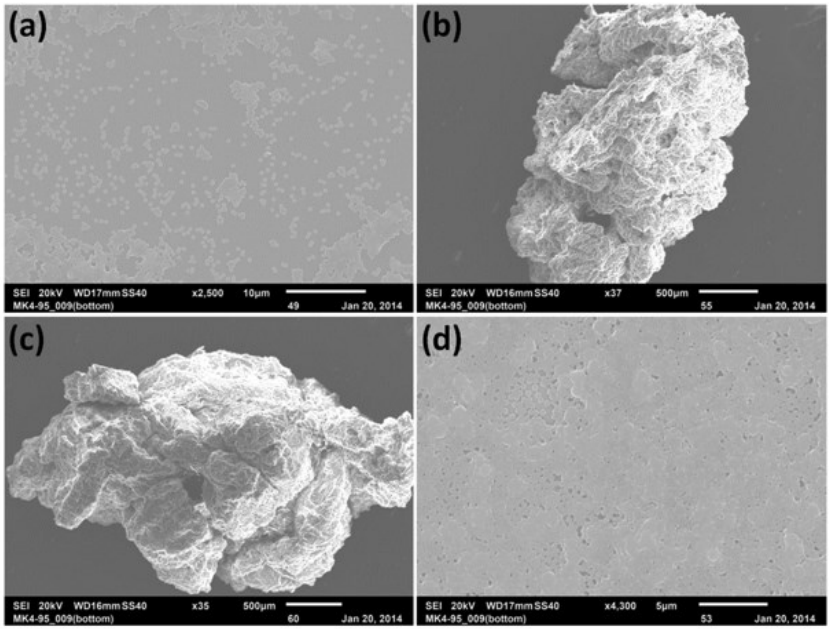

Figure 4-2. Scanning electron microscope (SEM) images of samples recovered after the two sets of microgels were mixed in solutions of pH (a) 2; (b) 5; (c) 7; (d) 12.

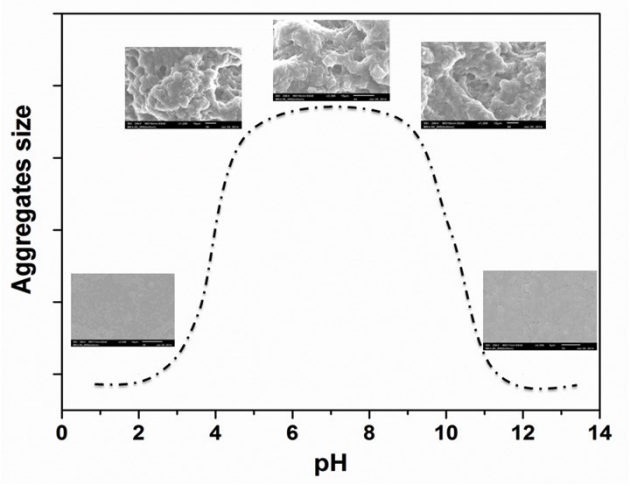

Figure 4-3. SEM images showing the relative aggregate sizes of the microgels at different pH values. Films were made for pH 2 and 12 since they did not form any

obvious aggregates. The aggregates from pH 5, 7 and 10 were freeze-dried and imaged.

When aggregates are formed in the presence of the dye molecule MB, the most efficient trapping is expected at pH 5, 7 and 9, while the least amount of aggregation is expected at pH 2 and 12. To generate the aggregates in the presence of MB, 1.0 mL of 0.5 mg/mL MB solution was added to the individual glass vials and diluted to a total volume of 10 mL with the appropriate pH solution, bringing the final concentration of MB to 0.05 mg/mL. For these experiments, pH solutions of 2, 4, 5, 7, 9, 10 and 12 were used; the solutions were vivid blue in each case, as can be seen in Figure 4-4a. Then, 50 μL of each microgel, directly taken from a centrifuged microgel pellet (see Experimental Section), were added one at a time to these pH solutions; pNIPAm-*co*-AAc microgels were always added to the solution first, immediately followed by pNIPAm-*co*-DMAPMA microgels.

The aggregates were formed upon addition of the two microgels to the appropriate pH solution. Figure 4-4b shows the dye was trapped inside the microgels that were aggregated in solutions of a certain pH, as is evidenced by the color of the aggregates and the associated decoloration of the solution. Almost no visual aggregates were formed in solutions of pH 2 and 12 (where one of the microgels is neutral, while the other is charged), while large aggregates were formed at pH 5, 7 and 9. Some aggregates were formed at pH 4 and 10 (near the two different pK_a values). This can be explained by the dissociation constant of the individual comonomers shift in a polymeric system;[184] however, these aggregates were much less efficient at trapping MB. To investigate

whether the MB dye molecules contributed to the formation of the aggregates, two control experiments were conducted; the results are shown in Figure 4-5. The addition of only one set of microgels to MB solutions of the various pH values had no effect on the aggregation state of the microgels, meaning that the aggregation is achieved only when the different microgels are together in their charged state.

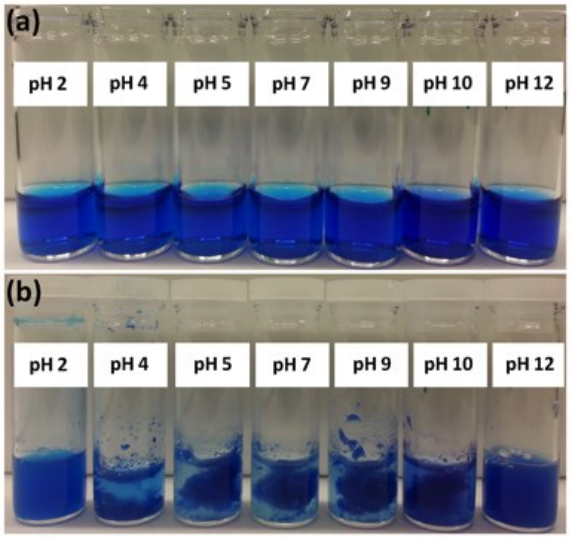

Figure 4-4. Photographs of methylene blue (MB) solutions at the indicated pH (a) before and (b) after addition and aggregation of the individual sets of microgels.

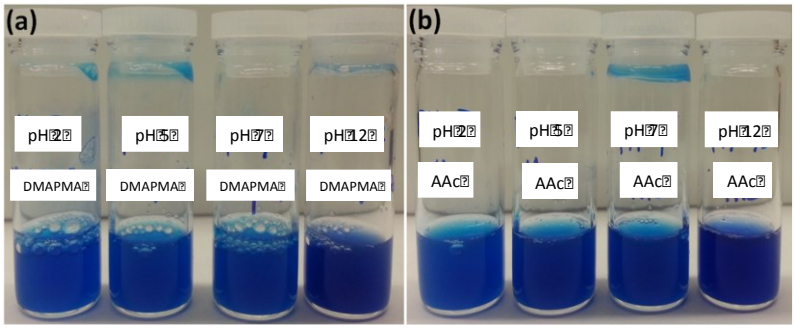

Figure 4-5. A control experiment with (a) only pNIPAm-*co*-DMAPMA microgels and (b) pNIPAm-*co*-AAc microgels at different pH values. This indicated that aggregation can only be achieved when the two microgels are mixed in their charged states.

Prior to studying the drug release properties of the aggregates, the ability of the aggregates to trap MB at the different pH values was investigated further. To do this, the absorbance of MB solutions was measured by UV-Vis spectroscopy, before and after the formation of aggregates, and after they have been removed from the MB solutions. Specifically, 200 µL of the MB solution (0.05 mg/mL) were diluted with 2.0 mL of a given pH solution, and the initial absorbance measured. In this case the absorbance value was measured at MB's λ_{max} of 664 nm (the full spectrum can be seen in Figure 4-6), and the results are shown in Figure 4-7.

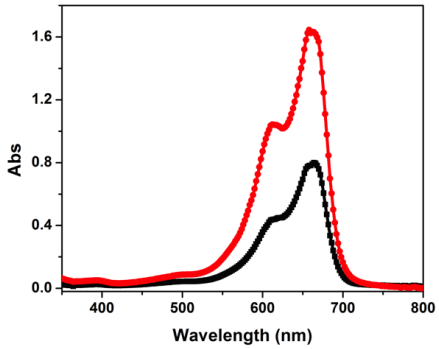

Figure 4-6. UV-Vis absorption spectrum for methylene blue at pH 5 (red) and pH 10 (black).

As can be seen, the solution pH minimally affects MB's optical properties. Similarly to what was observed above, the amount of MB left in solution after the aggregation of the microgels depends dramatically on pH. The most MB was removed from solution at pH values where the most efficient aggregation occurred. However, the absorbance of the remaining solutions when the "aggregates" were formed at pH 2 and 12 was high due to the presence of excess MB.

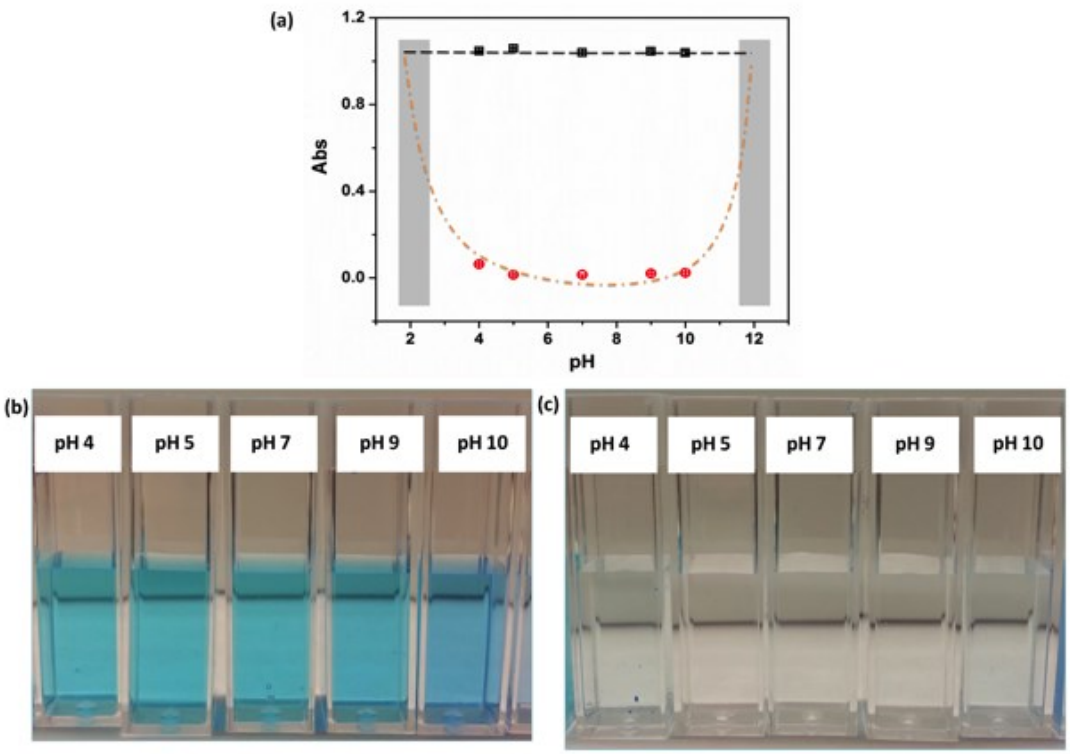

Figure 4-7. (a) UV-Vis absorbance values from MB solutions at the indicated pH (□) before and (●)□after microgel aggregation (and removal from solution). Photographs of the remaining solutions at the indicated pH (b) before and (c) after microgel aggregation.

---

pNIPAm-*co*-AAc microgels are negatively charged at high pH, which allows them to bind electrostatically with MB. However, the aggregation has a much greater effect on the uptake than electrostatics alone (see Figure 4-8). In this case, there are no aggregates formed, but the negative pNIPAm-*co*-AAc microgels will interact electrostatically with positive MB molecules. Zeta potential measurements of the individual pNIPAm-*co*-AAc and pNIPAm-*co*-DMAPMA microgels, shown in Figure 4-9, further confirm this aggregation behavior. At the extreme pH values (i.e., pH 2 and 12), only one set of the

microgels is charged (for example, pNIPAm-*co*-AAc is negatively charged at pH 12, while pNIPAm-*co*-DMAPMA is positively charged at pH 2, as shown in the shaded regions of Figure 4-9). However, at pH ranges between these shaded portions, the two sets of microgels have strong opposite charges, which promotes the formation of aggregates.

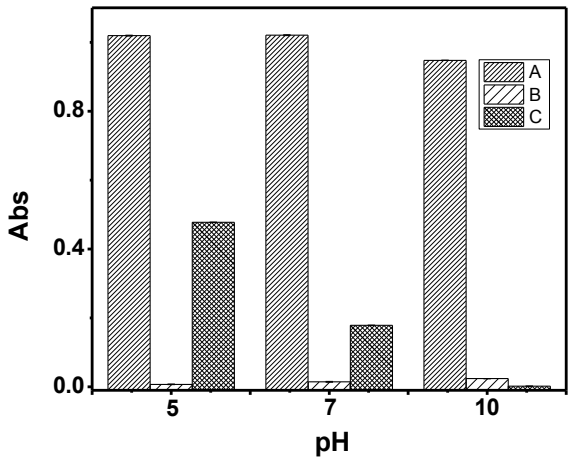

Figure 4-8. Absorbance values for MB solutions at the indicated pH values. (A) MB solutions before addition of microgels, (B) after microgel aggregation and (C) after addition of just the pNIPAm-*co*-AAc microgels alone and centrifugation to remove the microgels from solution. The electrostatic interaction between MB and the pNIPAm-*co*-AAc microgels becomes stronger as the solution pH increases. This leads to more uptake of MB and less MB left over in solution even though, at this pH, the amount of MB left over in solution after aggregation is the same, indicating that the aggregates are able to trap MB in addition to the electrostatic interactions.

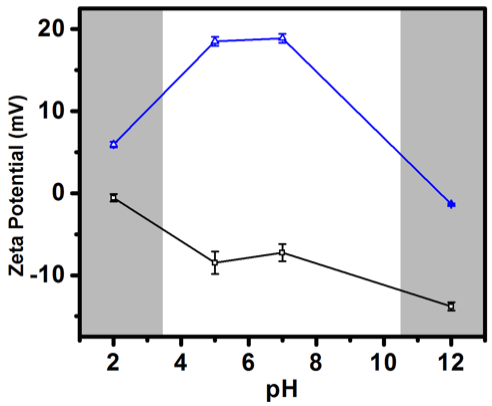

Figure 4-9. Zeta potential measurements of individual pNIPAm-*co*-AAc (black) and pNIPAm-*co*-DMAPMA (blue) microgels at different pH values. Shaded regions indicate regions of no aggregate as only one of the microgels is charged at those extreme pH values. Aggregates are expected for the microgels mixed at any pH values between these shaded portions.

Next, the ability of the aggregates to release MB at different pH values was investigated. This was done by isolating the aggregates formed at pH 5 and 7 and exposing them to solutions that have pH values rendering one of the sets of microgels neutral. To do this, a glass vessel containing 5.0 mL aqueous solution (either pH 2 or 10) was placed on a temperature controllable hot plate at 25 ^{o}C while the solution was stirred at 80 rpm. Then, a small vial containing the MB loaded aggregates was immersed into the glass container such that the liquid filled the small vial and contacted the aggregates; a timer was started at this point. The whole assembly was covered with a glass slide to prevent the water from evaporating. The aggregates were placed in the small vial to keep them from becoming damaged from the stirring. At given time intervals, 2.0 mL of the

solution were removed from the release vessel, and a UV-Vis spectrum acquired. In pH 2 solutions, the absorbance was taken every 5 min for the first hour, then every 10 min for the second hour and every 20 min for the third hour, until the release profile plateaued. In pH 10 solutions, the release was slow (due to the AAc charge). Therefore, the absorbance was taken at less frequent intervals. Following each UV-Vis measurement, all the liquid was carefully returned to the release vessel. The experimental setup is summarized in Scheme 4-2, while the results are shown in Figure 4-10. Figure 4-10a shows the release profiles for aggregates formed at pH 5. The MB is released very quickly from the aggregates at pH 2, with the release completing in ~ 5 h. At pH 10, the release was so slow that the absorbance was still lower than 0.2 even after 50 h, which is much slower than the release at pH 2 (absorbance reached this value in 15 min).

Scheme 4-2. A schematic representation of the drug release experimental set up.

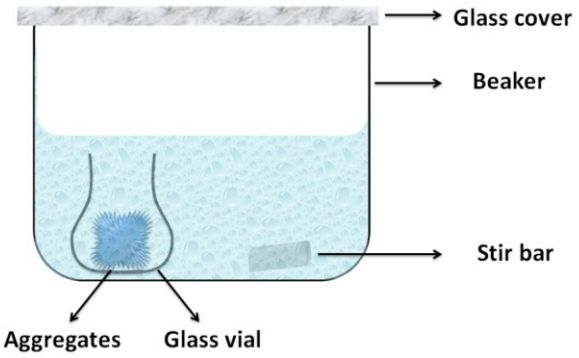

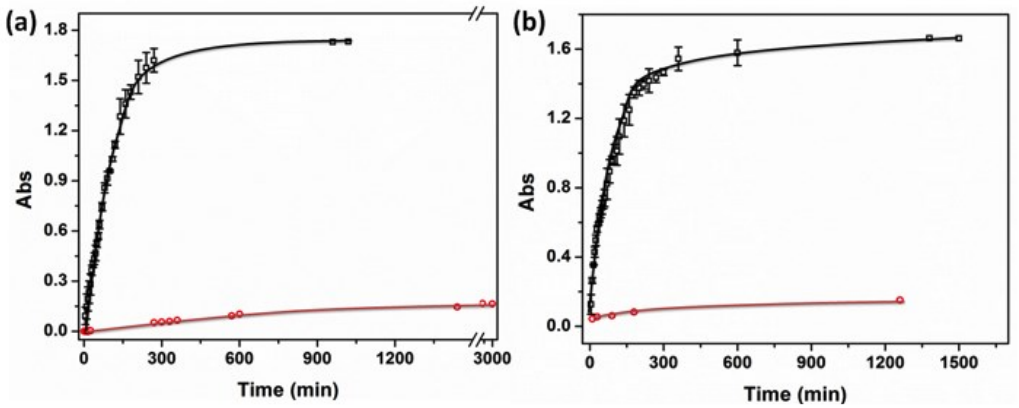

Figure 4-10. Drug release profiles in (□) pH=2 and (●) pH=10 solutions for aggregates formed at (a) pH=5 and (b) pH=7 solutions. Each point is the average of 3 individual experiments, while the error bars are their standard deviations.

Therefore, the MB can be released at a rate that is controlled by the pH. Figure 4-10b shows the same experiments, but for the aggregates formed at pH 7. The same phenomenon was observed for these aggregates; a very fast release for the aggregates exposed to a pH 2 solution, while a very slow release at pH 10. At a lower pH (~2), the electrostatic interaction between microgels disappeared and disaggregation occurred, making the diffusion of the MB molecules out of the microgels much easier. At the same time, pNIPAm-*co*-DMAPMA microgels are positively charged at this pH, giving rise to a repulsive force with the positively charged MB molecules. Hence dramatically increasing the diffusion of MB out of the microgel aggregates. Therefore, the disaggregation and repulsive forces, in combination with the AAc neutralization, are the collective forces that contribute to the faster release at pH 2. However, at pH 10, while the aggregates were still broken up due to the neutralization of the pNIPAm-*co*-DMAPMA microgels,

the pNIPAm-*co*-AAc microgels are fully negatively charged, causing them to form attractive electrostatic interactions with MB molecules (Figure 4-8). This makes the release of MB from the aggregates much slower. Photographs of the solution after releasing at different pH values are shown in Figure 4-11. One can see clearly that even after releasing, the solution color turned blue at pH 2 solution, while it is almost colorless in pH 10.

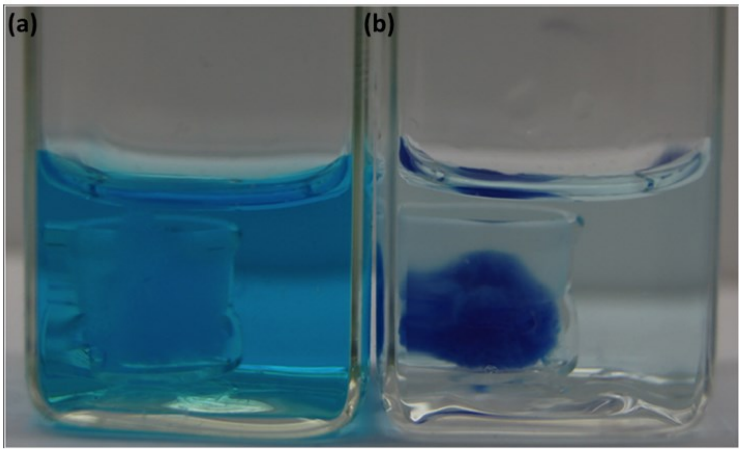

Figure 4-11. A photograph of the release of MB from the aggregates at (a) pH and at (b) pH 10.

Following this, the ability of the aggregates to release MB in a pH-triggered fashion was investigated. The aggregates were first immersed in a pH 10 solution and the release profile was measured over ~4 h. Next, the solution pH was reduced from pH 10 to 2 by the addition of HCl, and the release was monitored continuously. The results are shown in Figure 4-12. When the pH was changed from 10 to 2 at 270 min, the

absorbance increased immediately, eventually stabilizing at 0.8. This result shows that changing the pH can trigger the release of the model drug MB.

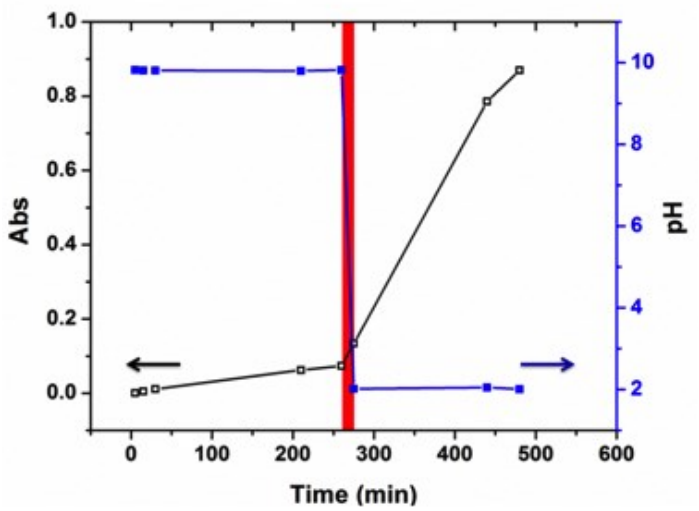

Figure 4-12. Triggered small molecule release from the microgel-based aggregates upon changing the solution pH from 10 to 2 at the time indicated by the shaded region.

4.4 Conclusions

pH responsive microgels that exhibited opposite charges over a given solution pH range were synthesized. The microgels aggregate when they are mixed in this pH range. This was used to trap/load a small molecule model drug, methylene blue. The loading efficiency was greater when the microgels aggregated in comparison to simply relying on electrostatic interactions for loading. Finally, methylene blue was released in a pH-dependent fashion over many hours/days under certain pH conditions. This was a clear demonstration of how microgel-based technology could be used for health related

applications, which could be used to release biologically relevant molecules at low pH environments typically found at tumour sites.

Chapter 5

Poly (*N*-Isopropylacrylamide)-Based Microgels as Sorbents for Pb^{2+} and Cd^{2+} Removal: Effect of Comonomer and Crosslinking Densities

Previously, the Serpe group has used poly (*N*-isopropylacrylamide)-based microgels and their assemblies as sorbents for the remediation of organic dyes.[94-98] The focus of this Chapter is on the use of these sorbents for the removal of toxic contaminants, using Pb^{2+} and Cd^{2+} as models. The influence of the microgel composition and comonomer contents on the removal efficiency is highlighted. The plausible sorption mechanism is presented also.

5.1 Introduction

Though natural causes exist, increased industrialization and anthropogenic activities have been the major contributors to environmental issues. The rising population is faced with threats, not only of water scarcity but also of access to quality water; more than a third of the human population is at risk of lack of safe drinking water.[73] Some toxic chemicals may degrade into less toxic forms after being discharged into the environment

for a long period of time. Heavy metals, however, do not degrade and may accumulate in an organism's body via the food chain. Heavy metal contamination has emerged as a great threat to the human race. Some of the contaminants of great concern are lead (Pb^{2+}) and cadmium (Cd^{2+}). Severe brain and kidney damage can occur at a high level of exposure to lead and may even result in death.[185] Industrial wastes from lead smelting, lead mining, dyeing, printing and rubber production have contributed to the increased sources of lead, and these sometimes find their way into the environment. Cadmium, on the other hand, has numerous applications in alloys, pigments, electroplating, nickel–cadmium batteries and many more. The wide spread applications of cadmium have paved the way for their ease of being transferred to animals and humans via smoke in the air, water and food, and their subsequent accumulation in the body. Like lead, long-term exposure to cadmium has a detrimental influence on the lungs, heart, bones and more importantly, the kidneys.[186]

There has been growing interest in finding efficient ways of removing contaminants from the environment, specifically from water. This is evident in the numerous studies that have been done in using different remediation technologies as applied to water decontamination. Among them are membrane filtration,[187,188] precipitation, coagulation[189-191] and adsorption.[192,193] Most of these technologies pose additional threats of leaving byproducts that are themselves potential hazards.[86] Adsorption technology has emerged as the method of choice in water remediation due to its simplicity, convenience and low cost.[192,193] In the current literature, carbon materials (for e.g., activated carbon, graphene, carbon nanotubes and carbon foam),[194-196] chitosan composites,[197] nanosized metal oxides[198] and low-cost adsorbents[199-202] have been shown

to be a promising choice for contamination control. However, most of these materials, used as adsorbents, are faced with the challenge of high production cost compared to other emerging adsorbents.[199-202] One of the greatest drawbacks to carbon based materials is the difficulty with their reusability.[203] The cost of regenerating these materials for reuse is comparable to producing fresh adsorbents; therefore, it is not viable economically to regenerate them. The problem is the large footprint of carbon that is left as a result of not regenerating these materials for reuse. In lieu of this, researchers have been looking into using low cost adsorbents in water remediation.

Recently, the use of polymeric materials, such as microgels, as sorbents has become attractive due to their facile means of synthesis and their ability to be regenerated for reuse. Our lab focuses on developing polymer and polymer-based (specifically microgels) materials for a myriad of applications, including sensing and biosensing,[32,124,204] drug delivery[17,55,56,67] and water remediation.[94-98] Microgels composed of poly(*N*-isopropylacrylamide) (pNIPAm) possess porous network structures, and have been shown to remove heavy metal ions.[205,206] The mechanism of removal has been thought to be mainly by absorption, whereby the networked microgel structure "entraps" contaminants at temperatures below the lower critical solution temperature (LCST) of 32 °C. Snowden and coworkers believed that the contaminants are "squeezed" out above the LCST, and that this system can act as a capture and release system for contaminants.[205] However, the same is not true for microgels with increased charge density. One of the promising and common means of increasing the charge density is by copolymerizing NIPAm with ionizable groups. The most common of these are acid ionizable groups, detailed in Chapter 1, specifically with acrylic acid backbones. Snowden and others have

studied the adsorption of lead onto *N*-isopropylacrylamide and acrylic acid copolymer microgels. These microgels tend to be pH sensitive. Hence, their adsorption of heavy metal ions is pH dependent. For instance, AAc has a pK_a of 4.25, and at a pH below 4.25, microgels composed of AAc remain neutral whereas at pH above 4.25, these microgels are ionized and present a larger charge density for enhanced adsorption. Thus, the presence of hydroxyl groups at high pH enhances adsorption of metal ions through coordination as well as via electrostatic interactions. The adsorbed metal ions are desorbed upon lowering the solution pH to below the pK_a of the ionizable group.

As shown in Chapter 3, the microgels made of varying acrylic acid backbones have different response kinetics to solution pH. This Chapter demonstrates how this difference in response kinetics resulted in different adsorption efficiency. Microgels made of varying composition of NIPAm and AAc (pNIPAm-*co*-AAc), NIPAm and MAAc (pNIPAm-*co*-MAAc) and NIPAm and BAAc (pNIPAm-*co*-BAAc) were synthesized by free radical precipitation polymerization; they were characterized previously in Chapter 2. Microgels with various degrees of crosslinking density were synthesized and characterized by scanning electron microscopy (SEM). These microgels were used in the removal of heavy metal ions, such as Cd^{2+} and Pb^{2+}, and quantified using an inductively coupled plasma-optical emission spectrometer (ICP-OES). The results obtained are in accordance with the previous studies described in Chapter 3;[57] microgels with increased alkyl chains in the backbone resulted in enhanced sorption capacity.

5.2 Experimental Section

*Synthesis of microge*ls. Free radical precipitation polymerization was employed to synthesize microgels similarly to a previously published procedure.[143,144] NIPAm (11.928 mmol) and BIS (0.702 mmol) were weighed into a 250 mL beaker with 99 mL deionized water. The mixture was stirred for 0.5 h on a stir plate and was filtered through a 0.2 μm filter into a 3-neck round-bottom flask. A reflux condenser was added to the flask, along with a N_2 gas inlet (needle) and a temperature probe. The solution was bubbled with N_2 gas and heated to 70 °C for 1.5 hr. BAAc/MAAc/AAc (1.403 mmol) was added to the heated reaction mixture in one aliquot, and the polymerization was initiated immediately by the addition of APS (0.2 mmol) in 1 mL of deionized water. The solution turned white/cloudy after ~ 1 min, indicating the successful initiation. Then, the reaction was allowed to proceed at 70 °C for 4 h under N_2 gas. The resulting suspension was allowed to cool overnight, followed by filtration through glass wool to remove any large aggregates. The microgel solution was distributed into centrifuge tubes and purified via centrifugation at ~10000 rpm for ~30 min to form a pellet, followed by removal of the supernatant and resuspending them in deionized water; this was repeated 6x. The purified microgels were stored for further use.

Adsorption experiment. A 10 mg/mL microgel solution at pH 7 with ionic strength (IS) 6 mM was prepared by adjusting the pH with 1.0 M NaOH and the IS with NaCl. Different concentrations of Pb^{2+} and Cd^{2+} were prepared from a 1000 ppm stock solution and spiked into 5 mL of a 10 mg/mL microgel solution, bringing the total volume to 25 mL using a pH 7 and 6 mM IS solution. The sorbent dose was studied by loading 10 ppm Pb^{2+} with final microgel solutions of 200 ppm or 2000 ppm, which were

allowed to stir on a gyration shaker for 1 h and then centrifuged at 10000 rpm for 30 min at 23 °C. The supernatant was removed carefully and analyzed for Pb^{2+} by ICP-OES, after acidification with 2 % (*wt/vv*) HNO_3.[206,207] The adsorption experiment is shown schematically in Scheme 5-1. The following equation was used to calculate the removal percentage of heavy metal ions by the microgel from a calibration curve, shown in Figure 5-1 for the respective heavy metal ions:

$$Uptake\ \% = \frac{Co - Ce}{Co} x\ 100\% \qquad (5\text{-}1)$$

where c_o is the initial concentration of sorbate, c_e is the equilibrium concentration, which is determined from the calibration curve of a series of concentrations of either Pb^{2+} or Cd^{2+}. The experiment was repeated, but for 15 h of contact, in order to estimate the minimum contact time required for sorption. The solution was centrifuged as described previously, and the supernatant analyzed by ICP-OES.

Scheme 5-1. A schematic presentation for the removal of heavy metal ions by the microgels and their quantitation by ICP-OES. MG represents microgels and M^{n+} represents metal ions.

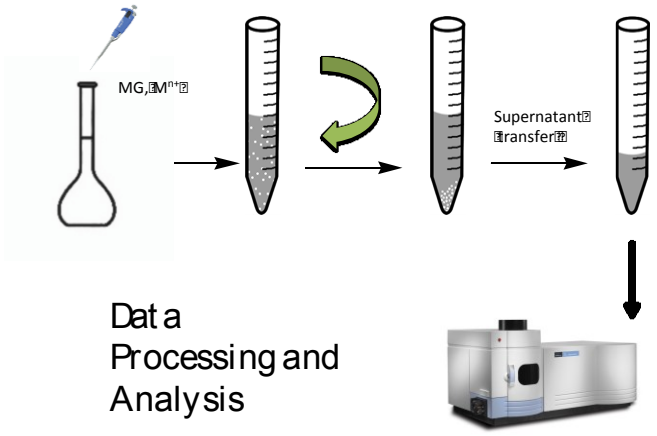

5.3 Results and Discussion

One of the hypothesized sorption mechanisms between the heavy metal ions (Cd^{2+} and Pb^{2+}) and the microgels was via electrostatic interaction, as shown in Scheme 5-2. Therefore, it was important to identify the role that pH plays on the removal of these ions. The effect of pH on adsorption of Pb^{2+} was studied using pNIPAm-*co*-BAAc at pH values from 3–11. To study the effect of pH on Pb^{2+} adsorption, the Pb^{2+} solution and the microgel solutions were all acidified to pH 2 and at IS of 6 mM. Then, the pH values of the mixture of Pb^{2+} and microgel solution for the adsorption experiment were adjusted with NaOH from pH 3–11. A calibration curve was established from standard Pb^{2+} and Cd^{2+} solutions, from which the amounts of Pb^{2+} and Cd^{2+} sorbed were calculated, as shown in Figure 5-1.

Scheme 5-2. Proposed sorption mechanism for Cd^{2+} and Pb^{2+} by microgels.

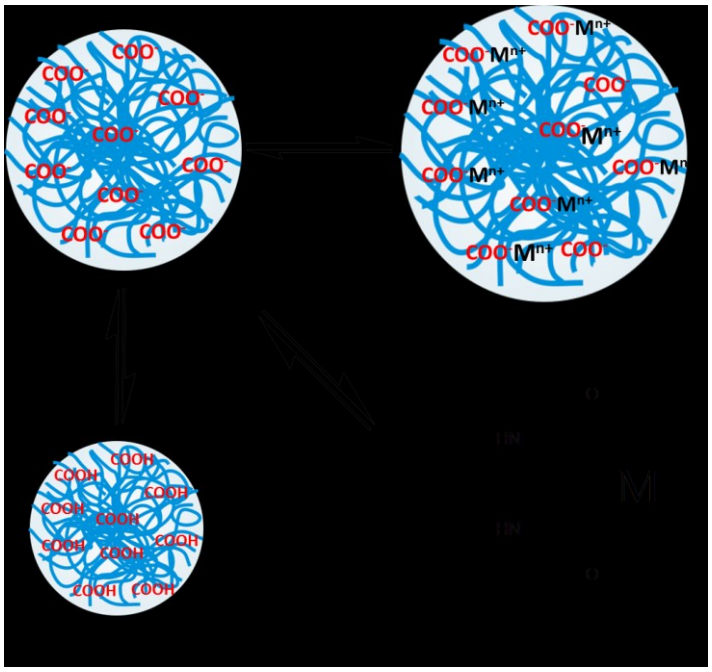

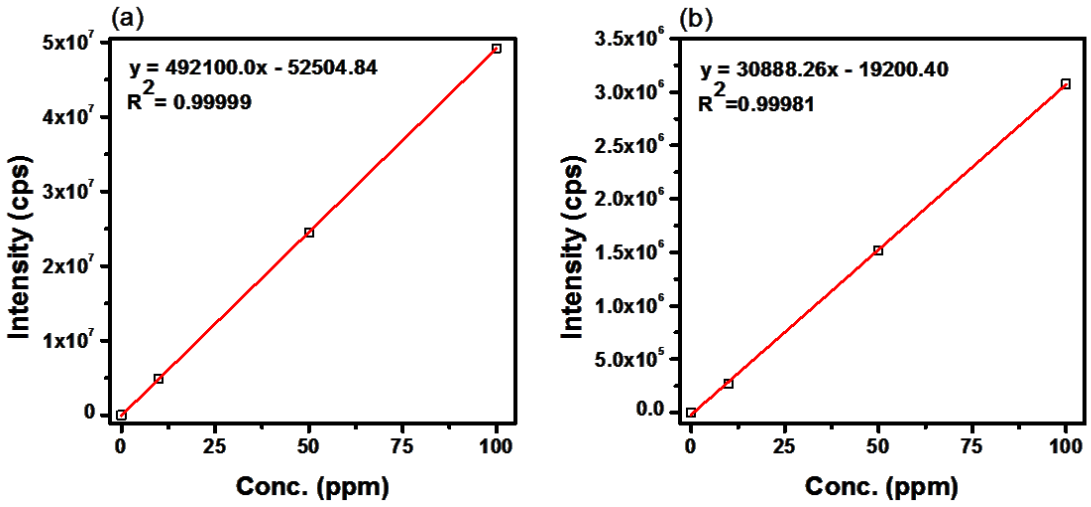

Figure 5-1. Calibration curves for (a) Cd^{2+} (226.502 nm) and (b) Pb^{2+} (220.353 nm) used to quantify the amount of Cd^{2+} and Pb^{2+} sorbed by the microgels. The straight line in each plot is a linear fit to the data using OriginLab Pro version 8.5 program software.

Because of the incorporation of ionizable groups in the microgels at the time of synthesis, the solution pH is hypothesized to play a critical role in the adsorption efficiency of heavy metal ions, as can be seen in Figure 5-2. An increase in the solution pH caused the metal ions to be hydrolyzed,[206] and at the same time deprotonation of the carboxylic acid groups of the microgel occurred. There was an overall increase in adsorption efficiency as the solution pH increased, plateauing at pH 7–10. The slight decrease in the adsorption efficiency beyond pH 10 at 25 °C can be attributed to the state in which lead or cadmium ion exists (either $M(OH)^+$ or $M(OH)_2$).[206] At this point, removal by precipitation dominates over adsorption. However, at lower pH values, the binding capacity may decrease as hydronium ions compete with the target heavy metal ions for their active

sites. Instead, as the pH increased, competition from the electrostatic repulsion force and the hydronium ions both decreased; hence, a gradual increase in uptake efficiency was observed. High sorption capacities were observed at pH values near the pK_a of the acid comonomer. This trend was expected because at such pH levels, the microgels are in their deprotonated states and can interact with metal ions via electrostatic interaction, as shown in Scheme 5-2. As pNIPAm is thermoresponsive, the influence of temperature on the uptake efficiency was studied at a temperature above (40 °C) and below (25 °C) the LCST (32 °C). The results from Figure 5-2 revealed that temperature did not influence the removal efficiency significantly, except at a higher pH (>10). As mentioned, the primary removal mechanism at these pH values is by precipitation rather than adsorption. Hence, the removal efficiency is expected to be higher at temperatures above the LCST. Above the LCST, pNIPAm-based microgels are said to precipitate[208,209] out of their medium and thus contribute to the enhanced sorption at higher pH values.

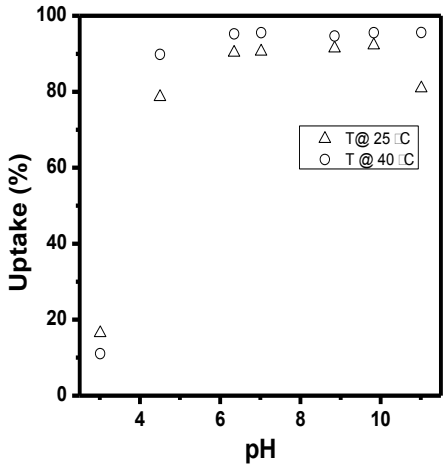

Figure 5-2. Influence of pH and temperature on 10 ppm lead uptake by 2000 ppm pNIPAm-*co*-BAAc (10Bu-10B). Error bars are about the size of the data points and have been omitted.

The influence of contact time on sorption studies is important to maximize the sorption of metal ions as well as the efficient use of time. In most adsorption experiments, maximum sorption have been observed for sorbents spanning contact times of >1 h.[210-212] However, in this Chapter, the maximum sorption efficiency was observed within 1 h of contact time. Hence, increasing the contact time to about 15 h, as shown in Figure 5-3, did not result in any significant change in the sorption efficiency. It is hypothesized that a shorter contact time is possible, however, this is currently limited owing to the time required to centrifuge the microgels.

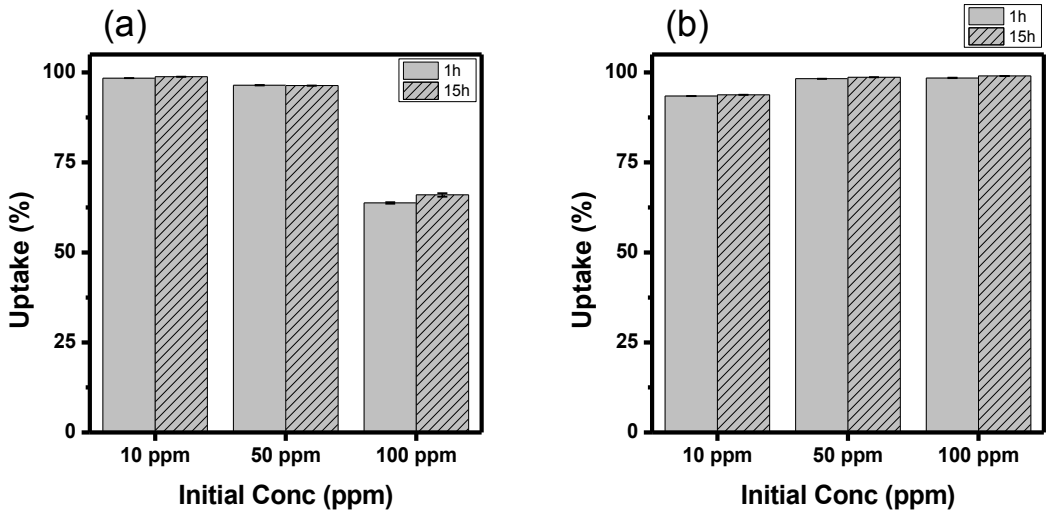

Figure 5-3. Contact time comparison on removal efficiency of (a) Cd^{2+} and (b) Pb^{2+} ions. A sorbent dose of 2 mg/mL of microgel solution was used in a 25 mL total

volume, with 10 ppm initial concentrations of the ions. The error bars represent the standard deviation of three measurements.

Again, to support further the hypothesis that a contributing factor to the sorption mechanism was due to an electrostatic interaction, different mole percent values of AAc groups were incorporated during the synthesis of the microgel. Increasing the charge density of ionizable groups led to increased sorption sites for heavy metal ions. Therefore, increasing the mole percent of AAc in the microgel led to an enhanced sorption efficiency, as can be seen in Figure 5-4. This shows further that the major contributor to the sorption mechanism is via electrostatic interaction involving the charged carboxylate groups from the AAc moieties and the metal ions. Although almost insignificant (in the case of Cd^{2+} ions, shown in Figure 5-4a), the minimal uptake of Pb^{2+} ions solely by pNIPAm (0A-5B), shown in Figure 5-4b, stems from the coordination bond between lone pairs of electrons on O and N atoms, which are donated into the empty orbitals of the metal ions, as depicted in Scheme 5-2. About 100% (>98%) uptake efficiency was observed for an initial sorbate dose of 10 ppm Cd^{2+} or Pb^{2+} ions, as shown in Figure 5-4, as the mole percent of AAc was increased from 0 to 10% while keeping the crosslinking density at 5 mole percent.

To demonstrate further the contribution of coordination to the overall sorption mechanism, the effect of the crosslinking density was investigated while keeping the mole percent of AAc constant. As shown in Figure 5-5, an increase in the crosslinking content from 5 to 10 mole percent resulted in an increase in the removal efficiency of Cd^{2+} ions. No significant increase in removal efficiency was observed for Pb^{2+} ions,

except at elevated sorbate concentrations. The marginal increase in removal efficiency of these metal ions at higher crosslinking density is attributed to the enhanced coordination sites presented by the increased crosslinking density.

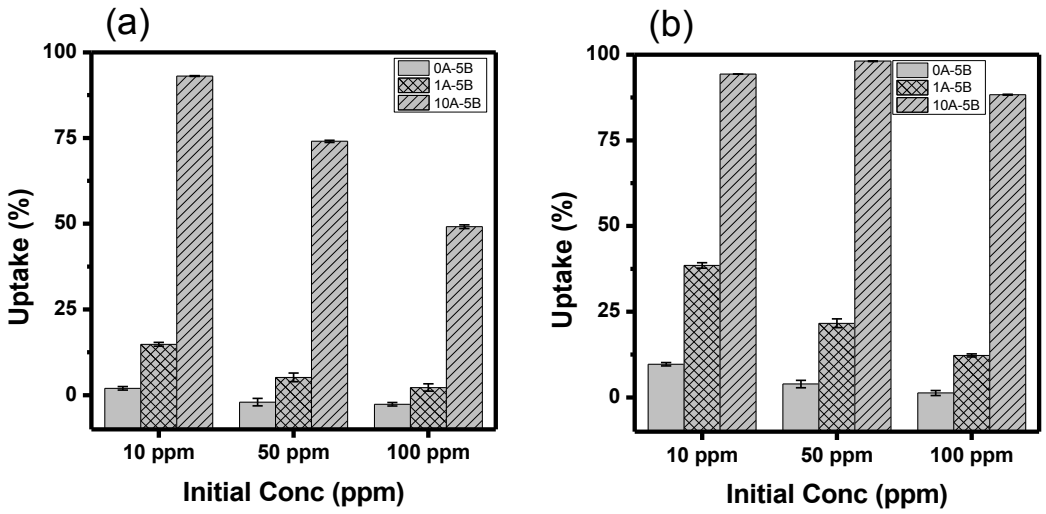

Figure 5-4. Effect of monomer composition on uptake of (a) Cd^{2+} and (b) Pb^{2+} ions. A: acrylic acid and B: BIS (numbers preceding letters represent amount in %). A sorbent dose of 2 mg/mL of microgel solution was used in a 25 mL total volume with the indicated initial concentrations of ions. The error bars represent the standard deviation of three measurements.

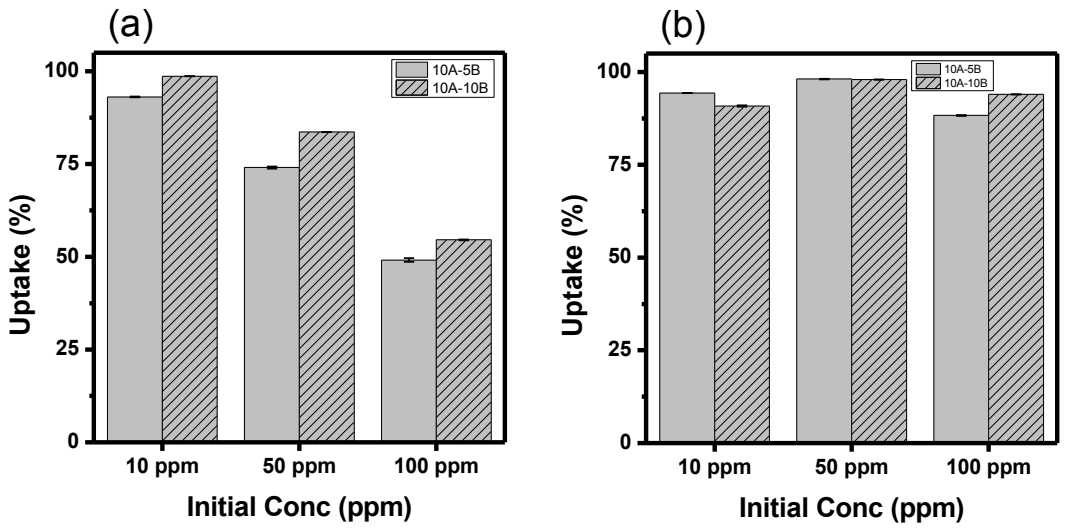

Figure 5-5. Effect of crosslinking density on removal efficiency of (a) Cd^{2+} and (b) Pb^{2+} ions. A: acrylic acid and B: BIS (numbers preceding letters represent amount in %). A sorbent dose of 2 mg/mL of microgel solution was used in a 25 mL total volume with the indicated initial concentrations of ions. The error bars represent the standard deviation of three measurements.

In Chapter 3, it was demonstrated how a series of ionizable groups differing only in their alkyl chain length revealed different response kinetics to solution pH changes; the longer alkyl chain groups responded faster to solution pH changes than those with shorter alkyl chains. This phenomenon was attributed to the increased void space presented by those with increased chain length. With this knowledge, it was hypothesized that the acid groups with increased chain length on their backbones could uptake more heavy metal ions compared to those with shorter chain length. While keeping the crosslinking density at 10 mole percent and varying the type of ionizable group, the ionizable group that contained the longer alkyl chain backbone showed enhanced sorption of Pb^{2+}, and the

sorption was even more significant at higher sorbate dose, as shown in Figure 5-6; this observed phenomenon is consistent with that described in Chapter 3. Furthermore, the increased sorption at increased alkyl chain length is attributed to the extent of charge distribution within the microgel. In accordance with Hoare's work[161,213] of functional group distribution with a MAAc group of microgels exhibiting a core-shell characteristic with dominant microgel surface charge, the same can be said for the BAAc–based microgels whose removal efficiency was in the order: BAAc>>MAAc>AAc, especially at a higher sorbate dose.

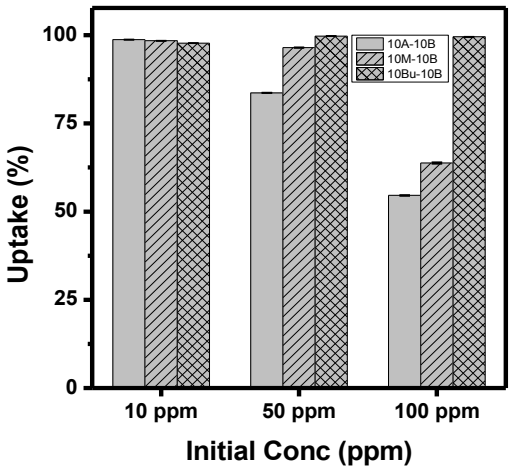

Figure 5-6. A Comparison of the removal efficiency of three comonomers with the same amount (10%) and the same crosslinking density (10%). A: acrylic acid, M: methacrylic acid and Bu: 2-butylacyrlic acid. A sorbent dose of 2 mg/mL of microgel solution was used in a 25 mL total volume with the indicated initial concentrations of Pb^{2+}. The error bars represent the standard deviation of three measurements.

To understand further the sorption mechanism by these microgels, the SEM images of microgels with different crosslinking densities and different monomer mole percent have been shown in Figure 5-7. Figures 5-7a and b compare the variation in monomer mole percent with the same amount of crosslinking density. Results in Figure 5-7a show a jam-packed structure of microgels in comparison to a loose structure in Figure 5-7b. It is possible to have increased number of microgel particles per surface area for Figure 5-7a. More sorption sites are, therefore, presented for the uptake of metal ions, and this is consistent with the removal efficiency shown in Figure 5-5. Further, the micrographs with the same amount of comonomer content and their crosslinking composition were compared, as shown in Figures 5-7 a,c,d. In accordance with the polymerization mechanism where the microgels are densely packed at the core compared to the corona, the SEM micrographs here showed the same phenomenon, observable by the "darker" regions in the core compared to the corona of the microgel particles. In addition, the diameter of the dried microgels decreased as the crosslinking density increased.[214]

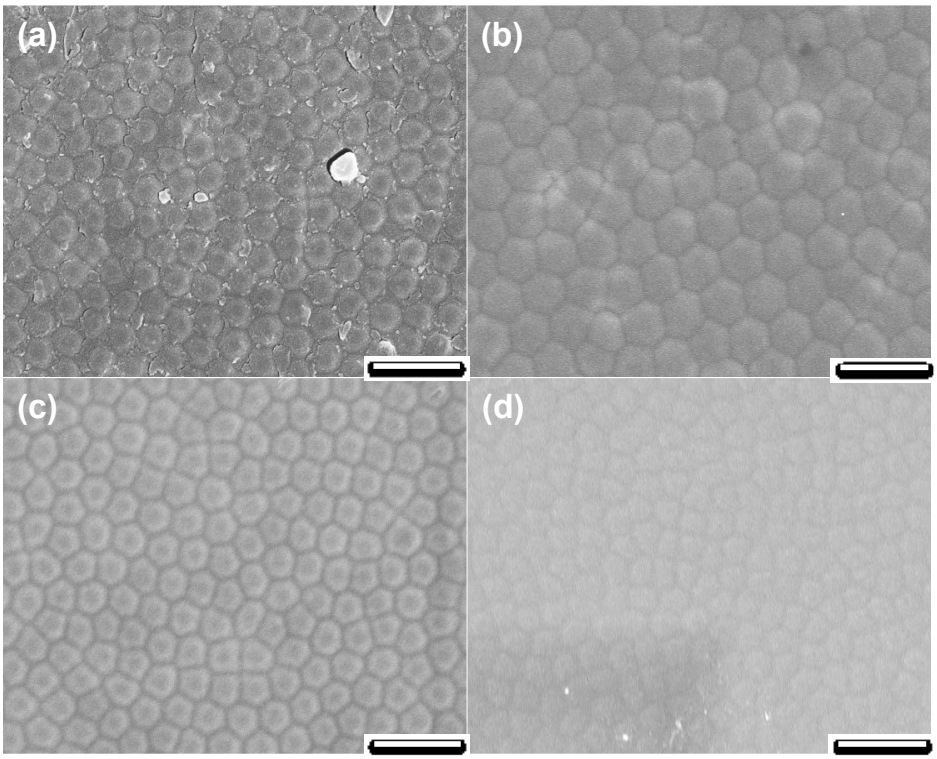

Figure 5-7. A scanning electron micrograph of different monomer and crosslinking density of pNIPAm-*co*-MAAc microgels. (a) 10M-10B (b) 1M-10B (c) 10M-5B (d) 10M-1B. M: methacrylic acid and B: BIS (numbers preceding letters represent amount in %). Dilute microgel solutions were deposited on a Si substrate to form uniform films. The scale bar is 1 μm.

Further evidence of microgel-metal ion binding was presented by the FTIR results, as shown in Figure 5-8. The amide I –C=O stretching and amide II –NH bending vibrations at about 1640 cm^{-1} and 1532 cm^{-1}, respectively, were present in all three types of gels: pNIPAm-*co*-AAc microgel (Gel), pNIPAm-*co*-AAc microgel bound to Cd (Gel-Cd) and pNIPAm-*co*-AAc microgel bound to Pb (Gel-Pb). The evidence of electrostatic

interaction between the carboxylate groups of the microgels and the metal ions was marked by the increased absorbance value at the amide I –C=O stretching and amide II –NH bending vibrations. This increase was about 0.0351 for Gel-Cd and 0.0669 for Gel-Pb at the amide I –C=O stretching vibrations. These results corroborate the work of Ooi and coworkers in determining the binding of Cu^{2+} ions to pNIPAm-*co*-AAc hydrogels.[215,216] The larger increase in absorbance for Gel-Pb (0.0669) over Gel-Cd (0.0351) evidently supports the results of Figures 5-3, 5-4 and 5-5, where Pb^{2+} removal efficiency was much higher at a higher sorbate dose. This preferential sorption of Pb^{2+} over Cd^{2+} could be attributed to the hydration energies associated with these ions.[217] The lower hydration energy for Pb^{2+} (-1425 kJ/mol) compared to that of Cd^{2+} (-1755kJ/mol) implies that Pb loses its hydration energy easily, hence, the preferential sorption.

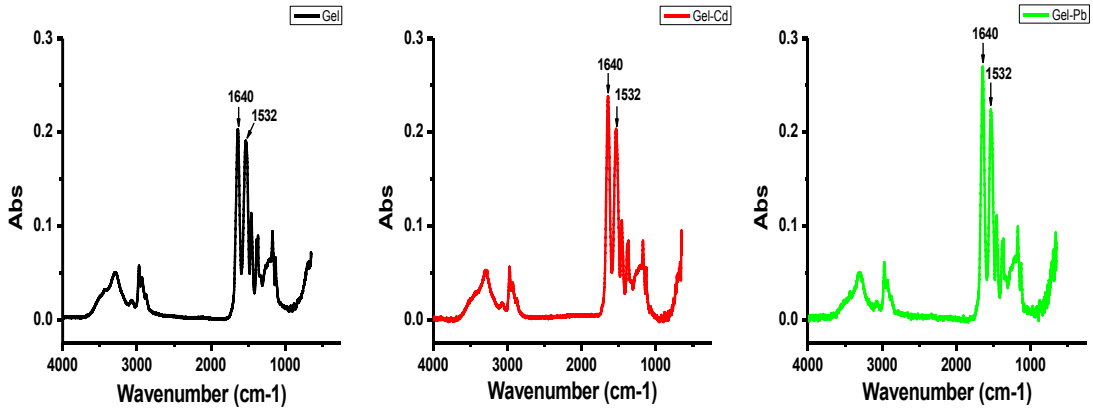

Figure 5-8. FTIR spectra of pNIPAm-*co*-AAc microgel (Gel), pNIPAm-*co*-AAc microgel sorbed Cd^{2+} (Gel-Cd) and pNIPAm-*co*-AAc microgel sorbed Pb^{2+} (Gel-Pb).

5. 4 Conclusions

Poly (*N*-Isopropylacrylamide)-based microgels sorbents have been synthesized and evaluated for their metal ion binding ability. The porous nature of the microgels made them attractive for removal of contaminants, and more importantly, the presence of ionizable groups presented binding sites for heavy metal ion uptake. Though coordination and electrostatic interactions are the main driving mechanisms for the removal of Pb^{2+} and Cd^{2+} studied in this work, the electrostatic interaction was more paramount. Increased crosslinking density increased the sorption of heavy metal ions through the provision of more donor atoms available for coordination interactions. As the charge density was increased by the incorporation of more ionizable groups, the uptake of Pb^{2+} and Cd^{2+} ions increased. Given the same group of ionizable moieties, differing only in their pendant carbon chain lengths, the longer chains presented more void spaces for entrapment of heavy metal ions as well as presenting more charged surfaces available for sorption.

Chapter 6

Enhanced Selenium Removal by Microgel Stabilized Zero Valent Iron

This Chapter describes the use of pNIPAm-based microgels as stabilizers for zero valent iron (ZVI) in the remediation of Selenium (Se), which is a metalloid, and whose removal efficiency is significantly low with the use of only the microgels. Severe aggregation of the ZVI occurs due to the highly electroactive nature and magnetic properties of pristine ZVI when using ZVI alone to remove Se or other recalcitrant contaminants. This Chapter demonstrates the significant role that the microgels play in dispersing the ZVI, leading to increased sorption sites on the ZVI and eventually enhancing the sorption capacity.

6.1 Introduction

Selenium's chemical properties are between those of metals and nonmetals, and it is considered a metalloid. Se has found applications in the semiconductor industry because of its peculiar semiconducting and photoactive properties.[218] Apart from its industrial applications, Se is also an essential micronutrient for humans and other mammals.[219] Selenium has three levels of biological activity: (i) trace concentrations are essential for normal growth and development; (ii) moderate concentrations can be stored

and homeostatic functions maintained and (iii) elevated concentrations can result in toxic effects. Because of the fine balance between its essential concentration and toxic regime,[219] Se has been coined the "necessary evil" element. Increased industrial and agricultural activities have accelerated the release of Se from geologic sources and are now accessible to fish and wildlife in both aquatic and terrestrial ecosystems. Sources of Se contamination range from agricultural drain water, sewage sludge, fly ash from coal-fired power plants, oil refineries, to the mining of phosphates and metal ores.[105] The discharge of Se-containing effluents into the environment has led to stringent regulations, especially by the US Environmental Protection Agency**.** These regulations have led to different remediation technologies, which have been applied over the years in remediating Se and other recalcitrant contaminants, including chemical, physical and biological methods.[219-222] Among these technologies is zero valent iron.[218,219]

Zero valent iron (ZVI) technologies have emerged as powerful remediation tools in the past few decades.[223] They have found applications in numerous contaminant sequestering technologies, ranging from organo-chlorine compounds to heavy metal ions and metalloids.[99,100] ZVI particles have been used in ground water remediation for the reduction of heavy metal ions, such as arsenate and chromate, and as a reducing agent for halogenated organic compounds.[106] Since their discovery for remediation, initially for the reductive dehalogenation of organo-chlorine compounds,[106] ZVI have been used for the remediation of a myriad of contaminants.[85,99,100,102,224] The versatile remediating ability of ZVI stems from their high surface area to volume ratio and high reactivity. Despite their potential as powerful remediating tools, their use in remediation is limited by their propensity to agglomerate.[225] Moreover, oxide layers always form on the surfaces of

prepared ZVI no matter how hard researchers try to degas the ZVI solution during its preparation;[101] this ultimately results in decreased removal efficiency. To decrease the oxide layer formation or to eliminate dissolved oxygen, so as to increase the removal efficiency, some researchers purge the system with high-purity nitrogen before the introduction of the ZVI.[99,102]

Research has been directed at stabilizing the ZVI particles to address the agglomeration of ZVI.[226,227] Two approaches are employed in the synthesis of stabilized ZVI particles: presynthesis and postsynthesis. The presynthesis approach was used in this Chapter, as it has been shown to yield nanoparticles of enhanced stability.[226] This approach involved the addition of microgel solutions to the precursor Fe solution, followed by an in-situ reduction of the Fe particles. Fewer studies use this approach compared to the postsynthesis method, which involves a mixing of the microgels with the Fe particles.[228] While some modifications have yielded an increased reactivity of the iron particles, others led to a two to four fold decreased reactivity.[228-230] This has been attributed to the modifiers blocking the adsorption sites of the ZVI.

Several stabilizers have been used[229,230] including polymers.[228] The potential of a polymer as stabilizer depends on the functional group, molecular weight, adsorbed mass, thickness layer of the polymer and molecular structure.[228] The porous structure of microgels offers an added advantage of capturing contaminants, as shown in studies using only microgels[94-98] and as detailed in Chapter 5. In this Chapter, pNIPAm-*co*-BAAc microgels were used as stabilizers for ZVI, and their removal efficiencies have been evaluated and compared to the removal efficiency of the pristine ZVI, the N_2 purged ZVI (ZVI–DG) and microgel stabilized ZVI (ZVI–MG). In previous Chapters, BAAc-

based microgels proved to be unusually fast in their response time to solution pH changes, due to their void spaces and other factors, detailed in Chapter 3,[57] as well as showing enhanced removal of Pb^{2+} and Cd^{2+} ions, in Chapter 5. However, the use of these microgels alone in the remediation of Se proved futile as will be seen in the discussion below.

6.2 Experimental Section

Materials: Unless otherwise specified, all reagents were from Sigma-Aldrich (Oakville, ON, Canada). *N*-isopropylacrylamide (NIPAm) was purified by re-crystallization from hexanes and vacuum dried. *N*, *N'*-methylene(bisacrylamide) (BIS), ammonium persulfate (APS), piperidine, formaldehyde, ethanol, n-butylmalonic acid, ethyl acetate and anhydrous $MgSO_4$ were used without further purification. 2-Butylacrylic acid was synthesized following the procedure reported by Pratt *et al.*[142] with some modifications.[57] A pH meter (JENCO 6173 pH, San Diego, CA, USA) was used to prepare solutions with known pH, using sodium hydroxide (NaOH) and hydrochloric acid (HCl) to adjust the pH. Millipore water (18.2 MΩ.cm) from a Milli-Q Plus system (Fisher, Z00QSVC01, Toronto, ON, Canada) was used for all experiments. A Rotovap RV 8 (IKA®, Wilmington, NC, USA) was used to remove organic solvents.

Synthesis of BAAc: BAAc was synthesized using a modified version of Pratt *et al.*[142] and is described in detail with characterization in Chapter 2. Specifically, piperidine (7.5 mmol, 0.74 mL) and formaldehyde (31.3 mmol, 2.3 mL) were added to a solution of n-butylmalonic acid (6.2, mmol, 1.00 g) in ethanol (11.6 mL). The solution

was heated to 85 °C under reflux while stirring, and a white precipitate appeared that steadily re-dissolved over 1 h. The mixture was stirred at 85 °C (under reflux) overnight and then cooled to room temperature. The solvent was removed under reduced pressure using rotovaporation. Then, the residue was dissolved in ethylacetate (12 mL) and transferred into a separatory funnel. The mixture was washed successively with 1.0 M HCl and brine (5%), dried over anhydrous $MgSO_4$ and vacuum-filtered (Whatman #1 filter paper) yielding a clear oil. ^{1}H NMR, MS and FTIR characterizations are shown in Chapter 2.

Synthesis of pNIPAm-based microgels: The microgels were synthesized by free radical precipitation polymerization, similarly to a previously published procedure[143,144] and also described in Chapter 1. NIPAm (11.928 mmol) and BIS (0.702 mmol) were weighed into a 250 mL beaker with 99 mL deionized water. The mixture was stirred for 0.5 h and filtered through a 0.2 μm filter into a 3-neck round-bottom flask. A reflux condenser was added to the flask, along with a N_2 gas inlet (needle) and temperature probe. The solution was bubbled with N_2 gas and allowed to heat to 70 °C over 1.5 h. BAAc (1.403 mmol) was added to the heated reaction mixture in one aliquot, and the polymerization was initiated immediately by addition of APS (0.2 mmol) dissolved in 1 mL of deionized water. The solution turned white/cloudy after ~1 min, indicating successful initiation. Then, the reaction was allowed to proceed at 70 °C for 4 h under N_2 gas. The resulting suspension was allowed to cool overnight, followed by filtration through glass wool to remove any large aggregates. The microgel solution was distributed into centrifuge tubes and purified via centrifugation at ~10000 rpm for ~30

min to form a pellet, followed by the removal of the supernatant and resuspending them in deionized water; this was repeated 6x. The purified microgels were stored for further use.

Synthesis of Zero Valent Iron and Microgel-Stabilized Zero Valent Iron

Zero valent iron particles were synthesized following the procedure of Zhang.[106] Briefly, 1.6 M $NaBH_4$ was added dropwise from a 50 mL burette at a flow rate of 2 drops/sec into a mechanically stirred (3000 rpm) $FeCl_3.6H_2O$ solution. The mixture was stirred under an N_2 atmosphere, and the reaction was allowed to proceed until the mixture turned black, signaling the formation of ZVI particles, according to equation 6-1. The mixture was filtered and purified by 3x centrifugation at 7500 rpm for 10 min with an ethanol/water mixture (70:30). The purified ZVI particles were stored in an ethanol/water mixture and refrigerated when not used immediately. The Microgel-ZVI particles were synthesized by the presynthesis approach: microgel solutions were added to the precursor Fe solution and allowed to stir vigorously for 24 h, followed by the dropwise addition of 1.6 M $NaBH_4$ from a burette at a flow rate of 2 drops/sec under mechanical stirring at 3000 rpm and N_2. The $NaBH_4$ was in excess to ensure complete reduction of the Fe precursor into Fe^0 particles, evidenced by the formation of black-like particles. The particles were purified by 3x centrifugation and stored under inert conditions until further use. A brief schematic of the synthesis set up is shown in Scheme 6-1.

$$Fe(H_2O)_6^{3+} + 3BH_4^- + 3H_2O \rightarrow Fe^0\downarrow + 3B(OH)_3 + 10.5H_2(g) \quad (6\text{-}1)$$

Scheme 6-1. A synthetic scheme for microgel stabilized zero valent iron. Adapted with modification from Ref.[106]

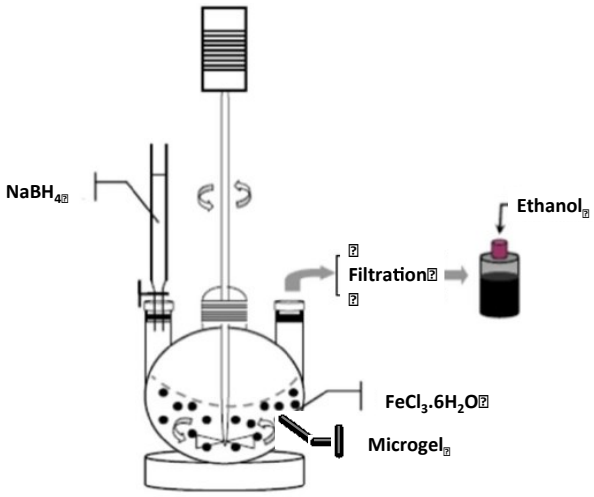

Characterization: Zeta potential (ζ) measurements were done on Malvern Instruments (Westborough, MA, USA) Zetasizer Nano ZS equipped with a 633 nm laser. TEM images were acquired using a JEOL, JEM 2100 (JEOL USA, Inc., MA, USA) operating at an accelerating voltage of 200 kV. Carbon coated copper grids, on which 5 µL of highly diluted aqueous solutions of the samples had been deposited, were allowed to air dry. Infrared spectra were collected on a Thermo Nicolet 8700 FTIR Spectrometer. X-ray diffraction (XRD) was performed on a Rigaku Ultima IV (Woodlands, Texas) multipurpose X-ray (Cu-source) diffraction system. Differential Scanning Calorimeter (DSC) measurements were recorded on a Perkin Elmer Pyris 1 DSC, held for 1 min at 25 °C and scanned from 25–600 °C at 10 °C/min. SEM was done on a Zeiss Orion NanoFab helium ion microscope operating on a helium ion beam with

an accelerated voltage of 34 kV and a beam current of 0.1–1.1 pA. XPS analysis was done using an XPS Spectrometer (Kratos AXIS 165).

Batch Experiments with Selenium. Batch experiments were conducted with the primary goal of evaluating the removal efficiency of pristine ZVI, ZVI purged with N_2 (ZVI–DG) and ZVI-stabilized with microgels (ZVI–MG). Samples containing 25 mL of 10 ppm Se (VI) and about 20, 40 and 60 mg of ZVI particles were charged into three different 50 mL centrifuge tubes and allowed to shake on the gyration shaker for 0.5 h at 100 rpm at 25 °C. The mixtures were centrifuged, and the supernatants were filtered to remove any suspended particles before their introduction into the ICP–OES for Se (196.026 nm) concentration determination. A series of Se (VI) ion concentrations between 0–100 ppm were prepared and taken through the same process but without the microgels. These concentrations were used to establish a calibration curve, and the concentration of the supernatant was determined from the calibration curve. Subsequently, the amount of Se (VI) removed by the microgels was determined by mass balance according to the following equation:

$$Uptake\ \% = \frac{Co - Ce}{Co} x\ 100\% \qquad 6\text{-}2)$$

where c_o is the initial concentration of sorbate and c_e is the equilibrium concentration, which is determined from the calibration curve. Samples were collected at 20 h and 70 h to estimate the maximum contact time required for maximum sorption. Based on the sorbent dose experiment, ~40 mg of ZVI was selected for subsequent sorption experiments. Kinetic studies were carried out using ~40 mg of sorbent and 10 ppm of sorbate, and taken through the above procedures.

6.3 Results and Discussion

As shown in previous publications, TEM images of the microgels show monodisperse, spherical particles with diameters of about 300 nm. ZVI particles without stabilizers show severe aggregation whereas in the presence of stabilizers, the aggregation is minimized, as shown in Figure 6-1. The ZVI particles aggregate because of the long-range magnetic attraction between the ZVI particles. The ZVI particles aggregate into fractal, chain-like clusters, as shown in Figure 6-1b. The aggregation has been shown to be apparent in the presence of an applied external magnet where the dipoles of the iron nanoparticles are oriented in a head-tail configuration along the direction of the field.[104] However, the presence of the microgels creates a repulsive condition for the ZVI particles and causes the particles to be dispersed.

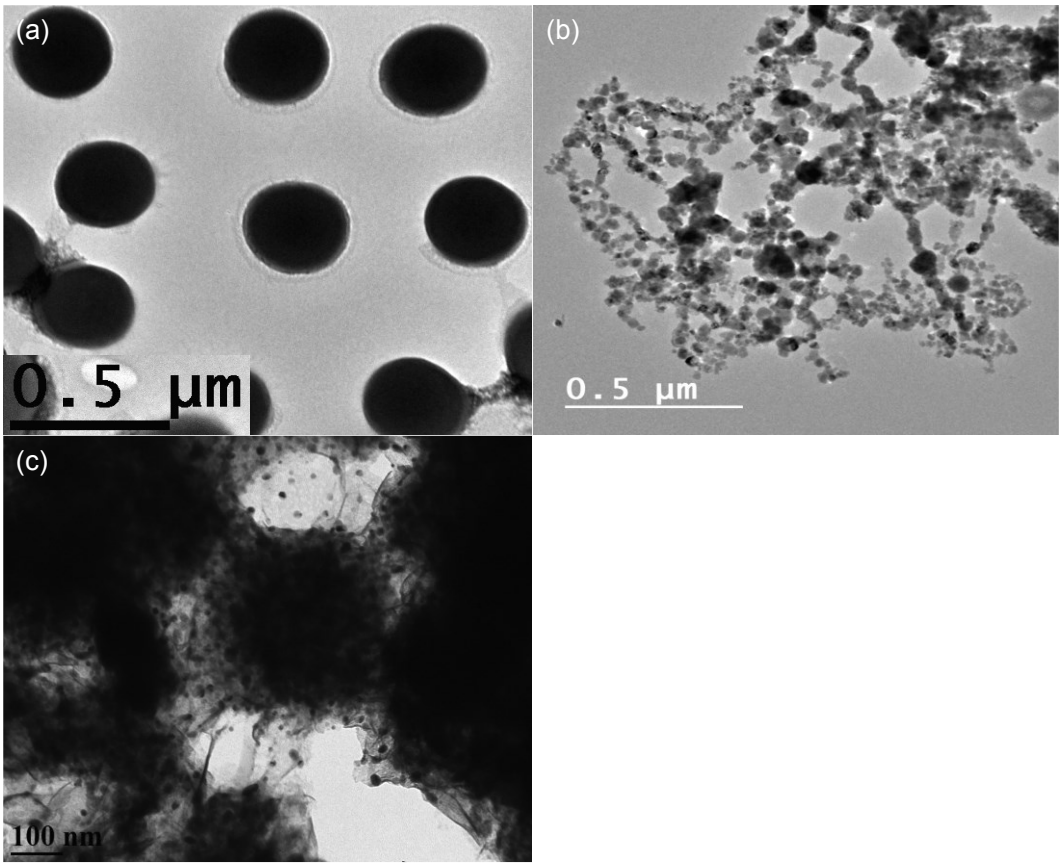

Figure 6-1. TEM images of (a) microgel, (b) zero valent iron and (c) microgel stabilized zero valent iron. Dilute sample solutions were coated on Cu grid and allowed to air-dry.

The microgels promoted colloidal stability of the ZVI through the existence of an energy barrier in the interparticle interaction potential. The conventional Derjaguin, Landau, Verwey, and Overbeek (DLVO) theory suggests that, the net interaction energy between particles is the sum of electrostatic double layer repulsion and van der Waals attraction forces. The attraction forces that exist in the ZVI particles are minimized by the introduction of the microgels. These microgels are in their charged state under the

experimental conditions, and their intraparticle repulsion further minimizes the potential of aggregation of the ZVI particles. Therefore, the microgels have improved the particle stability via surface charge/electrostatic stabilization, steric stabilization or both (electro-steric stabilization). The outcome of the reduced aggregation is the presence of increased surface area available for sorption studies. The helium ion micrographs, shown in Figure 6-2, are the structures of pristine ZVI particles (a), with severe aggregation that are polydispersed. Unlike those in Figure 6-1c, the microgels in Figure 6-2b are not obvious, and this may be due to the lower concentration of microgels relative to the ZVI particles. However, Figure 6-2c shows the micrograph of ZVI–MG after Se uptake; clearly, the surfaces of the particles are covered by the Se particles, shown as needle-like structures, similar to what was observed by Zhang and coworkers.[218]

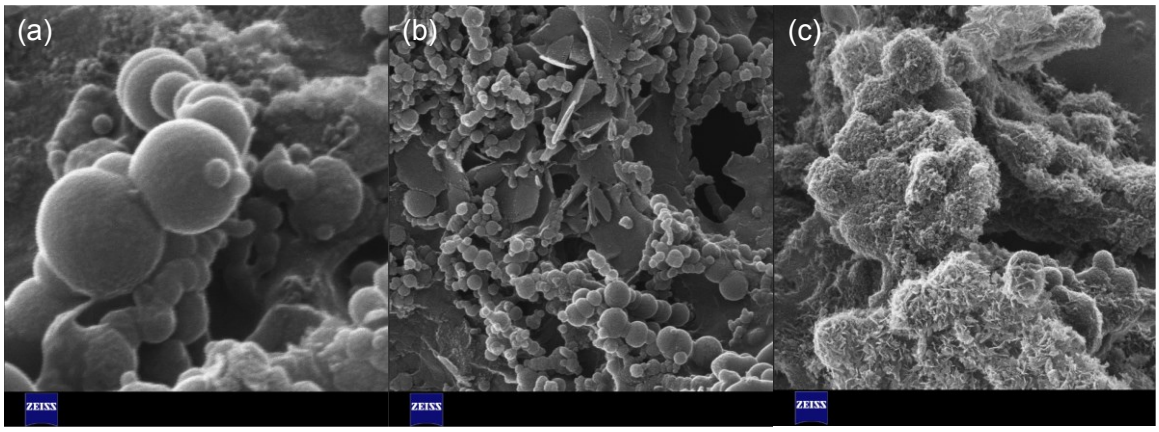

Figure 6-2. Helium ion micrographs of pristine (a) ZVI, with a scale bar of 100 nm, (b) microgel stabilized ZVI (ZVI–MG), with a scale bar of 200 nm and (c) ZVI–MG after Se uptake, with a scale bar of 500 nm, operating on a helium ion beam with an accelerated voltage of 34 kV and a beam current of 0.1–1.1 pA.

The DSC measurements in Figure 6-3a, show characteristic exothermic peaks for ZVI–MG whereas these peaks are absent in ZVI. Characteristic IR absorption peaks for ZVI are present in the ZVI–MG, suggesting the successful synthesis of ZVI–MG. The observed broad spectral feature for ZVI–MG is consistent with the literature.[231] XRD patterns for ZVI show intense crystalline domains with characteristic iron oxides and ZVI particles.[111] However, the presence of MG reduces the crystallinity, rendering more of an amorphous domain; the results are consistent with XRD patterns expected for a microgel-metal hybrid.[232]

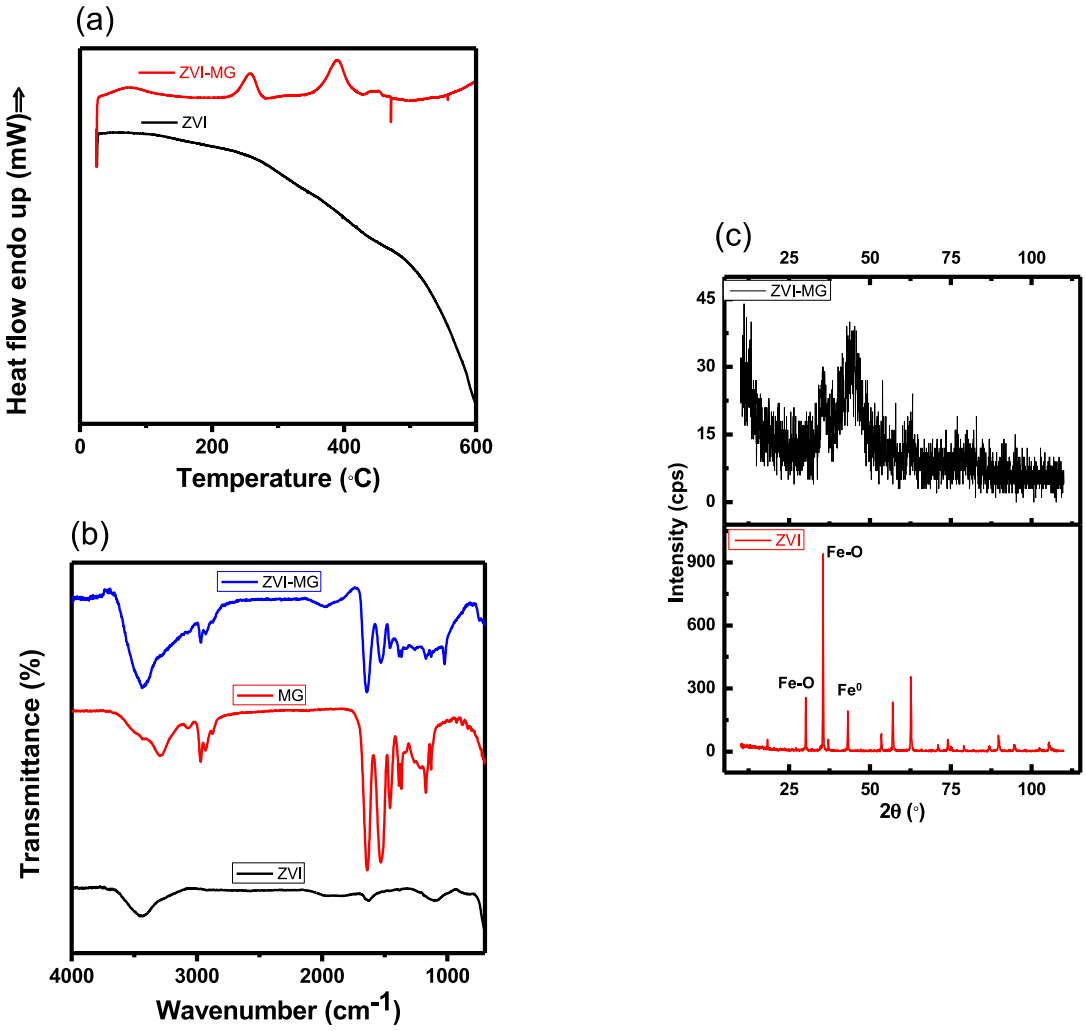

Figure 6-3. (a) DSC measurements of MG and ZVI-MG, (b) FTIR spectra of ZVI, MG and ZVI–MG and (c) XRD spectra of MG and ZVI-MG.

Survey scans for ZVI–MG, shown in Figure 6-4, show the presence of C, N and O peaks as well as Fe peaks, which are evidence of the presence of both ZVI and the microgels. A comparison of the survey scans of Figure 6-4 a and b do not reveal the presence of significant Se peaks in (b), which might be weak in comparison to other peaks in the spectrum. A focus scan, however, reveals two distinct Se peaks in the spent ZVI–MG (d) compared to a single peak in the blank ZVI–MG (c). High resolution scans for Fe 2p1/2 and Fe3/2 as well as C 1s peaks are shown in Figure 6-5. As expected, these peaks were present in both the blank and the spent ZVI particles.

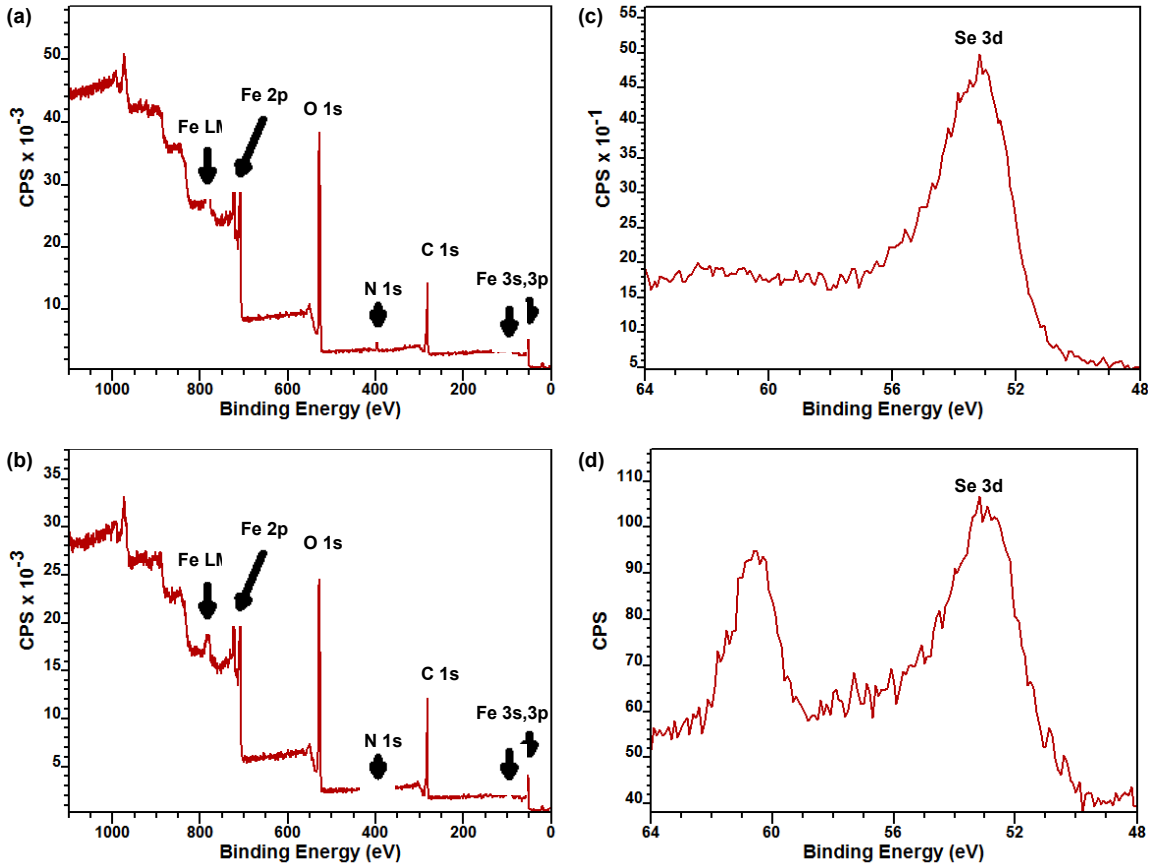

Figure 6-4. XPS survey scans of (a) blank ZVI–MG and (b) spent ZVI–MG after Se sorption. XPS focus scans for Se in (c) blank ZVI–MG and (d) after Se sorption. Note the scales in both (c) and (d). The peak at ca. 61 eV is likely in the form of Na_2SeO_4.

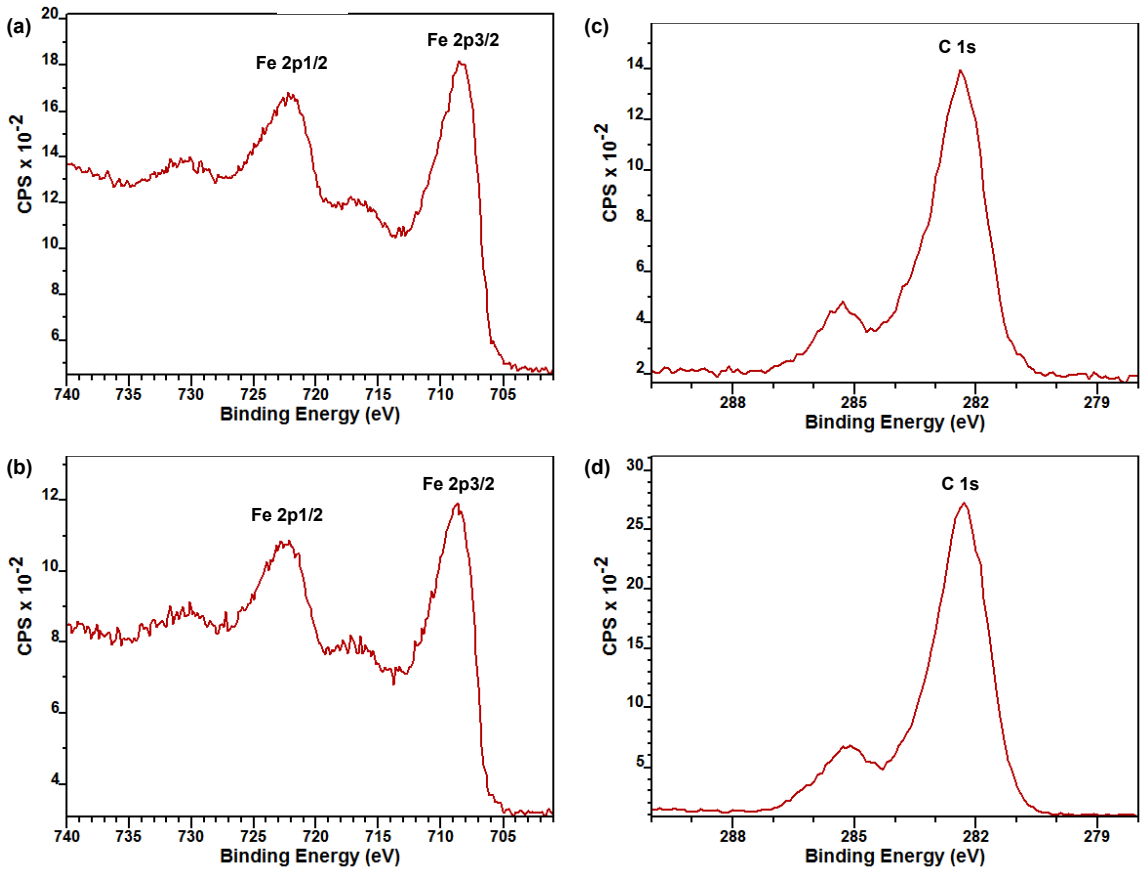

Figure 6-5. XPS focus scans for Fe peaks in (a) blank ZVI–MG and (b) spent ZVI–MG after Se sorption. XPS high resolution scans for C peaks in (c) blank ZVI–MG and (d) spent ZVI–MG after Se sorption.

The zeta potential measurement, often used to characterize the surface charge of ZVI particles, shown in Figure 6-6, was carried out to estimate the point of zero charge (pzc) for the particles. The surface charge, defined as the electric potential at the surface of shear relative to that in the distant bulk medium, is the major factor that determines the mobility of particles in an electrical field.

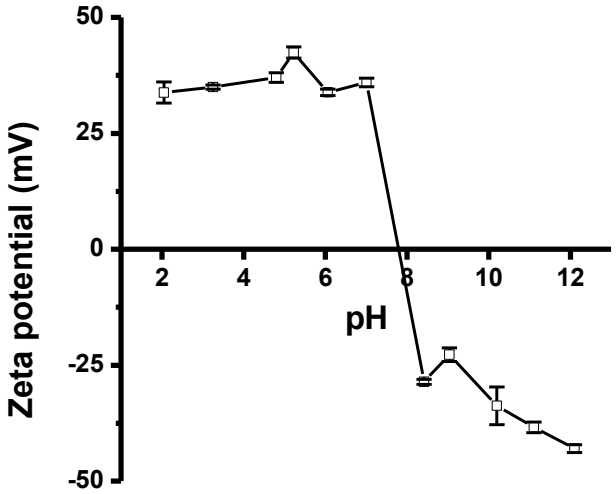

Figure 6-6. Zeta potential measurements of ZVI to estimate the point of zero charge. Measurements were done using 500 μL of dilute concentration of microgel solution.

Next, the sorption studies were conducted on the synthesized ZVI particles. The sorption study for only BAAc microgels was done as a control and the result is shown in Figure 6-7a. The amounts of Se removed as shown in Figure 6-7 were calculated using the calibration curve in Figure 6-8. In Figure 6-7a, it is evident the microgels by themselves are incapable of removing Se. The estimation of the minimum contact time required for maximum sorption was done in the form of kinetic studies, shown in Figure 6-7b. The ZVI reached its maximum sorption capacity within 1 h, irrespective of the sorbate dose. The presence of aggregates and sometimes oxide layers reduces the sorption efficiency of ZVI. A means of reducing the formation of oxide layers is through solution degassing with N_2.[99,102] In fact, it is known that ZVI works well under anaerobic conditions since it quickly oxidizes into iron oxides under aerobic conditions.[102,233] The

uptake efficiencies of the synthesized ZVI, ZVI degassed with N_2 and ZVI–MG were estimated. As can be seen in Figure 6-7c, the uptake efficiency increased upon degassing the ZVI solution. The enhanced uptake can be attributed to the reduced oxide layers formed on the surface of the ZVI, thereby exposing more active ZVI surface sites for sorption. Nearly a two-fold increase in uptake efficiency is observed for the ZVI–MG. Therefore, the major contributing factor to the poor performance of the synthesized and perhaps aged ZVI is their aggregation state. The reduced aggregation in the presence of MG exposes more of the ZVI particles' surface for sorption. It is hypothesized that the reduced aggregation led to an increased surface area available for the sorption of Se. Figure 6-7d shows the minimum sorbent dose required to achieve maximum sorption, estimated to be 40 mg. Almost 100% uptake is achieved within 30 min of contact time.

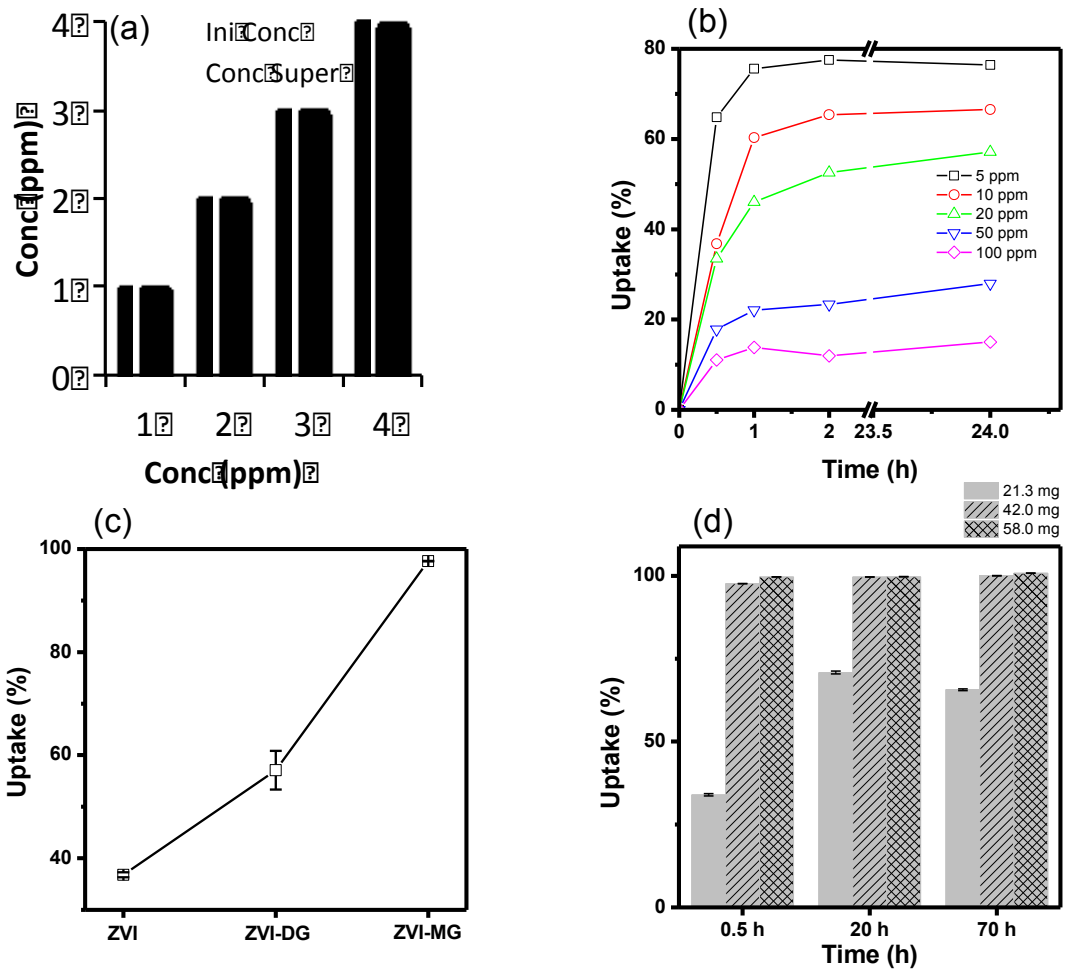

Figure 6-7. (a) Se uptake studies on only BAAc-based microgels, (b) kinetics of Se uptake by ZVI (c) uptake efficiency for ZVI, degassed ZVI and ZVI–MG using ~40 mg sorbent loaded with 10 ppm Se for 30 min and (d) ZVI–MG sorbent dose studies using 10 ppm Se. Lines in a–c are eye-guides.

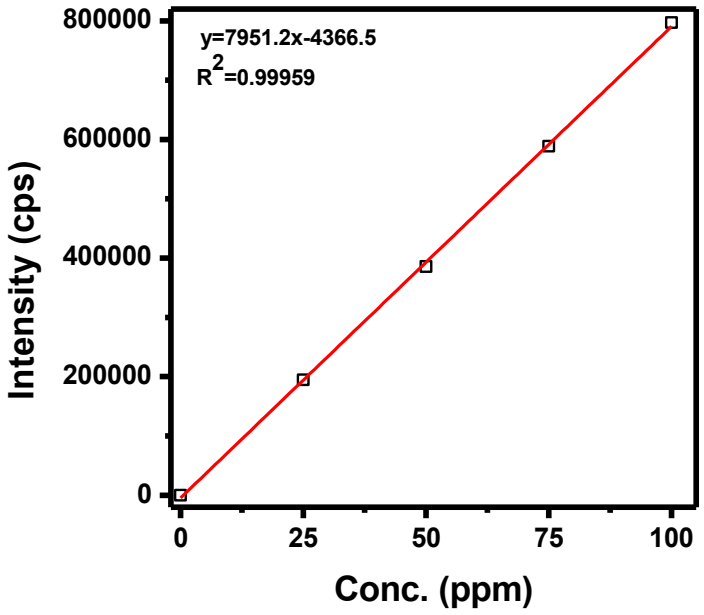

Figure 6-8. A calibration curve for Se (VI) (196.026 nm) used for the quantification of Se uptake by ZVI-based particles. The straight line is a linear fit to the data.

6.4 Conclusions

Zero valent iron has shown increasing potential for remediating a myriad of contaminants. Their limited applications have been due to the reduced surface area from aggregation. Through facile means, microgels have been incorporated into ZVI particles, reducing their propensity to aggregate, thereby increasing their surface area and enhancing their sorption capacity for Se. Characterization methods, such as SEM, TEM, XPS, FTIR, XRD and DSC were performed to support the presence of the microgels and the ZVI. The sorption capacity of Se was enhanced by a factor of three beyond the pristine ZVI.

Chapter 7

Conclusions and Future Outlook

This thesis was focused on the use of stimuli responsive polymers for pH sensing, establishing a relationship between different pH sensing groups, using these polymers as scaffolds for drug delivery and lastly, for water remediation applications. The pH sensors were shown to be sensitive to pH changes within their active pH windows. Because of the low cost of producing these sensors, efforts should be devoted in developing prototypes that can be deployed for field applications readily. An earlier work in collaboration with the Electrical Engineering Department at the University of Alberta to build a remote signaling platform for the devices should be revisited. One major drawback to the etalon devices, however, is their durability in an aqueous environment as the polymer layers peel off the glass substrate together with the Au layer. This happens due to the thin layer of microgels that are being deposited. Investigation into the means of increasing the shelf life of these sensors will be beneficial for field applications.

A comparison of the kinetic response to solution pH among different pH responsive acrylic acid based microgels, which differ only in their pendant alkyl groups, has been studied. A much faster response rate was observed by extending the chain length; this is attributed to the creation of void spaces and an increased hydrophobicity.

The conclusion from this study is important in building devices that are capable of producing a faster response for applications where rapid responses are essential.

Advantage was taken of the ability to incorporate different ionizable groups into the microgels to develop a facile means of loading and releasing model drug molecules. When different microgels of opposite charges are mixed together at specific pH ranges, aggregated microgels are produced. In the presence of model drug during the mixing, the aggregation process leads to drug loading. However, at certain pH values, the aggregates fall apart; this disaggregation was used to release the loaded model drug molecules. This simple, yet powerful approach to studying the controlled release of model drugs can be exploited for other applications, such as for artificial muscles.

The porous nature of the microgels made them attractive to be used as sorbents for environmental remediation applications. The ability to introduce ionizable groups during the microgel synthesis readily made them even more attractive. This offered the advantage of remediating numerous contaminants, including heavy metal ions, via electrostatic interaction and coordination, as shown in Chapter 5. The prepared microgels are not selective toward specific contaminants of interest over others. However, they display relative sorption depending on factors such as the size and hydration energy of the contaminants in question. To introduce specificity, ion selective membranes can be fabricated on top of the etalon, with the etalon acting as a transducer while the membrane does the selectivity by forming ion channels. The formation of the ion channels allows the passage of only the ions of interest that the membrane is specific to. An initial work in this regard is shown in the Appendix section; further work into completing this study is highly encouraged. Another approach to introducing specificity is through the

incorporation of ion selective ligands into the microgels during the synthesis. For example, an attempt was made to incorporate the polymerizable crown ether 4'-acrylamidobenzo 18-crown-6 (4'-AB18C6) into the microgel to impart selectivity to the microgels. A new synthetic method would have to be considered for the synthesis involving this macro monomer other than that for the microgel synthesis because using the usual synthetic procedure for microgels, causes the 4'-AB18C6 to precipitate out of solution. Synthesizing hydrogels composed of these groups could be explored.

Contaminants such as Se and other metalloids are not effectively removed by microgel sorbents. Instead, ZVI, emerging among the contaminant remediating technologies, has shown promise in remediating a wide category of contaminants, ranging from halogenated organic compounds to heavy metals and metalloids. Despite the superb remediating promises of ZVI, they suffer from aggregation due to their strong electroactive nature and magnetic properties. In this dissertation, a means of reducing the aggregation has been developed by using microgels as stabilizers to provide a dispersed medium for the ZVI and thus present more active sites for sorption. The presence of the microgels has been shown to enhance the sorption of Se by a factor of three. The mechanism(s) of action of these ZVI are still under debate, however, they are thought to be a combination of adsorption and precipitation. Further work is, therefore, encouraged to unravel the mechanism of sequestering by these novel particles. Their powerful remediating ability will make them limitless in decontamination implementation if more attention is paid to dealing with their propensity to aggregate.

References:

(1) Koetting, M. C.; Peters, J. T.; Steichen, S. D.; Peppas, N. A. Stimulus-Responsive Hydrogels: Theory, Modern Advances, and Applications. *Mat. Sci. Eng. R-Rep.* **2015**, *93*, 1-49.

(2) Tanaka, T.; Fillmore, D. J. Kinetics of Swelling of Gels. *J. Chem. Phys.* **1979**, *70*, 1214-1218.

(3) Bradley, M.; Ramos, J.; Vincent, B. Equilibrium and Kinetic Aspects of the Uptake of Poly(ethylene oxide) by Copolymer Microgel Particles of N-isopropylacrylamide and Acrylic Acid. *Langmuir* **2005**, *21*, 1209-1215.

(4) Chu, L. Y.; Kim, J. W.; Shah, R. K.; Weitz, D. A. Monodisperse Thermoresponsive Microgels with Tunable Volume-Phase Transition Kinetics. *Adv. Funct. Mater.* **2007**, *17*, 3499-3504.

(5) Plunkett, K. N.; Kraft, M. L.; Yu, Q.; Moore, J. S. Swelling Kinetics of Disulfide Cross-Linked Microgels. *Macromolecules* **2003**, *36*, 3960-3966.

(6) Zhang, X.-Z.; Chu, C.-C. Fabrication and Characterization of Microgel-Impregnated, Thermosensitive PNIPAAm Hydrogels. *Polymer* **2005**, *46*, 9664-9673.

(7) Cai, W.; Gupta, R. B. Fast-Responding Bulk Hydrogels with Microstructure. *J. Appl. Polym. Sci.* **2002**, *83*, 169-178.

(8) Mirzaei, B. E.; Ramazani, S. A. A.; Shafiee, M.; Danaei, M. Studies on Glutaraldehyde Crosslinked Chitosan Hydrogel Properties for Drug Delivery Systems. *Int. J. Polym. Mater. Polym. Biomater.* **2013**, *62*, 605-611.

(9) Barbosa, O.; Ortiz, C.; Berenguer-Murcia, A.; Torres, R.; Rodrigues, R. C.; Fernandez-Lafuente, R. Glutaraldehyde in Bio-catalysts Design: A Useful Crosslinker and a Versatile Tool in Enzyme Immobilization. *RSC Adv.* **2014**, *4*, 1583-1600.

(10) Slaughter, B. V.; Khurshid, S. S.; Fisher, O. Z.; Khademhosseini, A.; Peppas, N. A. Hydrogels in Regenerative Medicine. *Adv. Mater.* **2009**, *21*, 3307-3329.

(11) Hu, X.; Tong, Z.; Lyon, L. A. Synthesis and Physicochemical Properties of Cationic Microgels Based on Poly (N-isopropylmethacrylamide). *Colloid Polym. Sci.* **2011**, *289*, 333-339.

(12) Kodlekere, P.; Cartelle, A. L.; Lyon, L. A. Design of Functional Cationic Microgels as Conjugation Scaffolds. *RSC Adv.* **2016**, *6*, 31619-31631.

(13) Flory, P. J.; Rehner, J. Statistical Mechanics of Cross-linked Polymer Networks I Rubberlike Elasticity. *J. Chem. Phys.* **1943**, *11*, 512-520.

(14) Dalmont, H.; Pinprayoon, O.; Saunders, B. R. Study of pH-Responsive Microgels Containing Methacrylic Acid: Effects of Particle Composition and Added Calcium. *Langmuir* **2008**, *24*, 2834-2840.

(15) Hu, L.; Serpe, M. J. Controlling the Response of Color Tunable Poly(N-isopropylacrylamide) Microgel-Based Etalons with Hysteresis. *Chem. Commun.* **2013**, *49*, 2649-2651.

(16) Johnson, K. C.; Mendez, F.; Serpe, M. J.: Detecting Solution pH Changes Using Poly (N-Isopropylacrylamide)-co-acrylic Acid Microgel-Based Etalon Modified Quartz Crystal Microbalances. In *Anal. Chim. Acta*, 2012; Vol. 739; pp 83-88.

(17) Gao, Y.; Ahiabu, A.; Serpe, M. J. Controlled Drug Release from the Aggregation-Disaggregation Behavior of pH-Responsive Microgels. *ACS Appl. Mater. Interfaces* **2014**, *6*, 13749-13756.

(18) Schmaljohann, D. Thermo- and pH-Responsive Polymers in Drug Delivery. *Adv. Drug Deliv. Rev.* **2006**, *58*, 1655-1670.

(19) Jochum, F. D.; Theato, P. Temperature- and Light-Responsive Smart Polymer Materials. *Chem. Soc. Rev.* **2013**, *42*, 7468-7483.

(20) Yuk, S. H.; Cho, S. H.; Lee, S. H. pH/Temperature-Responsive Polymer Composed of Poly((N,N-dimethylamino)ethyl methacrylate-co-ethylacrylamide). *Macromolecules* **1997**, *30*, 6856-6859.

(21) Stuart, M. A. C.; Huck, W. T. S.; Genzer, J.; Mueller, M.; Ober, C.; Stamm, M.; Sukhorukov, G. B.; Szleifer, I.; Tsukruk, V. V.; Urban, M.; Winnik, F.; Zauscher, S.; Luzinov, I.; Minko, S. Emerging Applications of Stimuli-Responsive Polymer Materials. *Nat. Mater.* **2010**, *9*, 101-113.

(22) Dai, S.; Ravi, P.; Tam, K. C. Thermo- and Photo-Responsive Polymeric Systems. *Soft Matter* **2009**, *5*, 2513-2533.

(23) Lyon, L. A.; Meng, Z.; Singh, N.; Sorrell, C. D.; John, A. S. Thermoresponsive Microgel-Based Materials. *Chem. Soc. Rev.* **2009**, *38*, 865-874.

(24) Zhou, J.; Wang, G.; Hu, J.; Lu, X.; Li, J. Temperature, Ionic Strength and pH Induced Electrochemical Switching of Smart Polymer Interfaces. *Chem. Commun.* **2006**, 4820-4822.

(25) Shibayama, M.; Ikkai, F.; Inamoto, S.; Nomura, S.; Han, C. C. pH and Salt Concentration Dependence of the Microstructure of Poly (N-isopropylacrylamide-co-acrylic acid) Gels. *J. Chem. Phys.* **1996**, *105*, 4358-4366.

(26) Xu, W.; Gao, Y.; Serpe, M. J. Electrochemically Color Tunable Poly (N-isopropylacrylamide) Microgel-Based Etalons. *J. Mater. Chem. C* **2014**, *2*, 3873-3878.

(27) Thevenot, J.; Oliveira, H.; Sandre, O.; Lecommandoux, S. Magnetic Responsive Polymer Composite Materials. *Chem. Soc. Rev.* **2013**, *42*, 7099-7116.

(28) Zhang, Q. M.; Xu, W.; Serpe, M. J. Optical Devices Constructed from Multiresponsive Microgels. *Angew. Chem., Int. Ed.* **2014**, *53*, 4827-4831.

(29) Stuart, M. A. C.; Huck, W. T.; Genzer, J.; Müller, M.; Ober, C.; Stamm, M.; Sukhorukov, G. B.; Szleifer, I.; Tsukruk, V. V.; Urban, M. Emerging applications of stimuli-responsive polymer materials. *Nat. Mater.* **2010**, *9*, 101.

(30) Roy, D.; Cambre, J. N.; Sumerlin, B. S. Future Perspectives and Recent Advances in Stimuli-Responsive Materials. *Prog. Polym. Sci.* **2010**, *35*, 278-301.

(31) Heskins, M.; Guillet, J. E. Solution Properties of Poly (N-isopropylacrylamide). *J. Macromol. Sci., Chem.* **1968**, *2*, 1441-1455.

(32) Islam, M. R.; Serpe, M. J. Polymer-Based Devices for the Label-Free Detection of DNA in Solution: Low DNA Concentrations Yield Large Signals. *Anal. Bioanal. Chem.* **2014**, *406*, 4777-4783.

(33) Hendrickson, G. R.; Lyon, L. A. Bioresponsive Hydrogels for Sensing Applications. *Soft Matter* **2009**, *5*, 29-35.

(34) Gao, Y.; Zago, G. P.; Jia, Z.; Serpe, M. J. Controlled and Triggered Small Molecule Release from a Confined Polymer Film. *ACS Appl. Mater. Interfaces* **2013**, *5*, 9803-9808.

(35) Gao, Y.; Ahiabu, A.; Serpe, M. J. Controlled drug release from the aggregation–disaggregation behavior of pH-responsive microgels. *ACS Appl. Mater. Interfaces* **2014**, *6*, 13749-13756.

(36) Mura, S.; Nicolas, J.; Couvreur, P. Stimuli-responsive Nanocarriers for Drug Delivery. *Nat. Mater.* **2013**, *12*, 991-1003.

(37) Lee, K. Y.; Mooney, D. J. Hydrogels for Tissue Engineering. *Chem. Rev.* **2001**, *101*, 1869-1879.

(38) Zhai, L. Stimuli-Responsive Polymer Films. *Chem. Soc. Rev.* **2013**, *42*, 7148-7160.

(39) Tanaka, F.; Katsumoto, Y.; Nakano, S.; Kita, R. LCST Phase Separation and Thermoreversible Gelation in Aqueous Solutions of Stereo-Controlled Poly (N-isopropylacrylamide) s. *React. Funct. Polym.* **2013**, *73*, 894-897.

(40) Bae, Y. H.; Okano, T.; Kim, S. W. Temperature dependence of swelling of crosslinked poly(N,N′-alkyl substituted acrylamides) in water. *J. Polym. Sci. Part B: Polym. Phys.* **1990**, *28*, 923-936.

(41) Ward, M. A.; Georgiou, T. K. Thermoresponsive Triblock Copolymers Based on Methacrylate Monomers: Effect of Molecular Weight and Composition. *Soft Matter* **2012**, *8*, 2737-2745.

(42) Arndt, K.-F.; Schmidt, T.; Reichelt, R. Thermo-sensitive Poly(methyl vinyl ether) Micro-gel Formed by High Energy Radiation. *Polymer* **2001**, *42*, 6785-6791.

(43) Hoogenboom, R. Poly (2-Oxazoline) s: A Polymer Class with Numerous Potential Applications. *Angew. Chem. Int. Ed.* **2009**, *48*, 7978-7994.

(44) Meeussen, F.; Nies, E.; Berghmans, H.; Verbrugghe, S.; Goethals, E.; Du Prez, F. Phase Behaviour of Poly (N-vinyl caprolactam) in Water. *Polymer* **2000**, *41*, 8597-8602.

(45) Soeriyadi, A. H.; Li, G.-Z.; Slavin, S.; Jones, M. W.; Amos, C. M.; Becer, C. R.; Whittaker, M. R.; Haddleton, D. M.; Boyer, C.; Davis, T. P. Synthesis and Modification of Thermoresponsive Poly (oligo (ethylene glycol) methacrylate) via Catalytic Chain Transfer Polymerization and Thiol–ene Michael Addition. *Polym. Chem.* **2011**, *2*, 815-822.

(46) Karimi, M.; Ghasemi, A.; Sahandi Zangabad, P.; Rahighi, R.; Moosavi Basri, S. M.; Mirshekari, H.; Amiri, M.; Shafaei Pishabad, Z.; Aslani, A.; Bozorgomid, M.; Ghosh, D.; Beyzavi, A.; Vaseghi, A.; Aref, A. R.; Haghani, L.; Bahrami, S.; Hamblin, M. R. Smart Micro/Nanoparticles in Stimulus-Responsive Drug/Gene Delivery Systems. *Chem. Soc. Rev.* **2016**, *45*, 1457-1501.

(47) Kurkdjian, A.; Guern, J. Intracellular pH: Measurement and Importance in Cell Activity. *Annu. Rev. Plant. Biol.* **1989**, *40*, 271-303.

(48) Kocak, G.; Tuncer, C.; Butun, V. pH-Responsive Polymers. *Polym. Chem.* **2017**, *8*, 144-176.

(49) Schroeder, R.; Rudov, A. A.; Lyon, L. A.; Richtering, W.; Pich, A.; Potemkin, I. I. Electrostatic Interactions and Osmotic Pressure of Counterions Control the pH-Dependent Swelling and Collapse of Polyampholyte Microgels with Random Distribution of Ionizable Groups. *Macromolecules* **2015**, *48*, 5914-5927.

(50) Rizwan, M.; Yahya, R.; Hassan, A.; Yar, M.; Azzahari, A. D.; Selvanathan, V.; Sonsudin, F.; Abouloula, C. N. pH Sensitive Hydrogels in Drug Delivery: Brief History, Properties, Swelling, and Release Mechanism, Material Selection and Applications. *Polymers* **2017**, *9*.

(51) Phosphorus-Based Polymers: From Synthesis to Applications. *RSC* **2014**, *11*, 1-318.

(52) Gabaston, L. I.; Furlong, S. A.; Jackson, R. A.; Armes, S. P. Direct Synthesis of Novel Acidic and Zwitterionic Block Copolymers via TEMPO-Mediated Living Free-Radical Polymerization. *Polymer* **1999**, *40*, 4505-4514.

(53) Islam, M. R.; Serpe, M. J. Label-free Detection of Low Protein Concentration in Solution Using a Novel Colorimetric Assay. *Biosens. Bioelectron.* **2013**, *49*, 133-138.

(54) Islam, M. R.; Serpe, M. J. Poly (N-isopropylacrylamide) Microgel-Based Etalons and Etalon Arrays for Determining the Molecular Weight of Polymers in Solution. *Appl. Mater.* **2013**, *1*, 1-7.

(55) Gao, Y. F.; Xu, W. W.; Serpe, M. J. Free-Standing Poly (N-isopropylacrylamide) Microgel-Based Etalons. *J. Mater. Chem. C* **2014**, *2*, 5878-5884.

(56) Gao, Y.; Wong, K. Y.; Ahiabu, A.; Serpe, M. J. Sequential and Controlled Release of Small Molecules from Poly(N-isopropylacrylamide) Microgel-Based Reservoir Devices. *J. Mater. Chem. B* **2016**, *4*, 5144-5150.

(57) Ahiabu, A.; Serpe, M. J. Rapidly Responding pH- and Temperature-Responsive Poly (N-Isopropylacrylamide)-Based Microgels and Assemblies. *ACS Omega* **2017**, *2*, 1769-1777.

(58) Smiley-Wiens, J. B.; Serpe, M. J. Solvent Exchange Kinetics in Poly(N-isopropylacrylamide) Microgel-Based Etalons. *Colloid Polym. Sci.* **2013**, *291*, 971-979.

(59) Qiu, Y.; Park, K. Environment-Sensitive Hydrogels for Drug Delivery. *Adv. Drug Deliv. Rev.* **2012**, *64*, 49-60.

(60) Qiu, Y.; Park, K. Environment-Sensitive Hydrogels for Drug Delivery. *Adv. Drug Deliv. Rev.* **2001**, *53*, 321-339.

(61) Yu, H.; Cui, Z.; Yu, P.; Guo, C.; Feng, B.; Jiang, T.; Wang, S.; Yin, Q.; Zhong, D.; Yang, X.; Zhang, Z.; Li, Y. pH- and NIR Light-Responsive Micelles with Hyperthermia-Triggered Tumor Penetration and Cytoplasm Drug Release to Reverse Doxorubicin Resistance in Breast Cancer. *Adv. Funct. Mater.* **2015**, *25*, 2489-2500.

(62) Schmaljohann, D. Thermo- and pH-responsive polymers in drug delivery. *Adv. Drug Deliv. Rev* **2006**, *58*, 1655-1670.

(63) Zhou, T.; Xiao, C. F.; Fan, J.; Chen, S. M.; Shen, J.; Wu, W. T.; Zhou, S. Q. A Nanogel of on-site Tunable pH-Response for Efficient Anticancer Drug Delivery. *Acta Biomater.* **2013**, *9*, 4546-4557.

(64) Bai, Y. Y.; Zhang, Z.; Deng, M. X.; Chen, L.; He, C. L.; Zhuang, X. L.; Chen, X. S. Thermo- and pH-Responsive Microgels for Controlled Release of Insulin. *Polym. Int.* **2012**, *61*, 1151-1157.

(65) Lu, B.; Tarn, M. D.; Pamme, N.; Georgiou, T. K. Microfluidically Fabricated pH-Responsive Anionic Amphiphilic Microgels for Drug Release. *J. Mater. Chem. B* **2016**, *4*, 3086-3093.

(66) Lu, B.; Tarn, M. D.; Pamme, N.; Georgiou, T. K. Tailoring pH-Responsive Acrylic Acid Microgels with Hydrophobic Crosslinks for Drug Release. *J. Mater. Chem. B* **2015**, *3*, 4524-4529.

(67) Gao, Y. F.; Zago, G. P.; Jia, Z. H.; Serpe, M. J. Controlled and Triggered Small Molecule Release from a Confined Polymer Film. *ACS Appl. Mater. Interfaces* **2013**, *5*, 9803-9808.

(68) Gao, Y. F.; Ahiabu, A.; Serpe, M. J. Controlled Drug Release from the Aggregation-Disaggregation Behavior of pH-Responsive Microgels. A*CS Appl. Mater. Interfaces* **2014**, *6*, 13749-13756.

(69) Gao, Y. F.; Wong, K. Y.; Ahiabu, A.; Serpe, M. J. Sequential and controlled release of small molecules from poly(N-isopropylacrylamide) microgel-based reservoir devices. *J. Mater. Chem. B* **2016**, *4*, 5144-5150.

(70) Yu, L. L.; Ren, N.; Yang, K.; Zhang, M.; Su, L. Photo/pH Dual-Responsive Biocompatible Poly(methacrylic acid)-Based Particles for Triggered Drug Delivery. *J. Appl. Polym. Sci.* **2016**, *133*.

(71) Dadsetan, M.; Taylor, K. E.; Yong, C.; Bajzer, Z.; Lu, L. C.; Yaszemski, M. J. Controlled Release of Doxorubicin from pH-Responsive Microgels. *Acta Biomater.* **2013**, *9*, 5438-5446.

(72) Constantin, M.; Bucatariu, S.; Harabagiu, V.; Popescu, I.; Ascenzi, P.; Fundueanu, G. Poly(N-isopropylacrylamide-co-Methacrylic acid) pH/Thermo-Responsive Porous Hydrogels as Self-regulated Drug Delivery System. *Eur. J. Pharm. Sci.* **2014**, *62*, 86-95.

(73) Schwarzenbach, R. P.; Egli, T.; Hofstetter, T. B.; von Gunten, U.; Wehrli, B. Global Water Pollution and Human Health. *Annu. Rev. Environ. Resour.* **2010**, *35*, 109-136.

(74) Rappaport, S. M.; Smith, M. T. Environment and Disease Risks. *Science* **2010**, *330*, 460-461.

(75) Zahir, F.; Rizwi, S. J.; Haq, S. K.; Khan, R. H. Low Dose Mercury Toxicity and Human Health. *Environ. Toxicol. Pharmacol.* **2005**, *20*, 351-360.

(76) Papanikolaou, N. C.; Hatzidaki, E. G.; Belivanis, S.; Tzanakakis, G. N.; Tsatsakis, A. M. Lead Toxicity Update. A Brief Review. *Med. Sci. Monit.* **2005**, *11*, RA329-RA336.

(77) Järup, L.; Åkesson, A. Current Status of Cadmium as an Environmental Health Problem. *Toxicol. Appl. Pharmacol.* **2009**, *238*, 201-208.

(78) Denkhaus, E.; Salnikow, K. Nickel Essentiality, Toxicity, and Carcinogenicity. *Crit. Rev. Oncol. Hematol.* **2002**, *42*, 35-56.

(79) Gaetke, L. M.; Chow, C. K. Copper Toxicity, Oxidative Stress, and Antioxidant Nutrients. *Toxicol.* **2003**, *189*, 147-163.

(80) Kimbrough, D. E.; Cohen, Y.; Winer, A. M.; Creelman, L.; Mabuni, C. A Critical Assessment of Chromium in the Environment. *Crit. Rev. Environ. Sci. Technol.* **1999**, *29*, 1-46.

(81) Maret, W.; Sandstead, H. H. Zinc Requirements and the Risks and Benefits of Zinc Supplementation. *J. Trace Elem. Med. Biol.* **2006**, *20*, 3-18.

(82) Fu, F. L.; Wang, Q. Removal of heavy metal ions from wastewaters: A review. *J. Environ. Manage.* **2011**, *92*, 407-418.

(83) Deliyanni, E. A.; Kyzas, G. Z.; Triantafyllidis, K. S.; Matis, K. A. Activated Carbons for the Removal of Heavy Metal Ions: A Systematic Review of Recent Literature Focused on Lead and Arsenic Ions. *Open Chem.* **2015**, *13*, 699-708.

(84) Alsbaiee, A.; Smith, B. J.; Xiao, L.; Ling, Y.; Helbling, D. E.; Dichtel, W. R. Rapid Removal of Organic Micropollutants from Water by a Porous β-Cyclodextrin Polymer. *Nature* **2016**, *529*, 190-194.

(85) Zou, Y.; Wang, X.; Khan, A.; Wang, P.; Liu, Y.; Alsaedi, A.; Hayat, T.; Wang, X. Environmental Remediation and Application of Nanoscale Zero-Valent Iron and Its Composites for the Removal of Heavy Metal Ions: A Review. *Environ. Sci.Technol.* **2016**, *50*, 7290-7304.

(86) Richardson, S. D.; Ternes, T. A. Water Analysis: Emerging Contaminants and Current Issues. *Anal. Chem.* **2014**, *86*, 2813-2848.

(87) Yildiz, U.; Kemik, O. F.; Hazer, B. The Removal of Heavy Metal Ions from Aqueous Solutions by Novel pH-Sensitive Hydrogels. *J. Hazard. Mater.* **2010**, *183*, 521-532.

(88) Hazer, B. Synthesis of PS-PEG and PMMA-PEG Branched Block Copolymers by Macroinimers. *J. Macromol. Sci. A* **1991**, *28*, 47-52.

(89) Chen, J. J.; Ahmad, A. L.; Ooi, B. S. Thermo-Responsive Properties of Poly(N-isopropylacrylamide-co-acrylic acid) Hydrogel and its Effect on Copper Ion Removal and Fouling of Polymer-Enhanced Ultrafiltration. *J. Memb. Sci.* **2014**, *469*, 73-79.

(90) Jiang, L.; Liu, P. Covalently Crosslinked Fly Ash/Poly(acrylic acid-co-acrylamide) Composite Microgels as Novel Magnetic Selective Adsorbent for Pb2+ ion. *J. Colloid Interface Sci.* **2014**, *426*, 64-71.

(91) Hu, P.; Liu, T.; Zhou, G.; Duan, X.; Wu, W. Adsorption of Th4+ from Aqueous Solution onto Poly(N,N-diethylacrylamide-co-acrylic acid) Microgels. *J. Radioanal. Nucl. Chem.* **2014**, *301*, 65-73.

(92) Rehman, S. U.; Siddiq, M.; Al-Lohedan, H.; Aktas, N.; Sahiner, M.; Demirci, S.; Sahiner, N. Fast Removal of High Quantities of Toxic Arsenate via Cationic p(APTMACl) Microgels. *J. Environ. Manage.* **2016**, *166*, 217-226.

(93) Sahiner, N.; Demirci, S.; Sahiner, M.; Yilmaz, S.; Al-Lohedan, H. The use of Superporous p(3-acrylamidopropyl)Trimethyl Ammonium Chloride Cryogels for Removal of Toxic Arsenate Anions. *J. Environ. Manage.* **2015**, *152*, 66-74.

(94) Parasuraman, D.; Serpe, M. J. Poly (N-Isopropylacrylamide) Microgels for Organic Dye Removal from Water. *ACS Appl. Mater. Interfaces* **2011**, *3*, 2732-2737.

(95) Parasuraman, D.; Serpe, M. J. Poly (N-Isopropylacrylamide) Microgel-Based Assemblies for Organic Dye Removal from Water. *ACS Appl. Mater. Interfaces* **2011**, *3*, 4714-4721.

(96) Parasuraman, D.; Leung, E.; Serpe, M. J. Poly (N-isopropylacrylamide) Microgel Based Assemblies for Organic Dye Removal from Water: Microgel Diameter Effects. *Colloid Polym. Sci.* **2012**, *290*, 1053-1064.

(97) Parasuraman, D.; Sarker, A. K.; Serpe, M. J. Poly(N-Isopropylacrylamide)-Based Microgels and Their Assemblies for Organic-Molecule Removal from Water. *Chemphyschem* **2012**, *13*, 2507-2515.

(98) Parasuraman, D.; Sarker, A. K.; Serpe, M. J. Recyclability of poly (N-isopropylacrylamide) microgel-based assemblies for organic dye removal from water. *Colloid Polym. Sci.* **2013**, *291*, 1795-1802.

(99) Ling, L.; Pan, B.; Zhang, W.-x. Removal of Selenium from Water with Nanoscale Zero-Valent Iron: Mechanisms of Intraparticle Reduction of Se(IV). *Water Res.* **2015**, *71*, 274-281.

(100) Fu, F.; Dionysiou, D. D.; Liu, H. The use of Zero-Valent Iron for Groundwater Remediation and Wastewater Treatment: A Review. *J. Hazard. Mater.* **2014**, *267*, 194-205.

(101) Zhang, Y.; Chen, W.; Dai, C.; Zhou, C.; Zhou, X. Structural Evolution of Nanoscale Zero-Valent Iron (nZVI) in Anoxic Co2+ Solution: Interactional Performance and Mechanism. *Sci. Rep.* **2015**, *5*.

(102) Tuček, J.; Prucek, R.; Kolařík, J.; Zoppellaro, G.; Petr, M.; Filip, J.; Sharma, V. K.; Zbořil, R. Zero-Valent Iron Nanoparticles Reduce Arsenites and Arsenates to As(0) Firmly Embedded in Core–Shell Superstructure: Challenging Strategy of Arsenic Treatment under Anoxic Conditions. *ACS Sustain. Chem. Eng.* **2017**, *5*, 3027-3038.

(103) Huang, P.; Ye, Z.; Xie, W.; Chen, Q.; Li, J.; Xu, Z.; Yao, M. Rapid Magnetic Removal of Aqueous Heavy Metals and their Relevant Mechanisms Using Nanoscale Zero Valent Iron (nZVI) Particles. *Water Res.* **2013**, *47*, 4050-4058.

(104) Phenrat, T.; Saleh, N.; Sirk, K.; Tilton, R. D.; Lowry, G. V. Aggregation and Sedimentation of Aqueous Nanoscale Zerovalent Iron Dispersions. *Environ. Sci. Technol.* **2007**, *41*, 284-290.

(105) Lemly, A. D. Aquatic Selenium Pollution is a Global Environmental Safety Issue. *Ecotoxicol. Environ. Saf.* **2004**, *59*, 44-56.

(106) Wang, C.-B.; Zhang, W.-x. Synthesizing Nanoscale Iron Particles for Rapid and Complete Dechlorination of TCE and PCBs. *Environ. Sci. Technol.* **1997**, *31*, 2154-2156.

(107) Kanel, S. R.; Manning, B.; Charlet, L.; Choi, H. Removal of Arsenic(III) from Groundwater by Nanoscale Zero-Valent Iron. *Environ. Sci. Technol.* **2005**, *39*, 1291-1298.

(108) Lazar, P.; Otyepka, M. Dissociation of Water at Iron Surfaces: Generalized Gradient Functional and Range-Separated Hybrid Functional Study. *J. Phys. Chem. C* **2012**, *116*, 25470-25477.

(109) Liu, M.; Wang, Y.; Chen, L.; Zhang, Y.; Lin, Z. Mg(OH)2 Supported Nanoscale Zero Valent Iron Enhancing the Removal of Pb(II) from Aqueous Solution. *ACS Appl. Mater. Interfaces* **2015**, *7*, 7961-7969.

(110) Li, Y.; Cheng, W.; Sheng, G.; Li, J.; Dong, H.; Chen, Y.; Zhu, L. Synergetic Effect of a Pillared Bentonite Support on Se(VI) Removal by Nanoscale Zero Valent Iron. *Appl. Catal. B: Environmental* **2015**, *174–175*, 329-335.

(111) Bhowmick, S.; Chakraborty, S.; Mondal, P.; Van Renterghem, W.; Van den Berghe, S.; Roman-Ross, G.; Chatterjee, D.; Iglesias, M. Montmorillonite-Supported Nanoscale Zero-Valent Iron for Removal of Arsenic from Aqueous Solution: Kinetics and Mechanism. *Chem. Eng. J.* **2014**, *243*, 14-23.

(112) Pelton, R. H.; Chibante, P. Preparation of Aqueous Latices with N-isopropylacrylamide. *Colloids Surf.* **1986**, *20*, 247-256.

(113) Virtanen, O. L. J.; Brugnoni, M.; Kather, M.; Pich, A.; Richtering, W. The Next Step in Precipitation Polymerization of N-isopropylacrylamide: Particle Number Density Control by Monochain Globule Surface Charge Modulation. *Polym. Chem.* **2016**, *7*, 5123-5131.

(114) Zhang, D.; Yang, X.: Precipitation Polymerization. In *Encyclopedia of Polymeric Nanomaterials*; Kobayashi, S., Müllen, K., Eds.; Springer Berlin Heidelberg: Berlin, Heidelberg, 2014; pp 1-10.

(115) Tanaka, F.; Koga, T.; Kojima, H.; Xue, N.; Winnik, F. M. Preferential Adsorption and Co-nonsolvency of Thermoresponsive Polymers in Mixed Solvents of Water/Methanol. *Macromolecules* **2011**, *44*, 2978-2989.

(116) Hornig, S.; Biskup, C.; Grafe, A.; Wotschadlo, J.; Liebert, T.; Mohr, G. J.; Heinze, T. Biocompatible Fluorescent Nanoparticles for pH-Sensoring. *Soft Matter* **2008**, *4*, 1169-1172.

(117) Sun, H.; Scharff-Poulsen, A. M.; Gu, H.; Almdal, K. Synthesis and Characterization of Ratiometric, pH Sensing Nanoparticles with Covalently Attached Fluorescent Dyes. *Chem. Mater.* **2006**, *18*, 3381-3384.

(118) Motornov, M.; Zhou, J.; Pita, M.; Gopishetty, V.; Tokarev, I.; Katz, E.; Minko, S. "Chemical Transformers" from Nanoparticle Ensembles Operated with Logic. *Nano Lett.* **2008**, *8*, 2993-2997.

(119) Motornov, M.; Zhou, J.; Pita, M.; Tokarev, I.; Gopishetty, V.; Katz, E.; Minko, S. An Integrated Multifunctional Nanosystem from Command Nanoparticles and Enzymes. *Small* **2009**, *5*, 817-820.

(120) Tam, T. K.; Ornatska, M.; Pita, M.; Minko, S.; Katz, E. Polymer Brush-Modified Electrode with Switchable and Tunable Redox Activity for Bioelectronic Applications. *J. Phys. Chem. C* **2008**, *112*, 8438-8445.

(121) Ghosh, B.; Urban, M. W. Self-Repairing Oxetane-Substituted Chitosan Polyurethane Networks. *Science* **2009**, *323*, 1458-1460.

(122) Cao, P.-F.; Mangadlao, J. D.; Advincula, R. C. Stimuli-Responsive Polymers and their Potential Applications in Oil-Gas Industry. *Polym. Rev.* **2015**, *55*, 706-733.

(123) Li, J.; Mo, L.; Lu, C.-H.; Fu, T.; Yang, H.-H.; Tan, W. Functional Nucleic Acid-Based Hydrogels for Bioanalytical and Biomedical Applications. *Chem. Soc. Rev.* **2016**, *45*, 1410-1431.

(124) Islam, M. R.; Ahiabu, A.; Li, X.; Serpe, M. J. Poly (N-isopropylacrylamide) Microgel-Based Optical Devices for Sensing and Biosensing. *Sensors* **2014**, *14*, 8984-8995.

(125) Culver, H. R.; Clegg, J. R.; Peppas, N. A. Analyte-Responsive Hydrogels: Intelligent Materials for Biosensing and Drug Delivery. *Acc. Chem. Res.* **2017**, *50*, 170-178.

(126) Chen, Y.; Bai, Y.; Chen, S.; Ju, J.; Li, Y.; Wang, T.; Wang, Q. Stimuli-responsive Composite Particles as Solid-stabilizers for Effective Oil Harvesting. *ACS Appl. Mater. Interfaces* **2014**, *6*, 13334-13338.

(127) Sorrell, C. D.; Carter, M. C.; Serpe, M. J. A "paint-on" protocol for the facile assembly of uniform microgel coatings for color tunable etalon fabrication. *ACS Appl. Mater. Interfaces* **2011**, *3*, 1140-1147.

(128) Parasuraman, D.; Serpe, M. J. Poly (N-Isopropylacrylamide) Microgel-based Assemblies for Organic Dye Removal from Water. *ACS Appl. Mater. Interfaces* **2011**, *3*, 4714-4721.

(129) Shewan, H. M.; Stokes, J. R. Review of Techniques to Manufacture Micro-hydrogel Particles for the Food Industry and their Applications. *J. Food Eng.* **2013**, *119*, 781-792.

(130) Johnson, K. C.; Mendez, F.; Serpe, M. J. Detecting solution pH changes using poly (N-isopropylacrylamide)-co-acrylic acid microgel-based etalon modified quartz crystal microbalances. *Anal. Chim. Acta.* **2012**, *739*, 83-88.

(131) Marshall, A. J.; Blyth, J.; Davidson, C. A.; Lowe, C. R. pH-Sensitive Holographic Sensors. *Anal. Chem.* **2003**, *75*, 4423-4431.

(132) Richter, A.; Bund, A.; Keller, M.; Arndt, K.-F. Characterization of a Microgravimetric Sensor Based on pH Sensitive Hydrogels. *Sens. Actuators B Chem.* **2004**, *99*, 579-585.

(133) Bashir, R.; Hilt, J.; Elibol, O.; Gupta, A.; Peppas, N. Micromechanical Cantilever as an Ultrasensitive pH Microsensor. *Appl. Phys. Lett.* **2002**, *81*, 3091-3093.

(134) Yajima, Y.; Yamada, M.; Yamada, E.; Iwase, M.; Seki, M. Facile Fabrication Processes for Hydrogel-Based Microfluidic Devices Made of Natural Biopolymers. *Biomicrofluidics* **2014**, *8*, 1-11.

(135) Lu, B.; Tarn, M.; Pamme, N.; Georgiou, T. Microfluidically fabricated pH-responsive anionic amphiphilic microgels for drug release. *J. Mater. Chem. B* **2016**, *4*, 3086-3093.

(136) Gerlach, G.; Guenther, M.; Suchaneck, G.; Sorber, J.; Arndt, K. F.; Richter, A. Application of Sensitive Hydrogels in Chemical and pH Sensors. *Macromol. Symp.* **2004**, *210*, 403-410.

(137) Christodoulakis, K. E.; Vamvakaki, M. pH-Responsive Microgel Particles Comprising Solely Basic or Acidic Residues. *Macromol. Symp.* **2010**, *291-292*, 106-114.

(138) Ruan, C.; Zeng, K.; Grimes, C. A. A Mass-Sensitive pH Sensor Based on a Stimuli-Responsive Polymer. *Anal. Chim. Acta.* **2003**, *497*, 123-131.

(139) Sorrell, C. D.; Carter, M. C. D.; Serpe, M. J. A "Paint-on" Protocol for the Facile Assembly of Uniform Microgel Coatings for Color Tunable Etalon Fabrication. *ACS Appl. Mater. Interfaces* **2011**, *3*, 1140-1147.

(140) Ruan, C.; Ong, K. G.; Mungle, C.; Paulose, M.; Nickl, N. J.; Grimes, C. A. A wireless pH sensor based on the use of salt-independent micro-scale polymer spheres. *Sens. Actuators. B Chem.* **2003**, *96*, 61-69.

(141) Cai, Q. Y.; Grimes, C. A. A Salt-Independent pH Sensor. *Sens. Actuators B Chem.* **2001**, *79*, 144-149.

(142) Pratt, L. M.; Keavey, K. N.; Pain, G. D.; Mounier, L. Antibacterial Agents. US 6,846,825 BI Jan. 25, 2005.

(143) Debord, J. D.; Lyon, L. A. Synthesis and characterization of pH-responsive copolymer microgels with tunable volume phase transition temperatures. *Langmuir* **2003**, *19*, 7662-7664.

(144) Sorrell, C. D.; Carter, M. C.; Serpe, M. J. Color Tunable Poly (N-Isopropylacrylamide)-co-Acrylic Acid Microgel–Au Hybrid Assemblies. *Adv. Funct. Mater.* **2011**, *21*, 425-433.

(145) Sorrell, C. D.; Serpe, M. J. Glucose Sensitive Poly (N-Isopropylacrylamide) Microgel Based Etalons. *Anal. Bioanal. Chem.* **2012**, *402*, 2385-2393.

(146) Cheng, H.; Shen, L.; Wu, C. LLS and FTIR Studies on the Hysteresis in Association and Dissociation of Poly(N-isopropylacrylamide) Chains in Water. *Macromolecules* **2006**, *39*, 2325-2329.

(147) Higaki, Y.; Kobayashi, M.; Murakami, D.; Takahara, A. Anti-Fouling Behavior of Polymer Brush ImmobilizedSsurfaces. *Polym. J.* **2016**, *48*, 325-331.

(148) Grainger, S. J.; El-Sayed, M. E. Stimuli-sensitive particles for drug delivery. *Biol.-Responsive Hybrid Biomater. World Scientific Publishing Co. Pte. Ltd* **2010**, 171-189.

(149) Beebe, D. J.; Moore, J. S.; Bauer, J. M.; Yu, Q.; Liu, R. H.; Devadoss, C.; Jo, B. H. Functional Hydrogel Structures for Autonomous Flow Control Inside Microfluidic Channels. *Nature* **2000**, *404*, 588-590.

(150) Takashima, Y.; Hatanaka, S.; Otsubo, M.; Nakahata, M.; Kakuta, T.; Hashidzume, A.; Yamaguchi, H.; Harada, A. Expansion-Contraction of Photoresponsive Artificial Muscle Regulated by Host-Guest Interactions. *Nat. Commun.* **2012**, *3*, 1-8.

(151) Kumacheva, E. Hydrogels: The Catalytic Curtsey. *Nat. Mater.* **2012**, *11*, 665-666.

(152) Zhang, J.; Xie, R.; Zhang, S.-B.; Cheng, C.-J.; Ju, X.-J.; Chu, L.-Y. Rapid pH/Temperature-Responsive Cationic Hydrogels with Dual Stimuli-Sensitive Grafted Side Chains. *Polymer* **2009**, *50*, 2516-2525.

(153) Yan, H.; Fujiwara, H.; Sasaki, K.; Tsujii, K. Rapid Swelling/Collapsing Behavior of Thermoresponsive Poly(N-isopropylacrylamide)gel Containing Poly(2-(methacryloyloxy)decylphosphate) Surfactant. *Angew. Chem., Int. Ed.* **2005**, *44*, 1951-1954.

(154) Musch, J.; Schneider, S.; Lindner, P.; Richtering, W. Unperturbed Volume Transition of Thermosensitive poly-(N-isopropylacrylamide) Microgel Particles Embedded in a Hydrogel Matrix. *J. Phys. Chem. B* **2008**, *112*, 6309-6314.

(155) Yoshida, R.; Uchida, K.; Kaneko, Y.; Sakai, K.; Kikuchi, A.; Sakurai, Y.; Okano, T. Comb-type Grafted Hydrogels with Rapid De-Swelling Response to Temperature-Changes. *Nature* **1995**, *374*, 240-242.

(156) Zhang, J.; Chu, L.-Y.; Li, Y.-K.; Lee, Y. M. Dual Thermo- and pH-Sensitive Poly(N-isopropylacrylamide-co-acrylic acid) Hydrogels with Rapid Response Behaviors. *Polymer* **2007**, *48*, 1718-1728.

(157) Xia, L.-W.; Xie, R.; Ju, X.-J.; Wang, W.; Chen, Q.; Chu, L.-Y. Nano-Structured Smart Hydrogels with Rapid Response and High Elasticity. *Nat. Commun.* **2013**, *4*, 1-11.

(158) Kaneko, Y.; Sakai, K.; Kikuchi, A.; Yoshida, R.; Sakurai, Y.; Okano, T. Influence of Freely Mobile Grafted Chain Length on Dynamic Properties of Comb-type Grafted Poly (N-isopropylacrylamide) Hydrogels. *Macromolecules* **1995**, *28*, 7717-7723.

(159) Kaneko, Y.; Sakai, K.; Kikuchi, A.; Sakurai, Y.; Okano, T. Fast Swelling/deswelling Kinetics of Comb- type Grafted Poly (N- isopropylacrylamide) Hydrogels. *Macromol. Symp.* **1996**, *109*, 41-53.

(160) Zhang, X.-Z.; Yang, Y.-Y.; Wang, F.-J.; Chung, T.-S. Thermosensitive Poly(N-isopropylacrylamide-co-acrylic acid) Hydrogels with Expanded Network

Structures and Improved Oscillating Swelling−Deswelling Properties. *Langmuir* **2002**, *18*, 2013-2018.

(161) Hoare, T.; Pelton, R. Functional Group Distributions in Carboxylic Acid Containing Poly(N-isopropylacrylamide) Microgels. *Langmuir* **2004**, *20*, 2123-2133.

(162) Yin, X.; Hoffman, A. S.; Stayton, P. S. Poly(N-isopropylacrylamide-co-propylacrylic acid) Copolymers That Respond Sharply to Temperature and pH. *Biomacromolecules* **2006**, *7*, 1381-1385.

(163) Polotsky, A. A.; Plamper, F. A.; Borisov, O. V. Collapse-to-Swelling Transitions in pH- and Thermoresponsive Microgels in Aqueous Dispersions: The Thermodynamic Theory. *Macromolecules* **2013**, *46*, 8702-8709.

(164) Cho, J. K.; Meng, Z.; Lyon, L. A.; Breedveld, V. Tunable Attractive and Repulsive Interactions Between pH-Responsive Microgels. *Soft Matter* **2009**, *5*, 3599-3602.

(165) Wu, X.; Pelton, R.; Hamielec, A.; Woods, D.; McPhee, W. The kinetics of poly (N-isopropylacrylamide) microgel latex formation. *Colloid Polym. Sci.* **1994**, *272*, 467-477.

(166) Jones, C. D.; Lyon, L. A. Shell-restricted swelling and core compression in poly (N-isopropylacrylamide) core-shell microgels. *Macromolecules* **2003**, *36*, 1988-1993.

(167) Hoare, T.; Pelton, R. Engineering glucose swelling responses in poly (N-isopropylacrylamide)-based microgels. *Macromolecules* **2007**, *40*, 670-678.

(168) Das, M.; Sanson, N.; Kumacheva, E. Zwitterionic poly (betaine-n-isopropylacrylamide) microgels: properties and applications. *Chem. Mater.* **2008**, *20*, 7157-7163.

(169) Sorrell, C. D.; Carter, M. C.; Serpe, M. J. Color Tunable Poly (N-Isopropylacrylamide)-co-Acrylic Acid Microgel–Au Hybrid Assemblies. *Adv. Funct. Mater.* **2011**, *21*, 425-433.

(170) Sorrell, C. D.; Serpe, M. J. Glucose sensitive poly (N-isopropylacrylamide) microgel based etalons. *Anal. Bioanal. Chem.* **2012**, *402*, 2385-2393.

(171) Johnson, K. C.; Mendez, F.; Serpe, M. J. Detecting solution pH changes using poly (N-isopropylacrylamide)-co-acrylic acid microgel-based etalon modified quartz crystal microbalances. *Anal. Chim. Acta* **2012**, *739*, 83-88.

(172) Eke, I.; Elmas, B.; Tuncel, M.; Tuncel, A. A new, highly stable cationic-thermosensitive microgel: Uniform isopropylacrylamide dimethylaminopropylmethacryla mide copolymer particles. *Colloids Surf. A:* **2006**, *279*, 247-253.

(173) Suzuki, D.; Horigome, K. Binary Mixtures of Cationic and Anionic Microgels. *Langmuir* **2011**, *27*, 12368-12374.

(174) Kaur, J.; Harikumar, S. L.; Kaur, A. Interpolyelectrolyte Complexes as Prospective Carriers for Controlled Drug Delivery. *Int. Res. J. Pharm.* **2012**, *3*, 58-62.

(175) Oh, J. K.; Drumright, R.; Siegwart, D. J.; Matyjaszewski, K. The development of microgels/nanogels for drug delivery applications. *Progress in Polymer Science* **2008**, *33*, 448-477.

(176) Oh, J. K.; Lee, D. I.; Park, J. M. Biopolymer-based microgels/nanogels for drug delivery applications. *Prog. Polym. Sci.* **2009**, *34*, 1261-1282.

(177) Soppimath, K.; Aminabhavi, T.; Dave, A.; Kumbar, S.; Rudzinski, W. Stimulus-Responsive "Smart" Hydrogels as Novel Drug Delivery Systems. *Drug Dev. Ind. Pharm.* **2002**, *28*, 957-974.

(178) Zha, L.; Banik, B.; Alexis, F. Stimulus responsive nanogels for drug delivery. *Soft Matter* **2011**, *7*, 5908-5916.

(179) Gao, Y.; Zago, G. P.; Jia, Z.; Serpe, M. J. Controlled and Triggered Small Molecule Release from a Confined Polymer Film. *ACS Appl. Mater. Interfaces* **2013**, *5*, 9803-9808.

(180) Hoare, T. R.; Kohane, D. S. Hydrogels in drug delivery: progress and challenges. *Polymer* **2008**, *49*, 1993-2007.

(181) Kakde, D.; Jain, D.; Shrivastava, V.; Kakde, R.; Patil, A. T. Cancer Therapeutics- Opportunities, Challenges and Advances in Drug Delivery. *J. Appl. Pharm. Sci.* **2011**, *01*, 01-10.

(182) Parasuraman, D.; Sarker, A. K.; Serpe, M. J. Poly (N-Isopropylacrylamide)-Based Microgels and Their Assemblies for Organic-Molecule Removal from Water. *ChemPhysChem* **2012**, *13*, 2507-2515.

(183) Parasuraman, D.; Leung, E.; Serpe, M. J. Poly (N-isopropylacrylamide) microgel based assemblies for organic dye removal from water: microgel diameter effects. *Colloid Polym. Sci.* **2012**, *290*, 1053-1064.

(184) Rmaile, H. H.; Schlenoff, J. B. Internal pKa's in Polyelectrolyte Multilayers- Coupling Protons and Salt. *Langmuir* **2002**, *18*, 8263-8265.

(185) Jiang, L.; Liu, P.; Zhao, S. Magnetic ATP/FA/Poly(AA-co-AM) ternary nanocomposite microgel as selective adsorbent for removal of heavy metals from wastewater. *Colloids Surf. A:* **2015**, *470*, 31-38.

(186) Fu, F.; Wang, Q. Removal of Heavy Metal Ions from Wastewaters: A Review. *J. Environ. Manage.* **2011**, *92*, 407-418.

(187) Al-Rashdi, B. A. M.; Johnson, D. J.; Hilal, N. Removal of Heavy Metal Ions by Nanofiltration. *Desalination* **2013**, *315*, 2-17.

(188) Abdullah, N.; Gohari, R. J.; Yusof, N.; Ismail, A. F.; Juhana, J.; Lau, W. J.; Matsuura, T. Polysulfone/Hydrous Ferric Oxide Ultrafiltration Mixed Matrix Membrane: Preparation, Characterization and its Adsorptive Removal of Lead (II) from Aqueous Solution. *Chem. Eng. J.* **2016**, *289*, 28-37.

(189) Alvarez, M. T.; Crespo, C.; Mattiasson, B. Precipitation of Zn(II), Cu(II) and Pb(II) at Bench-scale Using Biogenic Hydrogen Sulfide from the Utilization of Volatile Fatty Acids. *Chemosphere* **2007**, *66*, 1677-1683.

(190) Chen, Q.; Luo, Z.; Hills, C.; Xue, G.; Tyrer, M. Precipitation of Heavy Metals from Wastewater Using Simulated Flue Gas: Sequent Additions of Fly Ash, Lime and Carbon Dioxide. *Water Res.* **2009**, *43*, 2605-2614.

(191) Ku, Y.; Jung, I.-L. Photocatalytic Reduction of Cr(VI) in Aqueous Solutions by UV Irradiation with the Presence of Titanium Dioxide. *Water Res.* **2001**, *35*, 135-142.

(192) Gupta, S.; Tai, N.-H. Carbon Materials as Oil Sorbents: A Review on the Synthesis and Performance. *J. Mater. Chem. A* **2016**, *4*, 1550-1565.

(193) Li, B.; Zhou, F.; Huang, K.; Wang, Y.; Mei, S.; Zhou, Y.; Jing, T. Highly Efficient Removal of Lead and Cadmium During Wastewater Irrigation Using a Polyethylenimine-grafted Gelatin Sponge. *Sci. Rep.* **2016**, *6*, 33573.

(194) Inagaki, M.; Qiu, J.; Guo, Q. Carbon Foam: Preparation and Application. *Carbon* **2015**, *87*, 128-152.

(195) Tofighy, M. A.; Mohammadi, T. Adsorption of Divalent Heavy Metal Ions from Water using Carbon Nanotube Sheets. *J. Hazard. Mater.* **2011**, *185*, 140-147.

(196) Lee, C.-G.; Song, M.-K.; Ryu, J.-C.; Park, C.; Choi, J.-W.; Lee, S.-H. Application of Carbon Foam for Heavy Metal Removal from Industrial Plating Wastewater and Toxicity Evaluation of the Adsorbent. *Chemosphere* **2016**, *153*, 1-9.

(197) Wan Ngah, W. S.; Teong, L. C.; Hanafiah, M. A. K. M. Adsorption of Dyes and Heavy Metal Ions by Chitosan Composites: A Review. *Carbohydr. Polym.* **2011**, *83*, 1446-1456.

(198) Hua, M.; Zhang, S.; Pan, B.; Zhang, W.; Lv, L.; Zhang, Q. Heavy Metal Removal from Water/Wastewater by Nanosized Metal Oxides: A Review. *J. Hazard. Mater.* **2012**, *211*, 317-331.

(199) Gupta, V. K.; Carrott, P. J. M.; Carrott, M.; Suhas. Low-Cost Adsorbents: Growing Approach to Wastewater Treatmenta Review. *Crit. Rev. Environ. Sci. Technol.* **2009**, *39*, 783-842.

(200) Babel, S.; Kurniawan, T. A. Low-cost Adsorbents for Heavy Metals Uptake from Contaminated Water: A Review. *J. Hazard. Mater.* **2003**, *97*, 219-243.

(201) Crini, G. Non-Conventional Low-cost Adsorbents for Dye Removal: A Review. *Bioresour. Technol.* **2006**, *97*, 1061-1085.

(202) Nguyen, T. A. H.; Ngo, H. H.; Guo, W. S.; Zhang, J.; Liang, S.; Yue, Q. Y.; Li, Q.; Nguyen, T. V. Applicability of Agricultural Waste and By-Products for Adsorptive Removal of Heavy Metals from Wastewater. *Bioresour. Technol.* **2013**, *148*, 574-585.

(203) Gautam, R. K.; Mudhoo, A.; Lofrano, G.; Chattopadhyaya, M. C. Biomass-Derived Biosorbents for Metal Ions Sequestration: Adsorbent Modification and Activation Methods and Adsorbent Regeneration. *J. Environ. Chem. Eng.* **2014**, *2*, 239-259.

(204) Islam, M. R.; Serpe, M. J. Label-free detection of low protein concentration in solution using a novel colorimetric assay. *Biosens. Bioelectron.* **2013**, *49*, 133-138.

(205) Snowden, M. J.; Thomas, D.; Vincent, B. Use of Colloidal Microgels for the Absorption of Heavy-Metal and Other Ions from Aqueous-Solution *Analyst* **1993**, *118*, 1367-1369.

(206) Morris, G. E.; Vincent, B.; Snowden, M. J. Adsorption of Lead Ions onto N-isopropylacrylamide and Acrylic Acid Copolymer Microgels. *J. Colloid Interface Sci.* **1997**, *190*, 198-205.

(207) Li, Y.; Chen, C.; Li, B.; Sun, J.; Wang, J.; Gao, Y.; Zhao, Y.; Chai, Z. Elimination Efficiency of Different Reagents for the Memory Effect of Mercury using ICP-MS. *J. Anal. At. Spectrom.* **2006**, *21*, 94-96.

(208) Bae, Y. H.; Okano, T.; Kim, S. W. Temperature-Dependence of Swelling of Cross-linked Poly(N,N'-alkyl substituted acrylamides) in Water. *J. Polym. Sci. B Polym. Phys.* **1990**, *28*, 923-936.

(209) Zhang, Q. L.; Weber, C.; Schubert, U. S.; Hoogenboom, R. Thermoresponsive Polymers with Lower Critical Solution Temperature: From

Fundamental Aspects and Measuring Techniques to Recommended Turbidimetry Conditions. *Mater. Horiz.* **2017**, *4*, 109-116.

(210) Martínez, M.; Miralles, N.; Hidalgo, S.; Fiol, N.; Villaescusa, I.; Poch, J. Removal of Lead(II) and Cadmium(II) from Aqueous Solutions Using Grape Stalk Waste. *J. Hazard. Mater.* **2006**, *133*, 203-211.

(211) Zhu, Q.; Li, Z. Hydrogel-Supported Nanosized Hydrous Manganese Dioxide: Synthesis, Characterization, and Adsorption Behavior Study for Pb2+, Cu2+, Cd2+ and Ni2+ Removal from Water. *Chem. Eng. J.* **2015**, *281*, 69-80.

(212) Gupta, V. K.; Agarwal, S.; Saleh, T. A. Synthesis and Characterization of Alumina-Coated Carbon Nanotubes and their Application for Lead Removal. *J. Hazard. Mater.* **2011**, *185*, 17-23.

(213) Hoare, T.; McLean, D. Kinetic Prediction of Functional Group Distributions in Thermosensitive Microgels. *J. Phys. Chem. B* **2006**, *110*, 20327-20336.

(214) Echeverria, C.; López, D.; Mijangos, C. UCST Responsive Microgels of Poly(acrylamide−acrylic acid) Copolymers: Structure and Viscoelastic Properties. *Macromolecules* **2009**, *42*, 9118-9123.

(215) Chen, J. J.; Ahmad, A. L.; Ooi, B. S. Poly(N-isopropylacrylamide-co-acrylic acid) Hydrogels for Copper Ion Adsorption: Equilibrium Isotherms, Kinetic and Thermodynamic Studies. *J. Environ. Chem. Eng.* **2013**, *1*, 339-348.

(216) Chen, J. J.; Ahmad, A. L.; Ooi, B. S. Thermo-responsive properties of poly(N-isopropylacrylamide-co-acrylic acid) hydrogel and its effect on copper ion removal and fouling of polymer-enhanced ultrafiltration. *J. Membr. Sci.* **2014**, *469*, 73-79.

(217) Wingenfelder, U.; Nowack, B.; Furrer, G.; Schulin, R. Adsorption of Pb and Cd by Amine-Modified Zeolite. *Water Res.* **2005**, *39*, 3287-3297.

(218) Xia, X.; Ling, L.; Zhang, W.-x. Genesis of Pure Se(0) Nano- and Micro-Structures in Wastewater with Nanoscale Zero-Valent Iron (nZVI). *Environ. Sci. Nano* **2017**, *4*, 52-59.

(219) Liang, L.; Yang, W.; Guan, X.; Li, J.; Xu, Z.; Wu, J.; Huang, Y.; Zhang, X. Kinetics and Mechanisms of pH-Dependent Selenite Removal by Zero Valent Iron. *Water Res.* **2013**, *47*, 5846-5855.

(220) Myneni, S. C. B.; Tokunaga, T. K.; Brown, G. E. Abiotic Selenium Redox Transformations in the Presence of Fe(II,III) Oxides. *Science* **1997**, *278*, 1106.

(221) Chen, Y.-W.; Li, L.; D'Ulivo, A.; Belzile, N. Extraction and Determination of Elemental Selenium in Sediments—A Comparative Study. *Anal. Chim. Acta* **2006**, *577*, 126-133.

(222) Breynaert, E.; Bruggeman, C.; Maes, A. XANES−EXAFS Analysis of Se Solid-Phase Reaction Products Formed upon Contacting Se(IV) with FeS2 and FeS. *Environ. Sci.Technol.* **2008**, *42*, 3595-3601.

(223) Crane, R. A.; Scott, T. B. Nanoscale Zero-Valent Iron: Future Prospects for an Emerging Water Treatment Technology. *J. Hazard. Mater.* **2012**, *211-212*, 112-125.

(224) Zhao, X.; Liu, W.; Cai, Z. Q.; Han, B.; Qian, T. W.; Zhao, D. Y. An Overview of Preparation and Applications of Stabilized Zero-Valent Iron Nanoparticles for Soil and Groundwater Remediation. *Water Res.* **2016**, *100*, 245-266.

(225) Tiraferri, A.; Chen, K. L.; Sethi, R.; Elimelech, M. Reduced Aggregation and Sedimentation of Zero-Valent Iron Nanoparticles in the Presence of Guar Gum. *J. Colloid Interface Sci.* **2008**, *324*, 71-79.

(226) Cirtiu, C. M.; Raychoudhury, T.; Ghoshal, S.; Moores, A. Systematic Comparison of the Size, Surface Characteristics and Colloidal Stability of Zero Valent Iron Nanoparticles pre- and post-Grafted with Common Polymers. *Colloids Surf. A Physicochem. Eng. Asp.* **2011**, *390*, 95-104.

(227) Sakulchaicharoen, N.; O'Carroll, D. M.; Herrera, J. E. Enhanced Stability and Dechlorination Activity of pre-Synthesis Stabilized Nanoscale FePd Particles. *J. Contam. Hydrol.* **2010**, *118*, 117-127.

(228) Singh, R.; Misra, V. Stabilization of Zero-Valent Iron Nanoparticles: Role of Polymers and Surfactants. *Handbook of Nanoparticles* **2015**, 1-19.

(229) Saleh, N.; Sirk, K.; Liu, Y.; Phenrat, T.; Dufour, B.; Matyjaszewski, K.; Tilton, R. D.; Lowry, G. V. Surface Modifications Enhance Nanoiron Transport and NAPL Targeting in Saturated Porous Media. *Environ. Eng. Sci.* **2007**, *24*, 45-57.

(230) Wang, Z.; Choi, F.; Acosta, E. Effect of Surfactants on Zero-Valent Iron Nanoparticles (NZVI) Reactivity. *J. Surfactants Deterg.* **2017**, *20*, 577-588.

(231) Xiao, S.; Wu, S.; Shen, M.; Guo, R.; Huang, Q.; Wang, S.; Shi, X. Polyelectrolyte Multilayer-Assisted Immobilization of Zero-Valent Iron Nanoparticles onto Polymer Nanofibers for Potential Environmental Applications. *ACS Appl. Mater. Interfaces* **2009**, *1*, 2848-2855.

(232) Khan, K.; Shaikh, A. J.; Siddiq, M.; Sherazi, T. A.; Nawaz, M. In Situ Formation of Copper Nanoparticles in a P(NIPAM-VAA-AAm) Terpolymer Microgel that Retains the Swelling Behavior of Microgels. *J. Polym. Eng.* **2016**, *36*, 287-292.

(233) Nurmi, J. T.; Tratnyek, P. G.; Sarathy, V.; Baer, D. R.; Amonette, J. E.; Pecher, K.; Wang, C.; Linehan, J. C.; Matson, D. W.; Penn, R. L.; Driessen, M. D. Characterization and Properties of Metallic Iron Nanoparticles: Spectroscopy, Electrochemistry, and Kinetics. *Environ. Sci. Technol.* **2005**, *39*, 1221-1230.

Appendices

The Appendix session shows unpublished works that have not formed a major part of the thesis. It also includes projects that have not been completed and may need further attention.

Appendix A

Crown Ether Functionalized Microgels for Selective Removal of Metal Ions

Microgels are excellent sorbents for the remediation of both organics and heavy metal ions. However, they are limited in their inability to perform selective sorption of contaminants. In order to introduce selectivity, this mini project was aimed at incorporating ion selective moieties, known as selectophores into the microgel network to impart selectivity to the microgel. Two approaches were used in this synthesis. The first involved the functionalization of pNIPAm-*co*-AAc microgels with amine containing crown ethers (specifically 4'-aminobenzo-18-crown-6) via the EDC coupling approach. The second method involved a direct copolymerization of NIPAm with 4'-acrylamidobenzo-18-crown-6 monomer. The bulky nature of the crown ether made the direct polymerization challenging, as the heavier crown ether precipitates early out of the solution and barely formed microgels. Though the EDC coupling method provided some means of functionalization, the success rate was relatively low.

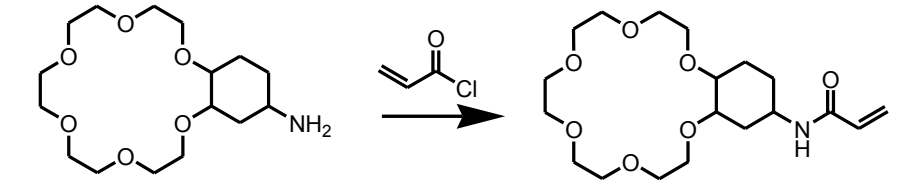

Figure A-1. Synthesis of 4-acrylamidobenzo-18-crwon-6 (4-AB18C6). The synthesized 4-AB18C6 was used to synthesize microgels similarly to that shown in previous Chapters.

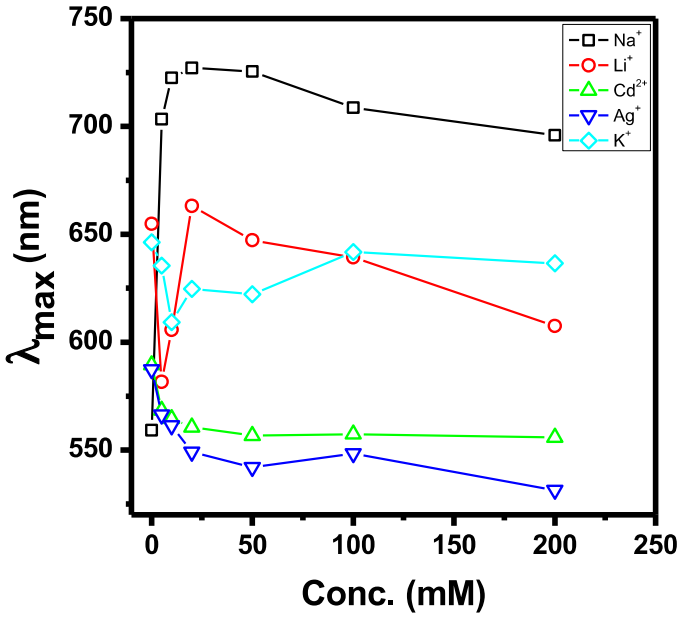

Figure A-2. 4'-AB18C6 based microgel- based etalons' response to different metal ions. Lines are eye-guides. The fabricated device was immersed in pH 6.5, 2 mM ionic strength solution and the response was monitored over the indicated salt concentration ranges.

Appendix B

Ion Selective Membranes for Selective Sensing of Chromium Ions

As mentioned in previous Chapters regarding the selectivity challenge with pNIPAm-based microgels, a facile method to introduce selectivity was developed. Briefly, ion selective membranes were fabricated on top of the pNIPAm-*co*-AAc microgel etalon. This membrane contains ionophores that are selective to the ion of interest and bars other ions from passing through. The mechanism is similar to the K^+ channel across the cell membrane found in most living organisms.

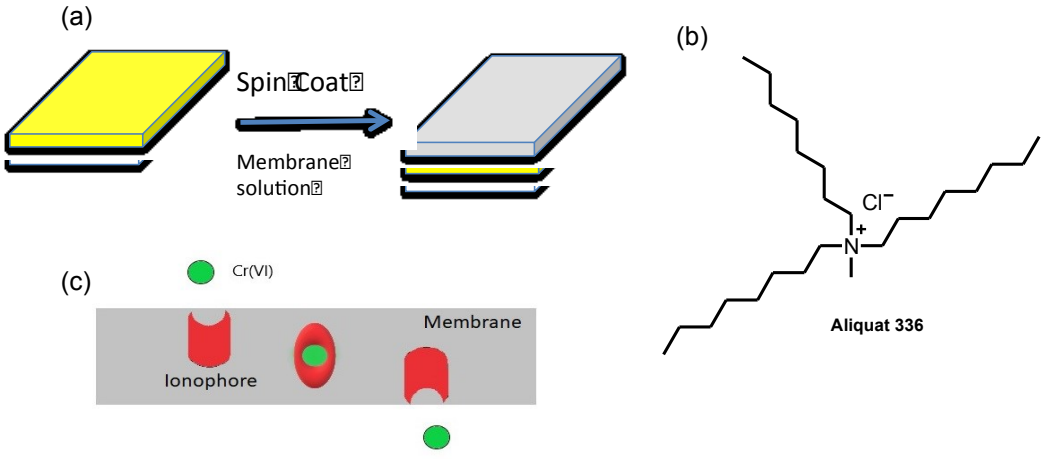

Figure B-1. (a) Experimental procedure for casting ion selective membrane on top of etalon, (b) chemical structure of Aliquat 336, the ionophore used in this study and (c)

schematic representation of Cr ion passage through the ion channels of the membrane.

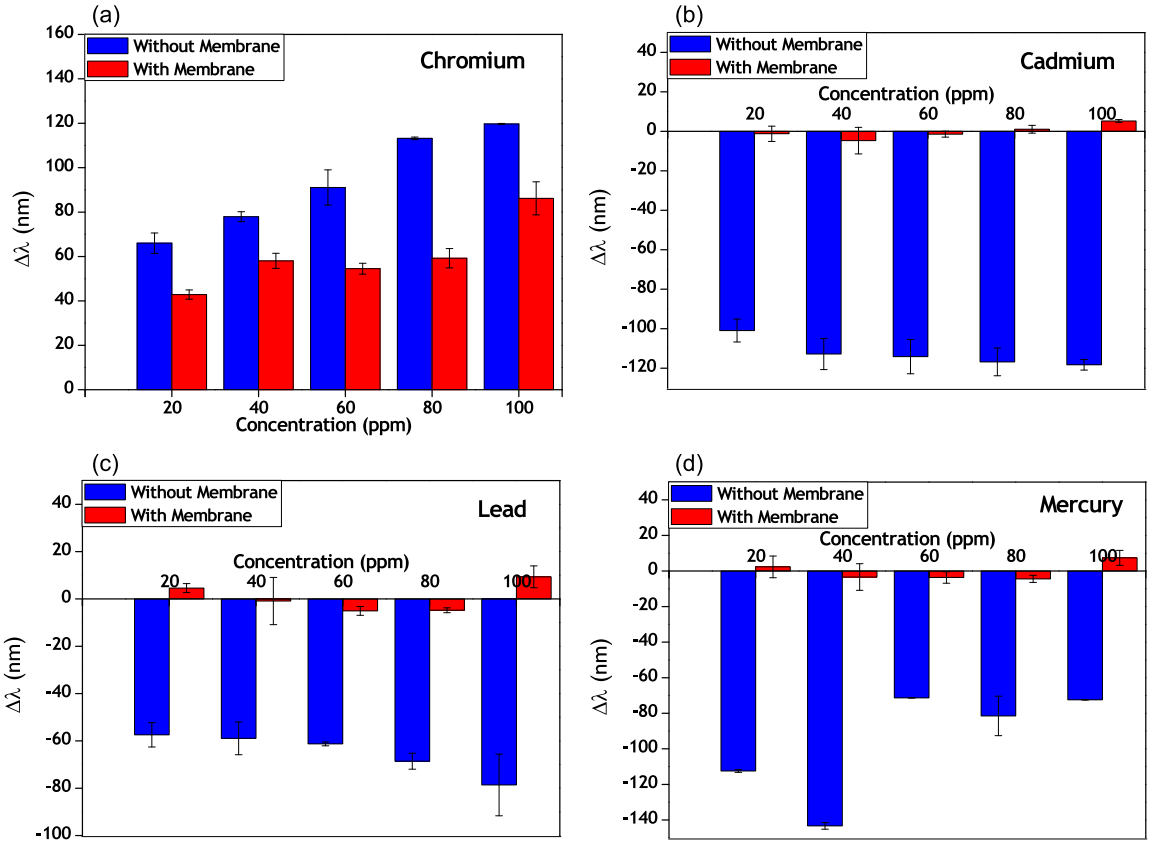

Figure B-2. Etalon response to different heavy metals with or without Cr ion selective membrane. All the etalons without membrane, show response to the metal ions tested. However, the etalon response in the presence of the membrane decreased significantly to almost no signal change in response to metal ion concentrations for other metal ions except for Cr. This proves that the membrane selectively created a channel specific for Cr and bared the other ions from passing through.

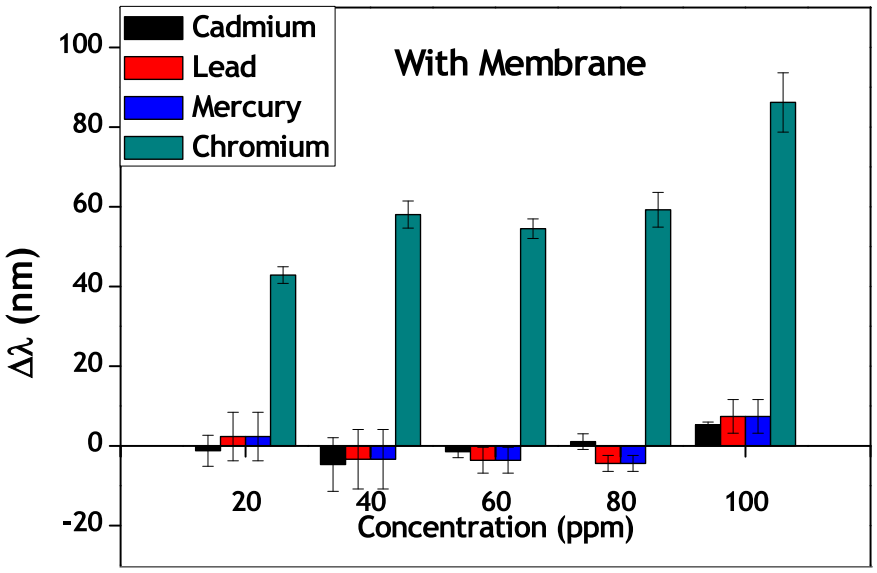

Figure B-3. A comparison of the membrane-etalon response to all metal ions, with Cr ions showing the highest response.

Appendix C

Oil Sands Processed Affected Clay (OSPC) as Sorbents for Organics and Heavy Metal Ions

The oilsands of Canada, mostly in the province of Alberta, contributes a significant part of the Canadian gross domestic product. The increased in mining operations lead to increased waste being generated that are of environmental concerns. Recently, the Alberta Energy Regulator (AER), a regulatory body that regulates the operations of the Oil Sands Company has set limits to the amount of OSPC that these companies can store onsite. Tons of these solids are generated and are mostly stored onsite. Due to the current regulation by AER, there is the need to find alternative means of storing these OSPC wastes. These OSPC contain toxic contaminants such as naphthenic acids (NAs) and other contaminants of environmental concerns. These are the focus of other research groups, but the main focus here was to utilize these OSPC wastes to remove organics and heavy metal ions. As these OSPCs contain NAs, they might have been templated to have affinity towards organics. Crystal violet (CV) was used as a model organic molecule. Kaolin and Bentonite are the common clay known to be found in the OSPC. Therefore, we sort to explore how the uptake of CV by OSPC compared to the sorption of CV by Kaolin and Bentonite.

Scheme C-1. Experimental procedure for removal of CV from aqueous solution by OSPC.

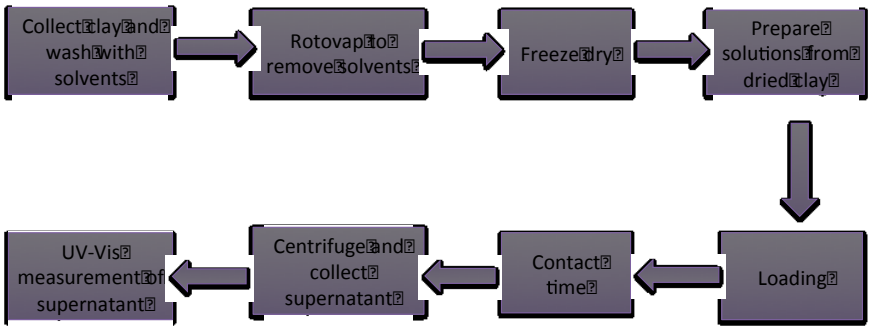

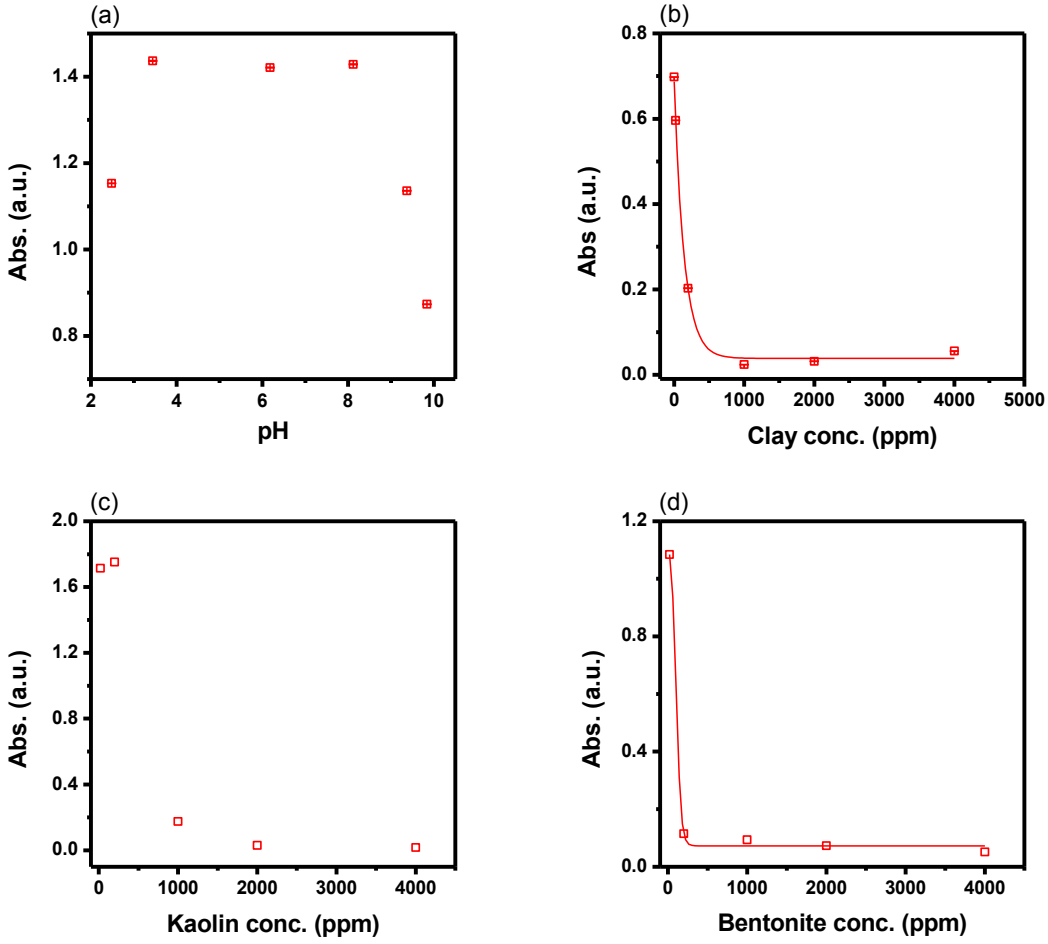

Figure C-1. PH effect and sorbent dose studies. (a) Effect of pH on stability of 4 ppm CV at 1 h contact time, sorbent dose studies with 20 ppm of CV for (b) OSPC, (c) Kaolin and (d) Bentonite. Symbols are data points and curves in b and d are fitted with non-linear weighted Boltzman curve fitting using OriginLab Pro version 8.5 program software.

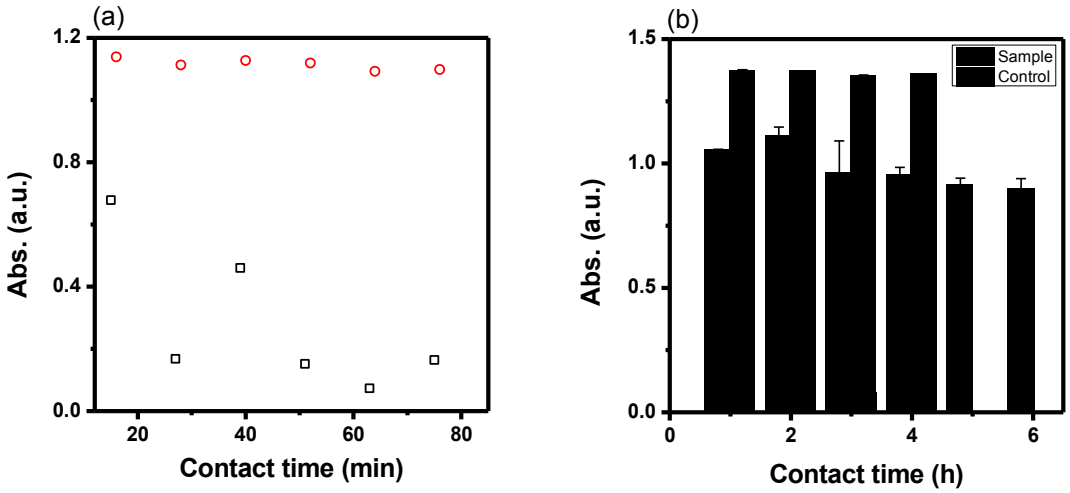

Figure C-2. A contact time study for removal of CV by OSPC at less contact time (a) and higher contact time (b). Red cycles in (a) represent control samples without the OSPC and the black squares are the data after CV contact with OSPC.

In Figure C-2b, the effect of contact time in uptake of CV by the sorbent was studied. The control experiment showed that the organic dye is stable over the duration of the experiment. The minimum contact time required for maximum uptake of CV is 1 h, as there is no significant difference in uptake beyond 1 h of contact time.

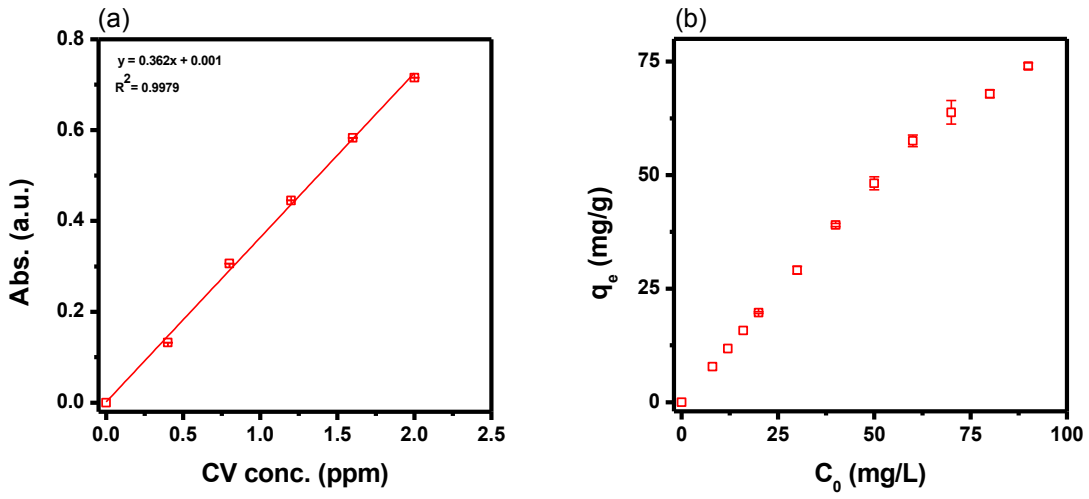

Figure C-3. (a) Calibration curve for CV used to calculate the removal efficiency of CV by the OSPC, (b) adsorption of CV by OSPC in the form of adsorbed amount (q_e) as a function of initial sorbate concentration (C_0). The maximum adsorption capacity is estimated at 74.0 mg/g.

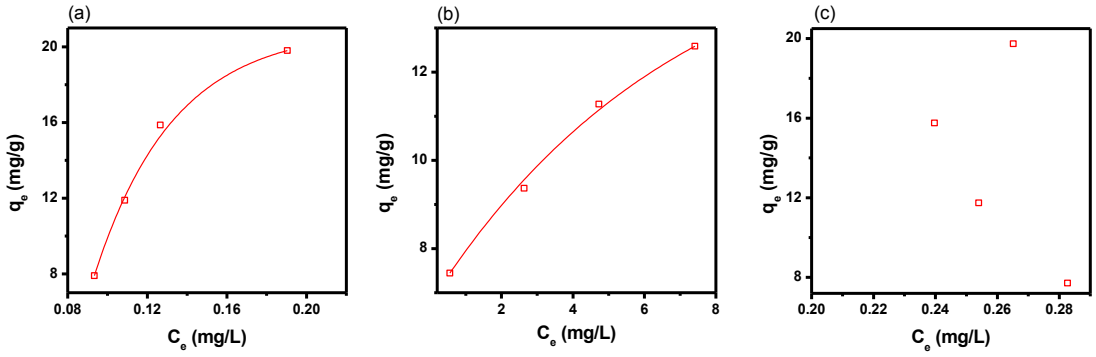

Figure C-4. Adsorption isotherms for (a) OSPC, (b) Kaolin and (c) Bentonite in their uptake of CV. Symbols represent data point and the curves are fitted to the Exponential Association model in OriginLab Pro version 8.5 software program.

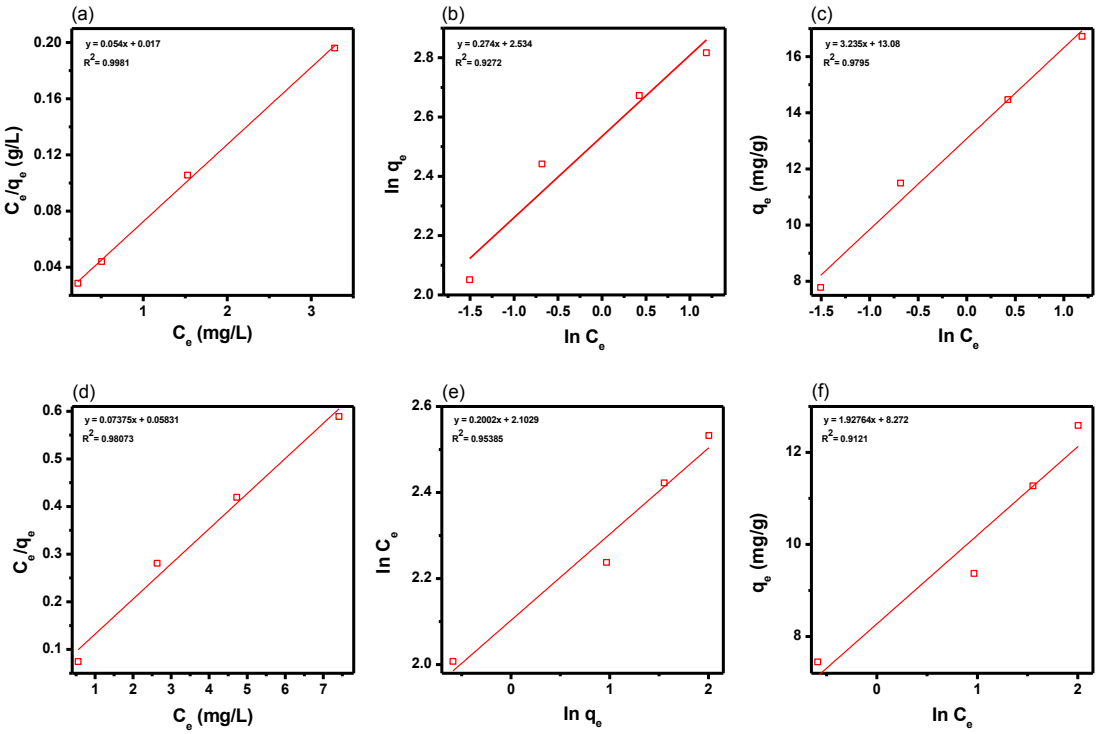

Figure C-5. (a,d) Langmuir, (b,e) Freundlich and (c,f) Temkin isotherms to fit the adsorption of CV data by (a-c) OSPC and (d-f) Kaolin. Symbols represent data points and the curves are fits to the linear best-fit model. The adsorption isotherm that best fits the adsorption process by OSPC is the Langmuir adsorption isotherm. The Temkin adsorption isotherm best fits the adsorption of CV by Kaolin. The best fits isotherms were judged based on the fit parameters such as the R^2 values.

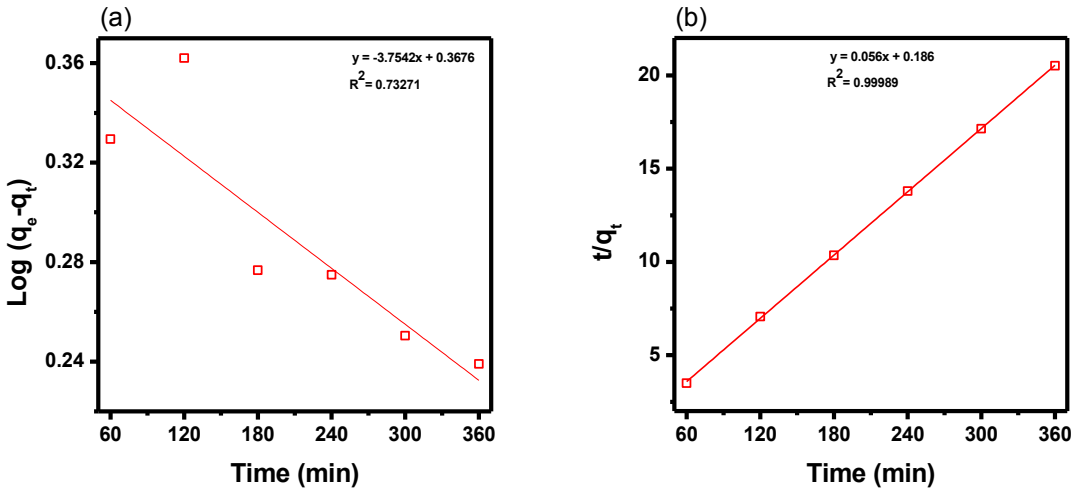

Figure C-6. Kinetics study of the adsorption of CV by the OSPC. (a) Pseudo first order kinetics and (b) Pseudo second order kinetics. Symbols represent data points and the curves are fits to the linear best-fit model. The adsorption kinetics suggests that the adsorption of CV by OSPC follows a Pseudo second order kinetics, as the data fits well to the linear least square fit model, judged by the R^2 value.

Table C-1. Zeta potential (ZP) measurements (mV) at different pH for sorbents used in this study.

	pH		
Sorbent	ZP @ 2.0	ZP @ 5.5	ZP @ 10
OSPC	-21.5	-28.8	-41.9
Bentonite	-24.8	-31.9	-23.0
Kaolin	-23.8	-28.8	-49.2

Table C-2. Adsorption capacity values at different initial concentrations of CV for the three sorbents studied. 1000 ppm solutions of sorbents were used at a contact time of 1 h.

	q_e (mg/g)		
C_0 (mg/L)	OSPC	Kaolin	Bentonite
8	7.91	7.44	7.72
12	11.9	9.37	11.7
16	15.9	11.3	15.8
20	19.8	12.6	19.7

The OSPC, though thought of as wastes, their potential for the remediation of organics, specifically CV, have been demonstrated. Their competitive adsorption makes them attractive for the removal of other environment contaminants. The potential of the OSPC to be used as sorbents were investigated for heavy metal ions, such as Cd^{2+} and Pb^{2+}. Calibration curves for their determination are shown in Figure C-7 using ICP-OES.

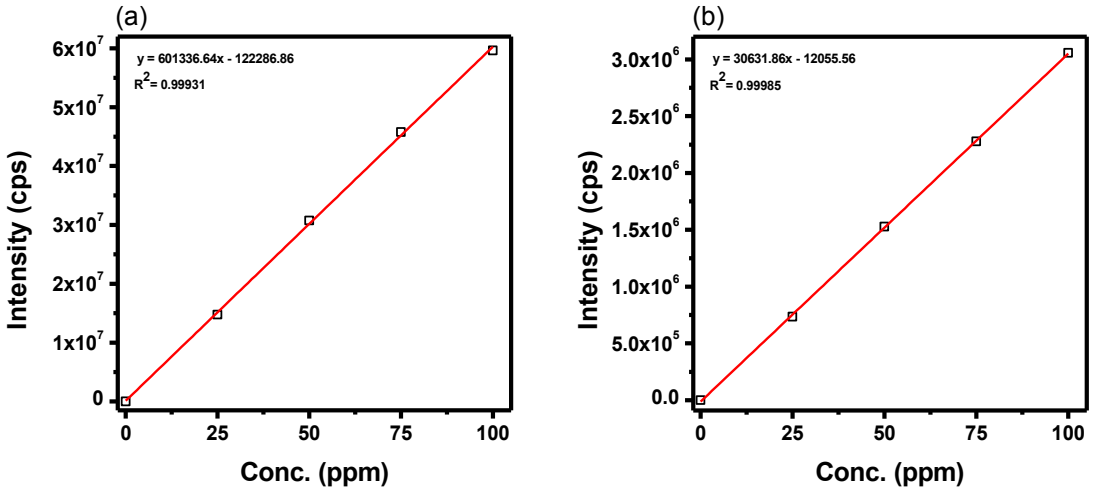

Figure C-7. Calibration curves for the Cd^{2+} and Pb^{2+} used to quantify the uptake efficiency of Cd^{2+} and Pb^{2+} by the OSPC.

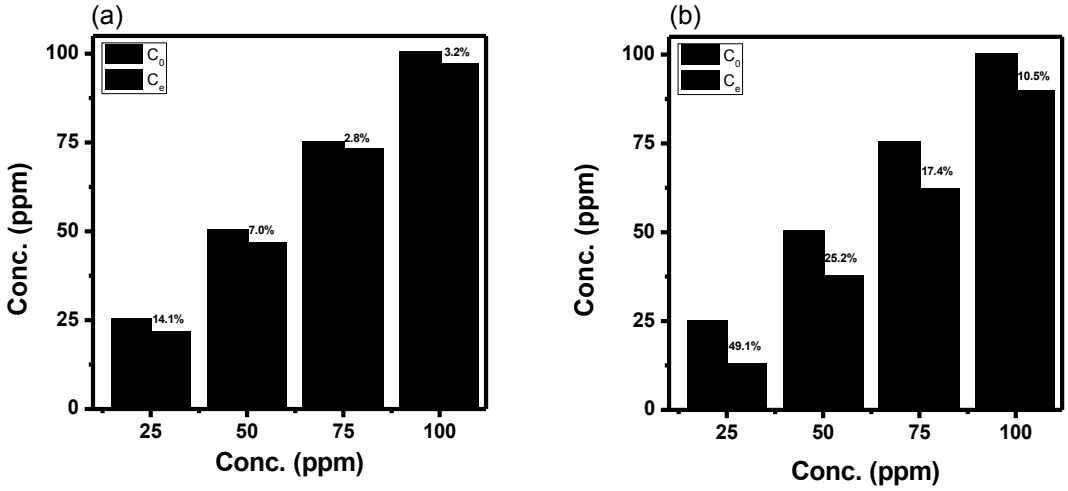

Figure C-8. Concentrations of ions before (black) and after removal by OSPC (red stripes) for (a) Cd^{2+} and (b) Pb^{2+}. Percentages denote removal efficiency in both cases. Even though the removal efficiencies were low in both cases, the OSPC have affinity towards Pb^{2+} than for Cd^{2+}.

Appendix D

Hybrid Clay-Hydrogel Sorbents for Organic Dye Removal from Water

This project sort to introduce a new functionality by making composite microgels using the spent OSPC. Because of the understanding of the behavior of microgels in removing organic dyes, as well as initial studies on removal of organic dyes with the OSPC, this project sort to generate a hybrid sorbents, composing of microgels and OSPC. Initial results show that removal of model organic dye, CV was enhanced by the incorporation of some mole % of the OSPC.

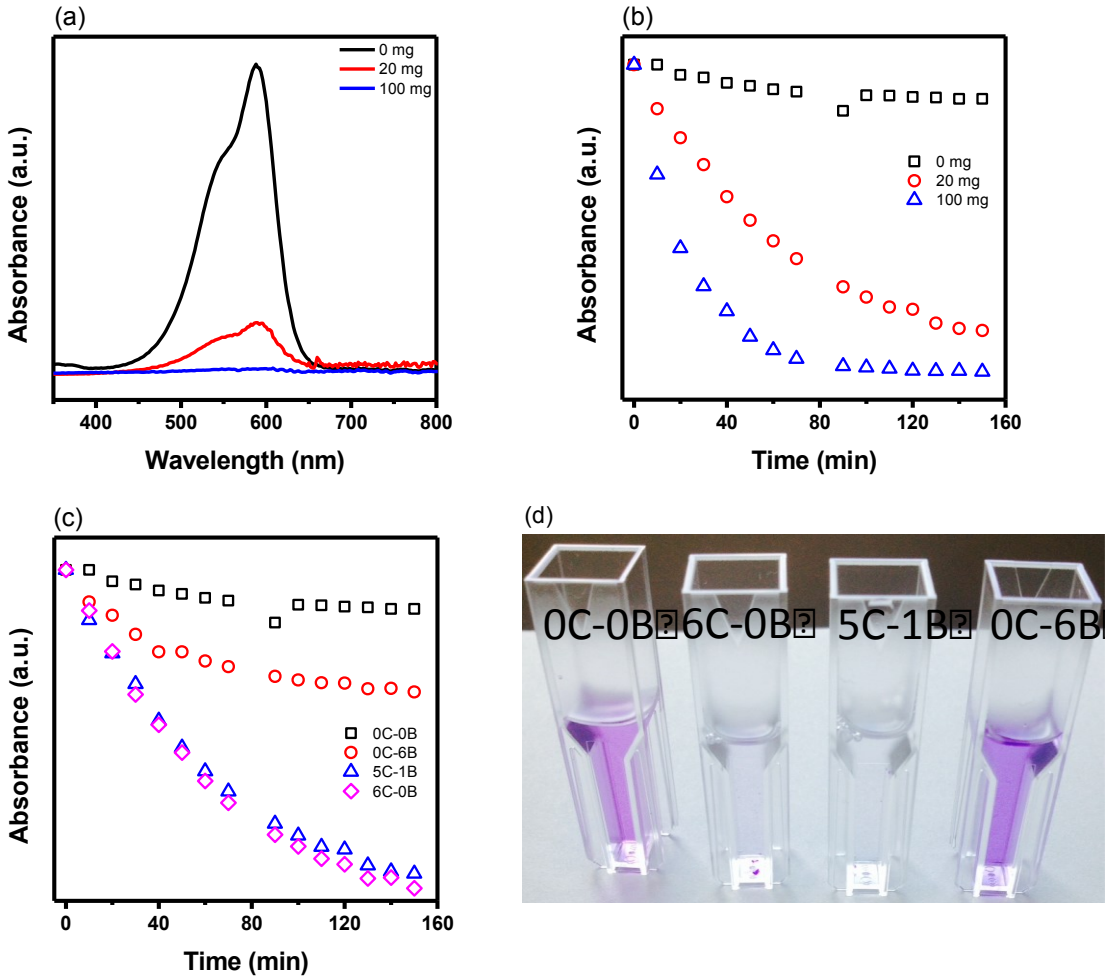

Figure D-1. (a) UV-Vis spectrum of CV showing the removal efficiency of different sorbent dose at 150 min of contact, (b) UV-Vis absorbance showing the uptake of CV over time at different sorbent dose, (c) absorbance showing the removal of CV by different composition of sorbents and (d) photographs of equilibrium concentrations of CV after 150 min contact time with 20 mg sorbent dose. C represents OSPC and B represents BIS. The numbers preceding the letters are the mole percent of the corresponding materials in the final hydrogel.

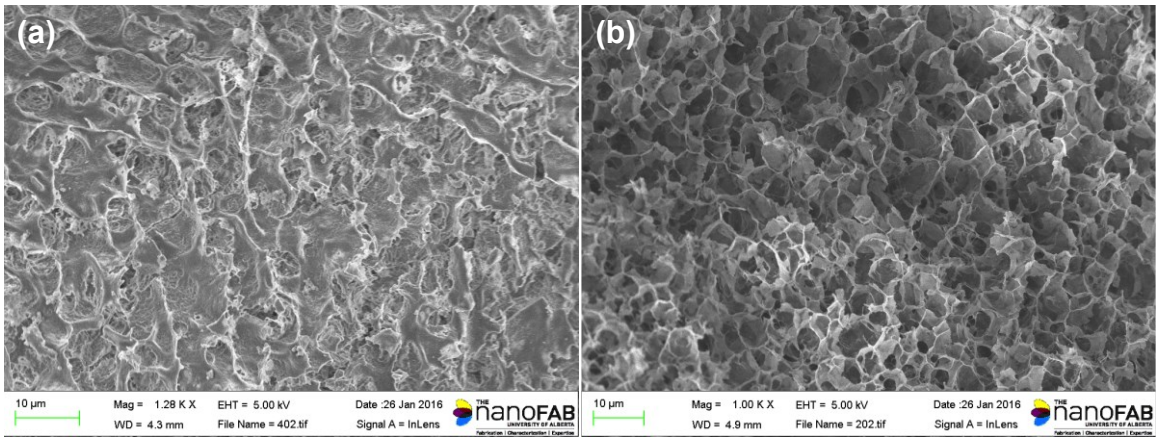

Figure D-2. SEM images of (a) 0C-6B and (b) 6C-0B. Figure (a) shows a dense packed structure of the sorbents, with a possible blocking of some sorption sites. Figure (b) shows honey-comb-like structures, with void spaces that can enhance removal of CV.

Appendix E

Putting Waste to Use: A Case of Cigarette Butts

This project sort to utilize the common things we see, yet are nuisance not only to the environment, but also to humans. According to the Surfrider Foundation's "Hold on to Your Butt campaign", cigarette butts are the most littered item in the world. It is estimated that 4.95-trillion of cigarette butts are tossed onto the ground or into water every year. Out of the $11-billion that the U.S. spends a year on litter clean-up, 32% of it goes into cleaning these cigarette butts.[d] Being interested in environmental remediation, this project put what is considered a nuisance to good use by utilizing them as sorbents for the removal of organic dyes with crystal violet (CV) and methylene blue (MB) as model organic molecules. The results so far, show incredible removal efficiency by these cigarette butts towards MB over CV, indicating their potential as sorbents for removing organic pollutants.

[d] https://sandiego.surfrider.org/2012/08/22/hold-on-to-your-butt-awareness-day-2012/ (accessed on October 22, 2017)

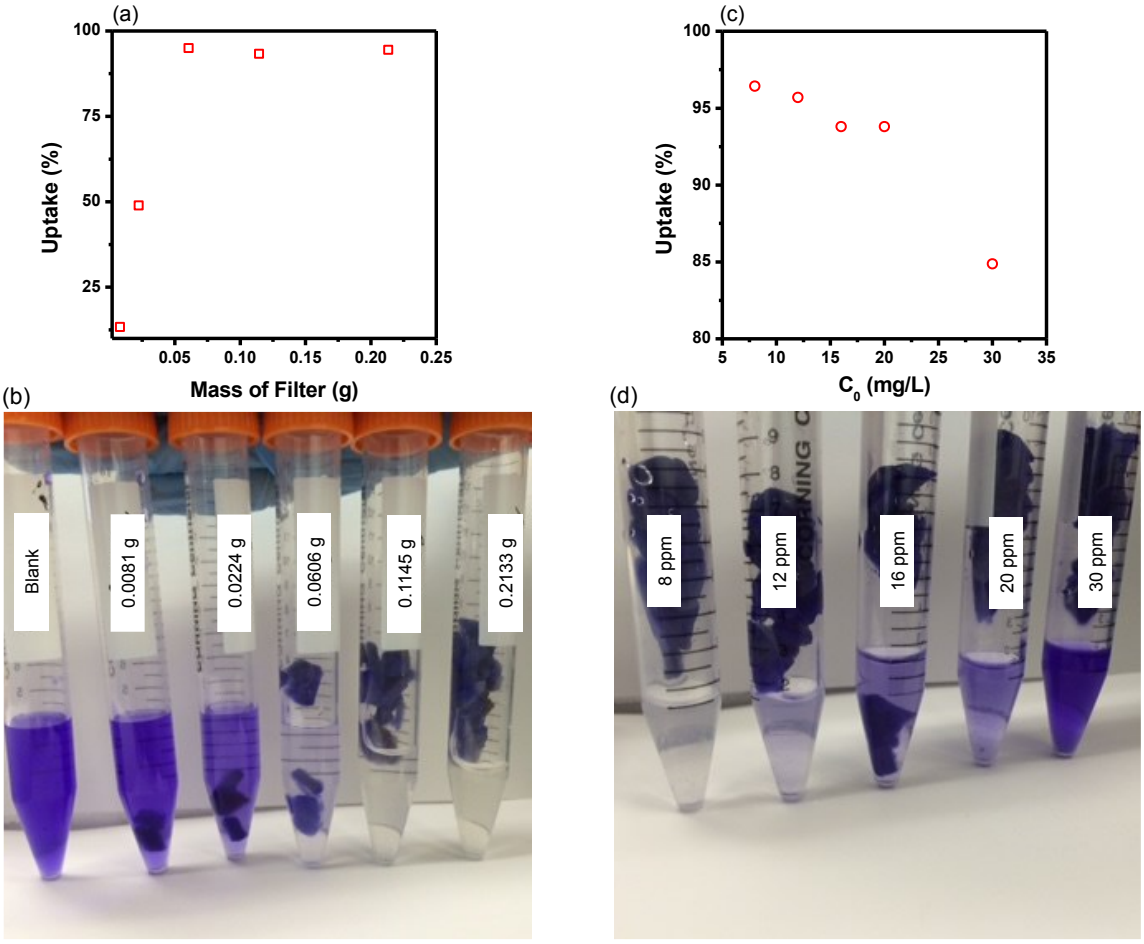

Figure E-1. Cigarette butt removal of CV from aqueous solution. (a) Sorbent dose effect on uptake of CV, (b) photographs showing uptake of initial 4 ppm CV after 30 min of contact time, (c) adsorption capacity studies shown as a plot of percent uptake as a function of initial concentrations of CV and (d) photograph showing the uptake capacity. Error bars are about the size of the data points.

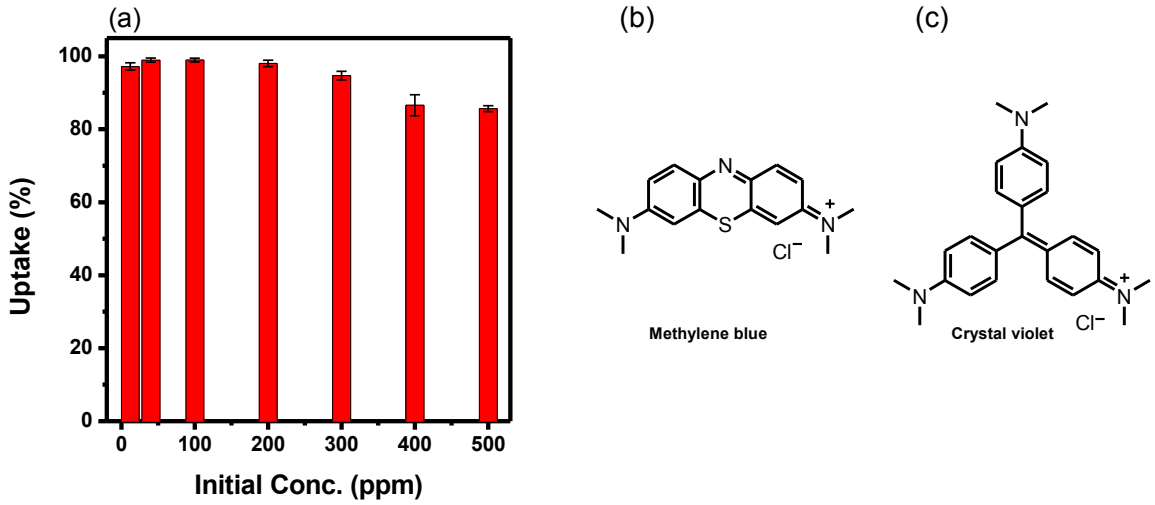

Figure E-2. (a) Uptake of MB as a function of initial concentration using 0.2 g of sorbent. As seen here, even at higher dose of sorbate, there is still a higher uptake. Chemical structures of (b) MB and (c) CV.

Appendix F

Unexpected Ionic Strength Response by Confined Microgels

The effects of ionic strength on microgels have been studied by a number of research groups. Generally, increased ionic strength results in decreased microgel diameter. This phenomenon can be explained mostly by employing the double layer theory. However, under confined conditions, such as in the case of etalon devices, a phenomenon that deviates from the double layer theory is observed, where the increase in salt concentration rather caused an increase in the microgel size at lower salt concentrations. Interestingly, the double layer theory explanation holds true only at higher concentrations according to the results of this work. At lower concentrations however, the hydration energy associated with the ions dominates the shielding effect from the ions at higher concentrations. Therefore, instead of a decreased diameter with increasing ionic strength, an initial increased in diameter was observed, as a result of an increased hydration sphere at lower concentrations.

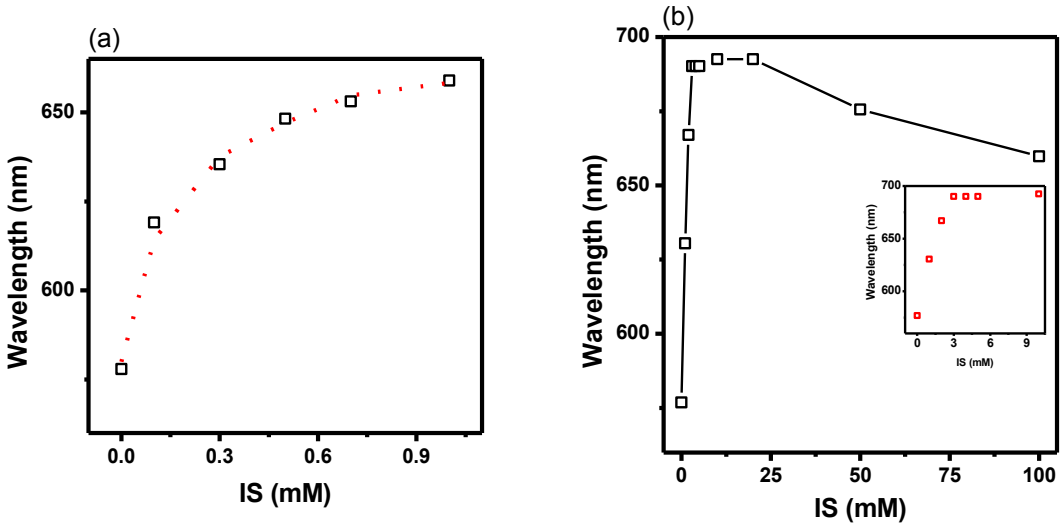

Figure F-1. Ionic strength response of p(NIPAm-*co*-AAc) microgel etalon at pH 6.5 at (a) low concentrations and (b) high concentrations. Signal smoothing in (a) was done with Savitzky-Golay using OriginLab Pro version 8.5 program software. The inset in (b) expands the low concentration region of the main figure.

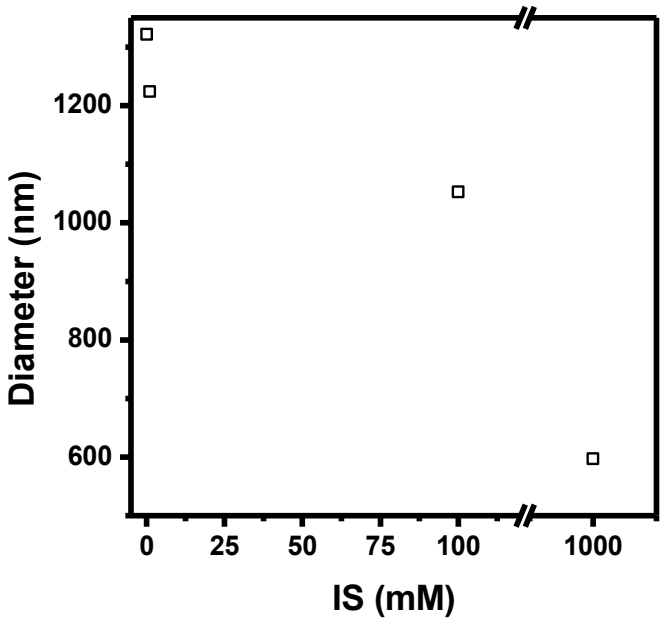

Figure F-2. Particle size dependence on ionic strength of p(NIPAm-*co*-AAc) microgel at pH 6.5. Particle size measurement was done with dynamic light scattering.